7cx

RECEIVED
OCT 18 1965
CENTAUR PROJECT OFFICE
NASA
LEWIS RESEARCH CENTER

CR-54609
4222-6043-KU000

FINAL REPORT

ADVANCED CENTAUR EXPLICIT GUIDANCE EQUATION STUDY

1 OCTOBER 1965

Prepared by
R. P. Davis
R. M. Staley
J. P. Ivaska

GPO PRICE $ ______
CFSTI PRICE(S) $ ______
Hard copy (HC) $6.00
Microfiche (MF) $1.50
ff 653 July 65

Prepared for

NATIONAL AERONAUTICS AND SPACE ADMINISTRATION
LEWIS RESEARCH CENTER

CONTRACT NAS 3-3231

FACILITY FORM 602

N66-19485 (ACCESSION NUMBER)
241 (PAGES)
CR 54609 (NASA CR OR TMX OR AD NUMBER)
______ (THRU)
1 (CODE)
21 (CATEGORY)

TRW SYSTEMS

4222-6043-KU000

FINAL REPORT

ADVANCED CENTAUR EXPLICIT GUIDANCE EQUATION STUDY

1 OCTOBER 1965

Prepared by
R. P. Davis
R. M. Staley
J. P. Ivaska

Prepared for
NATIONAL AERONAUTICS AND SPACE ADMINISTRATION
LEWIS RESEARCH CENTER

CONTRACT NAS 3-3231

TRW SYSTEMS

Prepared for
NATIONAL AERONAUTICS AND SPACE ADMINISTRATION
LEWIS RESEARCH CENTER

Approved A. A. Dzilvelis
A. A. Dzilvelis
Guidance and Control Project Engineer
Atlas/Centaur Launch Vehicle Study

Approved R K Whitford
R. K. Whitford, Director
Inertial Guidance and Control Laboratory

Errata for: Final Report, Advanced Centaur Explicit Guidance Equation Study,
dated 1 October 1965, TRW Report 4222-6043-KU000.

1. Page 2-12 In Figure 1 an arrowhead pointing down should appear on the right most vertical heavy line. Without this arrowhead the computation flow is ambiguous.

2. Page 5-2 In Figure 3 change x' to X, y' to Y, and z' to Z. These changes make the coordinate system shown on the right in Figure 3 compatible with the discussion in Section 5.1.2 on Page 5-3.

3. Page 5-37 In the middle of the page change "probe flight predictor" to read "free flight predictor".

4. Page 5-50 In Equation (165) C_{az} should be changed to C'_{az}.

5. Page 11-1 The primes should be removed from A'_x, A'_y, A'_z.

6. Page 11-11 The second entry for ϵ should be deleted.

R. P. Davis

R. P. Davis

CONTENTS

Page

1. SUMMARY 1-1

2. INTRODUCTION 2-1

2.1 Objectives 2-1

2.2 Why Generalized Equations 2-2

2.3 Why Explicit Equations 2-4

2.4 Ground Rules 2-7

2.4.1 Missions 2-7
2.4.2 Limitations of the Equations 2-8
2.4.3 Vehicle Configurations 2-8

2.5 Basic Methods 2-9

3. PRE-FLIGHT ACTIVITY REQUIREMENTS 3-1

3.1 Launch Azimuth Determination 3-1

3.2 Pre-Flight Targeting 3-2

4. SUMMARY OF RESULTS 4-1

4.1 Summary of Computer Requirements 4-1

4.2 Summary of Performance Results 4-8

5. THEORY AND DERIVATIONS 5-1

5.1 Descriptions of Coordinate Systems 5-1

5.1.1 Inertial Coordinate Systems 5-1
5.1.2 Earth Fixed System 5-3
5.1.3 Exo-Atmospheric Coordinate System 5-3

5.2 Exo-Atmospheric Steering Equations 5-4

5.3 Equations for Prediction of Cutoff Requirements 5-15

5.3.1 Optimum Intercept Targeting Routine 5-15
5.3.2 Specified Conic Routine 5-27

5.4 Coast Orbit Determination Guidance 5-31

5.4.1 Injection into Intercept Orbit 5-31
5.4.2 Injection into Hyperbolic Escape Trajectory 5-32
5.4.3 Injection into a Pre-Targeted Translunar Ellipse 5-33
5.4.4 Injection of ComSat into Synchronous Earth Orbit 5-33

5.5 Cutoff Routine 5-33

5.6 Maneuver Sequencing and Constant Redefinition 5-35

Page

5.7 Navigation Equations 5-35

5.7.1 The Advanced Centaur Navigation Problem 5-35
5.7.2 Overall Navigation Computations 5-37
5.7.3 Derivation of Navigation Equations 5-41

5.8 Atmospheric Steering 5-49

6. PERFORMANCE OF THE UPPER STAGE STEERING EQUATIONS 6-1

6.1 Parking Orbit and Elliptic Orbit Injection 6-6

6.2 Hyperbolic Orbit Injection 6-21

6.3 Intercept Orbit Injection 6-34

7. PERFORMANCE OF INTERCEPT EQUATIONS 7-1

7.1 General 7-1

7.2 P-Iteration Equations 7-1

7.3 Free-Flight Prediction Equations 7-2

7.4 Bias Equations 7-4

7.5 Search Logic 7-11

8. STABILITY INTERFACE OF GENERALIZED EXPLICIT EQUATIONS WITH THE CURRENT ATLAS/CENTAUR CONTROL SYSTEM 8-1

9. CONCLUSIONS 9-1

10. FLOW CHARTS 10-1

11. NOMENCLATURE 11-1

12. REFERENCES 12-1

CONTENTS (Continued)

Page

APPENDICES

A PRELIMINARY STUDY OF EXPLICIT GUIDANCE—CONTROL SYSTEM INTERFACE FOR ATLAS/CENTAUR

B DERIVATION OF ORBIT PARAMETERS, FROM THE MISSION CONSTRAINTS C_3, R_p, $\bar{s}$ FOR ESCAPE HYPERBOLA

C DERIVATION OR ORBIT PARAMETERS FROM THE MISSION CONSTRAINTS R_T, V_T AND R_p FOR TRANSLUNAR ELLIPTIC TRAJECTORIES

D ANGLE BETWEEN PERIGEE AND OUTWARD ASSYMPTOTE OF ESCAPE HYPERBOLA

E TABULATION OF INPUTS FOR EACH MISSION

ILLUSTRATIONS

		Page
1.	Guidance Computation Flow Chart	2-12
2	Intercept Targeting and Required Velocity Computation	2-13
3	Inertial and Earth Fixed Coordinates	5-2
4	Rotating Coordinate System	5-5
5	Overall Navigation Computation	5-42
6	Equivalent Block Diagram of the Attitude Control System for the Guidance Simulation	6-4
7	Unit Step Response of the Attitude Control System Used in the Guidance Simulation	6-7
8	Unit Ramp Response of the Attitude Control System Used in the Guidance Simulation	6-7
9	C_{az} Direction Cosine for a Parking Orbit Injection Using the Original Guidance Equations	6-9
10	C_{az} Direction Cosine for a Parking Orbit Injection Using the Final Guidance Equations	6-10
11	B Coefficient on a Parking Orbit Injection	6-11
12	Altitude Versus Time on a Parking Orbit Injection	6-13
13	Time to Go until Cutoff, T, on a Parking Orbit Injection	6-14
14	Predicted Change in Range Angle During Powered Flight, $\Delta\phi$, on a Parking Orbit Injection	6-15
15	Predicted Cutoff Position in Inertial Coordinates, X_D, and Present Position in Inertial Coordinates, X, on a Parking Orbit Injection	6-16
16	Predicted Cutoff Position in Inertial Coordinates, Y_D, and Present Position in Inertial Coordinates, Y, on a Parking Orbit Injection	6-18
17	Predicted Cutoff Position in Inertial Coordinates, Z_D, and Present Position in Inertial Coordinates, Z, on a Parking Orbit Injection	6-19
18	Velocity-to-be Gained, $\overline{V}_g$, in Inertial Coordinates	6-20

ILLUSTRATIONS (Continued)

		Page
19	C_{az} Direction Cosine for a Hyperbolic Orbit Injection Using the Unmodified Guidance Equations	6-23
20	C_{az} Direction Cosine for a Hyperbolic Orbit Injection Using Circular Orbit Steering up Until 400 Sec.	6-24
21	Time to go Until Cutoff, T, on a Hyperbolic Orbit Injection	6-25
22	Altitude Versus Time on a Hyperbolic Orbit Injection	6-27
23	Velocity-to-be Gained, V_g, in Inertial Coordinates, $K_{95} = 30$	6-28
24	Desired Radial Velocity at Cutoff on a Hyperbolic Orbit Injection	6-29
25	Desired Tangential Velocity at Cutoff on a Hyperbolic Orbit Injection	6-30
26	Magnitude of the Error in $\bar{V}_{\infty}$ Versus K_{95}	6-33
27	Cutoff Weight for Various Launch Times	6-36
28	Radial Velocity at Cutoff for Various Launch Times	6-38
29	Cutoff Altitude for Various Launch Times	6-38
30	Rendezvous Time, t_T, Various Launch Times	6-39
31	Perigee Altitude on the Transfer Orbit for Various Launch Times	6-39
32	Apogee Altitude on the Transfer Orbit for Various Launch Times	6-40
33	V_g Components Near Cutoff on the First Intercept Trajectory	6-43
34	Predicted Cutoff Position on the First Intercept Trajectory	6-44
35	Desired Velocity Components on the First Intercept Trajectory	6-46
36	Time to go to Cutoff on the First Intercept Trajectory	6-47
37	Diagram of the Lunar Biasing Problem	7-2

ILLUSTRATIONS (Continued)

		Page
38	The b Vector in Inertial Coordinates Versus Time of Impact	7-7
39	The b Vector in a Moon Oriented Rotating Coordinate Frame Versus Time of Impact	7-9
40	ΔV Versus t_r, Lunar Injection, 30 September 1965, Case 4	7-16

TABLES

		Page
1	Computer Estimate for LEM AGS Computer and Comparison with Current Centaur Computer	4-2
2	Computer Memor Requirements on On Board Computer Using Generalized Guidance Equations	4-5
3	Summary of Characteristics of Advanced Computer and Current -3 Centaur Computer	4-7
4	Summary of Performance Results	4-9
5	Values of Guidance Coefficients Which Remain Constant for All Missions	6-3
6	Special Guidance Coefficient for the Parking Injection Simulation	6-6
7	Special Guidance Coefficients for the Hyperbolic Orbit Injection	6-22
8	Special Guidance Coefficients for the Simulation of the Intercept of a Low Altitude Earth Satellite	6-35
9	Cutoff Errors in Radial and Out of Plane Velocity for Various Launch Times	6-42
10	Summary of Target Miss for Various Launch Times	6-42
11	Performance of the P-Iteration Equations	7-2
12	Performance of the Free Flight Prediction Equations	7-3
13	Error in Predicting the Position of the Moon	7-6
14	Lunar Impact Points Obtained From the Nominal Cutoff Condition	7-10
15	Lunar Impact Points Obtained from the Computed Desired Velocities	7-11
16	Coefficient Values for A-Shot Runs on Translunar Injection	7-12
17	Values of t_T From Nominal Trajectories and From A-Shot Results	7-13
18	A Comparison Between the A-Shot $\overline{V}_d$ Vectors and the Nominal Cutoff Velocities	7-14
19	Lunar Impact Points Obtained from the $\overline{V}_d$ Vectors Generated by the A-Shot Program	7-15

1. SUMMARY

This report is the final report on a portion of the work performed within Task VI under contract NAS3-3231. The work performed here was a study to investigate the feasibility of using a set of generalized guidance equations to direct a wide variety of future Centaur missions. The report discusses why explicit guidance techniques are best suited to the purposes of the generalized guidance required. It presents a set of ground rules which essentially define the missions which are considered to fall within the scope of a utility vehicle. Theoretical developments of the equations recommended are given and performance results reported. A set of computer requirements based on these equations is presented and the implications of these requirements are discussed.

The conclusions reached in the study are:

a) It is possible to design a set of generalized equations which will perform space tasks, and which can be accommodated by present day "advanced" flight computers.

b) The performance of these equations is comparable and can exceed the performance of contemporary procedures.

c) The current Centaur computer (-3 Librascope) is not adequate to handle the requirements of such an advanced set of equations. However, the possibility exists that the current computer could handle a version of the equations which had a reduced mission accomplishment capability (i.e. the ability to perform intercept guidance would be eliminated).

2. INTRODUCTION

2.1 OBJECTIVES

The objectives of this study were, in the broadest sense, to establish the feasibility of using a single set of generalized guidance equations to direct all the missions which could reasonably be predicted for the Centaur vehicle. It was further considered that this same set of equations should guide all stages through payload injection. The feasibility was to be evaluated within the context of the Advanced Centaur Guidance System Study contract (# NAS 3-3231, Task VI) which has as its purpose the investigation of requirements for an improved version of the guidance system for the Centaur vehicle with the appropriate lower stages. The two areas in which major improvements are contemplated are the inertial guidance hardware and the flight computer.

The guidance euqations and other associated guidance software are a primary function in determining the flight computer requirement. This is because a major portion of the computer memory is taken up by the guidance software and the speed at which the guidance computations must be made is a function of the complexity of the equations. The contribution to the computer requirements dictated by the hardware interface is more readily identifiable at a later stage in development when tradeoffs among available computer space, the computer input/output capability and the hardware characteristics can be made. Section 4.1 however, gives initial estimates for the requirements of these routines so that a gross maximum computer sizing estimate can be given.

The contribution to guidance system error due to the guidance software is generally small compared to the contribution of the measurement error and therefore is not critical to the performance of an advanced system. However, it is reasonable to place an accuracy requirement on any generalized equations approach to be comparable if not better than the current "special purpose" equations capability. Section 4 presents some of the performance capabilities of these equations.

For the above reasons, feasibility was evaluated primarily on the basis of whether the guidance equations could be reasonably accommodated in a computer currently existing or well along in development and of acceptable size and weight for the Centaur applications.

The guidance computational routines presented and discussed in this report are those which will form the major contribution from the guidance software to the definition of the computer requirements and which are unique to the guidance equation philosophy adopted. Other routines (such as navigational initialization, alignment, calibration, etc.) which in their essential forms are not dependent on the form of the guidance equations or which are dependent on the actual computer itself (such as mode sequencing logic, diagnostic and self tests, etc.) are not discussed in great detail. The contribution to the requirements of these routines can, however, be estimated from previous experience and these estimates are given in Section 4.1 together with overall computer requirements as prescribed from this study.

2.2 WHY GENERALIZED EQUATIONS

This section will discuss why there do, indeed, exist valid reasons for devoting considerable effort to the study of the use of generalized guidance equations; and also what general disadvantages can be identified in connection with guidance software generalization.

A basic role of the proposed Advanced Centaur is that of performing the functions of a highly reliable utility vehicle. An unavoidable implication of this concept is that such a space system be capable of carrying out many different classes of missions and, as a consequence, have a large repertoire of space maneuvers (i.e. high flexibility). Further is should be capable of performing any of these missions on relatively short notice which means, ideally no system modification, but more practically, a minimum of modification. Thus from the guidance software point of view a single set of guidance equations, programmed once and for all in the flight computer, capable of directing all of the proposed missions and requiring a minumum of pre-flight targeting would meet these flexibility and modification requirements admirably.

A further advantage of using a single set of guidance equations is the opportunity for continual evaluation of performance of the equations thereby gaining extensive knowledge of their capabilities with the resulting ultimate development of high levels of confidence in their operation. Also in this connection high ultimate reliability can be achieved using a standardized set of equations.

A less concrete reason but of possibly greater long term significance than the preceeding ones, is that the logical expectation of the eventual routine use of highly operational multipurpose spacecraft for various and sundry space duties (with the capability to meet changing mission requirements on very short notice or even in flight) will require a concommitant generality in guidance software. It would thus seem that the accumulation of experience in the formulation, evaluation, and use of generalized guidance techniques now and in the near future would be of significant value when it comes time to develop these advanced general purpose vehicles. Indeed the Advanced Centaur concept is an early version of such vehicles and would be a logical place to perform early evaluation of generalized guidance.

In terms of long term economy, the total program cost for a generalized approach should be less than for a mission-by-mission concept of guidance equation development. This saving would come from the minimization of not only total equation development "effort" but also from the minimization of supporting software requirements such as targeting and validation programs which are performed for each mission.

Another advantage of the particular generalized equation set presented in this report is that they are not sensitive to changes in the booster system configuration. Thus substitution of the Atlas booster vehicle by a Saturn or Titan vehicle would require only a change of constants with perhaps minor output processing to interface with the lower stage control system and discrete sequencing. Some minor modification of the atmospheric steering equations might also be appropriate when boosters other than the Atlas are used. This point is discussed in Section 5. 8.

The major disadvantage of the generalized approach is the necessary complexity of the equations and the fact that their evaluation must include proving that they function properly over the range of generality that they were designed for. This implies slightly more development and validation effort than for a specific mission approach where software is tailored to a smaller computer.

In summary then, the case for the use of generalized equations as opposed to the mission-by-mission approach is supported by the following attributes of the former.

a) High flexibility

b) High confidence levels in operation

c) High performance reliability

d) Lower total program cost

e) Low reaction time to booster configuration changes

f) Opportunity for accumulation of experience with highly generalized techniques.

The disadvantages arise primarily from the complexity of the generalized equations and the resultant level of initial effort needed to get the program operational.

2.3 WHY EXPLICIT EQUATIONS

In this section a brief discussion will be given on why explicit techniques were chosen in preference to perturbative methods. Such a discussion is appropriate since there exists a large fund of experience with the perturbative methods, and for a given mission the explicit techniques generally are more complex thus requiring more computer capacity and greater computational speed.

First, then, it can be stated that with the advancing state of the art in computer technology, the computer package has been reduced in weight and volume with significantly increased computational speeds. Thus, where in the past, hardware limitations militated against the use of explicit techniques, today, with such large, high speed machines as the TRW LEM AGS or UNIVAC 1824, it becomes feasible to take advantage of some of the significant advantages of explicit guidance. These advantages are principally that explicit equations are capable of being more flexible and require far less precomputation (targeting).

These two basic advantages arise from the fact that the inflight equations used to compute the required burnout (or engine cutoff) conditions result from using the fundamental principles of two body mechanics. Thus injection into any specified geo-focal orbit is achieved by computing the cutoff conditions utilizing the two basic equations,

$$r = \frac{p}{1 + e \cos f}$$

$$v^2 = \mu \left(\frac{2}{r} \pm \frac{1}{a} \right)$$

which can be recognized as the general equation for a conic and the vis-viva energy equation respectively (see below for the detailed application of these equations). Fundamentally then, all that needs to be provided are the parameters of the conical orbit discussed (i. e., p, e, a) and the same equations can be used to derive the cutoff conditions for circular, elliptic, parabolic, or hyperbolic orbits. This contrasts to the perturbative techniques where in general for each new conic attempted much pre-flight computation must be carried out in order to first, obtain the required nominal trajectory and burnout conditions and then, to determine a set of partial derivatives which relate the nominal burnout conditions to the required burnout conditions on a non nominal trajectory. Effectively then, using perturbative techniques often requires extensive new guidance software for many different objectives of a powered trajectory. In view of the above discussion, the basic difficulties in attempting to formulate generalized guidance equations using perturbative techniques, is that there would need to be stored within the flight computer the pre-targeted information for all of the maneuvers contemplated within the desired range of flexibility. Thus the storage capacity of the flight computer would quickly limit the degree of flexibility capable with the perturbative equations. An alternative would be to store the pre-targeted information in a ground facility computer, or to develope several special purpose programs neither of which appears as attractive as the one set.

The case for the use of explicit equations is further supported when it becomes necessary to have the guidance equations treat intercept and rendezvous problems as well as injections into specified orbits. In the intercept case the problem is one of guiding the spacecraft in such a way that it ultimately intercepts another vehicle (or point in space) whose position in general, is changing rapidly. The procedure for performing this type of maneuver using explicit techniques is to utilize the current position of the spacecraft, the position of the target from ephemeris data, and a time-to-intercept, in order to seek out a satisfactory intercept trajectory. These computations are done in flight (in-flight targeting) and the spacecraft can thus be put into the intercept trajectory from any position it might find itself, provided other constraints are not violated (e.g. propellant, perigee, etc.). If the same problem were to be solved using perturbative methods, the approach would be to develop a nominal intercept trajectory on the basis of a given set of spacecraft and target vehicle conditions. From this trajectory the appropriate error coefficients would be generated (i.e., pre-targeted quantities) from which the required cutoff conditions necessary to intercept from off-nominal conditions could be computed. In order to expand the capability to intercept from more than a single set of conditions, the error coefficients would have to be computed for each condition desired and then stored in the flight computer (or provision made to transmit the appropriate coefficients when and as needed from the ground). The storage of these coefficients in the form of time dependent polynomials, as is common, would alleviate the storage problem but accurate fits, good over long continuous periods or more than one injection opportunity, are difficult if not impossible to obtain. Thus, here again flexibility would be limited by storage and/or data retrival limitations. Furthermore even if it were feasible to adequately process the great amount of data needed by perturbative equations to approach the inherent flexibility of the explicit approach, the pre-flight targeting effort required to generate all of this information would make its usefullness highly questionable when there exist more direct techniques, involving less arduous preparations which can perform the same tasks.

An additional advantage of the explicit approach is that it is less sensitive to deviations in the booster trajectory. The reason for this is that the explicit procedures are not dependent on nominal trajectories and generate guidance commands on the basis of whole state variables instead of using approximate linear perturbation techniques.

In summary, the advantages in using explicit equations over perturbative techniques are:

a) Higher flexibility

b) Much less pre-flight computation (targeting)

c) Less sensitivety to deviations in booster trajectory

d) Less computer capacity for simultaneous multiple mission computation.

Thus, on balance, since the advanced hardware is available it seems evident that explicit techniques, though involving more complex in-flight computations at higher computing speeds, provide more flexibility and and require less mission dependent pre-computation than perturbative methods and are therefore preferable for space applications where frequent and varied missions and maneuvers are required.

2.4 GROUND RULES

2.4.1 Missions

The guidance equations presented in this report were designed to provide guidance for a multipurpose payload injection system with the Centaur as the upper stage and the Atlas booster system as the lower stages.* The missions which the equations were designed to direct are the following, and can be carried out in an appropriate single or two burn mode (or 3 burn in case of a synchronous orbit).

a) Boost and injection of a payload into an earth orbit.

b) Boost and injection of a payload into a translunar trajectory.

c) Boost and injection of a payload into an interplanetary trajectory.

d) Boost and injection of a communications satellite into an earth synchronous orbit.

---

*The use of the Atlas booster system in the development and evaluation of the equations does not restrict the use of the equations to this booster system.

e) Boost and injection of a payload into an intercept orbit for the purpose of effecting an ultimate rendezvous with an orbiting vehicle (it is assumed here that the Centaur would be passive, from at least the guidance command point of view, for the midcourse and terminal homing portions of the rendezvous).

These specific mission capabilities require a repertoire of maneuver capabilities which permit the system to be readily adaptable to future mission requirements. Thus, such advanced missions as satellite interception and/or inspection, or a refueling and support flight for an orbiting space station, for which there is presently no specific requirement, could be easily assimilated into the basic generalized capabilities of the equation set. In actuality the equations were designed with these advanced concepts in mind as well as those listed previously.

2.4.2 Limitations of the Equations

The equations as presented in this report are limited to the boost and injection functions. In addition there is no provision made for handling long term missions requiring external attitude updating or orbit determination because of the inherent limitations of the Centaur vehicle itself to these applications.

2.4.3 Vehicle Configurations

As stated above the vehicle which served as the model for this study was the Atlas Centuar configuration. Thus, as presented in this report, the equations provide guidance for the Atlas Booster, Atlas Sustainer, and Centaur stages. As such, the Atlas Booster was considered to complete the penetration of the atmosphere and thus uses a separate steering scheme designed to penetrate the atmosphere without violating the Atlas/Centaur loading and heating constraints. However, this atmospheric portion of the generalized equation set is designed as a modular component of the guidance computation system and may easily be replaced with another atmospheric steering scheme to accommodate changed ascent constraints. In addition, it was considered appropriate to consider the use of the Centaur with other booster packages (for example, Saturn or Titan), which might or might not have their own proven and operational atmospheric steering schemes. Thus, in addition to having the atmospheric steering modular, this initial guidance phase may be obviated altogether so that the generalized equations equations as presented in this report would not be initialized until the lower stage guidance system had completed its assigned function. The exo-atmospheric portion of the guidance equation set is designed nominally to begin during Atlas Sustainer flight (anywhere from sustainer ignition on) and continues to completion of the Centaur role. Thus the exo-atmospheric equations are nominally designed to act over two stages (this includes restarts of the Centaur engine), though, as suggested above no difficulty arises if it is desired to guide only the Centaur stage with the exo-atmospheric equations. The extension of the exo-atmospheric guidance equations to cover more than two distinct stages can be easily made, though, admittedly this would require a modification of the steering equations as presented in this report. It should be pointed out however, that this limit on the generality of the equations is not at all pertinent to the stated contractual objectives of this study, which were directed toward the Atlas/Centaur con configuration. Only when the question of the extent of "generalization" is posed or the prospect of extension of the equations to systems using more stages than Atlas/Centaur is considered, need these limits be defined or the means for the extension of the generality be considered.

2.5 BASIC METHODS

Before giving detailed derivations and descriptions of the explicit equations, a brief and general summary of the methods employed in these equations is given here so that the results and conclusions, presented in the next section, may be more fully appreciated.

Figure 1 shows the guidance computation flow chart with the main computational routines contained in the generalized set. Once this guidance program is initiated it automatically directs the particular flight to the completion of payload injection. The initial portion of the program is that of loading the various guidance inputs. These inputs fall under the following general categories.

a) Various constants related to the vehicle and its respective propulsion system

b) constants needed to sufficiently define the flight orbits to be achieved (i.e. orbital parameters, flight plane orientations, etc.),

c) constants which properly initiate maneuver sequencing logic,

d) constants associated purely with the guidance equations themselves such as initial values for starting iterations, proportionality constants, biases, etc., and

e) constants which define certain tolerances such as propellant pads and injection true anomaly limits, etc.

The actual guidance computations begin with the atmospheric steering phase which continues until the sensible atmosphere is penetrated sufficiently to permit employment of the exo-atmospheric equations. The equations used for this phase are designed to offer acceptable loading characteristics for the Atlas/Centaur structure and fall under the general category of velocity steering methods.

At a predetermined altitude the exo-atmospheric equations assume guidance of the flight and continue in this role through payload injection. The explicit scheme used for this portion of the flight consists of a procedure which divides logically into two parts:

a) Computation of desired cutoff conditions (i.e. velocity only or velocity-position constraints)

b) Incorporation of the cutoff constraints for the inflight derivation of an explicit steering regimen which will meet these constraints.

In other words, the procedure initially determines the cutoff conditions necessary to meet the current maneuver objectives, and then derives the appropriate steering commands. Since the nature of the powered flight problem does not permit of a sufficiently accurate analytic solution (of any practical importance) until the powered flight time becomes quite small, an iterative procedure is used throughout the powered flight whereby successive approximate solutions are carried out which converge to the sufficiently accurate solution as the burn time decreases. Thus, the iteration loop would run as follows:

a) A cutoff position is estimated.

b) From (a) the corresponding cutoff velocity is computed.

c) From (a) and (b) the appropriate steering signal is generated.

d) From (b) the powered flight burn arc remaining to cutoff is estimated from which the cutoff position estimate is made (i.e. return to 'a').

This loop is shown in heavy lines in Figure 1.

A "burn angle predictor" within the iterative loop is used in the process whereby the cutoff conditions are predicted. This computation is made by utilizing the computed angular momentum and position at cutoff and the current angular momentum and position in conjunction with the estimated time to go until cutoff.

The computation of the desired cutoff conditions is made by one of two routines depending on whether an intercept maneuver is being carried out (e.g. rendezvous, etc.) or whether an injection into a pre-targeted conic is desired (e.g. parking orbit, elliptic earth orbit, escape hyperbola for interplanetary missions, etc.). The former is the block entitled "Intercept Targeting and Required Velocity Computation" and the latter is the block entitled "Required Velocity for Specific Conic". The "Intercept Targeting and Required Velocity Computation" seeks out a propellant optimized intercept trajectory on the basis of the estimated cutoff position and the position of the target at intercept (see Figure 2). The ephemeris data of the target vehicle or body, obtained from the flight computer, together with a "Free Flight Prediction" routine (see Figure 2) is used to obtain the position of the target at intercept. Thus, in-flight targeting is carried out for intercept maneuvers. The "Required Velocity Computation for Specified Conic" routine uses the pre-launch targeted parameters of the desired conic to compute the required cutoff conditions. Thus, with a given estimate of the cutoff position specified, the corresponding cutoff velocity is determined by two-body equations.

With the cutoff conditions specified, the steering equations (E-steering) then derive the corresponding steering commands. This is done by solving the corresponding boundary value problem using the current position and velocity and the desired cutoff conditions at the specified end points. The steering commands are developed as attitude errors with respect to the vehicle body axes and transmitted to the control system as attitude rate commands.

Engine cutoff is commanded by the extrapolation of a second degree curve obtained by a fit to the "velocity to be gained" values just before cutoff. Thus, when the time until cutoff falls below a specified small

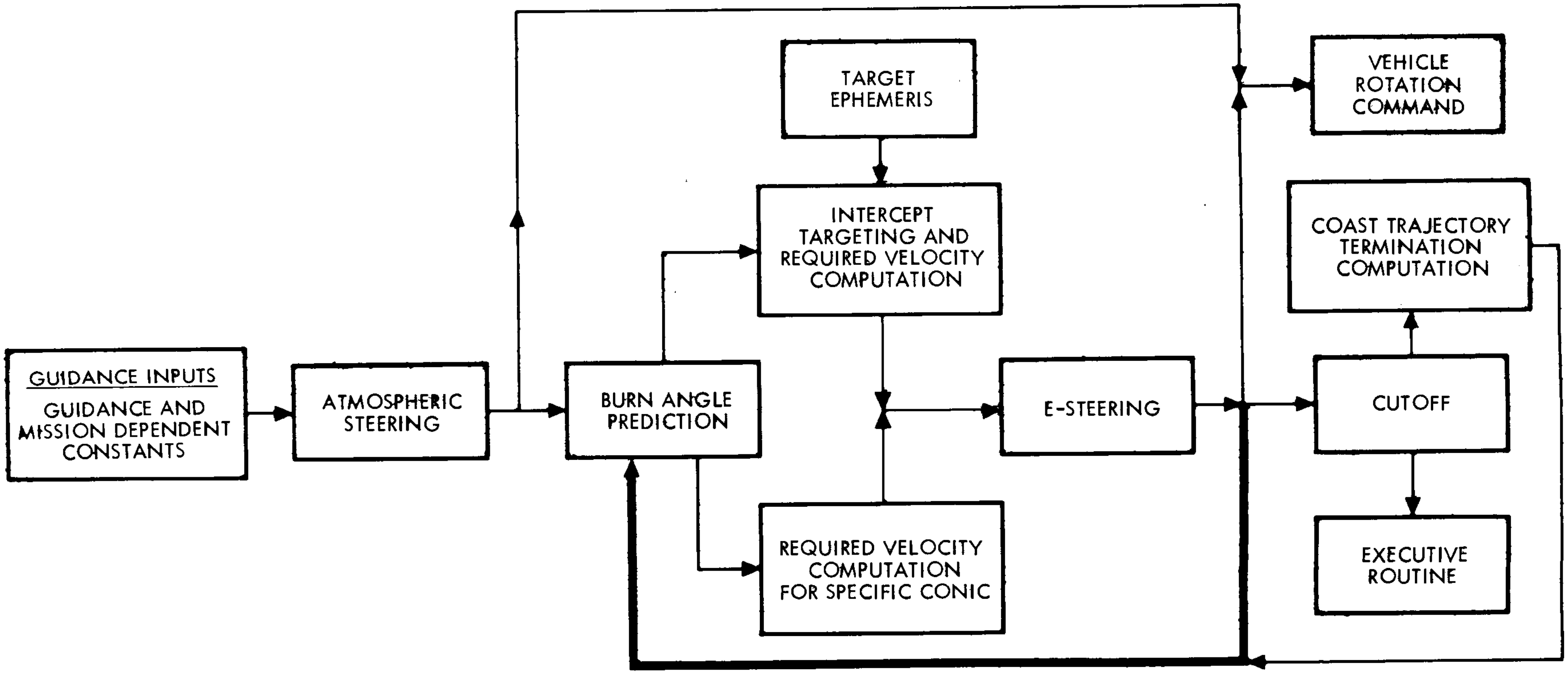
GUIDANCE INPUTS
GUIDANCE AND MISSION DEPENDENT CONSTANTS
ATMOSPHERIC STEERING
BURN ANGLE PREDICTION
TARGET EPHEMERIS
INTERCEPT TARGETING AND REQUIRED VELOCITY COMPUTATION
REQUIRED VELOCITY COMPUTATION FOR SPECIFIC CONIC
E-STEERING
VEHICLE ROTATION COMMAND
COAST TRAJECTORY TERMINATION COMPUTATION
CUTOFF
EXECUTIVE ROUTINE

Figure 1. Guidance Computation Flow Chart

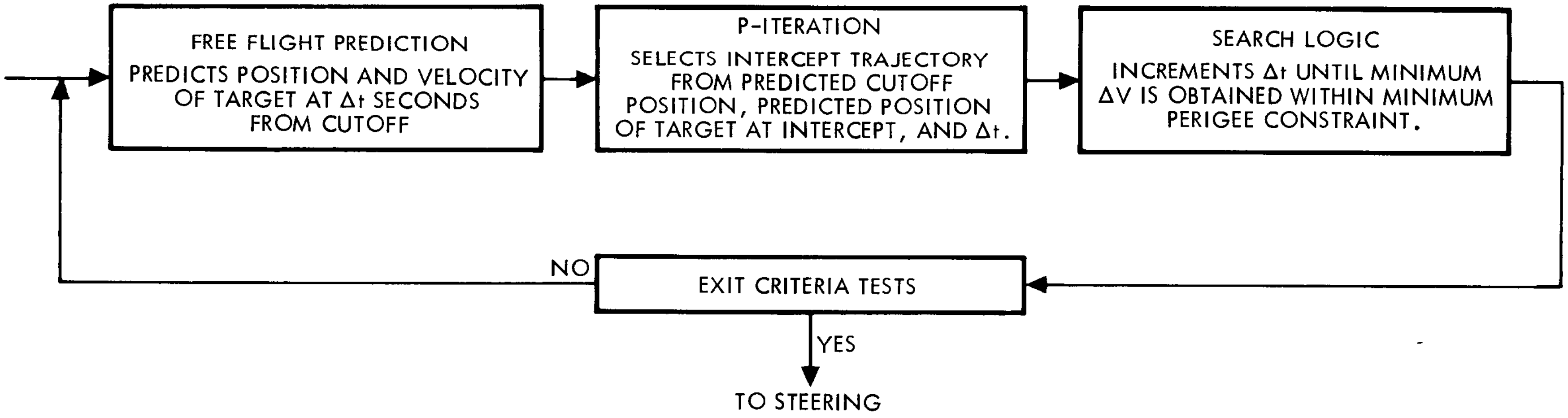
FREE FLIGHT PREDICTION
PREDICTS POSITION AND VELOCITY OF TARGET AT Δt SECONDS FROM CUTOFF
P-ITERATION
SELECTS INTERCEPT TRAJECTORY FROM PREDICTED CUTOFF POSITION, PREDICTED POSITION OF TARGET AT INTERCEPT, AND Δt.
SEARCH LOGIC
INCREMENTS Δt UNTIL MINIMUM ΔV IS OBTAINED WITHIN MINIMUM PERIGEE CONSTRAINT.
EXIT CRITERIA TESTS
NO
YES
TO STEERING

Figure 2. Intercept Targeting and Required Velocity Computation (in flight targeting loop)

value the last three "velocity to be gained" values are used to predict when the velocity to be gained will be zero and the engine is shut down at this predicted time.

With the accomplishment of engine shut down, the guidance equations continue to function (that is, provided the role of the equations for the mission has not been terminated) in order to determine when the next restart should occur. This computation is designated in Figure 1 as the "Coast Trajectory Termination Computation". The criteria for restarting are functions of the objectives of the ensuing powered flight phase and, depending on these objectives fall under one or more of the following:

a) The ensuing burn period (or periods) can be carried out within the limits of the propellant supply available. (This is of course a general requirement.)

b) The ensuing burn period should terminate with an injection within certain given true anomaly limits. This is the injection near perigee constraint.

c) The ensuing burn period should terminate with a position match accurate to within certain required limits.

d) The ensuing burn period will terminate in an orbit whose perigee is above a certain altitude.

This coast trajectory termination computation utilizes the "burn angle prediction" routine to predict the cutoff conditions of the subsequent burn phase and is designed to terminate parking orbits and unpowered intercept trajectories.

The role of these guidance equations is automatically terminated by an executive routine which issues the guidance termination discrete in accordance with the instructions loaded into the flight computer in the form of appropriate input constants.

3. PRE-FLIGHT ACTIVITY REQUIREMENTS

As discussed above, a primary aim in the design of these equations was the minimization of pre-flight mission-dependent computations. The use of explicit techniques goes far in accomplishing this objective as previously noted. However, even with the reduction of the pre-flight targeting effort, the equations to be presented in this report require a significant amount of pre-computed data. This section discusses the general extent of these requirements.

3.1 LAUNCH AZIMUTH DETERMINATION

It is assumed that the launch azimuth variation with launch time has been predetermined and is available to the vehicle guidance system as an input when the liftoff time has been established. This is the procedure used in the current Atlas/Centaur configuration. Thus, part of the development of an operational system using the guidance philosophy presented in this report, would be the determination of a body of launch azimuth information correlated with particular mission characteristics and launch times. This launch azimuth information might be made available in say, tabular form to a human controller, who, when the launch time were established, would manually "dial" the proper launch azimuth into the vehicle guidance system. Alternatively the launch azimuth information could be provided in the form of launch time dependent polynomials, programmed either in a ground based computer or in the flight computer (the former seems more attractive from the standpoint of limiting on-board computer capacity requirements). With these polynomials the launch azimuth computation would be a part of the automatic guidance system with no need for the human intermediary.

A brief look was taken at the advisability of attempting to develope an analytical non-empirically derived expression for the launch azimuth which would be a function of the launch time and the desired orientation of the initial orbit plane. Such a procedure was developed on a preliminary basis and it was found that it would, in general, require the knowledge of the orientation of the observed orbit, or equivantly its unit normal. This orientation is very strongly associated with launch window limits which in turn are based on paylaod capabilities. These limits must be determined before launch since the guidance equations are not sufficiently accurate at launch to predict payload capability of the boost and injection system. The process of determining these limits however involves the generation of acceptable launch azimuth data. It would therefore appear that the utilization of this launch azimuth information obtained in the activity described above, in the form of tables or polynomials would be more economical than including additional logic in the equation package to compute what has already been determined elsewhere. Thus for these reasons it was concluded inadvisable to include an explicit launch azimuth determination routine.

It might be pointed out however, that if the guidance equations were made capable of predicting payload limits with any precision at launch than an explicit routine for launch azimuth might then become appropriate. Any continued development in the area of generalized guidance equations should consider this possibility.

3.2 PRE-FLIGHT TARGETING

By targeting, is meant here, the generation of the proper values for those quantities that appear in the guidance equations and which are dependent on the nature and objectives of the mission to be flown and the vehicle configuration. In dealing with explicit guidance equations the targeted quantities are principally those which describe the orbit to be achieved rather than coefficients for required velocity and/or steering polynomials as in perturbative and open loop techniques. The pre-flight targeting effort for the guidance equations discussed in this report therefore falls into the following categories:

1) Determination of Atmospheric Steering Coefficients (See Section 5.8): For a given vehicle this determination could be done only once which would establish a standard ascent through atmosphere profile.

2) Determination of Exo-Atmospheric Steering Biases and Computation Switching Parameters (See Section 5.2): These are quantities which detailed performance analyses (See Section 6) indicated would optimize the performance of the equations. They compensate for the effect of staging discontinuities and specify when the switching between different steering modes should be accomplished. The values for these quantities were found to be generally mission dependent.

3) Determination of Desired Orbit Defining Parameters (See Section 5.3): These parameters are orbit parameters such as eccentricity, semi-latus rectum, etc., orbital inclinations, perigee magnitude and directions, target vector, and various other quantities which appear explicitly in the required velocity equations and are highly mission dependent.

4) Target Ephemerides: As explained in the body of the report (See Section 5.3.1) the guidance used to carry out intercept maneuvers requires a knowledge of the ephemeris of the target. Thus for such intercept maneuvers the appropriate ephemeris data would need to be determined and provided to the flight computer prior to launch.

5) Other Miscellaneous Mission Dependent Quantities: These are such things as control system gain constants which might be vehicle configuration and therefore mission dependent, satisfactory propellant pads, injection true anomaly, limits, etc.

4. SUMMARY OF RESULTS

4.1 SUMMARY OF COMPUTER REQUIREMENTS

As stated previously the principal criterion for establishing the feasibility of using a highly generalized set of guidance equations is how well such a set of equations can be accommodated by an advanced flight computer which is judged to be within the current state of the art. Three such computers are:

MIT/Raytheon Apollo Computer

Univac 1824

LEM AGS Computer, MARCO 4418 of TRW Systems

The LEM AGS is representative of these general purpose high speed machines so that requirements imposed on this machine by the generalized guidance equations of this report were taken to establish feasibility from the computer requirements standpoint.

Table 1 summarizes the results of capacity and timing requirement estimates made on the LEM AGS for the guidance equations alone. The estimates were made from the guidance equation flow charts shown in Section 10. The entries in Table 1 are on a flow chart by flow chart basis. Flow charts 2, 3, and 4 comprise the self-targeting routine for intercept guidance. The table shows timing estimates for the cases when this loop is deleted, when three cycles around this loop are made and when 15 cycles around the loop are made. These different values are given in order to:

a) show what the timing requirements would be if the self targeting loop were removed thus removing the ability of the equations to perform intercept guidance.

b) show the timing requirements during the powered portion of an intercept maneuver where three iterations around the loop are made.

c) show the timing requirements during the coast period preceding the powered portion of an intercept maneuver where as many as 15 iterations around the loop are made.

Table 1. Computer Estimate for LEM AGS Computer and Comparison with Current Centaur Computer

Flow Chart	Title	Number of Storage Locations		Worst Path Timing (m sec)	Timing With No Self Targeting (m sec)	Timing With Three Self Targeting Iterations	Timing With Fifteen Self Targeting Iterations
		With Self Targeting	Without Self Targeting				
1	Initial Guidance Loop Computations	225	225	5.5	5.5	5.5	5.5
2	Free Flight Prediction	265	-	10.2	-	(150)	(750)
3	P-Iteration	330	-	29.2	-		
4	Search Logic	115	-	1.7	-		
5	Cutoff Velocity Prediction	135	135	5.5	5.5	5.5	5.5
6	Exo-Atmospheric Steering	360	360	7.0	7.0	7.0	7.0
7	Error Signal Equations	60	60	4.2	4.2	4.2	4.2
8	Cutoff Routine	65	65	1.2	1.2	1.2	1.2
9	Coast Trajectory Termination	145	130	4.0	4.0	4.0	4.0
10	Maneuver Sequencing and Constant Redefinition	40	35	0.2	0.2	0.2	0.2
11	Atmospheric Steering	120	120	1.7	1.7	1.7	1.7
12	General Navigation Equations	275	275	7.9	7.9	7.9	7.9
13	Atmospheric Navigation Equations	100	100	1.0	1.0	1.0	1.0
14	Compensation Equations	90	90	1.4	1.4	1.4	1.4
	TOTALS	2325	1595		39.6 m sec	(189.6)	(789.6)
	Corresponding Totals for Current Centaur -3 Librascope Machine	2675	1835		2800.0 m sec	13300.0 m sec	55300.0 m sec

Table 1 also gives the total storage locations and timing requirements of the current Centaur -3 Librascope computer.

It can be seen from this table that the -3 machine requires somewhat more locations than the LEM AGS machine. The reason for this is the fact that the -3 is a drum machine and has a limited indexing capability. This means that different coding procedures are employed and additional logic must be provided in the -3 machine to perform the indexing function. The -3 computer has a total of 2800 locations available so it can be seen that programming the total guidance equation package barely leaves room for any of the other computer functions. If the self targeting feature of the equations is deleted (which eliminates the intercept guidance capability) there are about 1000 locations available for other functions, but the loss of the intercept capability constitutes a serious retreat from the position taken in the ground rules section of this report. Table 1 also indicates that the timing requirements imposed by the complete equation package are beyond practicality. This conclusion is supported by past experience and more explicitly, by a study entitled "Preliminary Study of Explicit Guidance Control System Interface for Atlas/Centaur", reproduced as Appendix A. Reference to this study shows that in order to preserve Atlas/Centaur control system stability, sampling periods of greater than 5 seconds can not be tolerated. Thus the requirement of more than 13 seconds indicated in Table 1 is quite out of limits. Note however, that if the self targeting feature of the equations is eliminated, the timing requirements are less than 3 seconds so that again, for a version of the equations which did not include an intercept guidance capability, the current Centaur machine might be acceptable.

In summary then, Table 1 shows that:

a) the current Centaur -3 Librascope computer is not adequate to handle the complete generalized equation package.

b) the current Centaur computer might be able to handle a reduced version of these equations (see the discussion below associated with Table 2 for a more complete answer to the question).

c) from the standpoint of timing requirements the LEM AGS (or a similar computer) can easily do the job, based on the requirements put forth in the study discussed in Appendix A.

Whether the LEM AGS and similar machines can meet the requirements with respect to instruction locations is discussed below in conjunction with Table 2.

Table 2 gives an estimate of the total memory locations needed to program the equations of this report plus the other computations usually required of the flight computer. It can be seen from the table that the guidance equations form the largest single part of the total requirement but that the other functions are by no means insignificant. The table is given in terms of four options. These options are as follows:

Option I

This option includes those computational functions which this report considers advisable to include as the responsibility of the on-board computer. Since the Centaur GSE is now being modified to include a separate ground computer to relieve the inflight computational load, it is a distinct possibility that that capability might be carried over to an advanced Centaur also. Some of these pre-flight computations are alluded to in the text of the report (e.g., the generation of the transformation from the equatorial oriented inertial to the platform coordinates, the computation of launch azimuth, and the calibration and alignment procedures, etc.). It was also felt that since it is, at present, difficult to identify a real requirement for the processing of externally received data, the memory requirements for these computations should be considered only for a maximum capability system.

Option II

This option included all the computer functions which might conceivably and reasonably be performed by the flight computer. This option can be viewed as a maximum system which provides an upper bound to the total computer requirements for an advanced Centaur guidance system.

Option III & IV

Reference to Table 1 shows that the largest contribution to the computer memory requirements is due to the self targeting or intercept

Table 2. Computer Memory Requirements for On Board Computer Using Generalized Guidance Equations

Function	Memory Locations				Remarks
	Option I	Option II	Option III	Option IV	
Pre-Flight Equations	▨	1000	▨	1000	OPTION I Includes flight computer functions as implied by the text of the report. OPTION II Includes all of the functions which might conceivably be performed by the flight computer. OPTION III Option I when intercept guidance is not included in the guidance equations. OPTION IV Option II when intercept guidance is not included in the guidance equations.
Pre-Launch Computations	150	200	150	200	
Guidance Equations (See Table 1 for breakdown)	2325	2325	1595	1595	
Executive Routine	420	420	420	420	
Telemetry	100	100	100	100	
Control System Computations	80	80	80	80	
External Command Interpretation and Execution	100	100	▨	▨	
Programmer and Switching	200	200	200	200	
External Data Processing	▨	200	▨	200	
Ephemeris Routine	150	150	▨	▨	
TOTALS FOR LEM-AGS	3525	4775	2545	3595	
Corresponding Totals for Current Centaur -3 Librascope Machine	3875	5125	2785	3835	

guidance feature of the guidance equations. Option III and IV gives the total computer requirements for the cases of Option I and II respectively if the intercept guidance capability is deleted from the equations. These last two options illustrate, in terms of practical requirements, the price paid for incorporating intercept guidance in a generalized set of equations. The requirements specified in these last two options also gives an indication of how far the guidance software can be modified before the capabilities of the current Centaur computer begin to be exceeded (see below).

Table 3 gives a summary of the characteristics of three representative advanced computers and the current -3 Librascope Centaur computer. A comparison of the data in Table 2 with the computer characteristics given in Table 3 shows that any of the advanced computers can accommodate the memory location requirements of even the maximum system of Option II. However, it can be seen that only with the most extreme "squeezing" could the minimum requirements of Option III (which has no intercept guidance capability) be accommodated by the current Centaur computer. In this connection it should also be pointed out that the current Centaur computer has available only about 1800 memory locations for in-flight computations, the remainder of the total 2800 being used for pre-flight computations. In addition, the current Centaur configuration does not provide a feasible method for continuous switching from one or the other of these two portions of the memory, so that even if the "squeeze" could be accomplished the computer would need to be modified to provide facile access to either of these sets of memory tracks.

In summary then, from the information given in Tables 1, 2, and 3 the following conclusions can be stated.

1) The total computer requirements for an advance guidance system using generalized explicit guidance equations can be met by any one of the three advanced computers of Table 3.

2) The current Centaur computer could not accommodate a system which employed generalized explicit guidance techniques and which included a capability to perform intercept guidance.

3) The current Centaur computer would possibly accomodate a system which did not have the intercept guidance capability, but only under the following conditions

Table 3. Summary of Characteristics of Advanced Computer and Current -3 Centaur Computer

Computer	Total Memory Locations Available	Basic Word Size (Bits) Including Sign Bit	Double Precision Capability	Computation Speed Relative To -3 Librascope	Remarks
Current -3 Librascope Centaur Computer	2800	26	No	X1	Current version has available only about 1700 locations for post launch computations. Remainder are used for pre-flight computations.
LEM AGS TRW Systems	8192	18	Yes	X70	Current version has 4096 locations but the machine has been designed for easy extension of the memory to 8192 locations
UNIVAC 1824	12288	16	Yes	X70	
M17/Raytheon Apollo	32000	15	Yes	X25	

a) extreme economy in computer function requirements, equation formulation and memory utilization.

b) Modification of -3 computer to allow use of total memory for inflight computations.

4.2 SUMMARY OF PERFORMANCE RESULTS

This section gives a summary of the results of the performance analyses made on the guidance equations presented in this report. The performance results were obtained from simulations using TRW System's N-Stage program. The current Atlas/Centaur vehicle model using an A/C-8 milestone was used, with various sections of the equations performing appropriate guidance functions. Time and resources did not permit the evaluation of all of the features of this equation set, but an effort was made however to simulate those segments of the set which would give indications of the capabilities and accuracies obtainable. Also the simulations were used as development tools in the design of certain features of the equations.

The portions of the equations which were simulated and for which results are quoted in this report are:

1) Injection into a 90 n. mi. circular parking orbit

2) Injection into a hyperbolic escape trajectory

3) Injection into an intercept trajectory for interception of a low altitude satellite

4) Injection into a translunar trajectory using intercept guidance.

Table 4 summarizes the performance results obtained with the simulations. The table by no means gives all of the results obtained, but does give those results which it is felt demonstrate that the accuracy capabilities of the equations are quite satisfactory. For more complete presentation and discussion of the results, the results section of the report should be consulted.

Table 4. Summary of Performance Results

	Injection Errors							
	Radial Position Error (ft)	Radial Velocity Error (ft/sec)	Out-of-plane Position Error (ft)	Out-of-plane Velocity Error (ft/sec)	Tangential Velocity Error (ft/sec)	Apogee Error (n. Miles)	Perigee Error (n. Miles)	Excess Pro-pellant (lbs)
Injection into 90 n. mi. Circular Orbit	15.75	0.02	19.50	0.015	0.15	0.05	0.03	19.0

	Excess* Weight (lbs)	$\Delta\overline{V}_\infty$** (ft/sec)	Eccentricity Error
Injection into Hyperbolic escape orbit	26.2	3	0.00001

	Maximum Target Miss With No Midcourse Correction (ft)	Minimum Target Miss With No Midcourse Correction (ft)
Intercept orbit Injection (Six Trajectories)	3800	236

	Impact Point Dispersion Circle (No Midcourse Correction)
Lunar Intercept Injection (Six Trajectories)	All trajectories fell within 2° circle about nominal impact point

*Excess of propellant used over calculus of variations optimum trajectory.

**A measure of software contribution to midcourse correction (see Section 6.2 for detailed explanation)

5. THEORY AND DERIVATIONS

5.1 DESCRIPTIONS OF COORDINATE SYSTEMS

5.1.1 Inertial Coordinate Systems

5.1.1.1 Platform Coordinate System

The inertial coordinate system employed to implement the equations presented in this report can be chosen as any which is convenient for the purpose to which the equations are to be used. For the purpose of the Atlas/Centaur it is convenient to use a u-v-w inertial coordinate system, which is an orthogonal triad related to the accelerometer input or inertial platform axes. The origin of this system is located at the center of the earth. The w-axis is along the negative of the measured gravitational acceleration vector at the launch site. The u-axis is assumed to be aligned to the particular alignment aximuth of the pad to be used (say 105° for pad 36A or 115° for pad 36B at Cape Kennedy) and the v-axis completes the set so that the u-v plane is parallel to the launch site horizontal plane at "go-inertial."

5.1.1.2 Pitch Plane Oriented Inertial

For the Atlas/Centaur the booster pitch profile shaping is assumed to be constant across both the launch window and launch opportunity, although the azimuth of this plane is variable across both the window and opportunity. It is therefore convenient during booster steering to use variables expressed in a coordinate system which has two axes defining a plane co-incident with the pitch plane and the third axis normal to the pitch plane. This is accomplished by defining a second coordinate system the u'-v'-w' system which is obtained by rotating about the w-axis an angle equal to the angular difference (Δu) between the platform azimuth (u-axis) and the trajectory azimuth. The latter is determined at the actual time of launch. The u' axis then lies along the intersection of the pitch plane and the launch site horizontal plane and the v'-axis completes the right handed set. Both of these coordinate systems (the u-v-w and u'-v'-w') are shown in Figure 3.

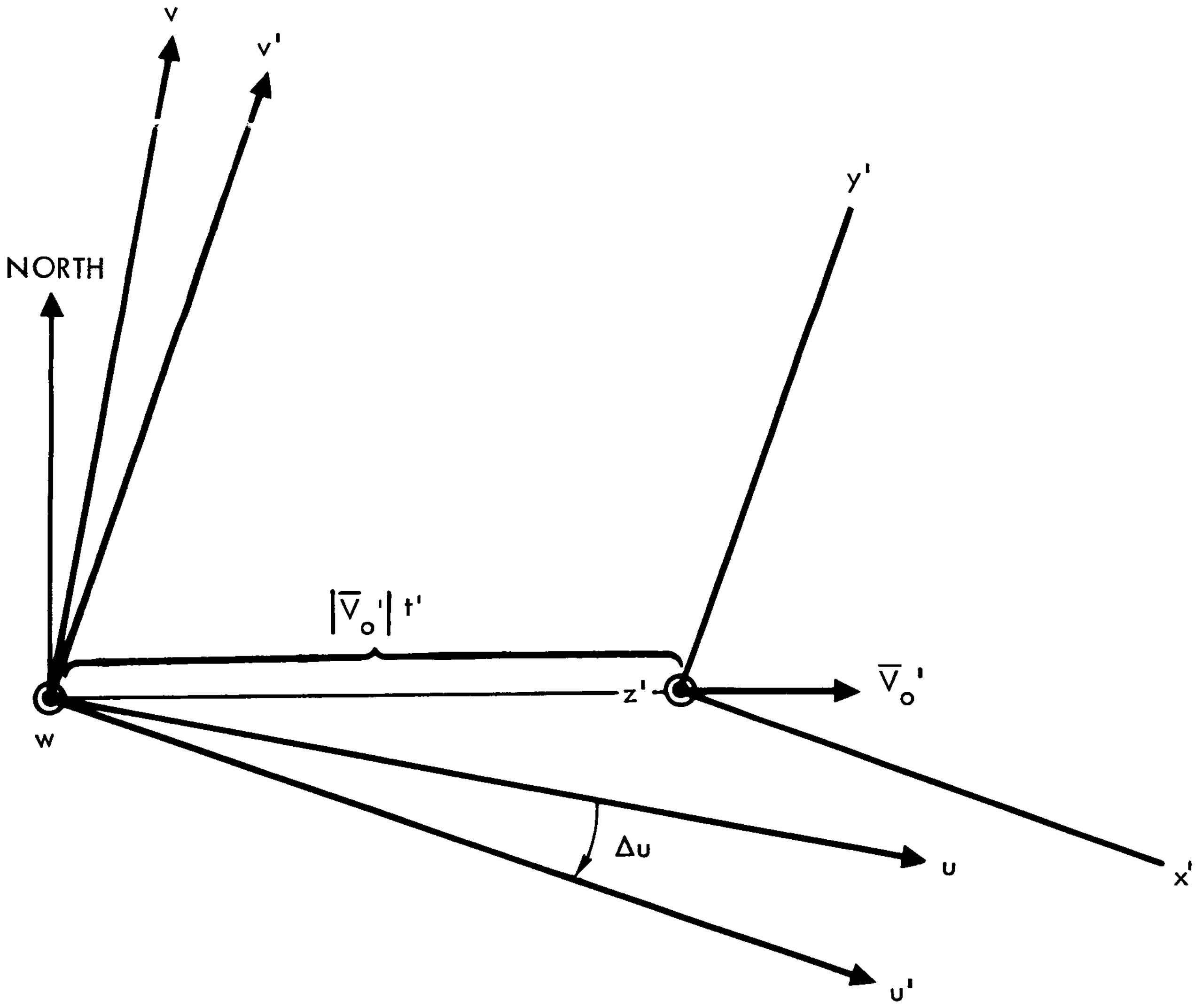
v
v'
NORTH
y'
$|\overline{V}_o'|\ t'$
z'
$\overline{V}_o'$
w
Δu
u
x'
u'

Figure 3. Inertial and Earth Fixed Coordinates

5.1.1.3 Equatorial Oriented Inertial

A third coordinate system should be mentioned at this point. This is the coordinate system in which pre-determined, mission describing vectors are initially expressed. These vectors ($\bar{s}$, $\bar{i}_{R_P}$, $\bar{j}$, $\bar{r}_T$ — see below for definitions) are determined prior to launch and must be converted to the platform coordinate system after this latter system is determined by the launch time. The coordinate system in which these vectors are assumed to be given is earth centered with the z' axis the polar axis and the x'-y' plane the equatorial plane. The specific orientation of the x' and y' axes in the equatorial plane is not essential to the purposes of this report. It will be seen in Section 5.7 that this is the coordinate system in which the numerical integration is carried out for the solution of the navigational parameters.

5.1.2 Earth Fixed System

To assist the development of load relief capability and to preclude the possibility of excessive loads or heating, it is useful to formulate the atmospheric steering law (see Section 5.8) in terms of quantities measured with respect to the nominal motion of the air mass. This is easily done by using a coordinate system, X-Y-Z, which translates with the air mass. To reduce position variable scaling problems, the origin of this system is placed at the launch site. At launch, the axes of the X-Y-Z systems are parallel to the u'-v'-w system axes respectively but the origin of the X-Y-Z system has, forever after launch, a velocity with respect to the u'-v'-w system which is equal to the launch site inertial velocity ($\bar{V}_o'$) at liftoff.* This X-Y-Z system is shown on Figure 3 t' seconds after liftoff.

5.1.3 Exo-Atmospheric Coordinate System

The exo-atmospheric computational coordinate system (henceforth called the computational system) is shown in Figure 4. The x, y, z system is a rotating right handed frame. The z axis is along the projection on the desired flight plane, of the instantaneous position vector $\bar{r}$ of the vehicle. The y axis is normal to the desired flight plane and the x axis completes the right handed set. The desired flight plane is defined by specifying a unit vector $\bar{j}$ which is normal to the desired flight plane. In terms of $\bar{r}$, $\bar{j}$ and $\bar{v}$ then,

---

*This is not truly an earth fixed system since the origin in an earth fixed system could not execute rectilinear motion as does the X-Y-Z axis after launch. However, for the purposes of atmospheric steering here, the motion of the X-Y-Z system approximates the motion of the air mass to a completely adequate degree.

$$\begin{aligned}
x &= o \\
y &= \bar{r} \cdot \bar{j} \\
z &= \sqrt{r^2 - y^2} \\
\bar{k} &= \frac{\bar{r} - y\bar{j}}{z} \\
\bar{i} &= \bar{j} \times \bar{k} \\
v_x &= \bar{v} \cdot \bar{i} \\
v_y &= \bar{v} \cdot \bar{j} \\
y_z &= \bar{v} \cdot \bar{k}
\end{aligned} \tag{1}$$

where $\bar{r}$, $\bar{j}$ and $\bar{v}$ are expressed in some convenient inertial coordinate system.

5.2 EXO-ATMOSPHERIC STEERING EQUATIONS (See flow chart 6)

This section of the report gives a derivation of the upper stage steering equations, i.e., the exo-atmospheric explicit steering equations used for the Atlas Sustainer and Centaur Stages. These equations are explicit because they are completely independent of any reference trajectory and require no nominal trajectory related pre-computed coefficients.

The derivations begin by assuming that the second derivatives of the y and z coordinates of the computational system are linear functions of time, except for a jump change in $\ddot{z}$ at the staging point. These quantities can thus be expressed as

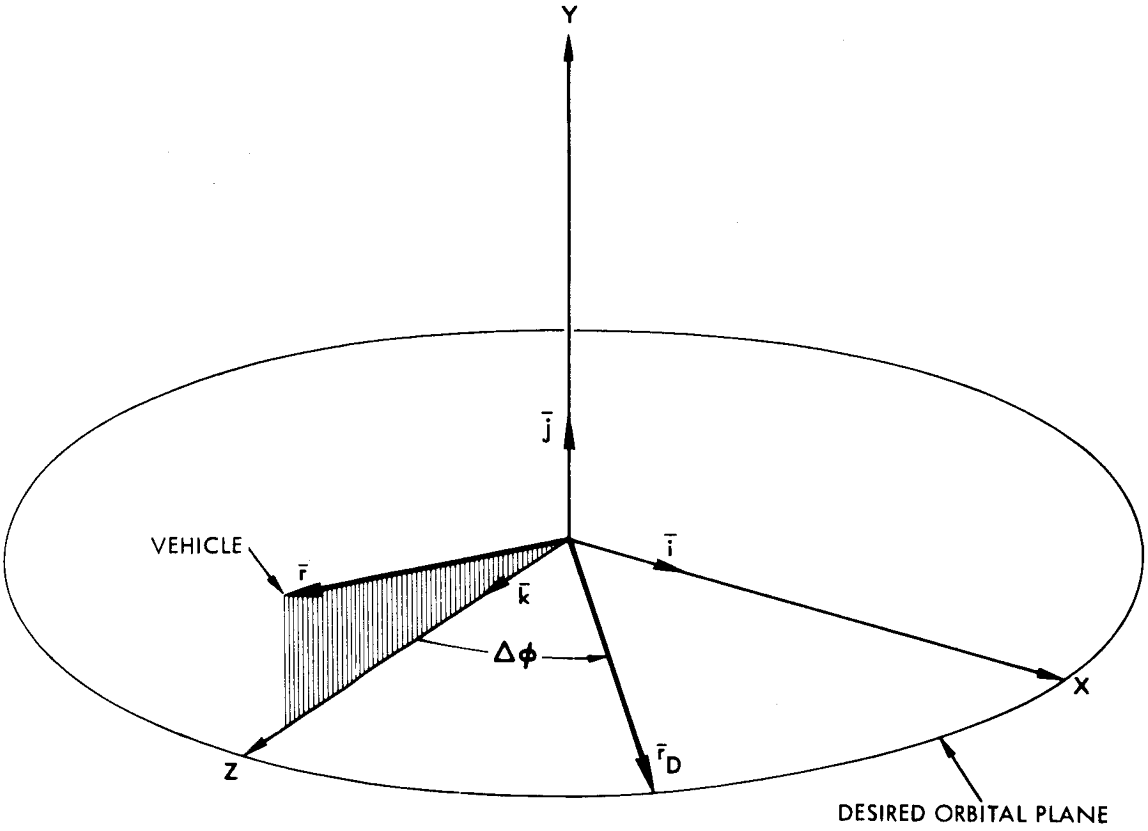
Y
$\bar{j}$
VEHICLE
$\bar{r}$
$\bar{k}$
$\bar{i}$
$\Delta\phi$
X
Z
$\bar{r}_D$
DESIRED ORBITAL PLANE

Figure 4. Rotating Coordinate System

$$\ddot{y} = A + Ct \tag{2}$$

$$\ddot{z} = B + Dt \qquad 0 \le t \le T_s \tag{3}$$

$$\ddot{z} = B_1 + Dt \qquad T_s < t \le T \tag{4}$$

In these expressions time t is measured from the present time, T_s is the time to go to staging, and T is the time to go to cutoff. It is assumed then that the coefficient B is used during the sustainer burn, and that B_1 is used during the Centaur burn.

If the above equations are integrated once, the results are

$$\dot{y}(t) - \dot{y}(0) = At + C\frac{t^2}{2} \tag{5}$$

and

$$\dot{z}(t) - \dot{z}(0) = Bt + \frac{Dt^2}{2} \qquad (0 \le t \le T_s) \tag{6}$$

$$\dot{z}(t) - \dot{z}(0) = B\,T_s + B_1(t-T_s) + D\frac{t^2}{2} \qquad (T_s < t \le T) \tag{7}$$

Evaluating these expressions at t = T, the results are

$$\dot{y}_D - \dot{y}(0) = AT + C\frac{T^2}{2} \tag{8}$$

and

$$\dot{r}_D - \dot{z}(0) = B\,T_s + B_1\,(T-T_s) + D\frac{T^2}{2} \tag{9}$$

where it has been assumed that $\dot{y}(T) = \dot{y}_D$, and $\dot{z}(T) = \dot{r}_D$, i. e. , the final values are equal to the desired values.

If the expressions for $\dot{y}(t)$ and $\dot{z}(t)$ are integrated from t = 0 to t = T the following equations can be obtained:

$$y_D - y(0) - \dot{y}(0)\,T = A\frac{T^2}{2} + C\frac{T^3}{6} \tag{10}$$

and

$$r_D - z(0) - \dot{z}(0)\,T = B\,T_s\left(T - \frac{T_s}{2}\right) + \frac{B_1}{2}\,(T - T_2)^2 + D\,\frac{T^3}{6} \tag{11}$$

where it has been assumed that $y(T) = y_D$ and $z(T) = r_D$.

Further simplification occurs if it is assumed that

$$B_1 = B + \Delta B \tag{12}$$

where ΔB is a known quantity. The in-plane equations then become

$$\dot{r}_D - \dot{z}(0) - \Delta B\,(T-T_s) = B\,T + D\,\frac{T^2}{2} \tag{13}$$

$$r_D - z(0) - \dot{z}(0)\,T - \frac{\Delta B}{2}\,(T-T_s)^2 = B\,\frac{T^2}{2} + \frac{DT^3}{6} \tag{14}$$

The right hand side of these equations are now of the same form as the yaw equations, i.e.,

$$\dot{y}_D - y(0) = A\,T + C\,\frac{T^2}{2} \tag{15}$$

$$y_D - y(0) - \dot{y}(0) = A\,\frac{T^2}{2} + C\,\frac{T^3}{6} \tag{16}$$

These equations can now be solved in two separate ways. If both position and velocity constraints are to be met then the pairs of equations must be solved simultaneously, which gives

$$B = -\frac{2}{T^2}\left[\dot{r}_D - \dot{z}(0) - \Delta B\,(T-T_s)\right] + \frac{6}{T^2}\left[r_D - z(0) - \dot{z}(0)\,T - \frac{\Delta B}{2}(T-T_s)^2\right] \tag{17}$$

and

$$A = -\frac{2}{T^2}\left[\dot{y}_D - y(0)\right] + \frac{6}{T^2}\left[y_D - y(0) - \dot{y}(0)\right] \tag{18}$$

There is no point in solving for the C and D coefficient because at $t = 0$ they drop out of the expression for $\ddot{y}$ and $\ddot{z}$.

On the other hand, if only the velocity constraint has to be met, then the position equation can be ignored, which leads to the expressions

$$B = \frac{\dot{r}_D - \dot{z}(0)}{T} - D\,\frac{T}{2} - \frac{\Delta B}{T}\,(T - T_s) \tag{19}$$

and

$$A = \frac{\dot{y}_D - y}{T} - C\,\frac{T}{2} \tag{20}$$

In these expressions it has to be assumed that C and D are known quantities. In the flow charts is has been assumed that $C = 0$, but the D coefficient has been included. It was felt that there might be some advantage to using a non-zero D coefficient, e. g. , in order to improve efficiency.

The mechanization given in the flow charts includes both the equations for position and velocity constraints ($\nu_2 = 0$) and the equations for velocity constraints only ($\nu_2 = 1$).

The equations of motion in the rotating computational frame are

$$\ddot{y} = a_T\, C_{ay} - \frac{\mu y}{r^3} \tag{21}$$

and

$$\ddot{z} = a_T\, C_{az} - \frac{\mu z}{r^3} + \frac{v_x^2}{z} \tag{22}$$

where C_{ay} and C_{az} are the direction cosines between the acceleration vector and the $\bar{j}$ and $\bar{k}$ axes, respectively.

These equations can be solved for C_{ay} and C_{az} as follows

$$C_{ay} = \frac{1}{a_T}\left[A + \mu \frac{y}{r^3}\right] \tag{23}$$

$$C_{az} = \frac{1}{a_T}\left[B + \mu \frac{z}{r^3} - \frac{v_x^2}{z}\right] \tag{24}$$

where it has been assumed that $\ddot{y} = A$ and $\ddot{z} = B$.

The reason for assuming that there is a jump change in B at the staging point can now be explained. It has been found from calculus of variation solutions that the direction cosine, C_{az}, should be continuous at the staging point. However, if B is continuous then the change in a_T at staging will cause a discontinuity in C_{az}. Hence, a discontinuity must be introduced into the B coefficient which will just cancel the discontinuity in a_T. In order to have continuity in C_{az} at staging we must have

$$(a_{T1} - a_{T0})\, C_{az}\Big|_{t=T_s} = B_1 - B = \Delta B \tag{25}$$

where a_{T1} is the acceleration at the beginning of Centaur and a_{T0} is the acceleration at the end of the sustainer stage. In order to solve for ΔB it is necessary to know $C_{az}\big|_{t=T_s}$. Since the burning time of the sustainer stage is fairly short, it can be assumed for the sake of simplicity that

$$C_{az}\Big|_{t=T_s} = C_{az}\Big|_{t=0}$$

The equation which was finally mechanized was

$$\Delta B = K_{91}\, C_{az} \tag{26}$$

where

$$K_{91} = (a_{T1} - a_{T0})$$

The entire discussion up to this point has assumed that $t = 0$ was some time prior to staging. Essentially the same results are obtained if $t = 0$ is subsequent to staging, except that it is necessary to assume $\Delta B = 0$. This assumption removes all the terms containing T_s from the expression for A and B, which might be expected.

Now it remains to obtain a suitable expression for the reciprocal of the thrust acceleration, $1/a(t)$, and the time to cutoff, T. For $1/a(t)$. a suitable expression, which will not blow up for low or zero sensed-accelerations, and which takes advantage of the filtering effect of an integration, can be derived in the following way.

Let V_c be the total thrust velocity accumulated by the stage up to the time of the current computation, t. Then

$$V_c(t) = \int_o^t a_T(t)\,dt \tag{27}$$

where $t = o$ is the time of initial ignition of the engine. From the rocket model chosen we have that

$$a_T(t) = \frac{V_e}{\frac{m_o}{\dot{m}} - t} \tag{28}$$

which when substituted into Equation (27) and integrated gives

$$V_c = -Ve \ln \left[1 - \frac{t}{\frac{mo}{\dot{m}}} \right] \tag{29}$$

or

$$\frac{\left[\frac{m_o}{\dot{m}} - t \right]}{\frac{m_o}{\dot{m}}} = e^{-\frac{v_c}{v_e}} \tag{30}$$

Dividing both sides by V_e and noting that

$$\frac{1}{V_e}\left(\frac{m_o}{\dot{m}} - t\right) = \frac{1}{a_T(t)} \tag{31}$$

and

$$\frac{m_o}{\dot{m}V_e} = \frac{1}{a_T(o)} \tag{32}$$

we get

$$\frac{1}{a_T(t)} = \frac{1}{a_T(o)}\, e^{-\frac{V_c}{V_e}} \tag{33}$$

Expanding the exponential in a Taylor series the expression becomes finally

$$\frac{1}{a_T(t)} = \frac{1}{a_T(o)}\left[1 - \frac{V_c}{V_e} + \frac{1}{2}\left(\frac{V_c}{V_e}\right)^2 - \frac{1}{6}\left(\frac{V_c}{V_e}\right)^3 + \frac{1}{24}\left(\frac{V_c}{V_e}\right)^4 - \frac{1}{120}\left(\frac{V_c}{V_e}\right)^5 + \frac{1}{720}\left(\frac{V_c}{V_e}\right)^6 + \dots\right] \tag{34}$$

To determine the time to burnout, T, the scheme used must account for the fact that two different stages* may be used to null a given $\bar{V}_g$. That is to say, the explicit guidance equations have been developed so as to be able to direct the flight from some time during the sustainer stage to ultimate burnout of the Centaur stage. Thus the scheme for computing T is developed as follows.

---

*The scheme can be used to guide more than two stages with a few simple modifications provided that the thrust velocity capability of all but the last stage can be specified prior to flight.

From the rocket model, we have that

$$a_T(t) = \frac{V_e \dot{m}}{m(t)} \tag{35}$$

But, the vehicle mass at first stage burnout, m_f, the present mass, m(t), and the mass rate are related by

$$m(t) = m_f + \dot{m} T_s \tag{36}$$

where T_s is the time to first stage burnout. Thus substituting (36) into (35) and inverting we have

$$\frac{1}{a_T(t)} = \frac{m_f}{V_e \dot{m}} + \frac{T_s}{V_e} \tag{37}$$

and solving for T_s,

$$T_s = \frac{V_e}{a_T(t)} - \frac{m_f}{\dot{m}} \tag{38}$$

gives the time to burnout of the first stage.

The time to go for cutoff of the second stage can be computed as follows. Rearranging Equation (28) we have

$$a_T(t) = \frac{V_e \dot{m}_2}{m_o - \dot{m}_2 t} \tag{39}$$

Integrating from the present (t = o) to cutoff of second stage (t = T)

$$v(T) - v(o) = \int_o^T \frac{V_e \dot{m}_2}{m_o - \dot{m}_2 t} dt = V_e \ln \frac{m_o}{m_o - \dot{m}_2 T} \tag{40}$$

But

$$v(T) - v(o) = V_g \tag{41}$$

where V_g is the velocity to be gained by the second stage. Thus

$$V_g = V_e \ln \frac{m_o}{m_o - \dot{m}_2 T} \tag{42}$$

or, expressed in exponential form

$$\exp\left(-\frac{V_g}{V_{e2}}\right) = 1 - \frac{\dot{m}_2 T}{m_o} \tag{43}$$

where the subscript 2 refers to the second or Centaur stage.

Expanding the right hand side in a Taylor series and performing some rearrangement we get

$$T = \frac{m_o V_g}{\dot{m}_2 V_{e2}} \left[1 - \frac{1}{2}\left(\frac{V_g}{V_{e2}}\right) + \frac{1}{6}\left(\frac{V_g}{V_{e2}}\right)^2 - \dots \right] \tag{44}$$

Then, noting that

$$a_T(t) = \frac{\dot{m}_2 V_{e2}}{m_o}$$

Equation (36) becomes finally

$$T = \frac{V_g}{a_T(t)} \left[1 - \frac{1}{2}\left(\frac{V_g}{V_{e2}}\right) + \frac{1}{6}\left(\frac{V_g}{V_{e2}}\right)^2 - \frac{1}{24}\left(\frac{V_g}{V_{e2}}\right)^3 + \dots \right] \tag{45}$$

When the two stages are used consecutively to null a given V_g Equations (38) and (45) are used if the computation is made during a first stage burn. That is, the time to go, T_g, until second stage cutoff is

$$T_g = T_s + T = \left[\frac{V_{e1}}{a_{T1}(t)} - \frac{m_{f1}}{\dot{m}_1}\right] + \frac{1}{a_T'}\left[1 - \frac{1}{2}\ \frac{V_g}{V_{e2}} + \frac{1}{6}\left(\frac{V_g}{V_{e2}}\right)^2 - \frac{1}{24}\left(\frac{V_g}{V_{e2}}\right)^3 + \ldots\right] \tag{46}$$

where subscript

1 → first stage

2 → second stage

a_T' = the initial acceleration of the second stage

If the computation is made during a second stage burn, then Equation (45) is used alone with the reciprocal of the acceleration given by Equation (34). It might be noted here that in the development of these equations it has been assumed that the sustainer stage will never be called upon to complete the nulling of a V_g which has been computed using the explicit (or exo-atmospheric) guidance equations. This means that the equations restrict the use of the sustainer to that of a part of the boost system only with the Centaur stage always performing the actual payload injection. However, minor modifications to the equations presented here would provide the capability to perform missions in the suborbital* start mode.

Equations (34), (38), (45) and (46) allow the determination of any of the direction cosine commands given by Equations (23) and (24) required by maneuver constraints. The Equations (34), (38), (45) and (46) in general give expressions by which the direction cosines are given as a function of the time from the computation. Thus, ideally it might be possible to compute the A and B coefficients only once and have explicit expressions from which the direction cosine requirements could be determined from the start of guidance to shut down. In practice, however, the determination of $y(T)$, $\dot{y}(T)$, $z(T)$ and $\dot{z}(T)$ involves certain inaccuracies which, as cut off is approached, become smaller and smaller (see below).

---

*Suborbital coast between sustainer burnout and Centaur ignition.

Thus the A and B coefficients accordingly are initially inaccurate and must be recomputed periodically if satisfactory terminal conditions are to be achieved.

5.3 EQUATIONS FOR PREDICTION OF CUTOFF REQUIREMENTS

The steering equations developed above require for their implementation two or more specified cutoff conditions. That is, depending on the manuever to be performed, at least two of the four quantities, $y(T)$, $\dot{y}(T)$, $z(T)$, $\dot{z}(T)$, must be specified. The means of obtaining these quantities is described in this section.

Essentially two routines are used to find the cutoff requirements. One routine is used for intercept maneuvers, where the Centaur is required to inject itself into an orbit which will intercept a given point in space at a given time. This routine is used for the on-board targeted intercept portions of rendezvous missions, Syn-Com missions, and for translunar missions. The second routine is used where the desired orbit is one which can be targeted prior to launch. These are taken to include, parking orbits and other earth orbits, interplanetary and pre-targeted translunar trajectories. The first routine will be called the "Optimum Intercept Targeting Routine" and the second the "Specified Conic Routine." These two routines are described below.

5.3.1 Optimum Intercept Targeting Routine (See flow charts 2, 3 and 4)

5.3.1.1 P-Iteration

This routine assumes two body dynamics, and specifies a conic on the basis of two points in space and a free fall time τ_{12}, between the two points. The computation proceeds by first assuming a value for h_D, the desired angular momentum on the transfer ellipse, and computing the corresponding free fall time to go from $\bar{r}_D$ to $\bar{r}_T$. This free fall time is compared to the required difference, $t_T - t_D$. Newton Raphson iteration is then used to find the value of h_D which causes the predicted free fall time to agree with $(t_T - t_D)$, once convergence has been obtained the desired velocity, $\bar{v}_D$, is computed from the parameters of the computed transfer orbit.

The particular algorithm used here for computing free fall time was developed at TRW Systems Group by F. A. Evans. It has the advantage of being valid even for zero eccentricity orbits. The development of these equations proceeds directly from Kepler's equations, which gives the free fall time between $\bar{r}_D$ and $\bar{r}_T$ as

$$\tau_{12} = \sqrt{\frac{a^3}{\mu}} \left[M_T - M_D\right] \tag{47}$$

where

$$M_T = E_T - e \sin E_T \tag{48}$$

$$M_D = E_D - e \sin E_D \tag{49}$$

where E_D and E_T are the eccentric anomalies at r_D and r_T respectively, on the transfer orbit.

The above equation can be rewritten as

$$\tau_{12} = \sqrt{\frac{a^3}{\mu}} \left[\Delta E - e \sin E_T + e \sin E_D\right] \tag{50}$$

where

$$\Delta E = E_T - E_D$$

Ordinary trigonometric identities then give

$$\cos \Delta E = \cos E_T \cos E_D + \sin E_T \sin E_D \tag{51}$$

$$\sin \Delta E = \sin E_T \cos E_D - \cos E_T \sin E_D \tag{52}$$

The following selections from astrodynamic theory are then quite useful

$$\cos E = \frac{e + \cos f}{1 + e \cos f} \tag{53}$$

$$\sin E = \frac{\sqrt{1 - e^2}\,\sin f}{1 + e \cos f} \tag{54}$$

where f is the true anomaly.

If these expressions are used in the cos ΔE and sin ΔE equations the results are

$$\cos \Delta E = \frac{\cos \phi + e \cos f_T + e \cos f_D + e^2 - (e \sin f_T)(e \sin f_D)}{1 + e \cos f_T + e \cos f_D + (e \cos f_T)(e \cos f_D)} \tag{55}$$

$$\sin \Delta E = \frac{\sqrt{1 - e^2}\left[\sin \phi + e \sin f_T - e \sin f_D\right]}{1 + e \cos f_D + e \cos f_T + (e \cos f_T)(e \cos f_D)} \tag{56}$$

where

$$\phi = f_T - f_D$$

The angle ΔE is then given by combining the above two equations, which gives

$$\Delta E = \tan^{-1}\left[\frac{\sqrt{1 - e^2}\,(\sin \phi + C_4 - C_3)}{\cos \phi + C_1 + C_2 + e^2 - C_3 C_4}\right] \tag{57}$$

where

$$C_1 = e \cos f_D$$

$$C_2 = e \cos f_T$$

$$C_3 = e \sin f_D$$

$$C_4 = e \sin f_T$$

The values of C_1 and C_2 are easily obtained from the standard equations

$$C_1 = \frac{p}{r_D} - 1 \tag{58}$$

$$C_2 = \frac{p}{r_T} - 1 \tag{59}$$

where

$$p = \frac{h^2 D}{\mu} \tag{60}$$

Then, using the fact that $\phi = f_T - f_D$, the following expressions can be obtained:

$$e \cos f_T = e \cos f_D \cos \phi - e \sin f_D \sin \phi \tag{61}$$

$$e \cos f_D = e \cos f_T \cos \phi + e \sin f_T \sin \phi \tag{62}$$

These equations can be rearranged into the forms

$$e \sin f_D = \frac{(e \cos f_D) \cos \phi - e \cos f_T}{\sin \phi} \tag{63}$$

$$e \sin f_T = \frac{e \cos f_D - (e \cos f_T) \cos \phi}{\sin \phi} \tag{64}$$

Using the previous notation, these equations become

$$C_3 = \frac{C_1 \cos \phi - C_2}{\sin \phi} \tag{65}$$

$$C_4 = \frac{C_1 - C_2 \cos \phi}{\sin \phi} \tag{66}$$

From the definitions of C_1 and C_2 it is clear that

$$e^2 = {C_1}^2 + {C_3}^2 \tag{67}$$

The semi-major axis, a, can then be computed from

$$a = \frac{p}{1 - e^2} \tag{68}$$

The sine and cosine of the range angle, ϕ, are computed from the relations

$$\cos \phi = \frac{\bar{r}_D \cdot \bar{r}_T}{r_D \, r_T} \tag{69}$$

and

$$\sin \phi = \pm \sqrt{1 - \cos^2 \phi} \tag{70}$$

The quantity $\sin \phi$ is first assumed to be positive, and the unit vector $\bar{1}_T$ normal to $\bar{r}_D$ and lying in the plane of $\bar{r}_D$ and $\bar{r}_T$ is then computed. The dot product of $\bar{i}$ and $\bar{1}_T$ will then be positive if the sign of $\sin \phi$ was proper, and will be negative otherwise. If a negative is obtained then the signs of $\bar{1}_T$ and $\sin \phi$ are changed appropriately.

The other quantities needed in the computation of τ_{12} are

$$C_5 = e \sin E_D \tag{71}$$

and

$$C_6 = e \sin E_T \tag{72}$$

The following equation can easily be derived from two body relations:

$$e \sin E = \frac{r}{p} \sqrt{1 - e^2} \, (e \sin f) \tag{73}$$

therefore,

$$C_5 = \frac{r_D}{p} \sqrt{1 - e^2} \quad C_3 \tag{74}$$

$$C_6 = \frac{r_T}{p} \sqrt{1 - e^2} \quad C_4 \tag{75}$$

The total time expression is then

$$\tau_{12} = \frac{a\sqrt{a}}{\sqrt{\mu}} \left\{ \tan^{-1} \left[\frac{\sqrt{1 - e^2} \; (\sin \phi + C_4 - C_3}{\cos \phi + C_1 + C_2 + e^2 - C_3 \, C_4} \right] - C_6 + C_5 \right\} \tag{76}$$

Since radial velocity is given by

$$\dot{r} = \frac{h}{p} \, e \sin f \tag{77}$$

the desired radial velocity cut off is clearly

$$\dot{r}_D = \frac{h_D}{p} \, C_3 \tag{78}$$

Since angular momentum is defined as the cross product of $\bar{r}$ and $\bar{v}$ it is evident that the desired tangential velocity at cutoff is just $\frac{h_D}{r_D}$. The total desired velocity is then

$$\bar{v}_D = \frac{h_D}{p} \, C_3 \left(\frac{\bar{r}_D}{r_D} \right) + \frac{h_D}{r_D} \, \bar{1}_T \tag{79}$$

Similar reasoning is used to compute $\bar{v}_T'$, the velocity on the transfer ellipse at time t_T. The only difference is that the unit vector in the tangential direction is given by $\left[\frac{\cos \phi}{\sin \phi} \left(\frac{\bar{r}_T}{r_T} \right) - \frac{\bar{r}_D}{r_D} \sin \phi \right]$.

Provision has also been made in these equations to handle the case where the free fall time is greater than the period of the transfer orbit. The required free fall time, $t_T - t_D$, is tested against the period, P, of the transfer orbit. If $t_T - t_D$ is greater than P then τ_{12} is increased by P. This procedure has been found to be necessary because the search logic will sometime require transfers through more than 360 deg.

It has been found that the p-iteration equations will not operate correctly if transfers very close to 180 deg are required. This problem will arise no matter what scheme is employed because the plane of the transfer orbit is no longer defined in that situation. In order to avoid this problem a test is made on sin ϕ to make sure it is above a minimum level defined by K_{31}. If it is not then the program transfers back to the free flight prediction routine and increases t_T until $\overline{r}_T$ is driven away from the 180 deg position.

5.3.1.2 Powered Flight Prediction. (See flow chart 6)

As described above, in order to make the p-iteration computation, the end points of the unpowered flight are required as well as the length of time of the unpowered flight. One end point is of course the cutoff point of the current burn period (which is seeking to inject the vehicle into the desired orbit). This end point designated as r_D can be estimated as follows:

We have that the expression for angular momentum is

$$h = r^2 \dot{\phi}$$

or in terms of finite differences and average values,

$$\Delta\phi = \frac{\widetilde{h}}{(\widetilde{r})^2}\,\Delta t = \frac{\widetilde{h}}{(\widetilde{r})^2}\,T \qquad (80)$$

where $\Delta\phi$ is the arc traversed in the T seconds to cutoff and where T is, as before, the remaining time for the current powered phase. An estimate of $\Delta\phi$ which becomes more accurate as cutoff is approached, can be made by assuming linear change in h and r. Thus if

$$\widetilde{h} = \frac{1}{2}(h_D + h) \qquad (81)$$

$$\widetilde{r} = \frac{1}{2}(r_D + r) \qquad (82)$$

we get

$$\Delta\phi = 2\frac{h + h_D}{(r + r_D)^2}T \qquad (83)$$

where

$h = zv_x$

$$h_D = \begin{cases} \text{given by the final computation for } h_D \text{ for the intercept case} \\ \text{given by } \sqrt{\mu p} \text{ for the specified conic case} \end{cases}$$

The value of r_D is pre-specified for the case of injection into a specified conic. For the case of an intercept orbit the value of r_D is not prespecified (although it could be) but it can be derived by integrating Equation (3) twice with D = 0. Thus

$$z(t) = \int_o^T \int_o^t B_o \, d\lambda d\tau + z \qquad (84)$$

$$r_D = z(T) = \frac{1}{2}B_oT^2 + \dot{z}_oT + z \qquad (85)$$

Similarly, a double integration of Equation (2) with B = 0, yields for the desired out of plane cutoff position y_D

$$y_D = y(t) = y + \dot{y}T + \frac{A_o T^2}{2} \qquad (86)$$

With $\Delta\theta$, z(T) and y(T) available, the desired cutoff position is

$$\bar{r}_D = z(t) \cos\Delta\phi\bar{k} + z(T)\sin \Delta\phi i + y(T) \bar{j} \qquad (87)$$

and we have thus established the first endpoint for the p-iteration computation.

5.3.1.3 Free Flight Prediction (see flow chart 2)

The second end point needed for the p-iteration computation is that of the target at the desired time of intercept. (See below for the method of selecting the time of intercept.) The term target, however, can have three different meanings depending on the mission being flown. For a rendezvous mission the target is another orbiting space vehicle. For a synchronous comsat mission the target is a point in space at the earth synchronous altitude and on a radial specified by the desired longitude of the satellite. For a translunar mission where the translunar trajectory has not been pre-targeted, the target is some pseudo aim point at some specific offset from the moon. In all of these cases the target's motion is predictable T seconds from the present provided the present position and velocity are known. Thus, for the rendezvous and lunar missions the corresponding ephemerides must be obtainable from the on board computer. For the com-sat the simple relation describing a circular equatorial orbit at synchronous altitude is sufficient.

With the initial conditions given, the expressions for the target's position and velocity T seconds later can be derived as follows. (See Reference 2 and 5)

Let $\bar{P} \equiv$ a unit vector in the perigee direction

$\bar{Q} \equiv$ a unit vector normal to $\bar{P}$ and in the orbit plane.

Let the origin be at the perifocus with the X and Y axes directed along $\bar{P}$ and $\bar{Q}$ respectively then

$$\begin{aligned} \bar{r} &= X\bar{P} + Y\bar{Q} \\ \dot{\bar{r}} &= \dot{X}\bar{P} + \dot{Y}\bar{Q} \end{aligned} \tag{88}$$

Solving (88) for $\bar{P}$ and $\bar{Q}$ we get

$$\begin{aligned} \bar{P} &= \frac{\dot{Y}\bar{r} - Y\dot{\bar{r}}}{X\dot{Y} - Y\dot{X}} \\ \bar{Q} &= \frac{X\dot{\bar{r}} - \dot{X}\bar{r}}{X\dot{Y} - Y\dot{X}} \end{aligned} \tag{89}$$

Now for an ellipse (See Reference 2 and 5)

$$\left.\begin{aligned} r &= a(1 - e\cos E) \\ X &= a(\cos E - e) \\ Y &= a(1 - e^2)^{1/2} \sin E \\ \dot{X} &= \frac{-(ua)^{1/2} \sin E}{r} \\ \dot{Y} &= [ua\,(1 - e^2)]^{1/2} \frac{\cos E}{r} \end{aligned}\right\} \tag{90}$$

Substituting (90) into (89) and after some manipulation P and Q become

$$\bar{P} = \frac{\cos E}{r}\bar{r} - \sqrt{\frac{a}{\mu}}\sin E\,\dot{\bar{r}} \tag{91}$$

$$\bar{Q} = \frac{1}{[1 - e^2]^{1/2}}\left[\frac{\sin E}{r}\bar{r} + \sqrt{\frac{a}{\mu}}(\cos E - e)\,\dot{\bar{r}}\right] \tag{92}$$

Now, if t is the present time, Δt is the remaining time of free flight and T is the time of rendezvous.

$$\bar{r}(t + \Delta t) = \bar{r}(T) = X(T)\,\bar{P} + Y(T)\,\bar{Q} \tag{93}$$

$$\dot{\bar{r}}(t + \Delta t) = \dot{\bar{r}}(T) = \dot{X}(T)\,\bar{P} + \dot{Y}(T)\,\bar{Q} \tag{94}$$

Substituting equations (90) into (93) and (94) gives

$$\bar{r}(T) = a(\cos E_T - e)\,\bar{P} + a(1 - e^2)^{1/2}\sin E_T\bar{Q} \tag{95}$$

$$\dot{\bar{r}}(T) = -\frac{\sqrt{\mu}\,a\sin E_T}{r_T}\,\bar{P} + \sqrt{\mu}\,a\,(1 - e^2)\,\frac{1}{2}\left(\frac{\cos E_T}{r_T}\right)\bar{Q} \tag{96}$$

and substituting (91) and (92) into (95) and (96)

$$\bar{r}(T) = \frac{a}{r}[\cos\Delta E - e\cos E]\,\bar{r} + \sqrt{\frac{a^3}{\mu}}[\sin\Delta E + e\,(\sin E - \sin E_T)]\,\dot{\bar{r}} \tag{97}$$

$$\dot{\bar{r}}(T) = -\frac{\sqrt{\mu a}}{r_T r}\sin\Delta E\,\bar{r} + \frac{a}{r_T}[\cos\Delta E - e\cos E_T]\,\dot{\bar{r}} \tag{98}$$

From (90) we have that

$$e\cos E = 1 - \frac{r}{a} \tag{99}$$

From Kepler's Equation

$$M = E - e\sin E$$

or

$$\sqrt{\frac{\mu}{a^3}}\,(t - \tau_P) = E - e\sin E \tag{100}$$

where τ_P = time since perifocal passage.

Similarly at $T = t + \Delta t$

$$\sqrt{\frac{\mu}{a^3}}\,(t + \Delta t - \tau_P) = E_T - e \sin E_T \tag{101}$$

Subtracting (100) from (101) we get

$$E_T - e \sin E_T = E - e \sin E + \frac{\sqrt{\mu}}{a^3}\,\Delta t \tag{102}$$

or

$$e\,(\sin E - \sin E_T) = \frac{\sqrt{u}}{a^3}\,\Delta t - \Delta E \tag{103}$$

Substituting (99) and (103) into (97) and (99) into (98) gives, finally

$$\bar{r}(T) = \frac{a}{r}\left[\cos \Delta E - \left(1 - \frac{\bar{r}}{a}\right)\right]\bar{r} + \left[\Delta t - \sqrt{\frac{a^3}{\mu}}\,(\Delta E - \sin E)\right]\dot{\bar{r}} \tag{104}$$

$$\dot{\bar{r}}(T) = -\frac{\sqrt{\mu a}}{r_T r}\sin \Delta E\,\bar{r} + \left[\frac{a}{r_T}\cos\Delta E + \left(1 - \frac{a}{r_T}\right)\right]\dot{\bar{r}} \tag{105}$$

Equations (104) and (105) can be used as free flight prediction equations provided ΔE is available. However since it is more convenient to treat the coast arc time, Δt, as the independent variable, ΔE must be derived from Δt. This can be done as follows:

We have for an ellipse (See Reference 5)

$$M_T - M = \frac{\sqrt{\mu}}{a^3}\,\Delta t \tag{106}$$

where M is the mean anomaly. Then, utilizing Kepler's Equation,

$$\Delta M = M_T - M = E_T - e \sin E_T - E + e \sin E$$

or

$$\Delta E = \Delta M + e \sin E_T - e \sin E \tag{107}$$

Now

$$\sin E_T = \sin (E + \Delta E) = \sin E \cos\Delta E + \cos E \sin\Delta E \tag{108}$$

Therefore,

$$\Delta E = \Delta M + e \sin E\,[\cos\Delta E - 1] + e \cos E \sin\Delta E \tag{109}$$

For an ellipse (See Reference 5)

$$e \cos E = \left(1 - \frac{r}{a}\right) \tag{110}$$

$$e \sin E = \frac{\bar{r} \cdot \dot{\bar{r}}}{\sqrt{\mu a}} \tag{111}$$

so that

$$\Delta E = \Delta M + \frac{\bar{r} \cdot \dot{\bar{r}}}{\sqrt{\mu a}} [\cos\Delta E - 1] + \left(1 - \frac{r}{a}\right) \sin\Delta E \tag{112}$$

Equation (112) is transcendental in ΔE so that an iterative solution for ΔE must be used. For this purpose we can write

$$\Delta E_K = \Delta E_{K-1} - \frac{f(\Delta E)}{\frac{df(\Delta E)}{d\Delta E}} \tag{113}$$

where $f(\Delta E)$, the error function, is defined from (112) as

$$f(\Delta E) = \Delta E - \Delta M - \frac{\bar{r} \cdot \dot{\bar{r}}}{\sqrt{\mu a}} [\cos\Delta E - 1] - \left(1 - \frac{r}{a}\right) \sin\Delta E \tag{114}$$

Then from (114)

$$\frac{df(\Delta E)}{d(\Delta E)} = 1 + \frac{\bar{r} \cdot \dot{\bar{r}}}{\sqrt{\mu a}} \sin \Delta E - \left(1 - \frac{r}{a}\right) \cos\Delta E \tag{115}$$

The iteration is repeated often enough to insure the required accuracy.

5.3.1.4 Selection of Optimum Coast Arc Time (See flow chart 4)

The means of selection of an optimum time for the intercept coast arc will now be discussed. The basic purpose of the procedure is to search for a time of intercept, t_T, which will result in the consumption of a minimum of propellant. This propellant is the sum of that needed for injection into the intercept orbit and that needed for the second burn (i. e. injection into the synchronous orbit for the ComSat, or the final closing maneuver for rendezvous). An additional constraint is that the minimum altitude, r_P, of the intercept arc be above a certain value, K_{13}. If this constraint cannot be met, then the search is carried out to find the t_T which maximizes r_P. The reason for this constraint on r_P is to prevent or minimize any reentry into a significantly sensible atmosphere during the transfer maneuver. The logic shown in flow chart 4 can be described as follows.

It is initially assumed that the goal is to maximize r_P, so a positive Δt_T is applied whenever $\partial r_P/\partial t_T$ is positive. The magnitude of Δt_T is held fixed until the derivative, $\partial r_P/\partial t_T$, changes sign, and then it is cut in half. This procedure is continued until r_P exceeds the constraint K_{13}. Once this occurs the search variable is switched over to ΔV. The problem is then re-initialized and a new constant magnitude of Δt_T is introduced. In this case the object is to minimize ΔV, so a negative Δt_T is applied whenever $\partial \Delta V/\partial t_T$ is positive. Again, the magnitude of Δt_T is cut in half whenever the derivative $\partial \Delta V/\partial t_T$ changes sign. If r_P falls below K_{13} while this process is attempting to minimize ΔV, then t_T is set back to the last acceptable value and the process is stopped.

In summary then, the "optimum intercept targeting routine" performs the function of seeking out an intercept trajectory which will be an optimum with respect to propellant consumption. The sequence of computations among the free flight prediction, the p-iteration, and the search logic is as follows.

a) The search logic provides a value for t_T*

b) The free flight prediction computes corresponding cutoff point

c) The p-iteration computes intercept trajectory with corresponding ΔV and r_P

d) The search logic adjusts t_T by $\pm \Delta t_T$

The above sequence is repeated for a given number of cycles after which the corresponding cutoff requirements are provided to the steering equations.

5.3.2 Specified Conic Routine (see flow chart 5)

The "specified conic routine" provides cutoff requirements to the steering equations for the cases where the desired trajectories have been specified before the Centaur guidance system has been activated (i.e. where the desired trajectories have been pre-targeted). These pre-targeted trajectories are escape hyperbolas for interplanetary missions and ellipses for earth orbits and the pre-targeted translunar trajectories.

---

*An initial value of t_T must be inserted to start the procedure.

Therefore common generalized conic equations can be used to obtain the cutoff requirements for these type trajectories.

It is assumed that the specification of the desired orbit includes the size and shape of the conic, the orientation of the orbit plane and as well the direction of the perigee vector. Thus the following quantities are assumed to be available.

$a \equiv$ semi-major axis

$p \equiv$ semi-latus rectum

$e \equiv$ eccentricity

$\bar{i}_{R_p} \equiv$ a unit vector in the direction of perigee

$\bar{j} \equiv$ the unit vector normal to the orbit plane

These quantities are obtained from a set of mission constraints, which implicitly define the characteristics of the conic to be achieved. Any set of constraints from which the above quantities can be obtained can be used. However, for the purposes of this study it was assumed that the desired conics would be defined in terms of the constraints described below. These choices were made on the basis of what is usually available for the particular mission and/or what was most effective in providing maximum control over the characteristics of the final conic. Appendices B and C show how the following constraints provide a, p, e and $\bar{i}_{R_p}$ for the "specified conic" guidance modes.

For the Interplanetary Escape Hyperbola the given mission constraints are:

1) Injection or vis-viva energy $\equiv C_3$
2) The perigee altitude $\equiv R_P$
3) The direction of the outward assymptote (unit vector) $\equiv \underline{s}$

For the translunar Ellipse the given mission constraints are:

1) Radius vector to the point of intersection of translunar trajectory with lunar sphere of influence $= \bar{R}_T$
2) Velocity at $\bar{R}_T \equiv V_T$

The above two quantities might be obtained by using a patched conic technique as described in Reference 5.

3) The perigee altitude $\equiv R_P$

For the Elliptic Earth Orbit the elliptic parameters a, e, p, can be obtained in a straightforward and familiar manner from the mission requirements. However it should be pointed out that, even if, as in many applications, there is no specific requirement on the line of apsides, the guidance equations require that the perigee vector, $\overline{i}_{R_P}$, be specified.

The two basic equations used for the "specified conic" computations are

$$r_D = \frac{p}{1 + \cos f} \tag{116}$$

and

$$v_D = \sqrt{\zeta \frac{\mu}{a} + \frac{2\mu}{r_D}} \tag{117}$$

Equation (116) provides the value of the cutoff radius r_D needed by the steering equations and Equation (117) forms the basis for computing the cutoff velocity. The sequence of computations may be taken to begin with the value of r_D computed at the previous guidance computation. From this value of r_D, the cutoff vector $\overline{r}_D$ can be computed from

$$\overline{r}_D = r_D \cos \Delta\phi \, \overline{k} + r_D \sin \Delta\phi \, \overline{i} + y_D \, \overline{j}. \tag{118}$$

In (118) the predicted powered flight burn arc $\Delta\phi$ is determined as described above in the "powered flight prediction" section. Also since it is desired to cut off with no out of plane position deviation, Y_D is zero. Using $\overline{r}_D$, the predicted cos f, (= cosine of true anomaly at cutoff) can be computed from

$$\cos f = \frac{\overline{r}_D \cdot \overline{i_{R_P}}}{r_D} \tag{119}$$

From this, the new predicted value of r_D can be computed from (116). The new value of predicted cutoff velocity at r_D is now computed from Equation (117). This, however, is the magnitude of the velocity at $\overline{r}_D$ but what is required by the steering equations is the component of V_D along $\bar{r}_D$, or $\dot{r}_D$. If we define

$$\Gamma = \text{flight path angle at } \bar{r}_D$$

then

$$\dot{r}_D = V_D \sin \Gamma \qquad (120)$$

The equation for the flight path angle can be easily obtained for both the ellipse and hyperbola as follows. At any point on the conic

$$\bar{r} \times \bar{v} = \bar{h} \qquad (121)$$

Therefore

$$rv \sin \left(\frac{\Pi}{2} - \Gamma\right) = rv \cos \Gamma = h \qquad (122)$$

or

$$\cos \Gamma = \frac{h}{rv} \qquad (123)$$

and

$$h = \mu a \,(1 - e^2)^{1/2}$$

From this

$$\sin \Gamma = \pm \sqrt{1 - \cos^2 \Gamma} \qquad (124)$$

where the plus or minus sign is chosen on the basis of a test which determines a positive or negative true anomaly (see flow chart). With Equations (123) and (124) the cutoff velocity vector is specified as follows

$$\bar{v}_D = v_D \,(\cos \Gamma)\, \bar{1}_D' + (\sin \Gamma) \frac{\bar{r}_D}{r_D} \qquad (125)$$

Here $\bar{1}_D'$ is a unit vector in the desired flight plane and normal to r_D and directed in such a way that

$$\bar{r}_D \times \bar{1}_D' = r_D \bar{j} \qquad (126)$$

if $\bar{j}$ bears a right handed screw relation to the direction of flight. With $\bar{v}_D$ defined, the velocity to be gained vector, $\bar{v}_g$, is given by,

$$\bar{v}_g = \bar{v}_D - \bar{v} \qquad (127)$$

5.4 COAST ORBIT DETERMINATION GUIDANCE (See flow chart 9)

This method monitors the vehicle state during the coast orbit, making continuous guidance computations. When these computations indicate that the conditions for beginning the next burn have been achieved, a restart signal is given and the guidance computations shift to the appropriate powered flight mode.

This method then involves a continuous computation during the coast period. A study of the equation mechanization flow chart set will show that the cutoff requirement computation and steering computations continue throughout unpowered flight as well as during powered flight. Thus a cutoff point estimate is available whether the vehicle is thrusting or not. What this means, as far as unpowered flight is concerned, is that an estimate of the cutoff point for the up coming burn is always available, so that the coast trajectory termination routine takes into consideration the burn arc in making the decision of when to restart.

Now, referring to the coast trajectory termination flow chart, if the vehicle is in powered flight mode, ψ will be unity, and the entire coast trajectory termination routine will be by-passed. If a coast trajectory is in progress then a test is made to see if the velocity increment needed to complete the mission from the present vehicle state is sufficiently less than the velocity increment remaining in the propellant tanks. If the answer is no, then no restart signal is given. If the answer is yes, further tests are made depending on the objective of the next burn. These tests are as follows:

5.4.1 Injection into Intercept Orbit (bb = o; aa = o)

Here the only additional test is to insure that the perigee altitude, r_p, of the computed intercept orbit is large enough so as to insure against a re-penetration of the sensible earth atmosphere. If r_p is sufficiently large the restart signal is given, and if not the coast period is continued. Notice that this criterion does not explicitly minimize the ΔV required for the maneuver. Since the intercept and rendezvous (or com-sat injection) burns are the last demands made on the Centaur propellant supply, minimization is not really required at this late phase of the mission.

5.4.2 Injection into Hyperbolic Escape Trajectory (bb = o, aa = 1).

The criterion for restarting the engine here is that of injecting the vehicle into the hyperbolic escape orbit as close as possible to perigee. Thus if f_T is the cosine of the angle between the perigee vector $\bar{r}_T$ and the direction of the outward assymptote, $\bar{s}$, the engine should be restarted when

$$C_T \quad \frac{\bar{r}_D \cdot \bar{s}}{r_D} = f_T \tag{128}$$

where f_T is given by (see Appendix D)

$$f_T = \cos \left[\pi - \tan^{-1} \sqrt{\frac{p}{a}} \right] \tag{129}$$

or, from the relation between cosine and tangent

$$f_T = - \frac{1}{\sqrt{1 + \frac{p}{a}}} \tag{130}$$

It is necessary however to make additional tests in order to avoid quadrant ambiguities. A check on the derivative of C_T establishes whether C_T is in the first or second quadrant, or whether it is in the third or fourth quadrant. Thus if

$$(C_T - C_{TO}) \begin{cases} < 0 & \text{3rd or 4th quadrant} \\ > 0 & \text{1st or 2nd quadrant} \end{cases}$$

where C_{TO} is the previously computed value of C_T. Two more tests establish whether C_T is within a range of values around f_T or, in other words, these tests tell whether the vehicle will be within a certain acceptable range of true anomaly at cutoff. Thus if injection will be allowed to occur between $+\theta'$ and $-\theta''$ degrees true anomaly, the two tests on C_T can be seen to make the proper restart decision if the following definitions are made.

$$\begin{aligned} \cos \theta' &= K_{110} \\ \sin \theta' &= K_{200} \\ \cos \theta'' &= K_{110} \\ \sin \theta'' &= K_{210} \end{aligned} \tag{131}$$

5.4.3 Injection into a Pre-Targeted Translunar Ellipse (bb = o, aa = 2)

As can be seen from the flow chart the procedure here is virtually the same as that for initiating the burn for injection into the hyperbolic escape trajectory. The only difference is the equation for computing the true anomaly cosine, f_T, of the target vector $\overline{r}_T$. The method of obtaining f_T is given in Appendix C with the result

$$f_T = \left[\frac{1}{e}\left(\frac{p}{r_T} - 1\right)\right] \tag{132}$$

It should be pointed out here that the computations using Equations (129) and (131) need not necessarily be done on board, since f_T is a function only of the quantities assumed to be pre-targeted.

5.4.4 Injection of ComSat into Synchronous Earth Orbit (bb = 1)

Here, the procedure is to initiate the burn when the predicted burn arc is equal to the angle between the instantaneous position vector of the vehicle $\overline{r}$, and the position vector of the desired injection point $\overline{r}_T$. The actual computation compares the cosines of these angles. Thus if C_T is the cosine of the angle between $\overline{r}$ and $\overline{r}_T$, then

$$C_T = \frac{\overline{r} \cdot \overline{r}_T}{r r_T} \tag{133}$$

Since a continued estimate of the burn arc, $\Delta\phi$, is being made upstream in the guidance computation, a comparison of C_T and cos $\Delta\phi$, can be made. When C_T approaches cos $\Delta\phi$, the restart command is issued. To avoid quadrant ambiguities, a check on the sign is also made on C_T.

5.5 CUTOFF ROUTINE (See flow chart 8)

After investigating several possible procedures a quadratic cutoff formula was employed and found highly satisfactory.

The other procedures attempted were (a) a linear extrapolation of the velocity to be gained parameter to obtain cutoff time and (b) a procedure which attempted to predict whether the velocity to be gained parameter would cease to decrease during the next computation time increment (see Reference 3 for a complete discussion of this procedure). The first of these discarded schemes was found to be accurate enough for circular orbit injections since it turned out that the velocity to be gained parameter changed very linearly as cutoff was approached. However, it was found that for injection into hyperbolic orbits, the change in the velocity to be gained parameter approaching cutoff was non-linear enough to produce significantly large errors in the linearly extrapolated time of cutoff. This large timing error was compounded by the fact that for hyperbolic injections the vehicle acceleration levels are considerably higher than for the near circular orbit injections (160 ft/sec^2 versus 60 ft/sec^2) so that any timing error in cutoff can become quite serious. The second discarded cutoff scheme did not prove adequate due to the fact that it used only the thrust acceleration to predict whether the cutoff would occur within the next computation time interval. This was acceptable for circular orbit injections since the velocity to be gained is nearly horizontal near injection and the gravitational acceleration has virtually no effect on the nulling of v_g. However, for hyperbolic orbit injections the flight path angle at injection is significantly different from zero (e. g. 5°) and the contribution of the gravitation acceleration is significant in how v_g changes.

The derivation of the quadratic cutoff equation is as follows:

Let v_{g0}, v_{g1}, v_{g2} be the value of the velocity to be gained at t_0, t_1, t_2 respectively. Then using a Legrange interpolating polynomial to fit a curve to these three values of v_g, we get that

$$t(v_g) = \frac{(v_g - v_{g1})(v_g - v_{g2})}{(v_{g0} - v_{g1})(v_{g0} - v_{g2})} t_o + \frac{(v_g - v_{g0})(v_g - v_{g2})}{(v_{g1} - v_{g0})(v_{g1} - v_{g2})} t_1 + \frac{(v_g - v_{g0})(v_g - v_{g1})}{(v_{g2} - v_{g0})(v_{g2} - v_{g1})} t_2 \qquad (134)$$

Since we desire that v_g be zero at cutoff, we have for the formula

$$t\ (\text{at cutoff}) = \frac{v_{g1}\ v_{g2}}{v_{g0}^{2} - v_{g0}\,(v_{g1} - v_{g2}) + v_{g1}\ v_{g2}}\, t_o + \frac{v_{g0}\ v_{g2}}{v_{g1}^{2}\ v_{g1}\,(v_{g0} + v_{g2}) + v_{g0}\ v_{g2}}\, t_1 + \frac{v_{g0}\ v_{g1}}{v_{g2}^{2} - v_{g2}\,(v_{g0} + v_{g1}) + v_{g0}\ v_{g}}\, t_2 \qquad (135)$$

Equation (135) is that shown in the cutoff routine flow chart in. It is in a form however, which promotes computational efficiency.

5.6 MANEUVER SEQUENCING AND CONSTANT REDEFINITION (See flow chart 10)

In order to have the various maneuvers of a given mission executed in the proper sequence automatically, a routine which provides this sequencing must be provided. What this really means is that the guidance program must provide logic which directs the computations to the proper area of the generalized equation set. In addition, since the same equations are often used for different maneuvers, it is necessary to redefine various coefficients and constants associated with a particular equation or equations. Flow chart 10 (together with other logic throughout the program) performs this function. Thus, by entering the proper set of constants into the ADC prior to launch, any of the missions described above can be performed, either in the direct ascent or parking orbit mode.

Appendix E gives a breakdown of the inputs necessary to perform any of the missions in either of the two modes.

5.7 NAVIGATION EQUATIONS

5.7.1 The Advanced Centaur Navigation Problem

The function of the navigation equations is to generate the quantities that describe the state of the vehicle and which are used by the guidance equations in determining the appropriate guidance commands. These quantities are in general the position, velocity and acceleration of the vehicle expressed in an appropriate coordinate system or systems.

The space system at which this study is directed is one with the navigation capability completely self-contained and with the principle sensing devices being inertial instruments. Thus, since such instruments can sense only accelerations due to the vehicle propulsion system and aerodynamic forces, the acceleration components due to gravity must be obtained by analytic means. That is, a mathematical expression which is a function of vehicle position and has the accuracy necessary for the proposed applications must be used to determine the acceleration imparted to the vehicle by the earth's gravity. With the total acceleration determined, appropriate numerical integration procedures are used to generate the vehicle's velocity and then its position.

The principal problem likely to be encountered from the standpoint of navigation in utilizing the Centaur vehicle for the various missions and modes as described above, is that of the serious degeneration of the accuracy of the results of the numerical integration when such calculations are carried out for extended lengths of time such as in parking orbits and transfer orbits. This degeneration is due to the build up of truncation and roundoff errors and as well to the use of an imperfect mathematical model for the gravitational acceleration. By roundoff errors is meant those errors which result from limiting the number of correct digits which are to be handled by the computing device (in this case a digital computer using binary digits). By truncation errors is meant those errors due principally to the necessarily approximate nature of the numerical integration procedure, though truncation errors are generally taken to describe all those errors associated with the computing system not due to roundoff or gross mistakes.

The roundoff errors are not much affected by the design of the navigation equations since these errors are determined principally by the word length (or number of bits) allotted to the numbers appearing in the navigation computations. On the other hand the truncation errors can be reduced by a judicious choice of the numerical integration scheme and the overall inherent accuracy improved further by choosing as accurate a gravity model as is practical.

From the ground rules stated previously (see Section 2.4) it is evident that for many of the missions and/or mission modes the Centaur guidance and navigation system will be active for lengths of time significantly greater than those required for the current Centaur missions. Thus the navigation computations for the Advanced Centaur configuration as envisioned in this report, would have to be carried out with accuracies greater than those possible in the current configuration, and the immediate software avenues available for making such improvements are as suggested above in the reduction of truncation and gravity model errors. A third possible way of reducing errors is to abandon the numerical integration during the longer non-powered portions of the flight and instead utilize the "free flight prediction" routine described earlier. Thus as described in Section 5.3.1.3, given the position and velocity at some point on the coast orbit (say, Centaur main engine cutoff), the position and velocity at some later time on the same coast orbit is completely determined. Such a computation would satisfy completely the navigation requirements except for the fact that the "free flight prediction" makes the "two body" assumption which of course is not absolutely valid, and as a result this procedure also incurs errors.

Below are given detailed derivations and descriptions of the integration scheme and gravity models suggested, Flow Chart 12 shows the basic navigation combinations with the logic set up to use the "probe flight predictor" for navigation during coast periods. If it is not desired to use the "free flight predictor" for navigation purposes, then the ψ test in Flow Chart 12 should be eliminated and the $\psi = 0$ branch deleted. Time and task budgets did not allow for a performance analysis of these suggested navigation procedures. What is provided in this report are procedures which are are fundamentally more accurate than those procedures currently used, and which are reasonable worst cases from the standpoint of the burden navigation computations would place on Advanced Centaur computer requirements.

5.7.2 Overall Navigation Computations

The navigation computations can be divided into two general areas as follows:

a) Navigation Initialization and Derivation of the parameters required for the atmospheric equations.

b) Derivation of the basic navigation parameters.

5.7.2.1 Navigation Initialization and Atmospheric Steering Parameters

Prior to the time of "go-inertial" ($t_e = 0$) all input vectors which have been specified have been specified in the equatorial oriented inertial system. (See Section 5.13.) At "go inertial" the orientation of the platform coordinate axes are determined and the appropriate transformation from the equatorial oriented to the platform coordinates may be computed. This is assumed to be done on a ground computer. Using this transformation the above input vectors are transformed to the platform system (also done in a ground computer) and loaded in this form into the flight computer.

At "go inertial" it is also necessary to define the pitch plane oriented inertial system. Since this system is related to the platform system by an orthogonal rotation about the w-axes, the transformation is

$$T = \begin{bmatrix} a_{11} & a_{12} & 0 \\ -a_{12} & a_{11} & 0 \\ 0 & 0 & 1 \end{bmatrix} \tag{136}$$

where

$$a_{11} = \cos \Delta u \tag{137}$$

$$a_{12} = \sqrt{1 - a_{11}^2} \tag{138}$$

The angle Δu is the difference between the alignment azimuth and the pitch plane azimuth at launch where the launch time dependence of this quantity can be determined prior to launch. Thus

$$a_{11} = a_{11}(t_e) \tag{139}$$

where t_e is the launch time, referenced conveniently.

Now, it will be recalled (Section 5.1.2) that the atmospheric equation parameters are expressed in a coordinate system which is parallel to the pitch plane oriented inertial system but which is moving with respect to it with the velocity of the launch site at launch time. This coordinate system has been referred to as the earth fixed system in Section 5.1.2. The necessary position and velocity information in this coordinate system is obtained by transforming first from the platform system to the pitch plane inertial system and thence to the earth fixed system by subtracting the initial velocity of the launch site. The transformation from platform to pitch plane inertial is carried out by using the T matrix described above or, in terms of components

$$\left.\begin{aligned}
r_u' &= a_{11}\, r_u + a_{12}\, r_v && \text{(not used)}\\
r_v' &= -a_{12}\, r_u + a_{11}\, r_v &&\\
r_w' &= r_w && \text{(not used)}\\
v_u' &= a_{11}\, v_u + a_{12}\, v_v &&\\
v_v' &= a_{12}\, v_u + a_{11}\, v_v &&\\
v_w' &= v_w &&
\end{aligned}\right\} \qquad (140)$$

Since the atmospheric steering scheme selected required only cross range position information (see Section 5. 8) the first and third equations above may be eliminated as indicated.

The transformation from the pitch plane oriented quantities to the earth fixed quantities is accomplished by subtracting the velocity and position of the launch site at launch, expressed in the pitch plane oriented system, from the position and velocity expressed in the pitch plane oriented inertial system, or

$$\left.\begin{aligned}
V_x' &= v_u' - v_{uo}'\\
V_y' &= v_v' - v_{vo}'\\
V_z' &= v_w'\\
P_y' &= r_v' - r_{vo}' - v_{vo}'\, t_e
\end{aligned}\right\} \qquad (141)$$

Here v_{uo}', v_{vo}', r_{vo}' are the required position and velocity components at launch of the launch site expressed in the pitch plane oriented inertial system. These quantities are obtained from the corresponding position and velocity components of the launch site at launch expressed in the platform system, by using again the elements of the T matrix, or

$$\left.\begin{aligned} v'_{uo} &= a_{11}\, v_{uo} + a_{12}\, v_{vo} \\ v'_{vo} &= -a_{12}\, v_{uo} + a_{11}\, v_{vo} \\ r'_{vo} &= -a_{12}\, r_{uo} + a_{11}\, r_{vo} \end{aligned}\right\} \qquad (142)$$

The quantities v_{xo}, v_{yo}, r_{uo}, r_{vo} are the required velocity and position components of the launch site at launch expressed in the platform system.

The computations described above are summarized in flow chart 13. It might be mentioned here that a look at flow chart 13 will show that the quantities used to compute v'_{uo}, v'_{vo} and r'_{vo} do not possess the zero subscript as do the equations (142) above. This is because the actual navigation computation need not make this distinction since the initial navigation computation (K = 0) proceeds in a different way from the subsequent computations.

5.7.2.2 Basic Navigation Parameters

By basic navigation parameters is meant here the position and velocity information needed by the guidance equations and the coordinate system in which these parameters are expressed. Since the guidance equations make no restriction on what coordinate system can be used (other than it be inertial) one that is convenient with respect to the application of the guidance equations can be chosen. For the purposes of this report such a coordinate system is the accelerometer input or platform coordinate system. This choice was made for the following reasons:

1) The use of platform coordinates reduces the complexity necessary to derive the atmospheric steering parameters. This is true because the atmospheric parameters are related to the platform coordinates parameters by only a single rotation and a subtraction, whereas the relationship with some other operationally definable inertial coordinate system would involve, in general, a three rotation transformation to the platform system and then the additional rotation and subtraction to the earth fixed system.

2) The transformation from the atmospheric attitude commands to attitude error signals is likewise less complex owing to the fact that only the negative of the single rotation mentioned above (the translation is not necessary since direction cosines are being dealt with here) need be made while a system other than the

platform coordinates would require multiple rotations again.

3) The transformation elements from computational coordinates to the vehicle fixed system may be obtained directly using the gimbal pickoff angles, or by means of a resolver chain relating platform gimbal angles to body coordinates. The use of some other computational coordinate system would involve an additional transformation from the platform system to it.

It is, however, convenient to express the gravitational function in an earth centered equatorial plane oriented coordinate system. This convenience comes from the fact that expressing the gravitational function in this coordinate system permits taking advantage of certain symmetry characteristics and this results in a less complex function (see below). This coordinate system is that described in Section 5.1.1.3. Thus the actual navigation computation which consists of a numerical integration routine and the gravitational computation is conveniently carried out in this earth centered equatorial plane oriented coordinate system.

Since the inputs to the navigation computation are velocity increments in platform coordinates and the output of the navigation computation must likewise be in platform coordinates, two transformations are required on either end of the navigation computation, one from platform to earth centered equatorial oriented and one which is its inverse. The elements of these transformations are considered here to have been made on the ground computer as soon as the launch time has been established and loaded into the flight computer before actual liftoff.

The overall navigation computation flow chart is given in Figure 5 and summarizes the discussion of the above sections. The lines shown dotted indicate the computations which are performed at or before "go inertial". This figure does not show the literal computation flow but only the flow in principal. The literal computation flow can be understood by studying the corresponding equations flow charts.

5.7.3 Derivation of Navigation Equations

This section gives the mathematical justifications for the two major segments of the navigation equations. These segments are the gravity computation and the numerical integration procedure.

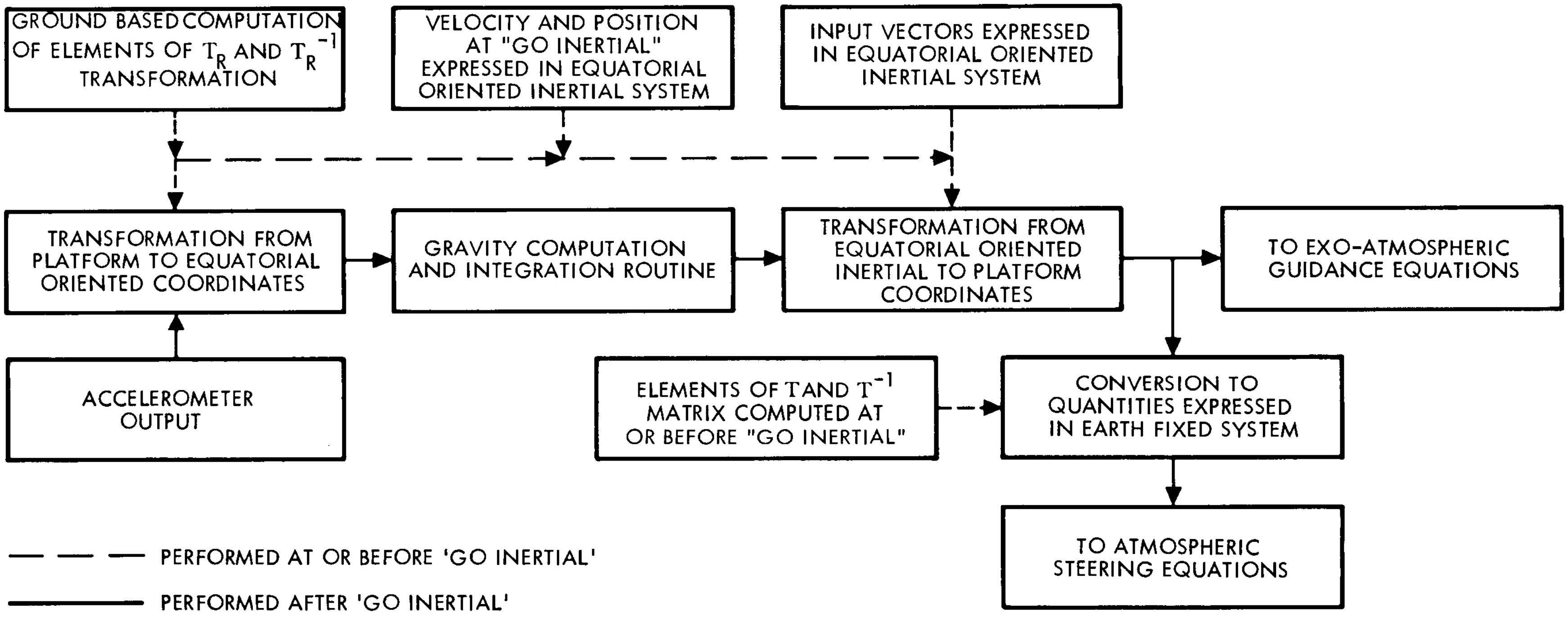
GROUND BASED COMPUTATION OF ELEMENTS OF T_R AND T_R^{-1} TRANSFORMATION
VELOCITY AND POSITION AT "GO INERTIAL" EXPRESSED IN EQUATORIAL ORIENTED INERTIAL SYSTEM
INPUT VECTORS EXPRESSED IN EQUATORIAL ORIENTED INERTIAL SYSTEM
TRANSFORMATION FROM PLATFORM TO EQUATORIAL ORIENTED COORDINATES
GRAVITY COMPUTATION AND INTEGRATION ROUTINE
TRANSFORMATION FROM EQUATORIAL ORIENTED INERTIAL TO PLATFORM COORDINATES
TO EXO-ATMOSPHERIC GUIDANCE EQUATIONS
ACCELEROMETER OUTPUT
ELEMENTS OF T AND T^{-1} MATRIX COMPUTED AT OR BEFORE "GO INERTIAL"
CONVERSION TO QUANTITIES EXPRESSED IN EARTH FIXED SYSTEM
TO ATMOSPHERIC STEERING EQUATIONS
PERFORMED AT OR BEFORE 'GO INERTIAL'
PERFORMED AFTER 'GO INERTIAL'

Figure 5. Overall Navigation Computation

5.7.3.1 Gravity Equation

An expression for the earth's gravitational potential is (See Reference 2)

$$V(r, \varphi) = \frac{\mu}{r}\left[1 - \sum_{k=2}^{\infty} J_k \left(\frac{a_g}{r}\right)^k P_k(\cos\varphi)\right] \tag{143}$$

where

J_k = the kth coefficient in the summation

J_k = 0 for k odd

$V(r, \varphi)$ = the potential at coordinates r, φ

r = radial distance from the center of the earth

φ = angle measured from the earth's polar axis

a_g = radius of the earth at the equator

$P_k(\cos\varphi)$ = the kth order Legendre polynomial

This expression is reduced to the above from a relatively untractable form, by making the following justifiable assumptions

- The earth's mass is distributed symmetrically about its polar axis
- The origin of coordinates coincides with the earth's center of gravity
- The earth is symmetrically shaped with respect to the equatorial plane

The Legendre polynomials are obtained from the expression

$$P_k(\cos\varphi) = \frac{1}{k}\left[(2K - 1)\cos\varphi\, P_{k-1}(\cos\varphi) - (k-1)P_{k-2}(\cos\varphi)\right] \tag{144}$$

with

$$p_o(\cos\varphi) = 1$$

Now, from analytical mechanics, the gravitational acceleration is obtained by taking the gradient of the potential, or,

$$\overline{G} = \overline{\nabla} V (r, \varphi) \tag{145}$$

which can be shown to be (see Reference 2)

$$\overline{G} = \frac{\overline{V}\mu}{r^2} \left\{ \overline{i}_r - \sum_{k=2}^{\infty} J_k \left(\frac{a_g}{r} \right)^k \left[P'_{k+1} (\cos \varphi) \overline{i}_r - P'_k (\cos \varphi) \overline{i}_z \right] \right\} \tag{146}$$

where $\overline{i}_k$ and $\overline{i}_z$ are unit vectors in the radial and polar directions respectively and the derivatives of the Legendre polynomials are obtained from the formula

$$P'_k (\cos \varphi) = \frac{1}{k-1} \left[(2k - 1) \cos \varphi \; P'_{k-1} (\cos \varphi) - k P'_{k-2} (\cos \varphi) \right] \tag{147}$$

with

$$P'_0 = 0$$

$$P'_1 = 1$$

Now, if an orthogonal coordinate system is defined with z' being along the polar axis and x' and y' axes being fixed in inertial space and lying in the equatorial plane, we have as described in Section 5.1.1.3, an equatorial plane oriented inertial coordinate system. The components of $\overline{r}$ in this x', y', z' coordinate system are r_x, r_y, r_z respectively. Thus in this coordinate system,

$$\overline{i}_r = \frac{r_x}{r} \overline{1}'_x + \frac{r_y}{r} \overline{1}'_y + \frac{r_z}{r} \overline{1}'_z \tag{148}$$

$$\cos \varphi = \frac{z}{r} \tag{149}$$

where $\overline{1}'_x$, $\overline{1}'_y$, $\overline{1}'_z$, are unit vectors in the x', y', z' directions respectively. Now if (148) and (149) are substituted into (146) and if the terms beyond k=4 are omitted, the components of the gravitational acceleration in the x', y', z' system are

$$G_x = -\frac{\mu}{r^2}\left[\frac{r_x}{r} + \frac{J_2}{2} a_g{}^2 \left(\frac{15\, r_z{}^2\, r_x}{r^5} - \frac{3r_x}{r^3}\right) - \frac{J_4}{8} a_g{}^4 \left(315\, \frac{r_z{}^4\, r_x}{r^9} - \frac{210\, r_z{}^2\, r_x}{r^7}\right)\right]$$

$$G_y = -\frac{\mu}{r^2}\left[\frac{r_z}{r} - \frac{J_2}{2} a_g{}^2 \left(\frac{15\, r_z{}^2\, r_y}{r^5} - \frac{3r_y}{r^3}\right) - \frac{J_4}{8} a_g{}^4 \left(315\, \frac{r_z{}^4\, r_y}{r^9} - \frac{210\, r_z{}^2\, r_y}{r^7}\right)\right] \qquad (150)$$

$$G_z = -\frac{\mu}{r^2}\left|\frac{r_z}{r} - \frac{J_2}{2} a_g{}^2 \left(\frac{15\, r_z{}^3}{r^5} - \frac{3r_z}{r^3} + \frac{6r_z{}^2}{}\right) - \frac{J_4}{8} a_g{}^4 \left(315\, \frac{r_z{}^5}{r^9} - \frac{210r_z{}^3}{r^7} - \frac{15r_z}{r^5} - \frac{14r_z{}^4}{r^8} + \frac{60r_z{}^2}{r^6}\right)\right]$$

Equations (150) represents a maximum complexity for the gravity functions. It is probable that performance analysis on these functions would show that the above equations would do an acceptable job with fewer terms than shown. However, time and budget did not permit the completion of such investigations. Equations (150) were used never the less, in making the computer requirements estimate and constitute a worst case contribution to these requirements. (See Section 4.)

5.7.3.2 Numerical Integration Procedure

The numerical integration scheme presented here attempts to provide improved accuracy by employing second degree numerical integration procedures rather than the currently used linear methods. This requires the temporary storage of two previously computed values of the parameter to be integrated, rather than just the storage of the result of the last computed value of the parameter.

The procedure for integrating the gravitational acceleration to obtain the contribution to the total velocity increment from the earth's gravity is as follows.

An estimate of the derivative of the gravity function at the time of the present computation is made by fitting a second degree curve to the last three values of the computed gravity and then establishing the derivative of the curve at the time of the current computation. Mathematically, however, the first step need not be explicitly taken, as the derivative may be obtained using the method of undetermined coefficients as follows. Let the derivative at t = T be approximated by the following formula

$$\frac{d\,G_x}{dt} = A_0\,(G_x)_{k-2} + A_1\,(G_x)_{k-1} + A_2\,(G_x)_k \tag{151}$$

where A_0, A_1, A_2 are coefficients to be determined and subscripts k, k-1, k-2 refer to the current, last and next to last values of computed gravity respectively. We impose the constraint that Equation (151) be exact for functions of 2nd degree or less. That is, we say that when

$$\begin{aligned} G_x &= 1 \\ G_x &= (t - t_{k-2}) \\ G_x &= (t - t_{k-2})^2 \end{aligned} \tag{152}$$

formula (151) will yield the correct result for $\frac{dG_x}{dt}$. Differentiating equations (152) we get

$$\begin{aligned} G'_x &= 0 \\ G'_x &= 1 \\ G'_x &= (t - t_{k-2}) \end{aligned} \tag{153}$$

and if we assume a constant computation time increment, Δt

$$\begin{aligned} t_{k-2} &= t_{k-2} \\ t_{k-1} &= t_{k-2} + \Delta t \\ t_k &= t_{k-2} + 2\Delta t \end{aligned} \tag{154}$$

Substituting Equations (153) and (154) into (151) then gives the three Equations,

$$
\begin{aligned}
0 &= A_0 + A_1 + A_2 \\
1 &= \Delta t\, A_1 + 2\Delta t\, A_2 \\
4 &= \Delta t\, A_1 + 4\Delta t\, A_2
\end{aligned}
\tag{155}
$$

from which

$$
\begin{aligned}
A_0 &= \frac{1}{2\Delta t} \\
A_1 &= \frac{2}{\Delta t} \\
A_2 &= \frac{3}{2\Delta t}
\end{aligned}
\tag{156}
$$

The formula for the derivative is then

$$
\left(\frac{d\,G_x}{dt}\right)_k = \frac{1}{\Delta t}\left[\frac{1}{2}\,(G_x)_{k-2} - 2\,(G_x)_{k-1} + \frac{3}{2}\,(G_x)_k\right] \tag{157}
$$

With the value of the derivative obtained, the increment of velocity added between t_k and t_{k+1} is obtained using the trapezoidal relation

$$
\begin{aligned}
\left(\Delta G_x\right)_{k+1} &= \left(G_x\right)_k\,\Delta t + \frac{1}{2}\left[\left(\frac{d\,G_x}{dt}\right)_k \Delta t\right]\Delta t \\
&= \left(G_x\right)_k\,\Delta t + \frac{1}{2}\,\frac{1}{\Delta t}\left[\frac{1}{2}\left(G_x\right)_{k-2} - 2\left(G_x\right)_{k-1}\right. \\
&\qquad \left. + \frac{3}{2}\left(G_x\right)_k\right] \\
&= \frac{1}{2}\left[\frac{1}{2}\left(G_x\right)_{k-2} - 2\left(G_x\right)_{k-1} + \frac{7}{2}\left(G_x\right)_k\right]\Delta t
\end{aligned}
\tag{158}
$$

The same formula is used for ΔG_y and ΔG_z.

These values of $(\Delta G_x)_{k+1}$, $(\Delta G_y)_{k+1}$, $(\Delta G_z)_{k-1}$ become the $(\Delta G_x)_k$ $(\Delta G_y)_k$, $(\Delta G_z)_k$, on the next computation of total integrated velocity. The total integrated velocity is computed by adding to the last value of total integrated velocity the contribution from the integrated gravity computation (Equation 158) and the incremental thrust velocity accelerometer output (ΔV_{sx}, etc.). These computations are shown in the upper left portion of flow chart 12.

In order to determine the vehicle position components a numerical integration of the total integrated velocity is carried out. This procedure utilizes the last three computations of integrated velocity to provide a second degree approximation, and is derived as follows.

Fundamentally we wish to find the increment of position contributed to the total position between the time increments t_{k-1} and t_k, from the three values of total integrated velocity at t_k, t_{k-1} and t_{k-2}, $(V_x)_k$, $(V_x)_{k-1}$, $(V_x)_{k-2}$, and etc. for the other two components. To do this we set the integral equal to the following polynomial

$$\int_{t_{k-1}}^{t_k} V_x \, dt = A_{k-2} (V_x)_{k-2} + A_{k-1} (V_x)_{k-1} + A_k (V_x)_k \qquad (159)$$

and impose the condition that Equation (159) be exact for functions of V_x of second degree or less. That is, Equation (159) is to be exact for

$$\begin{aligned} V_x &= 1 \\ V_x &= [t - t_{k-2}] \qquad (160) \\ V_x &= [t - t_{k-2}]^2 \end{aligned}$$

If again the computation time increments are uniform,

$$\begin{aligned} t_{k-2} &= t_{k-2} \\ t_{k-1} &= t_{k-2} + \Delta t \qquad (161) \\ t_k &= t_{k-2} + 2\Delta t \end{aligned}$$

Thus integrating Equations (160) from t_{k-1} to t_k and substituting the results into Equation (159), we get three equations, as follows:

$$\begin{aligned}\Delta t &= A_{k-2} + A_{k-1}\ A_k \\ \frac{3}{2}\Delta t &= A_{k-1} + 2\ A_k \\ \frac{7}{3}\Delta t &= A_{k-1} + 4\ A_k\end{aligned} \tag{162}$$

which yields for the constants

$$\begin{aligned}A_{k-2} &= -\Delta t \\ A_{k-1} &= \frac{2}{3}\Delta t \\ A_k &= \frac{5}{12}\Delta t\end{aligned} \tag{163}$$

Thus the integration formula becomes

$$\int_{t_{k-1}}^{t_k} V_x\ dt = \left[\frac{5}{12}t_k + \frac{2}{3}t_{k-1} - \frac{1}{12}t_{k-2}\right]\Delta t \tag{164}$$

and etc. for the other two components. The position of this computation in flow chart 12 is in the upper right hand corner.

5.8 ATMOSPHERIC STEERING

The discussion in this section is based on the work performed under contract NAS3-3231 amendment 7 for the NASA Lewis Research Center. This work was a study to determine the feasibility of employing closed loop booster steering for the Atlas/Centaur vehicle. The results of the study are reported in full in Reference 1. A major portion of this study was devoted to the investigation of various booster steering laws for use in the closed loop mechanization. The investigation was aimed at determining, from a wide range of possible steering functions, which best satisfied the following atmospheric steering requirements for the Atlas/Centaur vehicle.

a) Acceptable stability characteristics throughout booster flight.

b) Acceptable dispersion control (position and velocity).

c) Improved load relief characteristics over the current A/C time programmed booster steering.

d) Acceptable response to other common disturbances such as thrust misalignment, C. G. offsets, and changes in aerodynamic parameters.

e) Acceptable response to the effect of finite navigation information sampling intervals.

An initial conclusion of the study was that of all the candidate pitch plane steering laws investigated (some 39 in all involving position, velocity and acceleration terms) four were acceptable for continued study*. These four were:

$$\begin{aligned}
1)\quad C_{az} &= C_{27} V'_x + C_{28} V'_z + C_{29}\left(V'_x\right)^2 + C_{30}\left(V'_z\right)^2 \\
&\quad + C_{31} V'_x V'_z \\
2)\quad C_{az} &= C_{27} V'_x + C_{28} V'_z + C_{29}\left(V'_x\right)^2 + C_{30}\left(V'_z\right)^2 \\
&\quad + C_{31} V'_x V'_z + C_{32} A_x + C_{33} A_z \\
3)\quad C_{az} &= C_{24} P_x + C_{25} P_z + C_{26}\left(V'_z\right)^2 + C_{27} V'_x \\
&\quad + C_{28} V'_z + C_{30}\left(V'_z\right)^2 + C_{31} V'_x V'_z \\
4)\quad C_{az} &= C_{24} P_x + C_{25} P_z + C_{27}\left(V'_x\right) + C_{28}\left(V'_z\right) \\
&\quad + C_{30}\left(V'_z\right)^2 + C_{31} V'_x V'_z + C_{32} A_x + C_{33} A_z
\end{aligned}\tag{165}$$

The coefficients in these laws (and the discarded ones) were obtained by making least square fits of the particular law to a nominal A/C-5 trajectory. The field was narrowed to the above four laws by

a) Discarding laws whose fits to the nominal trajectory were such as to result in unacceptably large residuals.

b) Discarding laws which were not inherently stable. This was ascertained by checking the various partial

---

*Yaw plane laws were not investigated since the problems encountered in pitch plane steering were considered to be much more severe.

> derivatives (with respect to the appropriate independent variables - position, velocity and acceleration) and discarding laws for which the partials were of the wrong sign at a critical point in the flight or for significantly long durations. A wrong sign here means a sign which would result in pitching the vehicle in the wrong direction to correct a given deviation from the nominal trajectory.

The results of the analysis performed on these remaining four laws is summarized from Reference 1 below. For a complete description of this analysis Reference 1 should be consulted.

Once the inherent stability of the four laws had been established, each law was analyzed further to determine what its effect would be on the overall stability of the control system with the guidance loop closed. This was done by a standard technique of linearizing the system equations at three critical points of the flight. Then the effect of the given booster steering law in the closed guidance loop was determined by noting the appropriate stability margins on a gain-phase portrait. The three critical points were:

1) Pitchover start
2) Max-Q (maximum aerodynamic loading)
3) Booster engine cutoff

Of these the Max-Q point is the most important since in the current Atlas/Centaur configuration the aerodynamic gain margin is only barely acceptable at this point. The results showed that the degradation of the aerodynamic gain margin and the rigid body phase margin due to any of the four steering laws was not severe. However, since the aerodynamic gain margin at max-Q is dangerously small to begin with, even a small degradation is serious. For this reason a redesign of the Atlas/Centaur autopilot was dictated. When the four laws were analyzed with the redesigned autopilot it was found that laws 1 and 3 produced acceptable margins but that laws 2 and 4 produced instability due to the presence of acceleration terms in these functions. This would leave laws 1 and 3 in the running if the redesigned autopilot were to be employed.

When the four laws were evaluated in terms of their ability to keep position and velocity perturbations small all gave satisfactory results with law 4 giving the best position dispersion results and law 2 giving the best velocity dispersion results. However it was found from simulation runs that the load relief characteristics* were best with laws 1 and 2, giving 12.5% improvement over the performance with the present time programmer.

All of the four laws gave satisfactory results when disturbances such as thrust misalignments, C.G. offsets, and changes in aerodynamic parameters were simulated.

When the sampling periods for obtaining navigation information was varied using each of the four laws it was found that for the laws incorporating acceleration terms (2 and 4) the sampling period had to remain less than 0.25 seconds to prevent instability. For the laws incorporating only position and velocity terms (1 and 3) the sampling times had to remain less than 1.25 seconds though for law 1 instability did not occur until the sampling time was above 2 seconds. For law 3 a significant increase in the maximum bending moment at station 770 was experienced for values of 1.25 and above and instability occurred at 2 seconds.

From these results, the balance favors law 1, because of its good load relief characteristics and its ability to interface properly with an advanced autopilot for the Atlas/Centaur. Though the other laws offer somewhat better dispersion control, law 1 still keeps these dispersions within limits which are entirely acceptable. Thus on the basis of the work outlined above, the velocity law (law 1) is incorporated in this set of generalized equations to perform the booster steering function with the actual mechanization shown on flow chart 11.

It might be pointed out here that the work reported on in Reference 1 and outlined here was specifically directed at the Atlas/Centaur vehicle with its own unique structural and control interfaces with guidance schemes. For example, if the aerodynamic gain margin were not so small to begin with a redesigned autopilot would not be necessary, and the acceleration terms, in law 2 and 4 would not induce the instability mentioned above. Then, laws 2 and 4 might be recommended in order to take advantage of their ability to reduce dispersion more effectively than the velocity law. The other equations (that is the exo-atmospheric equation) in the generalized set, are not so organically connected to the Atlas/ Centaur vehicle which points up the fact that, in general, atmospheric equations are highly vehicle dependent where the explicit equations are not. In view of this any design of "generalized equations" where the generalization is intended to encompass different vehicle configurations, would be hardpressed to provide a "generalized" scheme for ascent through the atmosphere applicable in an efficient manner to the various booster vehicles, and a design approach which admitted the atmospheric equations as a module would be called for. This modular approach was taken in the design of the equation set presented in this report, with the specific atmospheric steering equations being here, for the obvious reasons, Atlas/Centaur motivated.

---

*Load relief is taken to be indicated by the reduction in the maximum bending moment at station 770 of the Atlas/Centaur over that using the current time programmed steering.

5.9 COMPENSATION EQUATIONS

Flow chart 14 shows the general form of the equations assumed to account for the inertial instrument compensation computations. These equations can be considered representative of the equations used to compensate for

accelerometer biases
gyro drifts
scale errors
nulling errors

However, since the actual compensation equations are determined in the first instance by the inertial hardware itself, these equations do not constitute a recommendation but rather are included in this general way so that the overall characteristics and implication of a complete guidance equation set may be more accurately determined.

6. PERFORMANCE OF THE UPPER STAGE STEERING EQUATIONS

This section of the report has been purposely separated from any overall performance summary to emphasize the fact that the steering equations which have been developed are independent of the methods used to compute required cutoff conditions. The explicit methods of computing required cutoff conditions recommended in this report are not essential to the steering equations, and could be replaced by the more conventional finite series representations if desired.

A goal of the development effort on this contract was to show that the upper stage steering equations could give the required efficiency and accuracy over a wide variety of missions and still remain entirely explicit, i. e., not require any trajectory dependent pre-targeted steering coefficients. This goal was achieved, as is shown in the following paragraphs. However, there was little time left for an exhaustive study of the effect of various perturbations on a particular mission. Such a study should be made if the development effort is continued. It should be pointed out, however, that this scheme is not as sensitive to perturbations as are some. In the case of injection into a fixed elliptical or hyperbolic trajectory the steering is designed to remove any deviations in the initial conditions at the start of the Centaur stage. Hence, the only effects of winds, booster stage perturbations, or sustainer perturbations, are to change the amount of fuel consumed in Centaur. In the case of intercept guidance the desired velocity is computed explicitly, and hence there is no increase in the error due to variations in cutoff position as there would be with a finite series representation. There may, of course, be some steering errors due to center of gravity offsets, etc., in Centaur, and these should certainly be studied.

The following paragraphs describe the simulation results which were obtained for some typical nominal missions, and some of the steps which were taken in the development process. The simulations were made with an AC-8 configuration, which was slightly modified to eliminate certain items not essential to the present study. The values of the guidance coefficients which stayed the same in all of these runs are listed in Table 5.

It was first suspected that it might be necessary to stop the guidance equations a few seconds before cutoff in order to avoid a situation where a division by a near zero time to go (T) might be required. The tests on T against the coefficient K_{14} was designed to prevent this situation. However, in the course of the study it was found that the test was really unnecessary, and actually caused increased steering error unless K_{14} was held at 1.0 sec. No excessively large attitude rates were observed near cutoff with the value of K_{14}. The value of K_{16} was held at 1.0 sec, which means that the cutoff routine is entered as soon as T becomes less than 1.0 sec. Since the normal guidance computations are halted once the cutoff routine is entered, the test employing K_{14} is not really necessary.

This test was included in the flow charts to accurately describe the existing simulation.

The value of K_{55} was held at 400 sec., which caused the vehicle to be steered towards a circular orbit up until 400 seconds after liftoff. It was found that this procedure gave a better trajectory shaping and decreased the fuel consumption on the hyperbolic and intercept flights, as is explained below in the sections on those particular simulations. The value of K_{56} was chosen to give this circular orbit a 90 n.mi. altitude.

The value of K_{90} was chosen empirically to give good results under a variety of conditions. This correction is necessary to acount for gravity losses and rotation of the $\overline{V}_g$ vector when computing time to go until Cutoff, T.

The value of K_{91}, i.e., -32.3, was chosen from the difference between the final acceleration of the Atlas Sustainer and the initial acceleration of the Centaur. This choice is in agreement with the theory of Section 5.2.3.

The value of K_{95} was chosen as 30 sec, which means that over the last 30 seconds the steering equations abandon the position constraints and drive towards the velocity constraints only. It had been observed in the simulation that if this switch were not used the equations would satisfy the position constraints quite accurately, but have rather large errors in

Table 5. Values of Guidance Coefficients Which Remain Constant for All Missions

$K_6 = 36,000$
$K_7 = 23,00$
$K_{11} = 0.027159570$
$K_{12} = 0.0375$
$K_{14} = 1.0$
$K_{15} = 0.0$
$K_{16} = 1.0$
$K_{17} = 4,014.2$
$K_{18} = 9,840$
$K_{19} = 13,800$
$K_{51} = 4.0$
$K_{52} = 4.0$
$K_{55} = 400$
$K_{56} = 21,472,863$
$K_{90} = 0.0930$
$K_{91} = 32.3$
$K_{95} = 30.0$

velocity. This action is quite undesirable since the velocity errors are usually much more serious than the position errors. The switch to velocity steering at T = 30 seconds remedies this problem.

The coefficients K_6, K_7, K_{11}, K_{12}, K_{17}, K_{18} and K_{19} describe the accelerations and velocity change capabilities of the rocket engines. They have been chosen in a straightforward manner from the known characteristics of the Atlas and Centaur vehicles.

The coefficients K_{51} and K_{52} are used in the computation of the commanded body angular rates. The first coefficient, K_{51}, multiplies the angular error in body coordinates, and the second multiplies the integral of that error. This control law gives rise to a linear constant coefficient 2nd order servo system on the body attitude. The fact that the commands are computed only at the guidance cycle times, i.e., once every half second, causes this control system to behave as a sampled data system. The equivalent block diagram is shown in Figure 6.

The integral term was included in the control law in order to eliminate the study state attitude error due to a constant commanded angular rate. The problem of designing a realistic autopilot is not considered in this part of the report. However, it was necessary to choose the gain

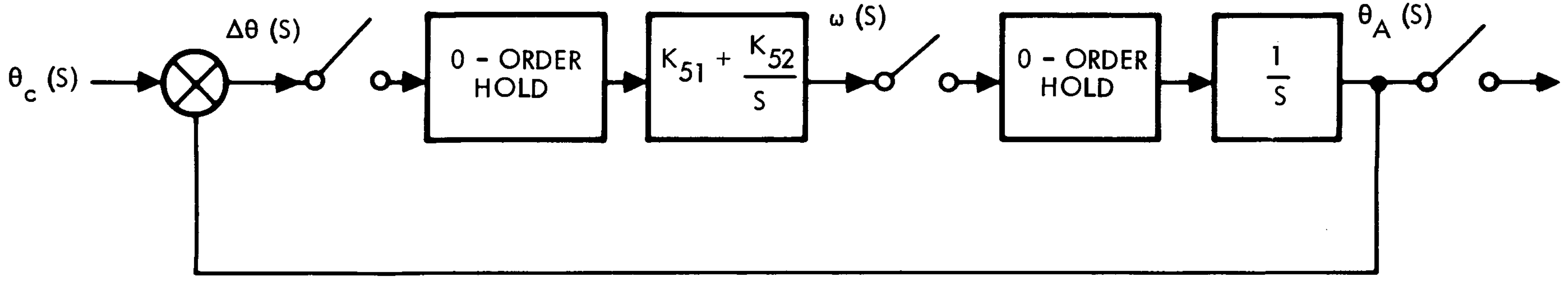
θ_c (S)
$\Delta\theta$ (S)
0 - ORDER HOLD
$K_{51} + \frac{K_{52}}{S}$
ω (S)
0 - ORDER HOLD
$\frac{1}{S}$
θ_A (S)

Figure 6. Equivalent Block Diagram of the Attitude Control System for the Guidance Simulation

K_{51} and K_{52} to give a good response in the simulation of the guidance equations. The error in body attitude is related to the commanded attitude by the expression

$$\Delta\theta_\rho(Z) = \frac{(Z-1)^2}{Z^2 + Z\,(K_{51}\,\Delta t_f - 2) + (1 - K_{51}\,\Delta t_f + K_{52}\,\Delta t_f^{\,2})}\;\theta_c(Z) \qquad (166)$$

where Z is the usual transform variable used in sampled data analysis. If $\theta_c(t)$ is a ramp function then

$$\theta_c(Z) = \frac{\Delta t_f Z}{(Z-1)^2} \qquad (167)$$

and so

$$\Delta\theta_\rho(Z) = \frac{\Delta t_f\, Z}{Z^2 + Z\,(K_{51}\,\Delta t_f - 2) + (1 - K_{51}\,\Delta t_f + K_{52}\,\Delta t_f^{\,2})} \qquad (168)$$

Application of the final value theorem then shows that the steady state error in body attitude is zero for a ramp input. For a cycle time of $\Delta t_f = 0.5$ sec. a system with the minimum response time to a step or ramp input is obtained with $K_{51} = 4.0$, $K_{52} = 4.0$. With these values of gain the expression for the Z-transform of $\Delta\theta_\rho(t)$ is

$$\Delta\theta_\rho(Z) = \frac{(Z-1)^2}{Z^2}\quad\theta_c(Z) \qquad (169)$$

The Z-transform of $\Delta\theta_\rho(t)$ for a unit step input in $\theta_c(t)$ is then

$$\Delta\theta_\rho(Z) = 1 - Z^{-1} \qquad (170)$$

whereas the corresponding expression for a unit ramp input is

$$\Delta\theta_\rho(Z) = \Delta t_f\, Z^{-1} \qquad (171)$$

The corresponding time responses are shown in Figures 7 and 8.

These values of gain generally gave quite good results in the simulations. For example, in the last thirty seconds before cutoff on the parking orbit injection, the worst error was $13 \ \widehat{\sec}$ in pitch and $10 \ \widehat{\sec}$ in yaw.

6.1 PARKING ORBIT AND ELLIPTIC ORBIT INJECTION

Much of the initial work concentrated on getting good performance for a special case of elliptic orbit injection, i.e., for injection into a 90 n.mi. circular parking orbit. Since only the performance over the Atlas sustainer and Centaur stages was of interest, the simulations were made from a nominal set of initial conditions at the beginning of the sustainer phase. The $\bar{j}$ vector describing the orientation of the desired orbital plane was chosen so that it contained the position and velocity vectors at booster burnout. The special values of the guidance coefficients needed for the particular run are listed in Table 6.

Table 6. Special Guidance Coefficient for the Parking Injection Simulation

1. $\nu = 0$
2. $K_{58} = 1$
3. $\bar{j} = 0.14080116, 0.49383428, 0.85808085$
4. $K_{23} = 21,472,863$
5. $K_{24} = 0.0$
6. $K_{25} = 21,472,863$

The original set of equations presented in Reference 3 were found to be inadequate because they caused excessive fuel consumption. The cutoff weight for a simulation using these equations was 14,106.5 lbs. An open loop simulation using the calculus of variation to find the optimum steering profile gave a cutoff weight of 14,169.5 lbs., a savings of 63.0 lbs. It was found that most of the difference was due to poor steering over the Atlas sustainer stage, which caused poor initial conditions at the beginning of Centaur. This fact was proven by making a guided simulation over the Centaur stage with a set of initial conditions taken off the

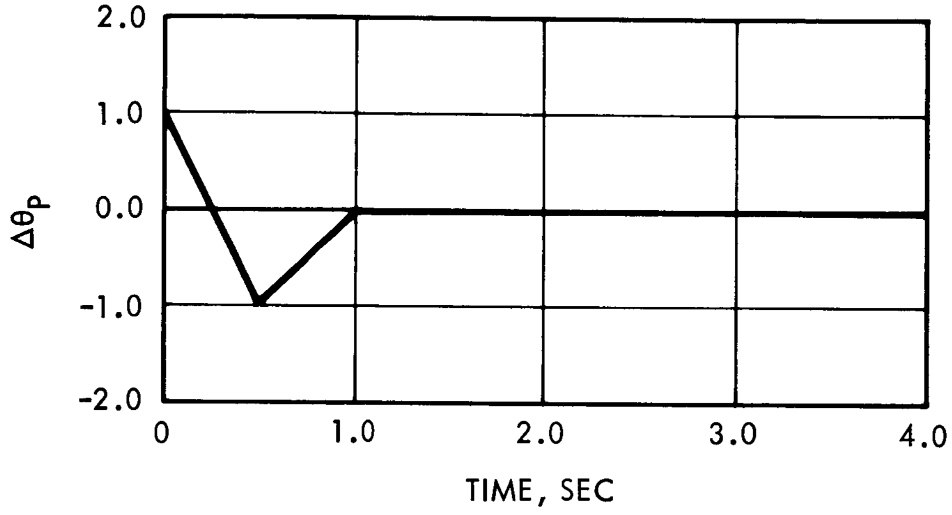

Figure 7. Unit Step Response of the Attitude Control System Used in the Guidance Simulation

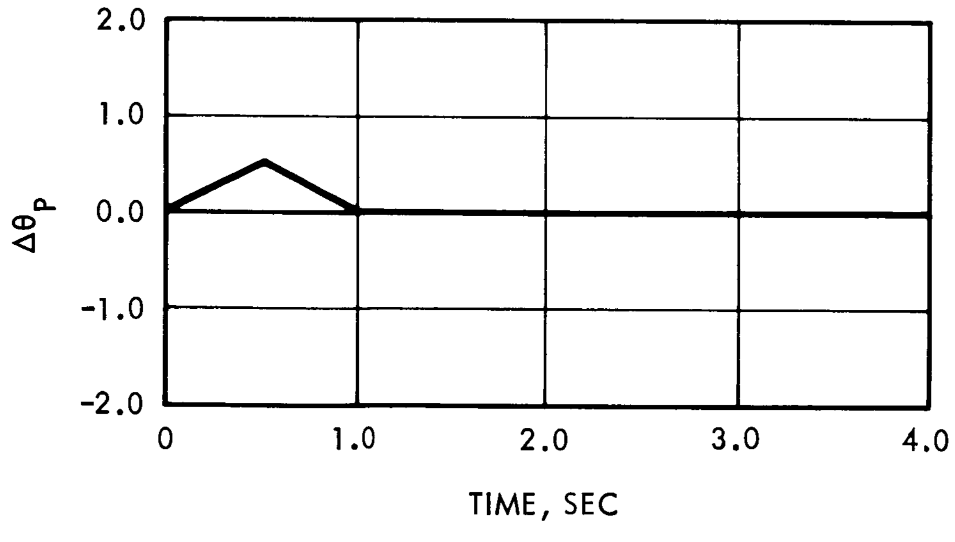

Figure 8. Unit Ramp Response of the Attitude Control System Used in the Guidance Simulation

open loop simulation. The cutoff weight in this case was 14,163.0 lbs., which shows that the steering equations waste only 6.5 lbs., over the Centaur stage when the proper initial conditions are provided.

The original equations were inefficient because no attempt had been made to force the attitude to be continuous across the staging region. Figure 9 shows a plot of C_{az}, the direction cosine between the desired thrusting direction and the local vertical, for the original set of equations and for the optimum solution using the calculus of variations. Since C_{az} is approximately equal to Cos θ_p, where θ_p is the desired pitch angle from the local vertical, it is a measure of the desired attitude angle. The optimum C_{az} is continuous and has a continuous derivative across the staging region, whereas the original guidance equations gave a very large change in C_{az} across the region. Once this problem had been recognized the equations were modified with a ΔB correction which is designed to give a smooth C_{az} across the staging region. The theory behind this correction is discussed in Section V.B.3.

Figure 10 shows the behavior of C_{az} after the ΔB correction had been included. This profile has a much smaller C_{az} change than that of the original equations, and generally follows the optimum C_{az} much more closely. There is still a small discontinuity remaining because of the approximations which were made in mechanizing the guidance equations. The required change in attitude is only 4 deg, however, which is quite an improvement over the 16 deg. of the original equation. The cutoff weight was increased to 14,150.5 lbs., which means that only 19.0 lbs. of fuel were wasted. This final loss was judged to be acceptably small, so development work on this problem was stopped. Further improvement could probably be made at the price of increased guidance equation complexity.

Figure 11 shows the behaviour of the B coefficient during the powered flight region of the parking orbit injection simulation. The large change between the values at sustainer cutoff and Centaur ignition was purposely induced by means of the ΔB correction. This change in the B coefficient causes the C_{az} direction cosine to be more smoothly behaved. The straight line behavior of the B coefficient after Centaur ignition is

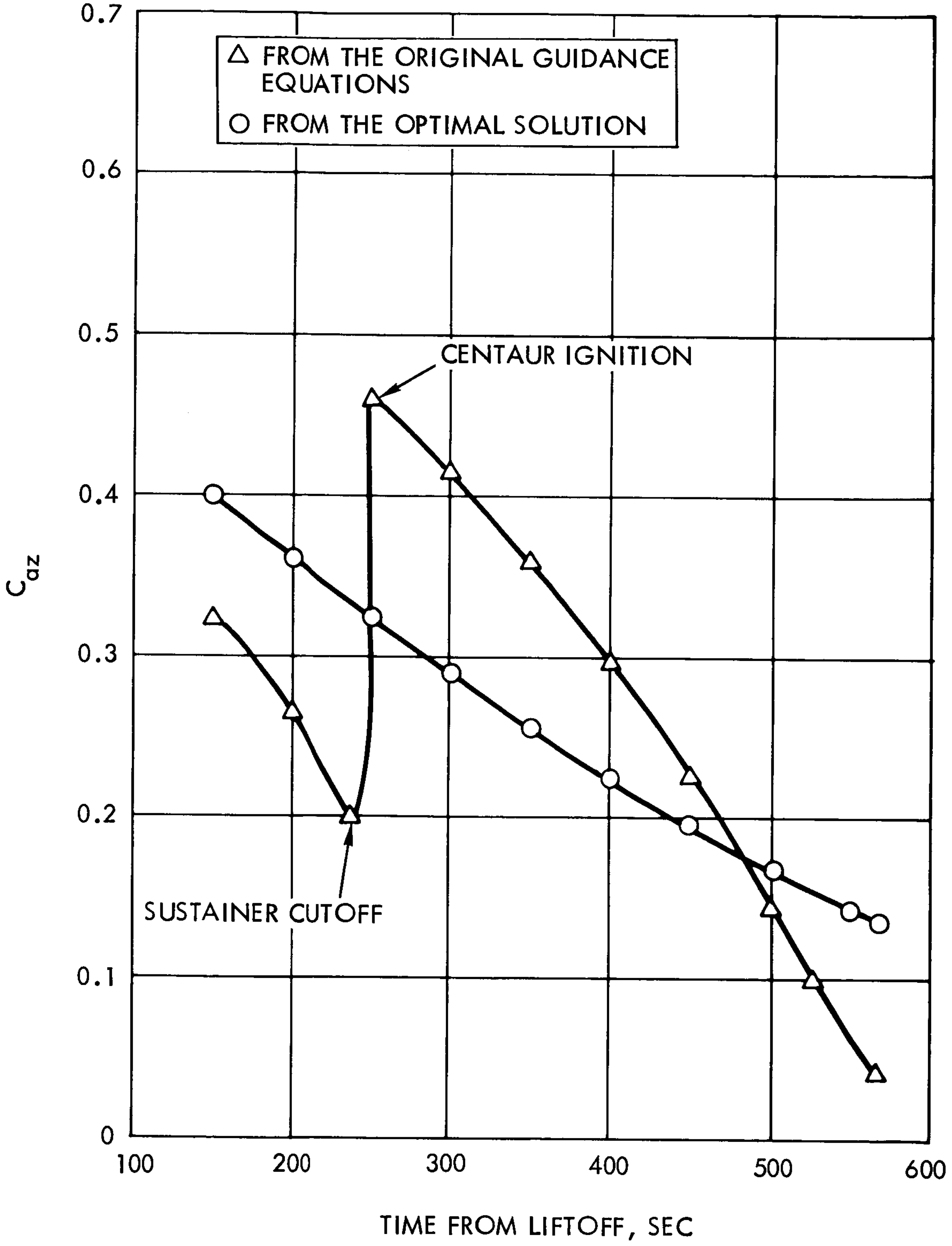

Figure 9. C_{az} Direction Cosine for a Parking Orbit Injection Using the Original Guidance Equations

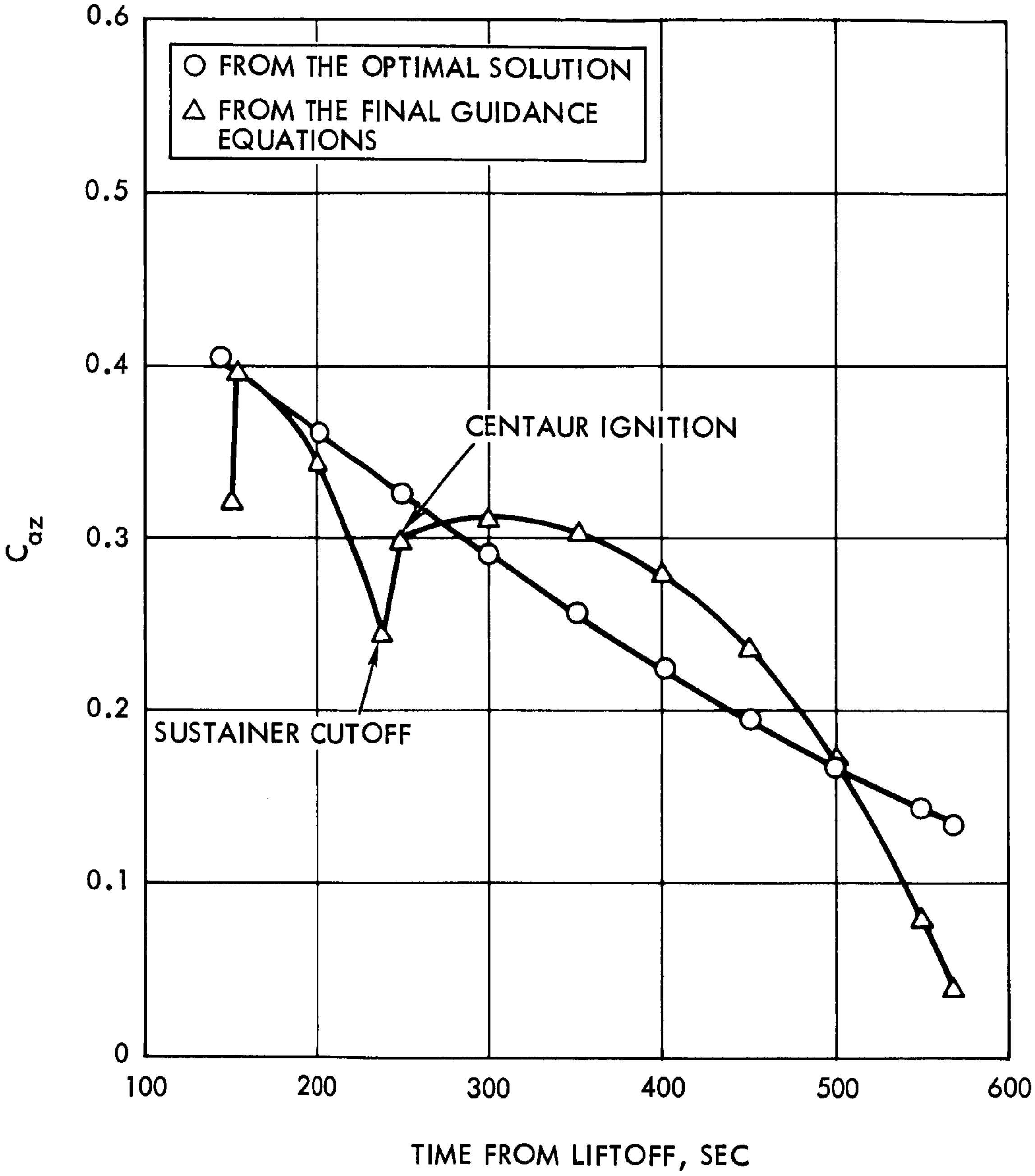

Figure 10. C_{az} Direction Cosine for a Parking Orbit Injection Using the Final Guidance Equations

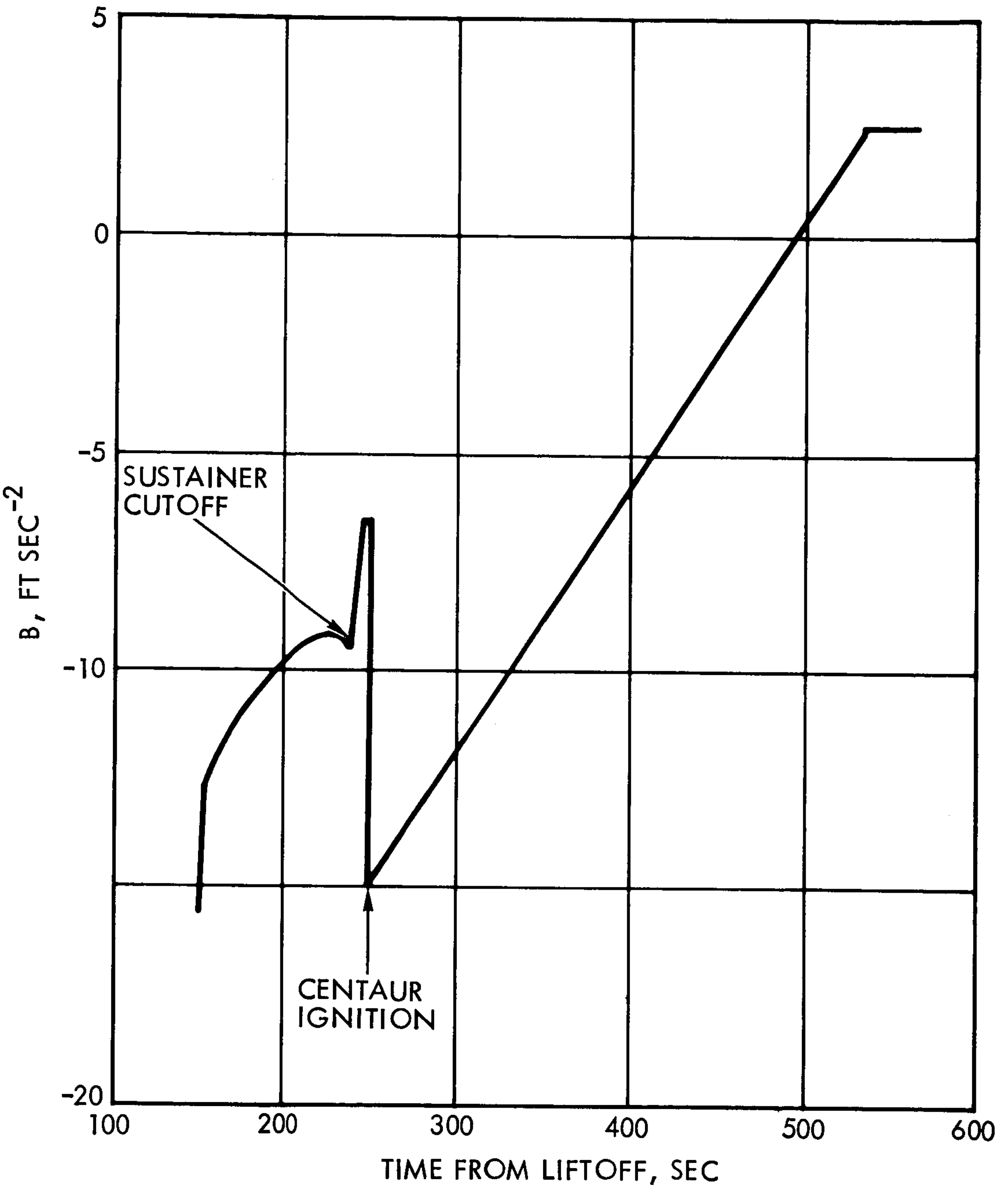

Figure 11. B Coefficient on a Parking Orbit Injection

due to the fact that $\ddot{r}$ was assumed to be a straight line in the derivation of the guidance equations. The B coefficient is identical to $\ddot{r}$, as can be seen from the derivation in Section 5.2.3. The B coefficient becomes nearly constant over the last 30 seconds of flight because of the switch to velocity steering during that time.

Some of the other characteristics of the parking orbit injection simulations are represented by Figures 12 through 18. Figure 12 shows a plot of altitude vs. time. The altitude rises above the desired value during the Centaur phase, then drops down to its final value. This behavior is fairly typical of most parking orbit injection schemes.

Figure 13 shows a plot of time to go until cutoff, T, for the same simulation. It is clear from this curve that T is extremely linear and quite accurate over both stages. The small irregularity which occurs between stages is due to the fact that the acceleration goes to zero in the region, and hence V_c and V_g become constant, causing T to become constant.

The accuracy of the cutoff point prediction scheme is also of interest. Figure 14 shows a plot of the predicted change in range angle during powered flight $\Delta\phi$, on the parking orbit injection. The components of the predicted cutoff position in inertial coordinates, as computed from $\Delta\phi$ and the present position vector, are plotted in Figures 15 through 17. The components of the present position vector in inertial coordinates are also shown in these figures. It is clear from these curves that the prediction becomes increasingly accurate as the cutoff time approaches, and that the error goes to zero at the end. Even at the beginning the error is less than 30 miles, while the total position change being considered is on the order of 1,500 miles. Hence the worst error is on the order of 2% of the total position change, which is quite low considering the number of approximations involved.

The accuracy of the steering equations was found to be quite good, i.e., the vehicle was driven through the required final condition with very little error. Figure 18 shows a plot of the magnitude and plot of the inertial components of the $\overline{V}_g$ vector over the last few seconds of flight. The steering accuracy is demonstrated by the fact that all these

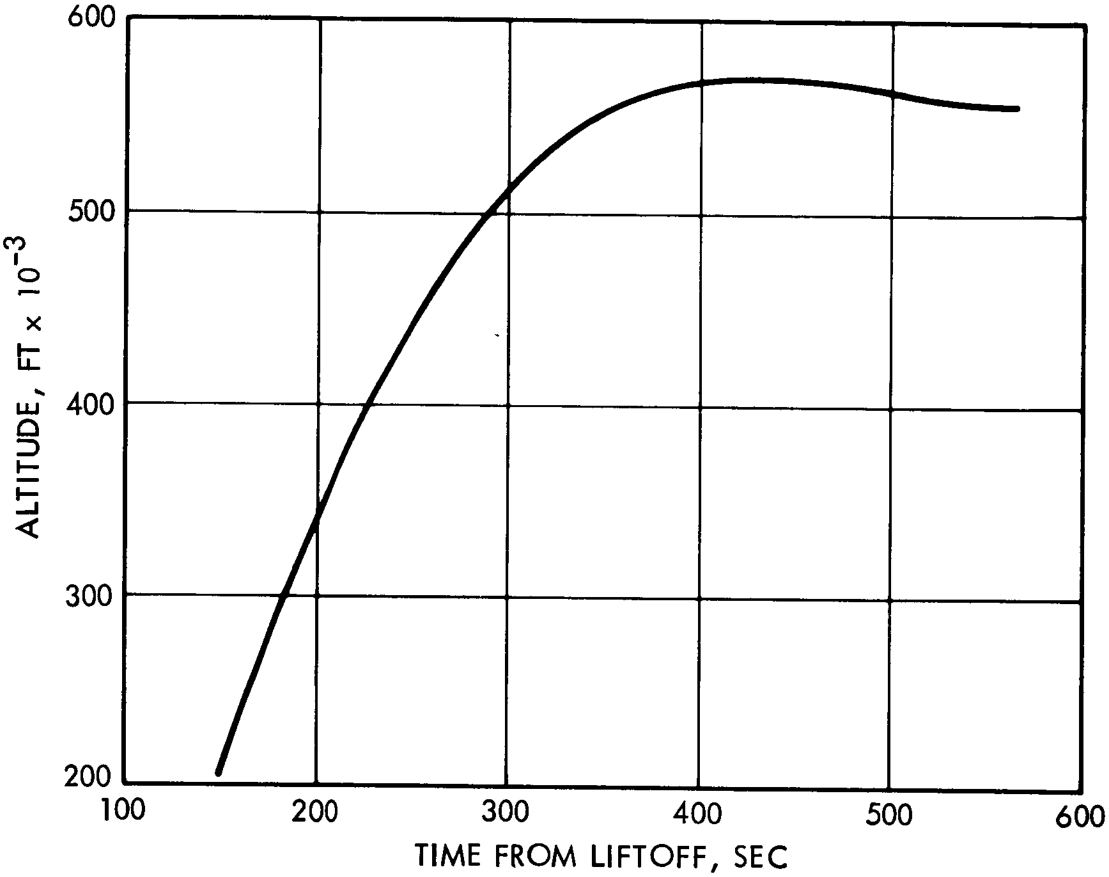

Figure 12. Altitude Versus Time on a Parking Orbit Injection

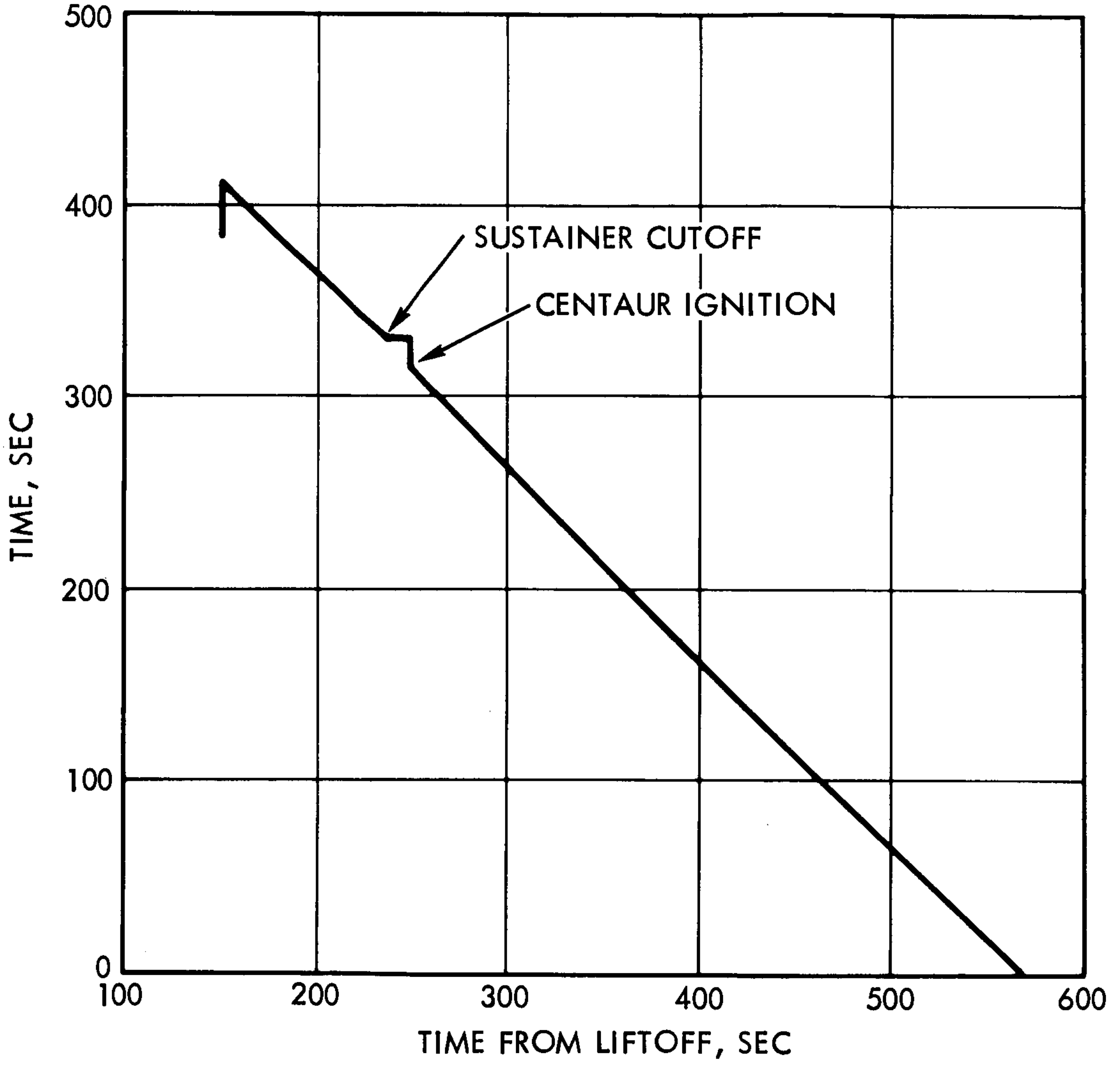

Figure 13. Time to Go until Cutoff, T, on a Parking Orbit Injection

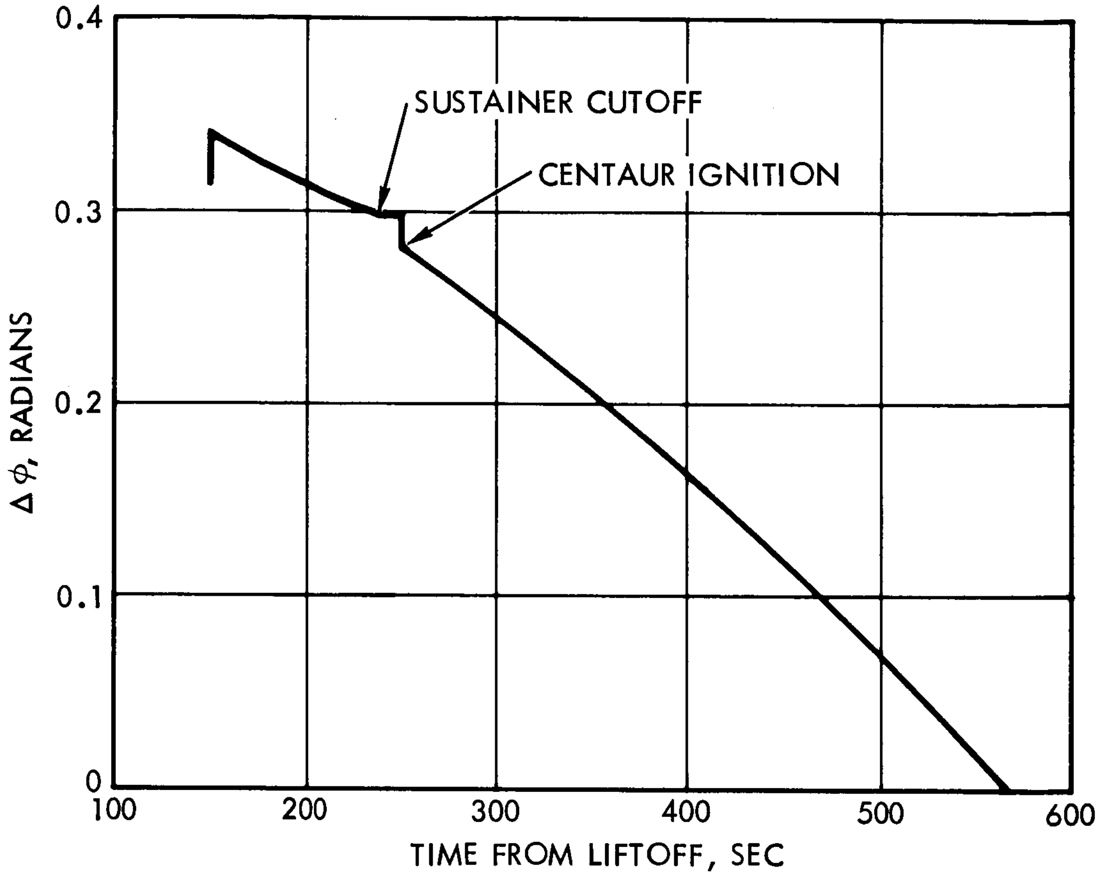

Figure 14. Predicted Change in Range Angle During Powered Flight, Δ φ, on a Parking Orbit Injection

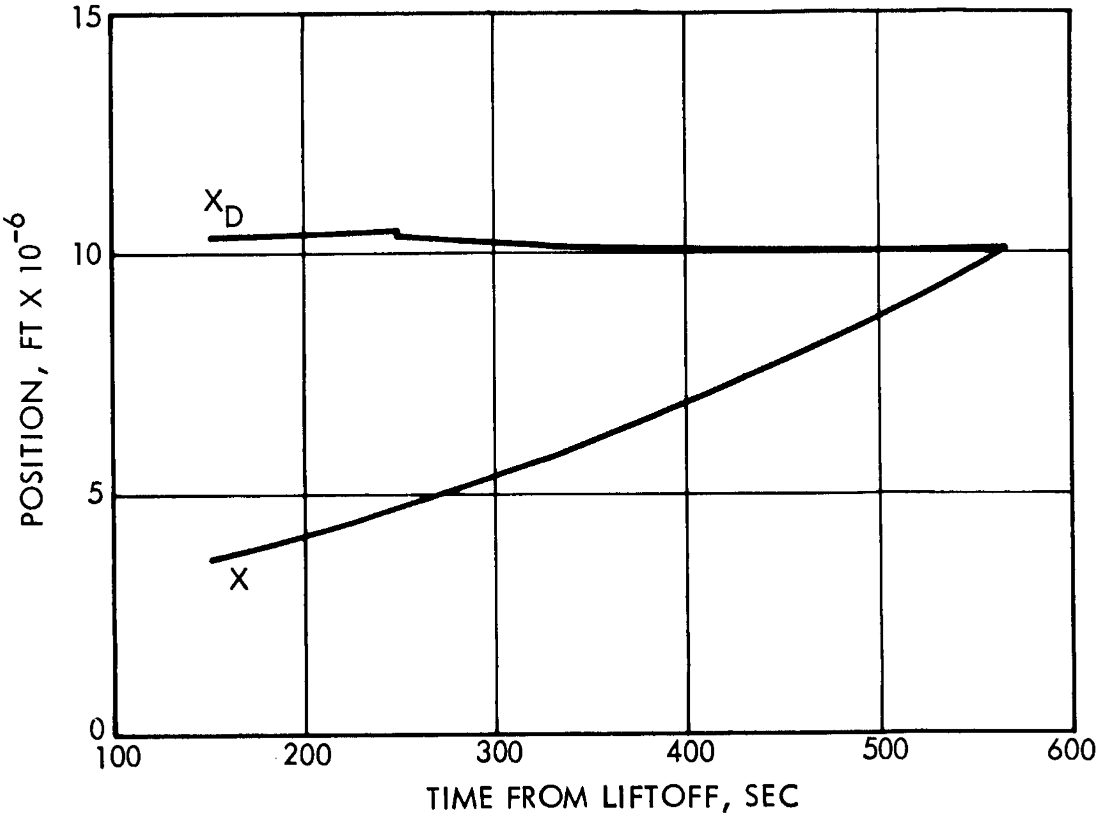

Figure 15. Predicted Cutoff Position in Inertial Coordinates, X_D, and Present Position in Inertial Coordinates, X, on a Parking Orbit Injection

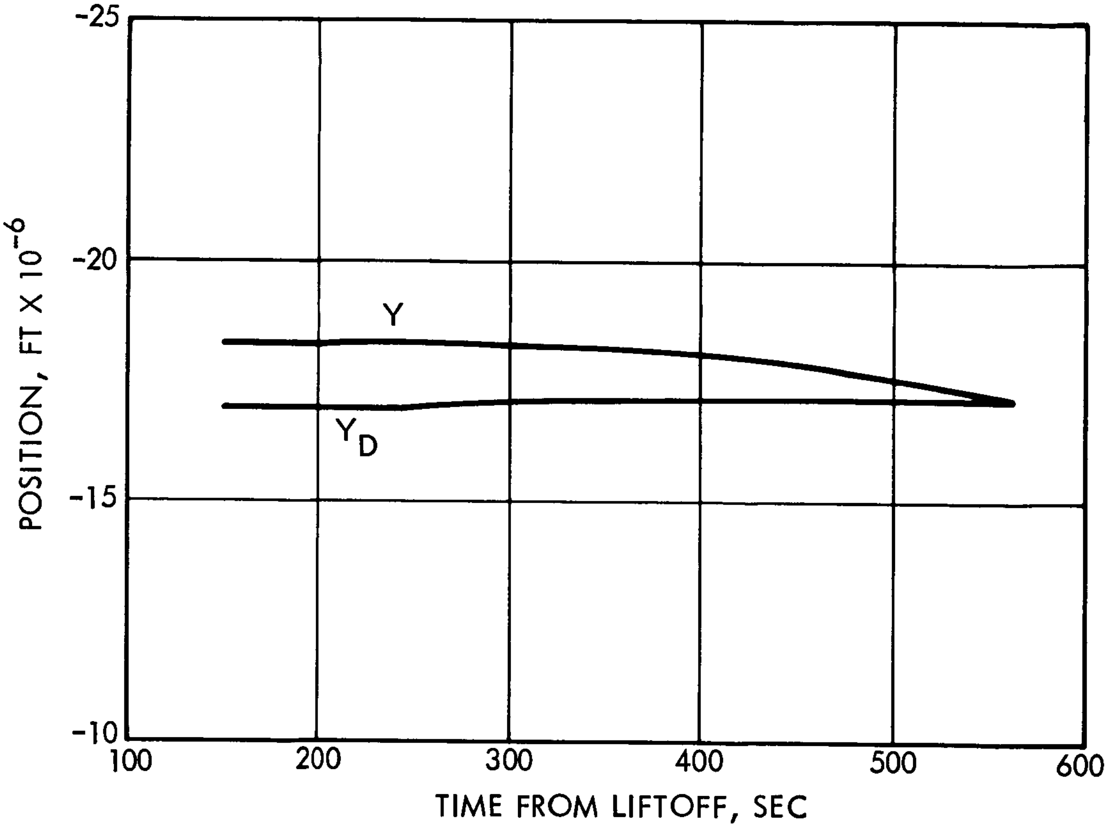

Figure 16. Predicted Cutoff Position in Inertial Coordinates, Y_D, and Present Position in Inertial Coordinates, Y, on a Parking Orbit Injection

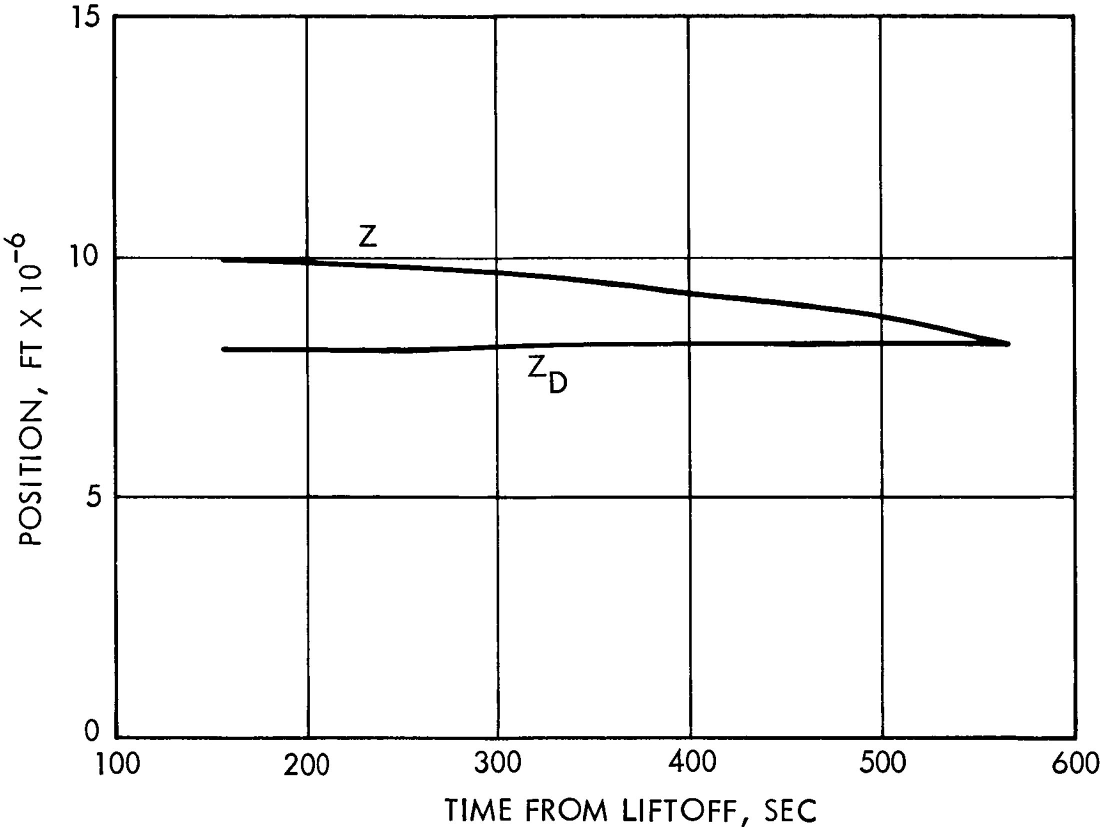

Figure 17. Predicted Cutoff Position in Inertial Coordinates, Z_D, and Present Position in Inertial Corrdinates, Z, on a Parking Orbit Injection

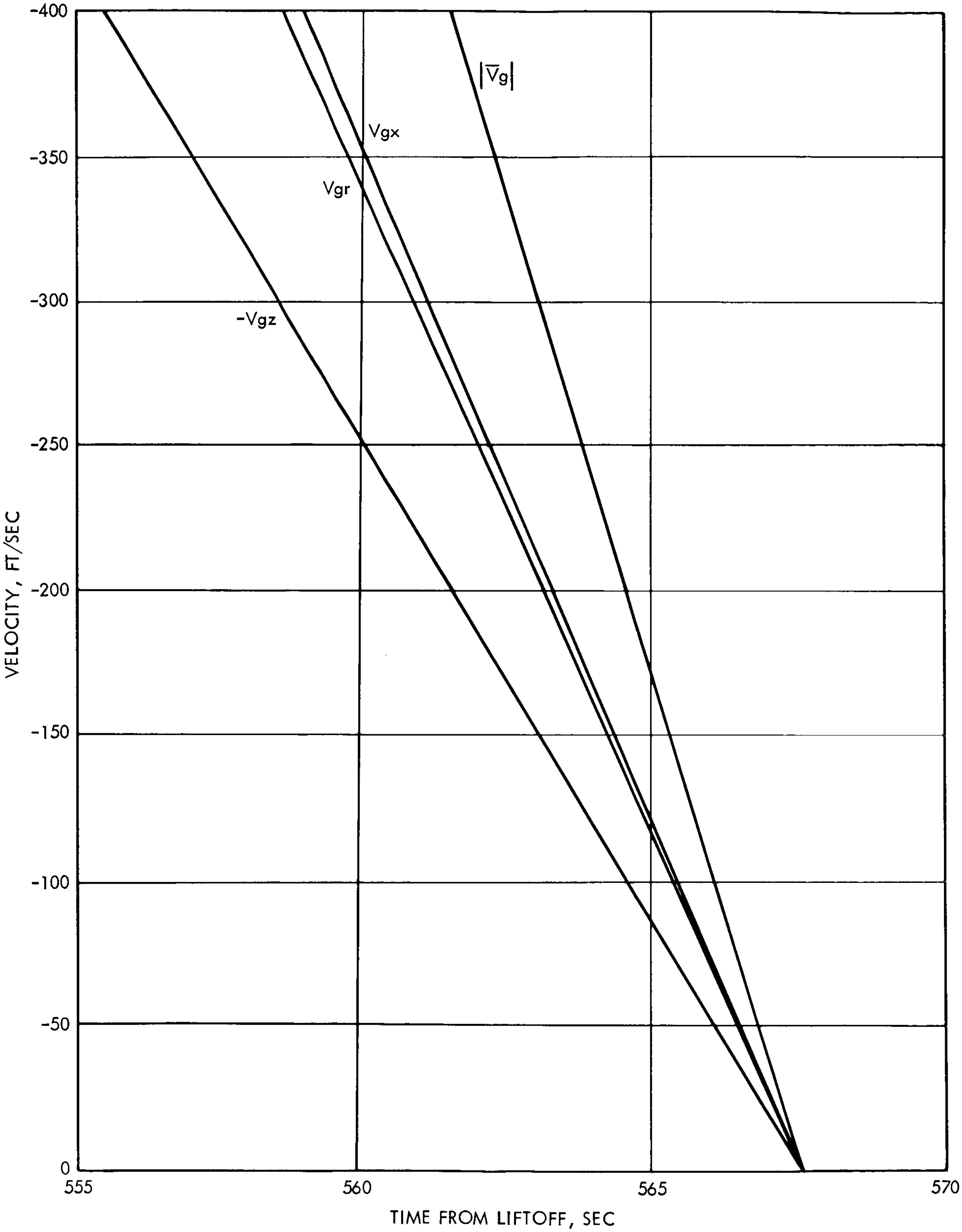

Figure 18. Velocity-to-be Gained, $\overline{V}_g$, in Inertial Coordinates

components appear to be driven through zero simultaneously. On the parking orbit injection the vehicle is thrusting nearly horizontally at cutoff. Hence the errors in radial position and velocity and out of plane position and velocity are measures of the steering error, whereas the error in tangential velocity is determined by the cutoff routine. The errors in radial position and velocity at cutoff were 15.75 ft and 0.020 ft $\sec^{-1}$ respectively. The errors in out of plane position and velocity were 19.5 ft and 0.015 ft $\sec^{-1}$ respectively. These errors are certainly much lower than can be expected from any inertial guidance hardware which can be built in the near future. The tangential velocity was in error by 0.15 ft $\sec^{-1}$, which is largely due to the cutoff routine. The resulting apogee error was 0.05 miles, and the perigee error was 0.03 miles. There was little effort devoted to determining just why the cutoff routine gave this relatively large error. However, there is no reason to believe that it cannot be improved to the point where the tangential velocity error is as low as the steering error.

It can be stated, then, that the steering equations give satisfactory efficiency and accuracy in the parking orbit injection mission.

6.2 HYPERBOLIC ORBIT INJECTION

Several simulations were made using the hyperbolic injection option of the guidance equations on a direct ascent mission. The special guidance coefficients used for making these runs are listed in Table 7. The $\bar{j}$ vector describes the desired orbital plane, the $\bar{1}_{R_P}$ vector describes the desired orientation of the hyperbola in this plane, and K_{23} and K_{21} define its desired shape, representing semi-major axis and eccentricity, respectively.

The initial simulations which were made showed that the guidance equations were causing excessive fuel consumption. The final weight at cutoff was 5501.8 lbs., when these equations were used without modification. A calculus of variations solution with the same initial and final conditions had a final weight of 5686.2 lbs., a savings of 184.4 lbs. It was found that the C_{az} direction cosine profile given by the guidance equations was vastly different from that of the optimal solution, as shown

Table 7. Special Guidance Coefficients for the Hyperbolic Orbit Injection

1. $\nu = 0$
2. $K_{58} = +1$
3. $\bar{j} = 0.14080116; 0.49383428; 0.85808085$
4. $K_{23} = 9.7708476 \times 10^{7}$ ft.
5. $K_{25} = 4.7607574 \times 10^{7}$ ft
6. $K_{24} = 1.2195252$
7. $\bar{1}_{R_P} = 0.4694073573; -0.7965397313; 0.3810265139$
8. $\bar{s} = 0.1140066981; 0.8529953211; -0.503146562$

in Figure 19. It was also noted, however, that the optimal C_{az} direction cosine profile was almost identical with that of the circular parking orbit injection, as can be seen by comparing Figure 19 and 9. From these results it was decided that the equations should be modified to steer toward a circular parking orbit in the early part of the burn, i.e. for time less than K_{55}. As was mentioned earlier, K_{55} has been chosen to be 400 seconds. This resulted in a steering profile somewhat closer to the optimal solution, as shown in Figure 20. The cutoff weight was increased to 5660.0 lbs., which is only 26.2 lbs., less than that obtained using the calculus of variations. This loss was judged to be acceptably small.

This method of steering causes the time to go computation to be incorrect for time less than 40 seconds. Figure 21 shows a plot of time to go, T, as a function of time.

The jump change in T at 400 seconds amounts to about 100 seconds. The computations past that point are not quite as linear as on the circular orbit injection, but are still satisfactory.

Some initial difficulties were encountered in computing the reciprocal of the acceleration, i.e., γ, on the hyperbolic orbit injection because the velocity consumed, V_c, becomes so very large toward the end. When V_c

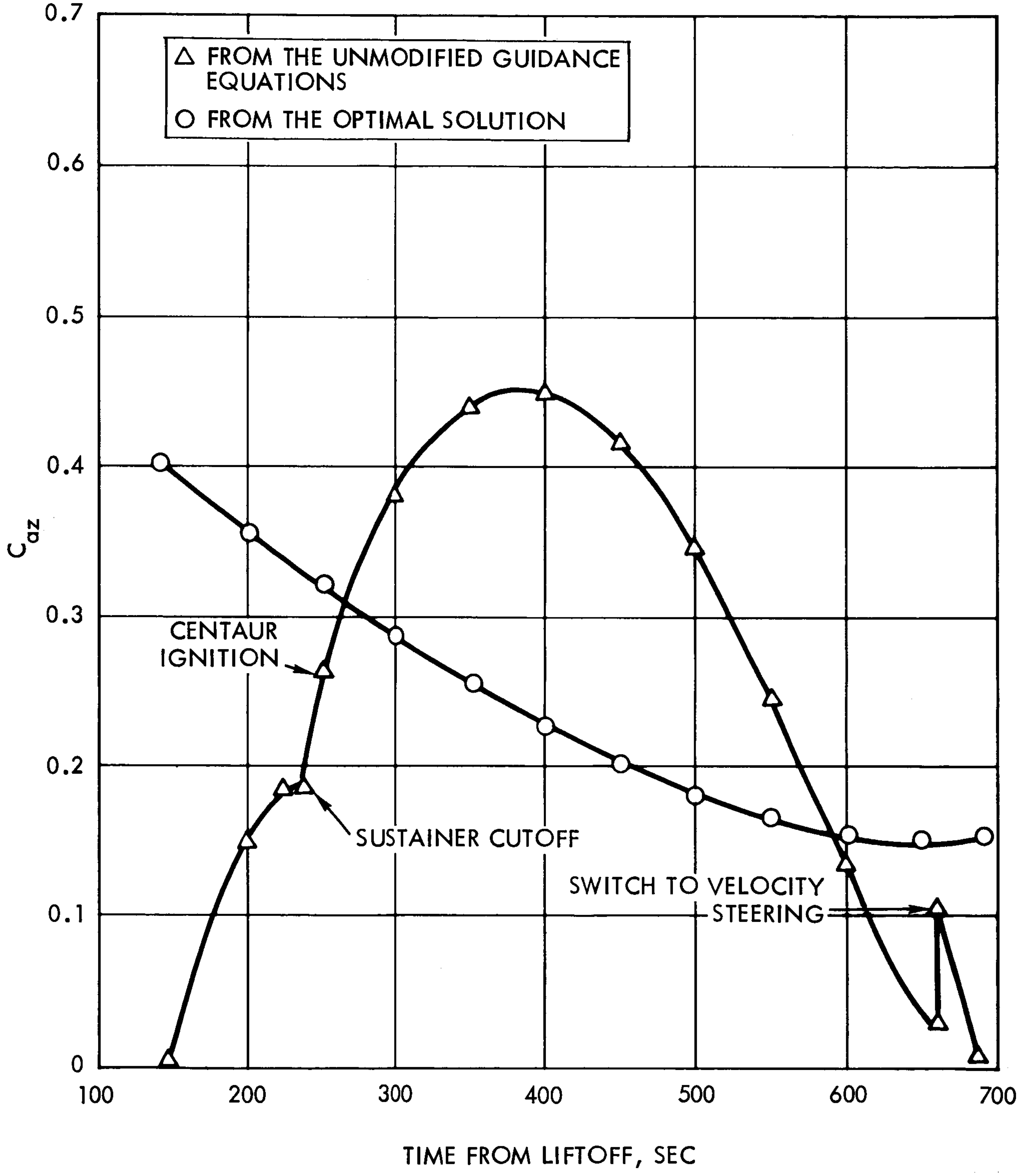

Figure 19. C_{az} Direction Cosine for a Hyperbolic Orbit Injection Using the Unmodified Guidance Equations

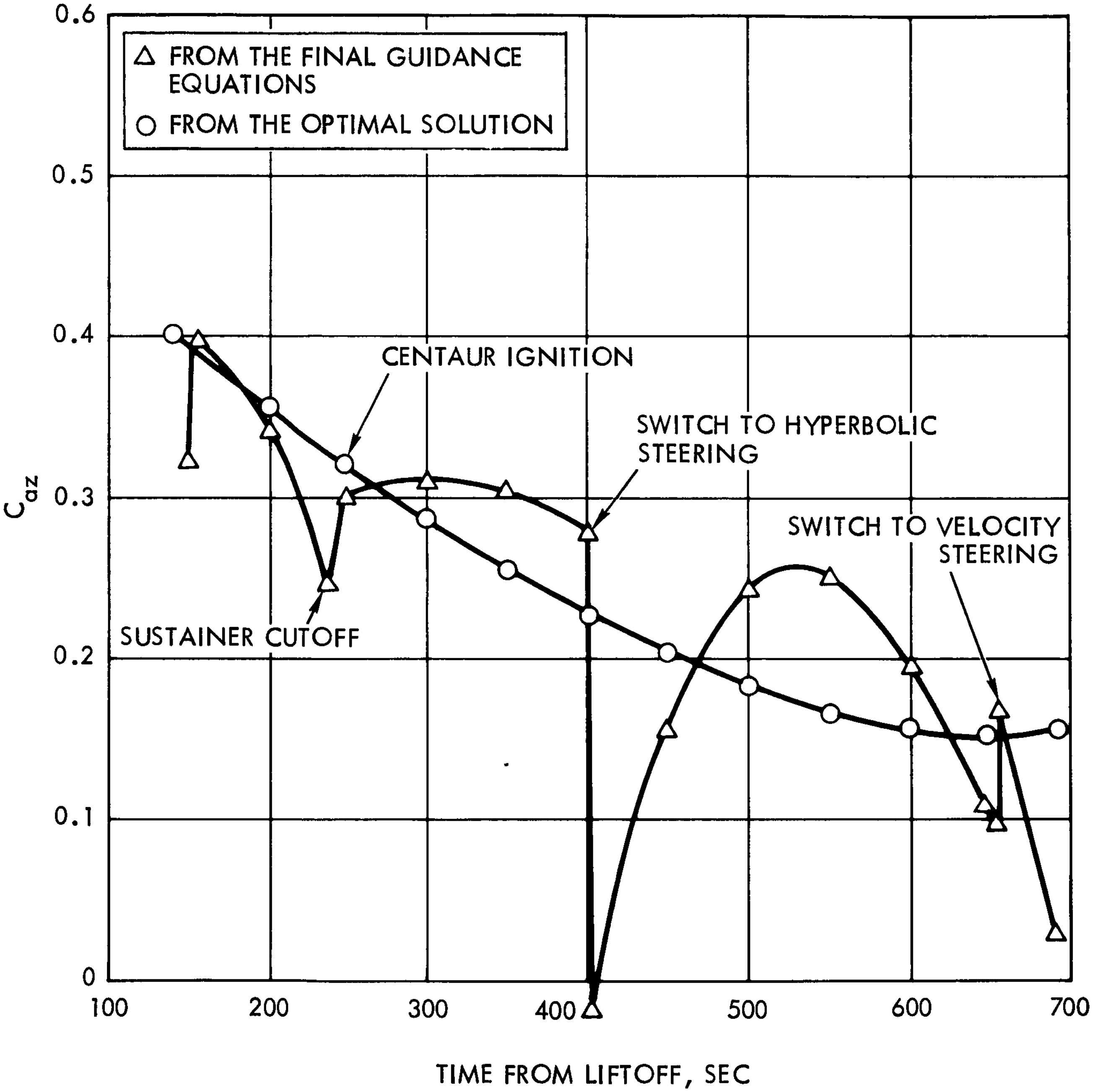

Figure 20. C_{az} Direction Cosine for a Hyperbolic Orbit Injection Using Circular Orbit Steering up Until 400 Sec.

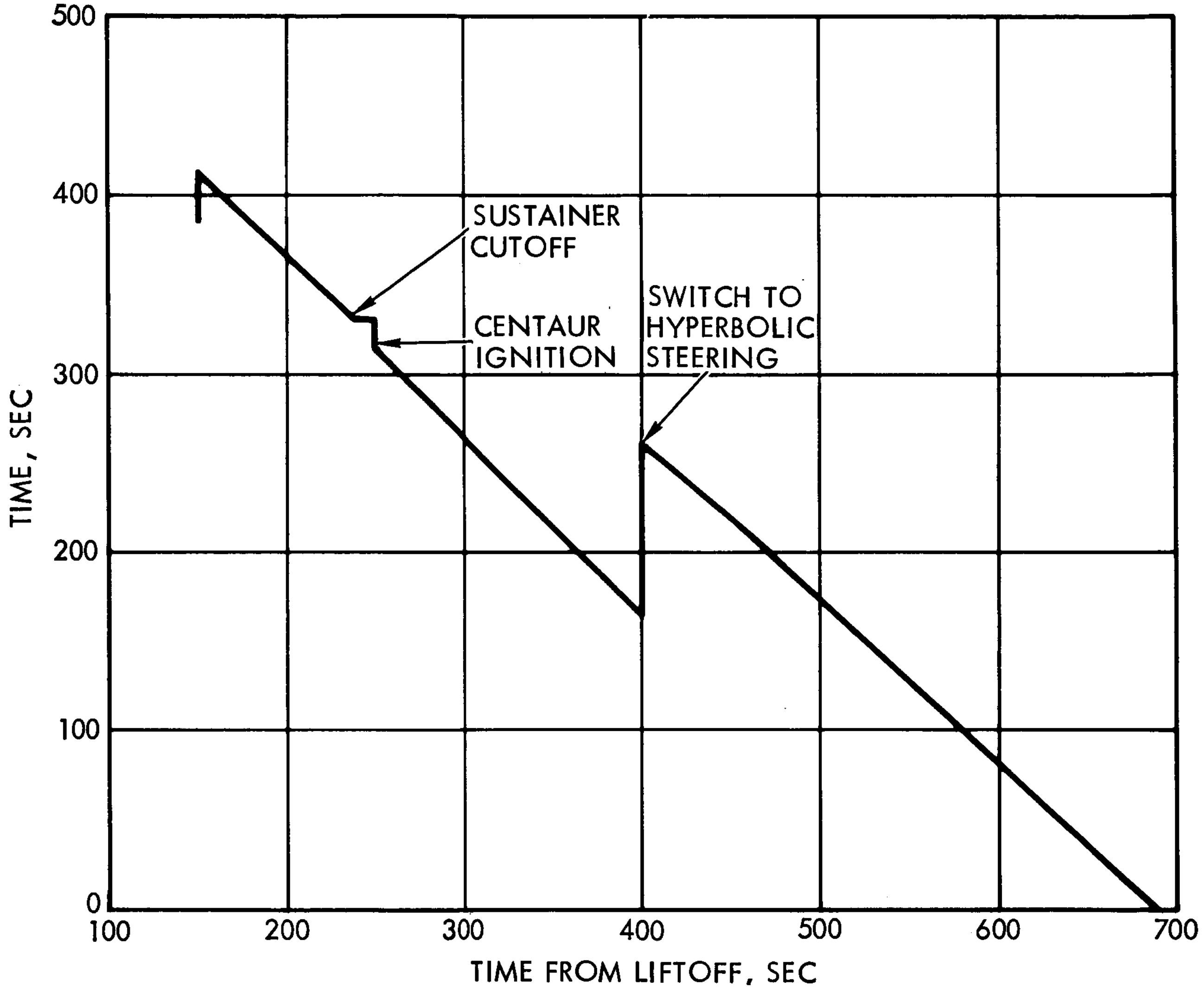

Figure 21. Time to go Until Cutoff, T, on a Hyperbolic Orbit Injection

becomes larger than the exhaust velocity of the gases, K_{19}, then the accuracy of the expansion of exp $\frac{V_c}{K_{19}}$ tends to become poor. It was found that a six term expansion of this function was needed in order to insure the proper accuracy.

Figure 22 shows a plot of the altitude vs. time on the hyperbolic orbit injection. This curve is, of course, identical with the parking orbit injection curve up until 400 seconds. The altitude then drops down below the 90 n. mile of the circular parking orbit before rising back up to the final cutoff value. The altitude at cutoff was 716,674 ft., and the radial velocity was 3675.38 ft $\sec^{-1}$.

Figure 23 shows a plot of the components and the magnitude of $\overline{V}_g$ in inertial coordinates. These curves again illustrate the accuracy of the steering equation, since all components appear to be driven to zero simultaneously. The vehicle is thrusting in a nearly horizontal direction at cutoff, so the error in radial and out of plane position and velocity are indicative of the steering error. The error in the tangential velocity is caused by the cutoff routine.

The hyperbolic orbit injection differs somewhat from the parking orbit injection in that the radial and tangential components of desired velocity are varying continuously throughout the flight. Figures 24 and 25 show the variations in these quantities in the region near cutoff. These variations are caused by errors in predicting the cutoff position. The variations in $\overline{V}_g$ in Figure 23 are thus due to variations in $\overline{V}_d$ as well as $\overline{V}$. The fact that $\overline{V}_g$ essentially goes to zero means that $\overline{V}_g$ is very nearly equal to $\overline{V}$ at cutoff, in spite of these variations in $\overline{V}_d$.

If the curves in Figures 24 and 25 are extrapolated to the known cutoff time it appears that the desired radial and tangential velocities were 3675.52 ft $\sec^{-1}$ and 37,840.84 ft $\sec^{-1}$ respectively. The actual radial and tangential velocities at cutoff were 3675.38 ft $\sec^{-1}$ and 37,840.66 ft $\sec^{-1}$ respectively. The 0.14 ft $\sec^{-1}$ error in radial velocity is essentially a steering error, and the 0.18 ft $\sec^{-1}$ error in tangential velocity is due to the cutoff routine. There was, in addition, a 0.030 ft $\sec^{-1}$ error in out of plane velocity. The corresponding position

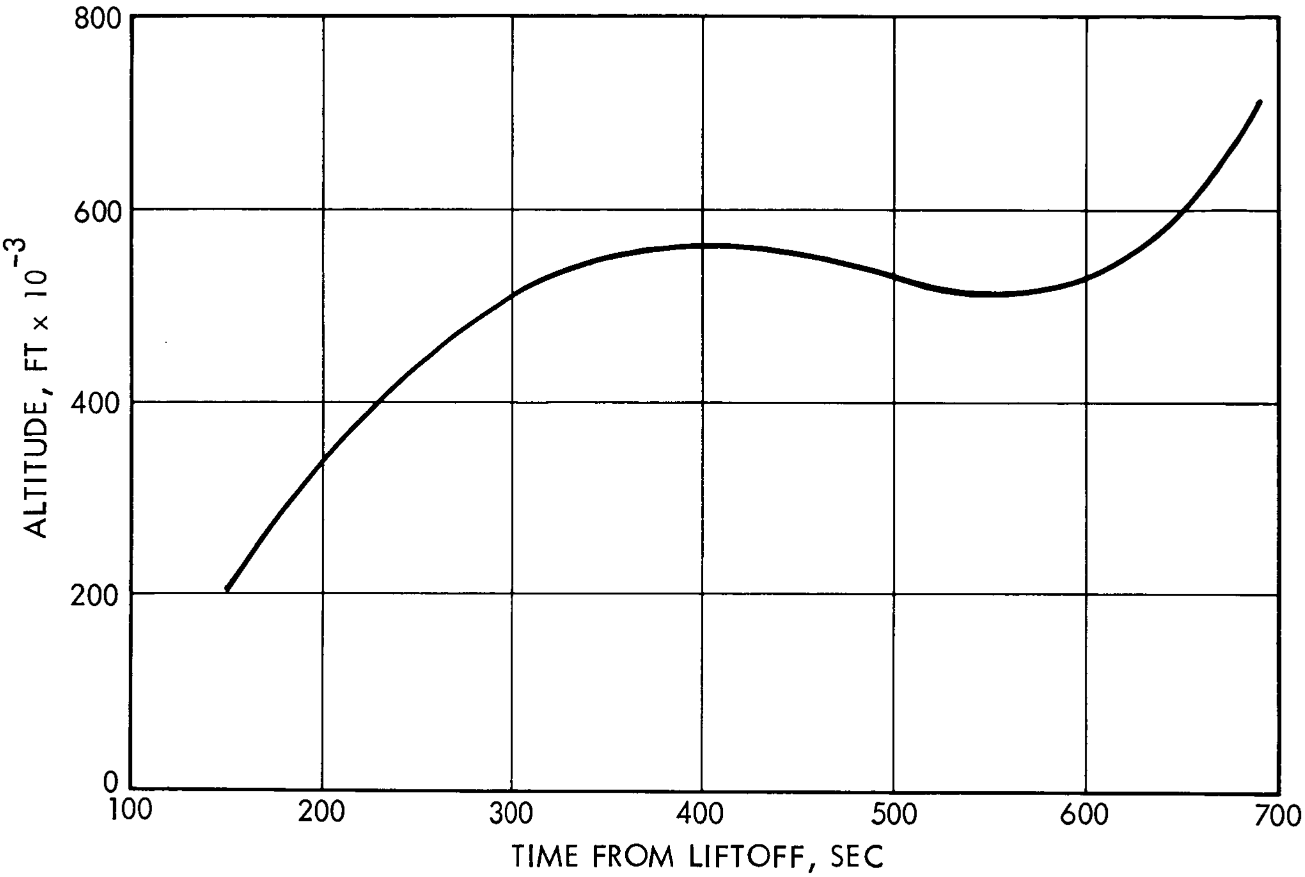

Figure 22. Altitude Versus Time on a Hyperbolic Orbit Injection

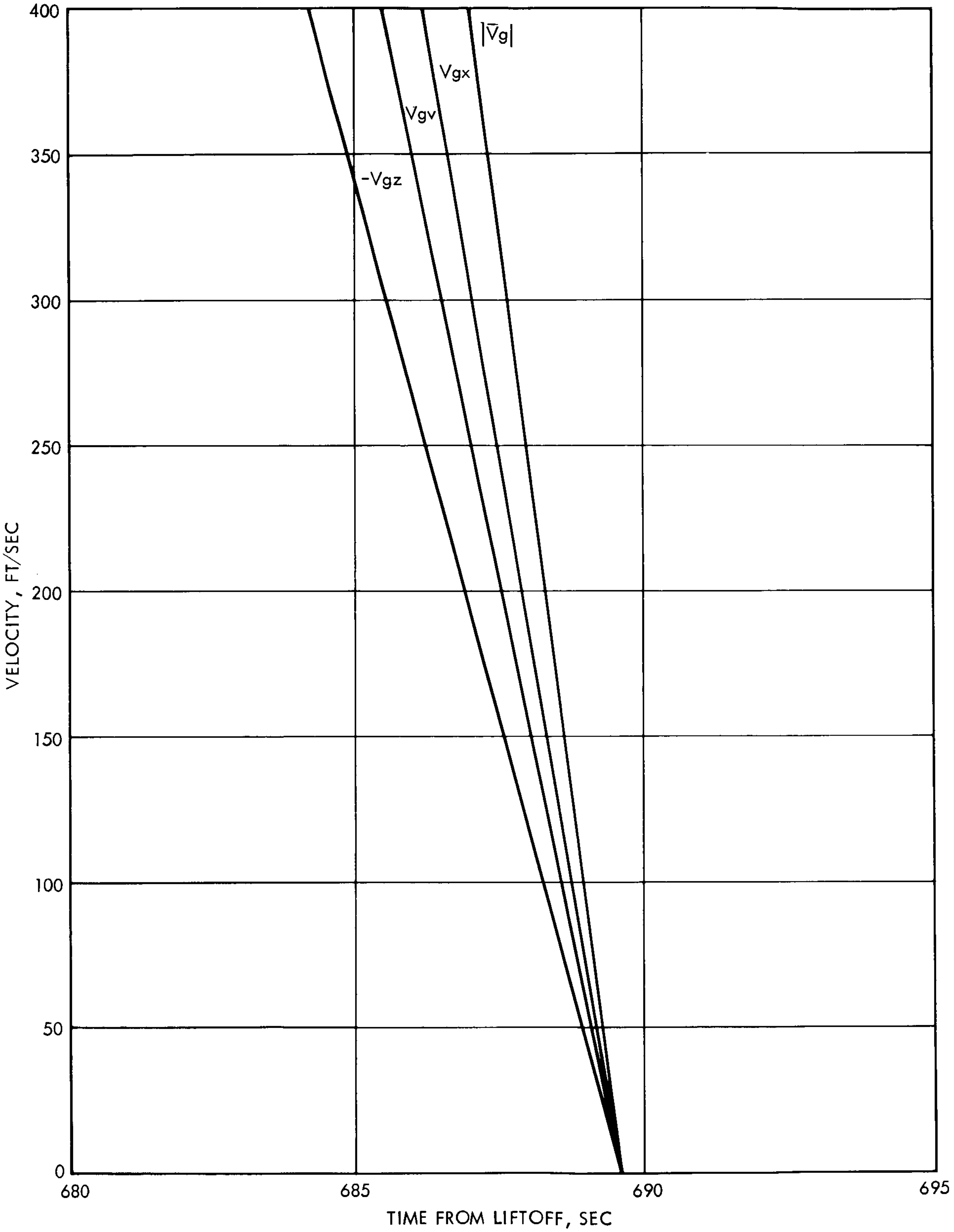

Figure 23. Velocity-to-be Gained, $\overline{V}_g$, in Inertial Coordinates, $K_{95} = 30$

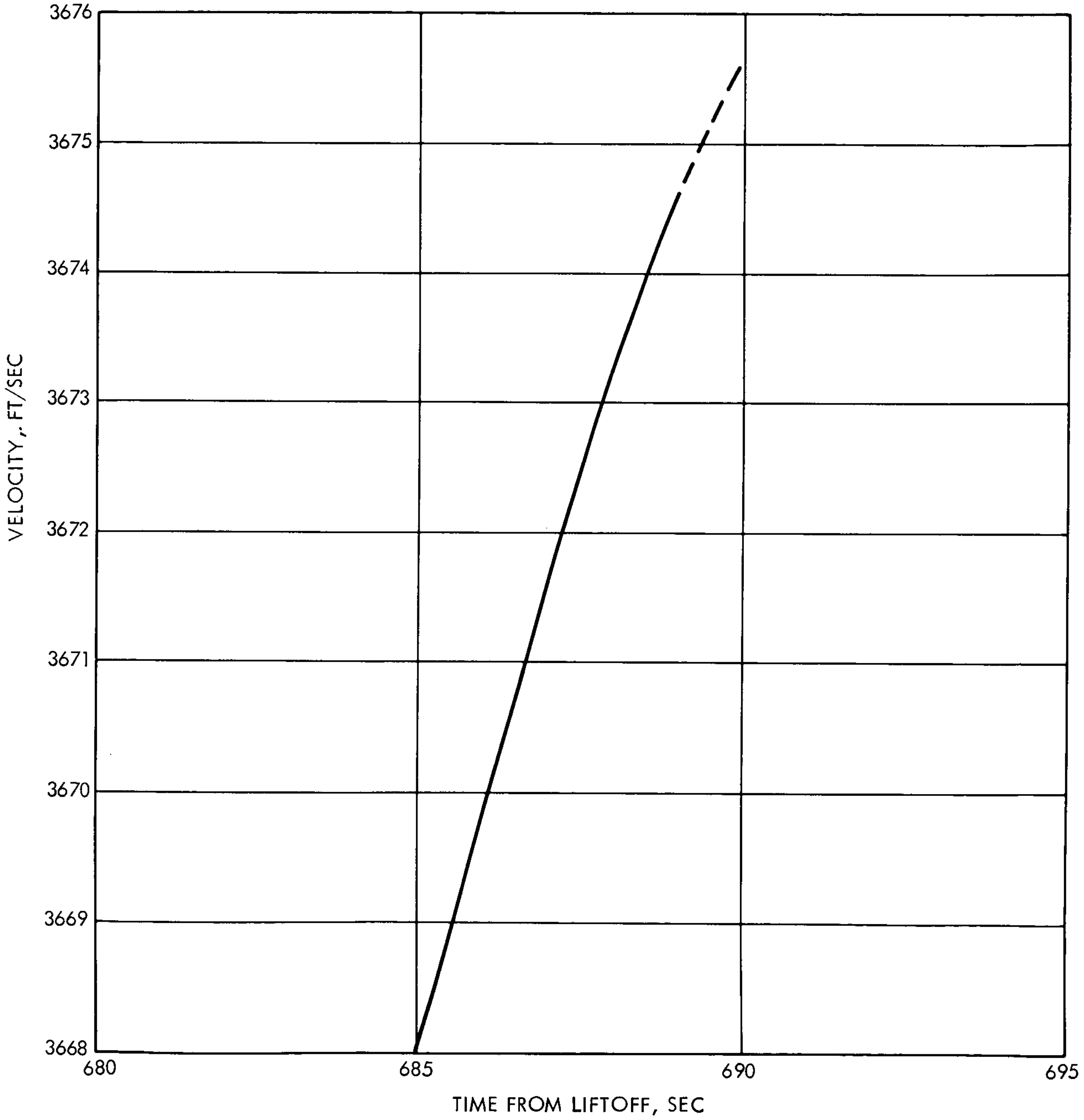

Figure 24. Desired Radial Velocity at Cutoff on a Hyperbolic Orbit Injection

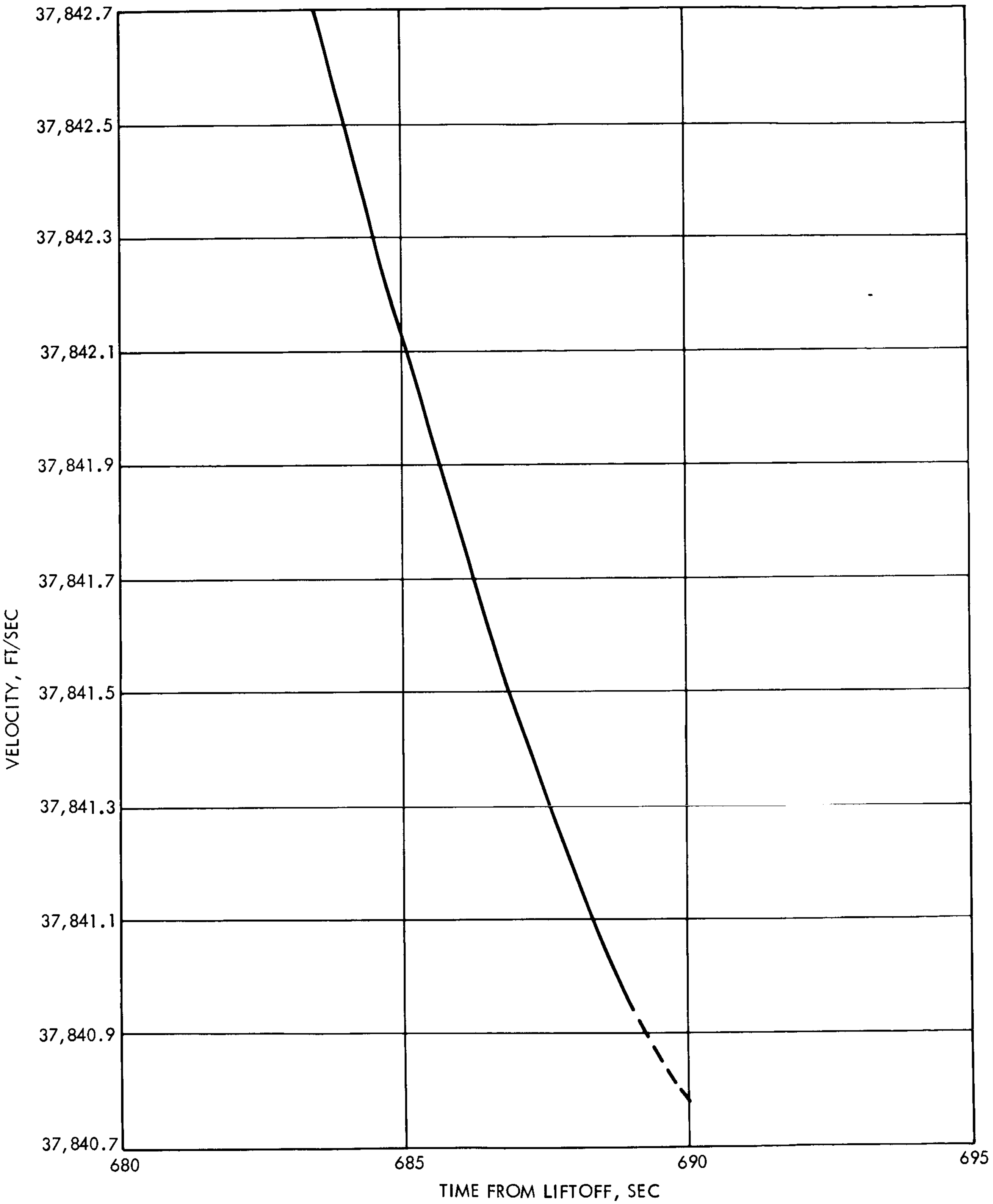

Figure 25. Desired Tangential Velocity at Cutoff on a Hyperbolic Orbit Injection

errors were 2,055 ft in the radial direction and 15 ft in the out of plane direction. These figures were all taken from a simulation with $K_{95} = 30$. The overall performance can be improved slightly by changing K_{95}, as shown below.

The objective of the hyperbolic injection is to obtain a prescribed escape velocity with respect to the earth, $\overline{V}_{oo}$, which insures that the vehicle will have some desired velocity with respect to the sun. The error in attaining $\overline{V}_{oo}$ is then a measure of the software performance. This error is a function of both the velocity and position errors at cutoff. From the vis-viva integral one has

$$v_{oo}^2 = -\frac{\mu}{a} \tag{172}$$

so the magnitude of the final velocity depends only on the semi-major axis of the orbit. This semi-major axis is in turn related to the radius, r_c, and velocity, v_c, at cutoff by the equation

$$a = \frac{1}{\left(\frac{2}{r_c} - \frac{v_c^2}{\mu}\right)} \tag{173}$$

The partial derivatives of "a" with respect to r_c and v_c are

$$\frac{\partial a}{\partial r_c} = 2 \left(\frac{a}{r_c}\right)^2$$

and

$$\frac{\partial a}{\partial v_c} = \frac{2a^2 v_c}{\mu}$$

When the numerical values of this particular simulation are substituted into the above expressions the results are

$$\frac{\partial a}{\partial r_c} = 43$$

$$\frac{\partial a}{\partial v_c} = 48,500 \text{ sec}$$

It might appear at first that the velocity error at cutoff is much more critical than the position error. However, the position error can make important contributions too. For example, the run with $K_{95} = 30$ seconds, the errors were

$$\Delta r_c = + 2,055 \text{ ft}$$

$$\Delta v_c = - 0.21 \text{ ft sec}^{-1}.$$

so that Δr_c contributed + 88,500 ft to Δa, whereas Δv_c contributed -10,200 ft. The actual error observed in this case was $\Delta a = + 72,966$ ft, which is very close to the value predicted by the above linear theory. The resulting error in the magnitude of $\bar{v}_{oo}$ was 4.1 ft sec^{-1}. This simple treatment says nothing about the error in the direction of $\bar{v}_{oo}$. It does, however, point out the fact that both position and velocity error at cutoff are important to the final performances.

By varying K_{95}, the value of time to go at which velocity steering is commanded, it is possible to obtain a compromise between position and velocity errors at cutoff. If K_{95} is made large then the velocity steering is begun early and the velocity errors at cutoff are kept low, while the position errors may be rather larger. On the other hand, if K_{95} is decreased then the position errors are kept small, but the velocity errors get worse. It is clear, then, that there is some optimum value of K_{95} which will give a minimum to the magnitude of the error in $\bar{v}_{oo}$.

Figure 26 presents a plot of the magnitude of the error in $\bar{v}_{oo}$ vs. K_{95}, which shows that the best value of K_{95} is about 15 sec. The error in $\bar{v}_{oo}$ at the value of K_{95} is 3 ft sec^{-1}. The total midcourse Δv provided for interplanetary missions is usually several hundred ft sec^{-1}, so the nominal error is almost negligible.

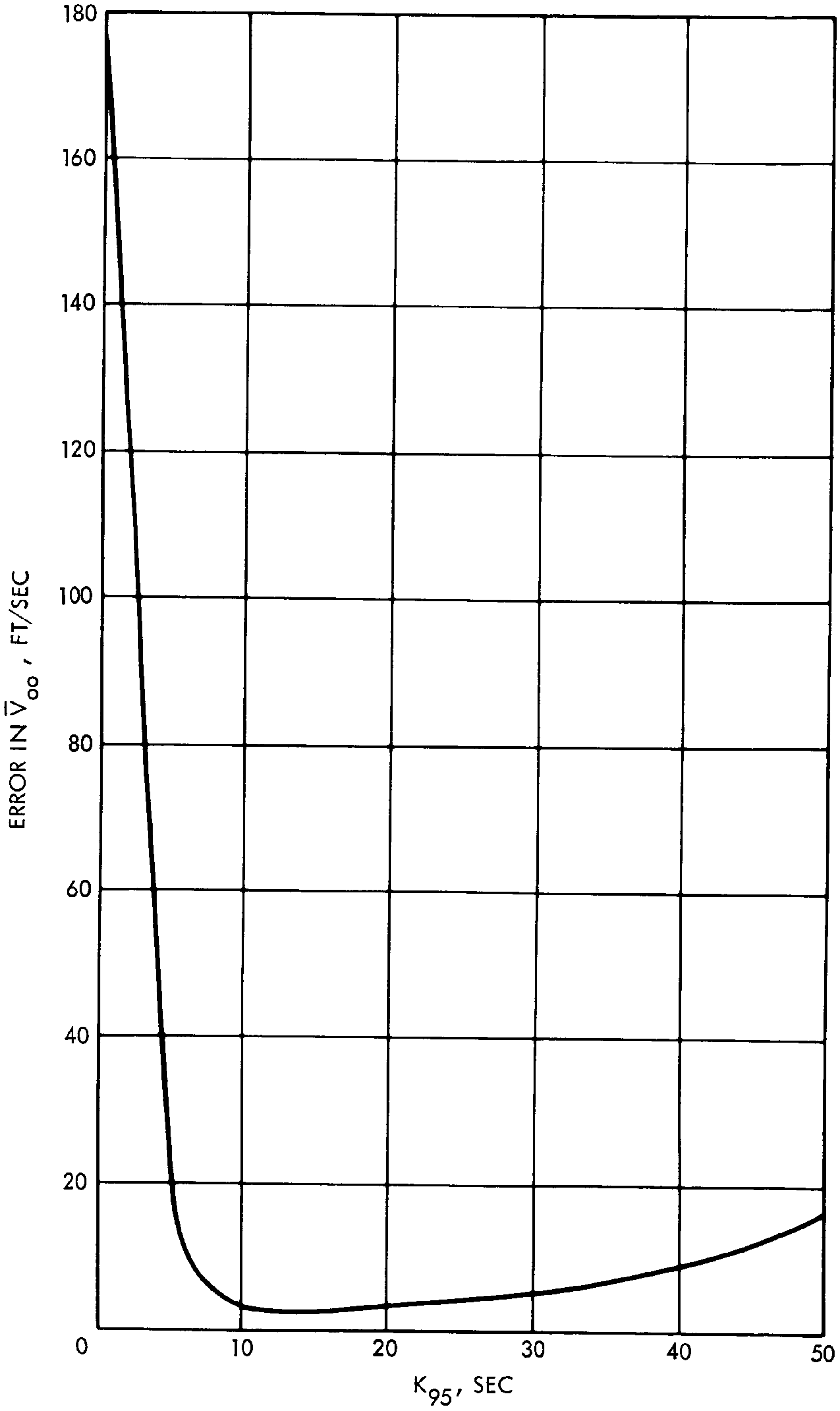

Figure 26. Magnitude of the Error in $\overline{\overline{V}}_{\infty}$ Versus K_{95}

The steering equation performance on a nominal hyperbolic orbit injection is then quite satisfactory from the point of view of both fuel consumption and accuracy.

6.3 INTERCEPT ORBIT INJECTION

The steering equations were checked in the intercept mode by simulating the direct ascent intercept of an artificial earth satellite which had a 148.5 n mi perigee and a 158.5 n mi apogee. It was assumed that the launch site was very close to the orbital plane of the target, and that the two orbital planes were coincident at booster burnout. The simulations were again initialized at the beginning of the sustainer stage, assuming a nominal trajectory up to that point. Table 8 gives the values of the special guidance coefficients used in these simulations. The meanings of the symbols used there are given in Section 9.

The free flight prediction equations, p-iteration equations and search routine were used in these runs to compute the desired velocity at cutoff. The search procedure was used to find the best rendezvous time, t_T, to minimize fuel consumption, subject to the constraint that the perigee altitude be above 300,000 ft. The launch window limits were established by running a number of trajectories with different launch times and noting the time limits on the region of acceptable performance. It was found that excessively high attitude rates were required prior to the opening of the window, and that the perigee altitude became too low after the closing of the window. The window which was finally established was over seven minutes wide. Simulations were obtained for five different launch times within this window. The effects of earth's rotation on the launch site location were ignored in this study, since the earth rotates only 1.75 deg during the launch window.

The general procedure of guiding towards a 90 n mi circular orbit until t = 400 seconds was retained in these simulations, since it seems to give better trajectory shaping and lower fuel consumption. For example, on the trajectory which had a starting time at 6 minutes after the opening of the launch window, the cutoff weight was increased by 421 lbs. by the use of this procedure.

Table 8. Special Guidance Coefficients for the Simulation of the Intercept of a Low Altitude Earth Satellite

K_1 = 5.50×10^9 ft^2 sec^1

K_2 = 5

K_3 = 550×10^9 ft^2 sec^{-1}

K_4 = 300 sec.

K_5 = 3200 sec.

K_{10} = 50 sec.

K_{13} = 21,200,000 ft.

K_{20} = 0.0

K_{22} = 300 sec

K_{30} = 3.0

K_{31} = 0.050

$\bar{r}_o$ = 10,294,364.2; + 17,423,723.0; - 8,338,014.7 ft.

$\bar{v}_o$ = 22,082.41; - 8,849.13; + 8,729.5 ft sec^{-1}

t_o = 3593.1

ν = 1

$\bar{j}$ = 0.14051799; 0.49381829; 0.85813647

Figure 27 shows a plot of the final Centaur weight for various launch times. The weight is increasing for later launch times, which means less fuel is being used. At the end of the window the cutoff weight is almost equal to the 14,150 lbs. observed on the circular parking orbit injection. At the opening of the window the cutoff weight is 13,274 lbs. The increase in final consumption at the opening of the window is due to the fact that the trajectory has to be lofted somewhat to allow the target vehicle to catch up with the Centaur. Towards the end of the window the

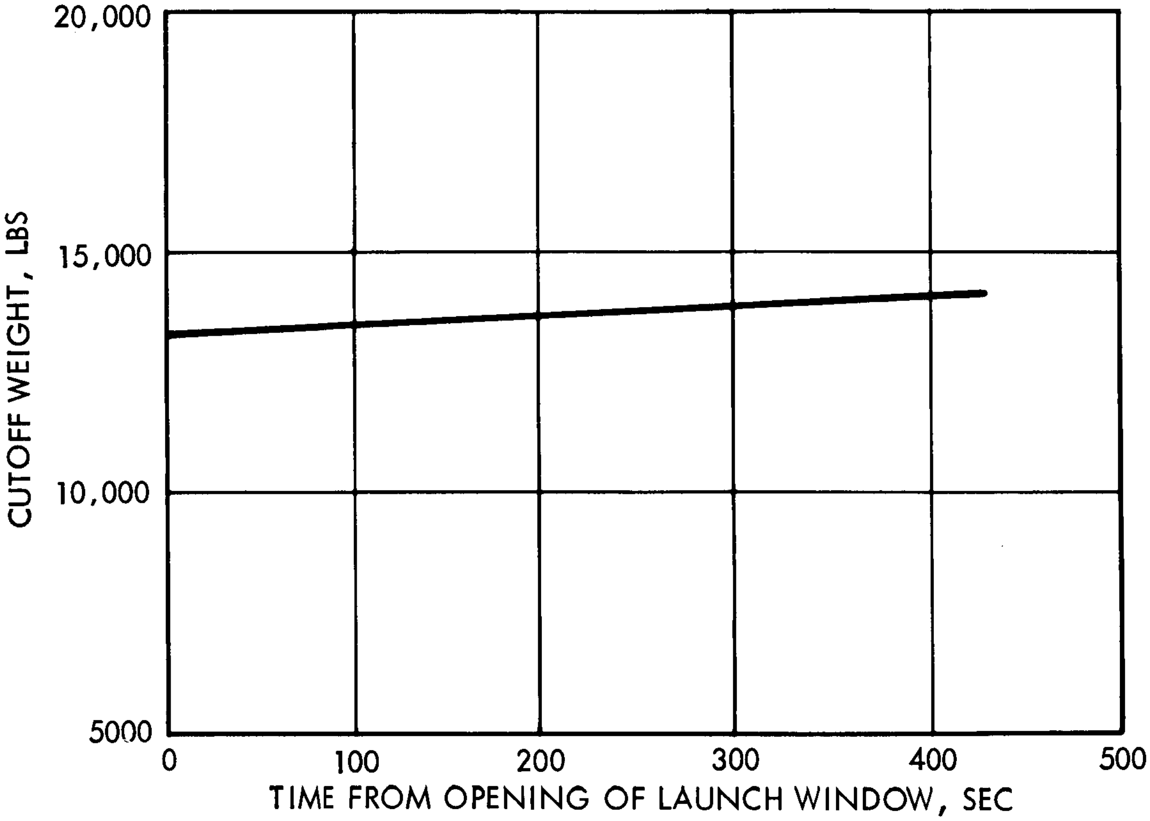

Figure 27. Cutoff Weight for Various Launch Times

phase lead of the Centaur is greatly reduced, so the trajectory is much flatter.

The value of the D coefficient in the steering equations was held at zero in all the simulations. It is possible that even better fuel economy could be obtained if some other value of D were used. The optimum value of D could easily be found by making a number of simulations with different D coefficients.

The lofting required for early launch times is illustrated in Figures 28 and 29 which show the radial velocity and altitude at cutoff for various launch times. It is clear from Figure 28 that the radial velocity at cutoff is a large positive number at the opening of the window, then decreases, goes through zero, and becomes negative at the end of the launch window. At 347 sec, the lift off time for which the radial velocity at cutoff is zero, an almost perfect Hohmann transfer condition prevails. If the launch occurs prior to that time, then the vehicle passes through the apogee of the transfer orbit and comes down on the target vehicle from above. If the launch occurs later than 347 sec then the vehicle passes through perigee on the transfer orbit, and comes up to the target vehicle from below.

The rendezvous time, t_T, chosen by the search routine is plotted in Figure 30. The longest t_T occurs at the launch time corresponding to the Hohmann transfer. All other rendezvous times are higher than this, indicating a transfer of over 180°.

The perigee and apogee altitude on the transfer orbits for various launch times are shown in Figures 31 and 32 respectively. Note that the perigee altitude is always considerably lower than the cutoff altitude except at the launch time corresponding to the Hohmann transfer condition. At that time the two are essentially equal. The perigee altitude decreases very rapidly past the 347 sec. lift off time, soon hitting the 300, 000 ft lower limit at the edge of the launch window. The apogee altitude is very high at the opening of the launch window, because the Centaur must go high above the target vehicle to reduce the phase lead. Increasing liftoff time then produces a linear decrease in apogee altitude until 340 sec point. The apogee altitude then becomes essentially constant at the altitude of the target vehicle.

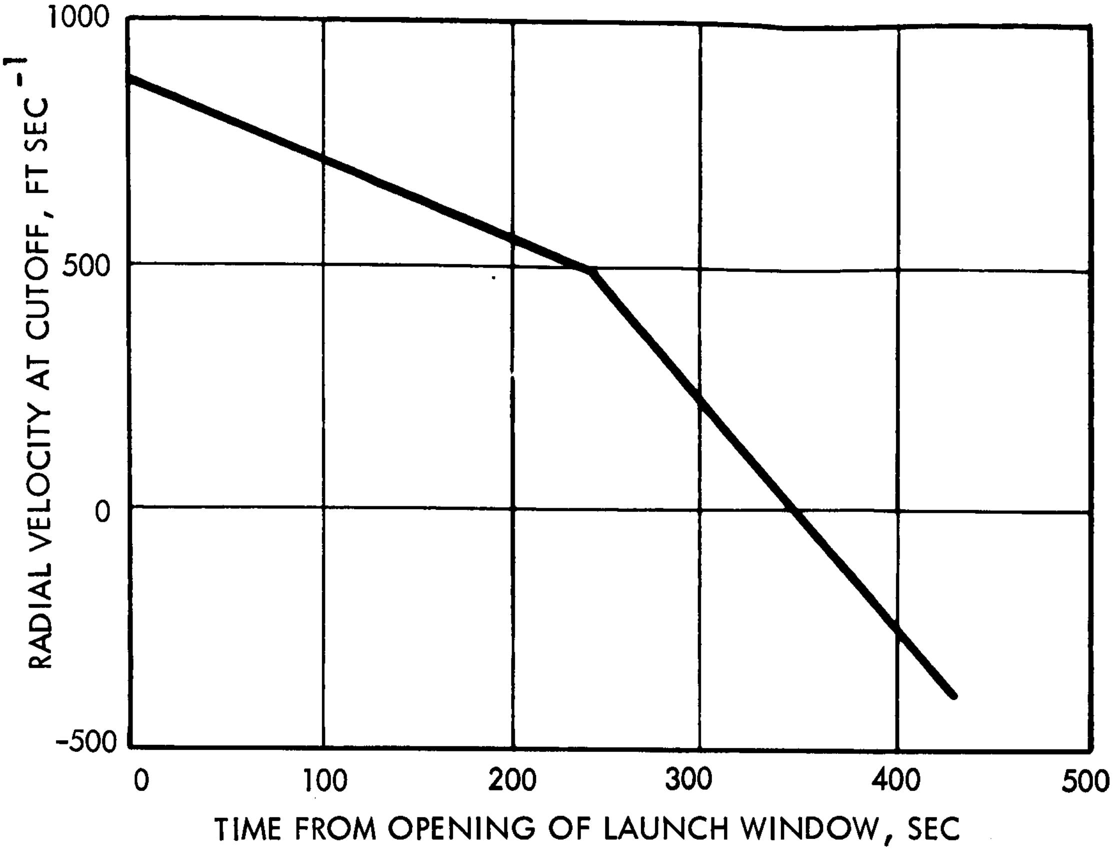

Figure 28. Radial Velocity at Cutoff for Various Launch Times

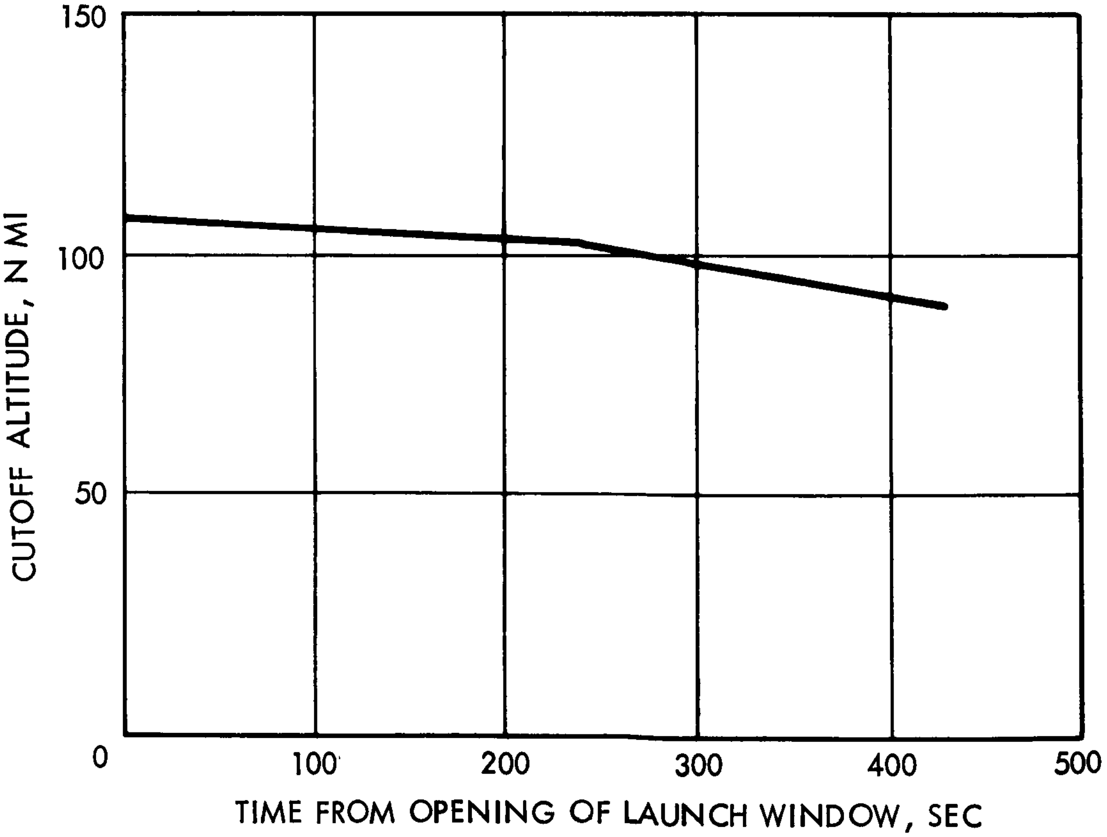

Figure 29. Cutoff Altitude for Various Launch Times

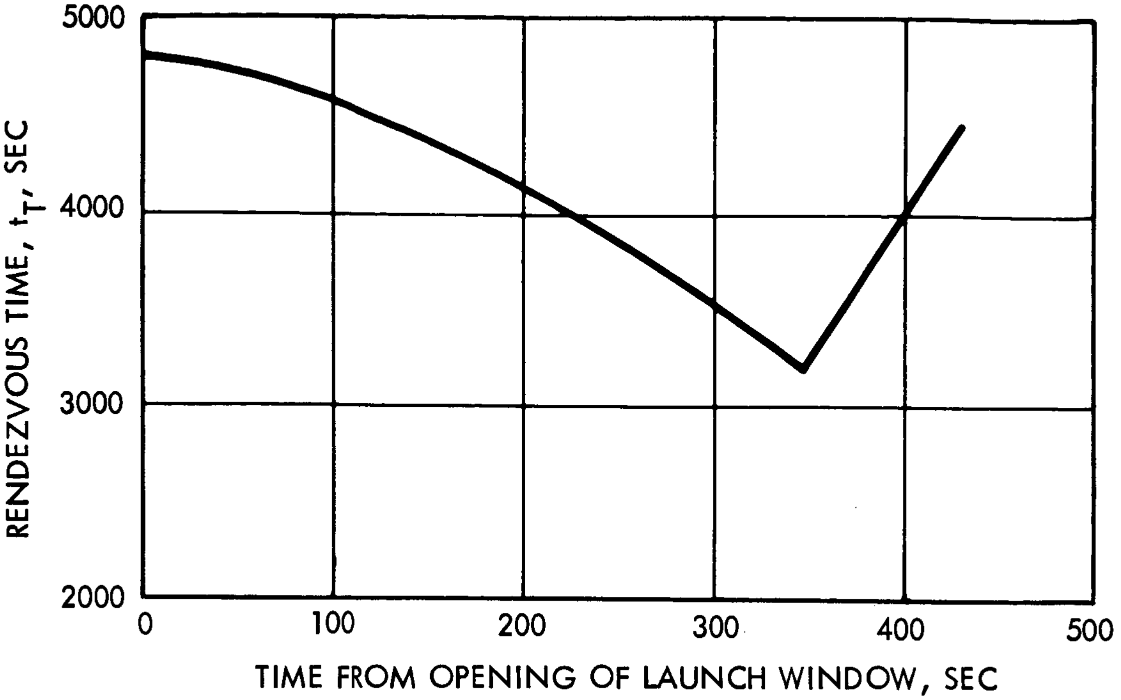

Figure 30. Rendezvous Time, t_T, for Various Launch Times

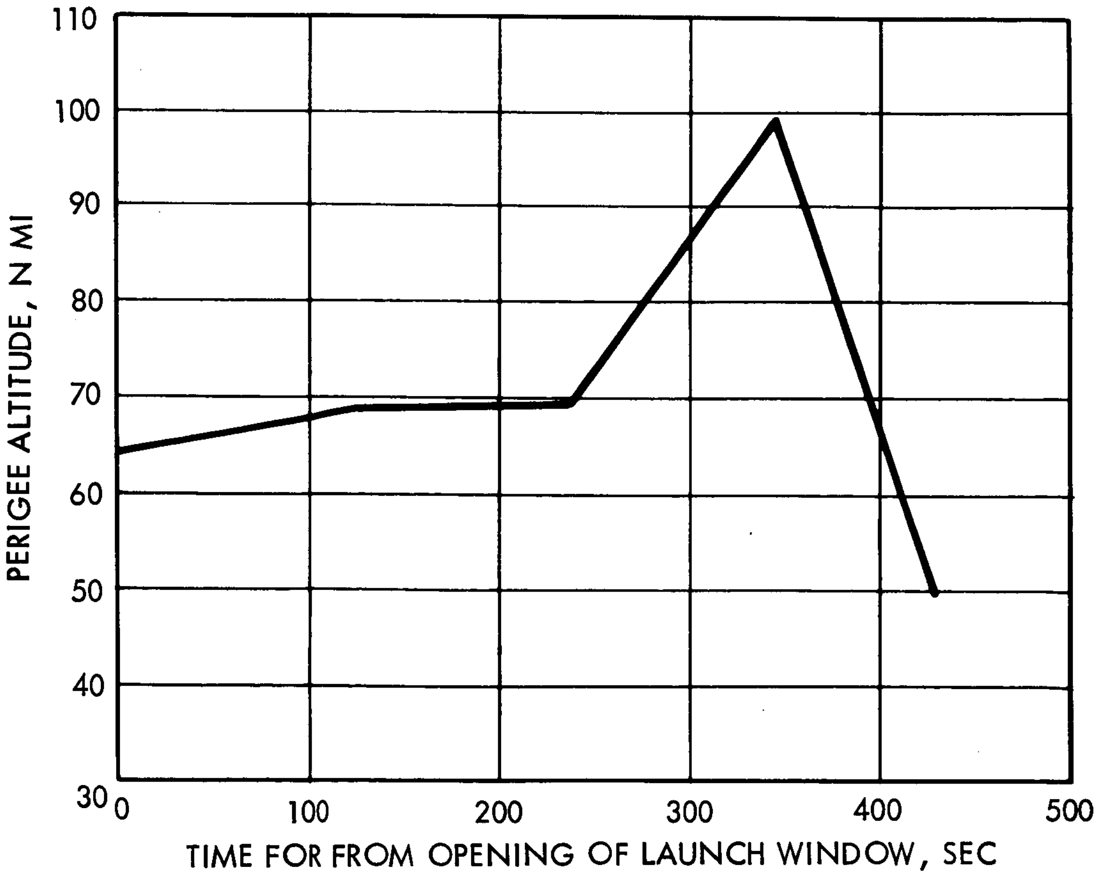

Figure 31. Perigee Altitude on the Transfer Orbit for Various Launch Times

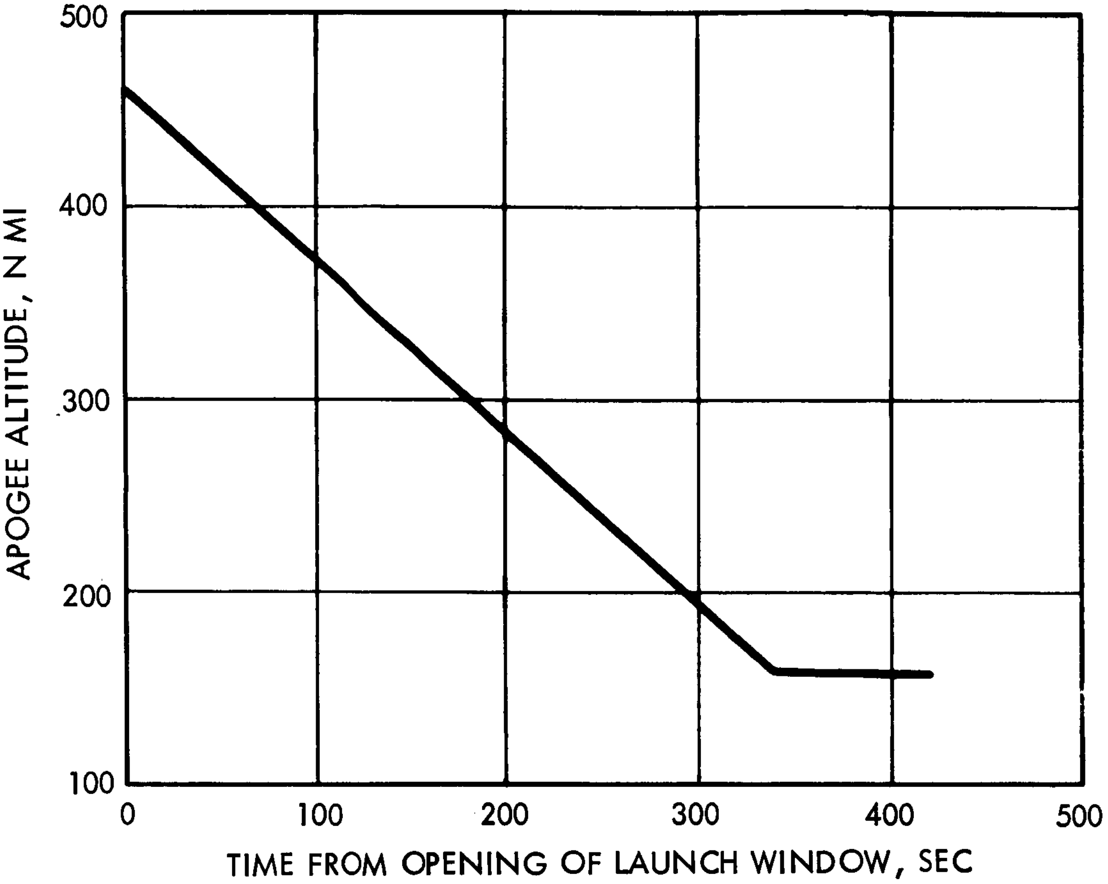

Figure 32. Apogee Altitude on the Transfer Orbit for Various Launch Times

The steering accuracy was again quite good. The cutoff errors in radial and out of plane velocity are summarized in Table 9. The worst error in radial velocity is 0.05 ft sec^{-1}, and the errors in out of plane velocity are all less than 0.01 ft sec^{-1}. These good results are due to the fact that the guidance equations are in the velocity steering mode for the entire time that the intercept equations are being used. The equations are designed to stop the search procedure some time before cutoff is reached, so that the rendezvous time, t_T, and position, $\overline{r}_T$, becomes constant. The desired velocity then becomes nearly constant, except for small variations due to errors in predicting the cutoff position. These variations do not cause any significant problems, as shown by the above accuracy figures.

The target misses observed at the chosen rendezvous time are not as small as might be expected from the figures on steering accuracy. These misses are summarized in Table 10 for the various launch time. The worst miss is 3908 ft, which occurs at the opening of the launch window. Because the steering errors are so low, these misses must largely be attributed to the cutoff routine. The observed misses are still low compared to what can be expected from IMU errors, tracking errors, and oblateness effects. The gravity forces due to the earth's oblateness have been neglected in the computation of desired velocity, and hence will be a source of target miss. It should also be pointed out that the miss figures given here are for a fixed time. The miss at the point of closest approach will be somewhat smaller in every case.

The characteristics of the trajectories flown for various launch times are all quite different. Only the data on the first trajectory will be given here to avoid unnecessary detail. The first trajectory was chosen because the vehicle will always be launched at the opening of the launch window unless mechanical difficulties have occurred.

Table 9. Cutoff Errors in Radial and Out of Plane Velocity for Various Launch Times

Launch Times	$(\Delta\dot{r})$	$(\Delta\dot{y})$
0 sec	0.05 ft sec^{-1}	0.01 ft sec^{-1}
120	0.02	0.01
240	0.02	0.01
360	0.03	0.01
420	0.02	0.01

Table 10. Summary of Target Miss For Various Launch Times

Launch Time	ΔX	ΔY	ΔZ	$\sqrt{(\Delta X)^2 + (\Delta Y)^2 + (\Delta Z)^2}$
0 sec	-1,697 ft.	+3,110 ft.	+1,398 ft.	3,809 ft.
120	- 958	+2,747	-1.426	3,240
240	+ 408	+2,146	-1,303	2,544
360	1,241	+1,595	-1,124	2,312
420	+ 58	+ 202	- 108	236

Figure 33 shows the inertial components of $\bar{v}_g$ in the vicinity of cutoff. These components are all driven through zero simultaneously, which again demonstrates the accuracy of the steering equations.

Figure 34 shows the inertial components of the predicted cutoff position, $\bar{r}_D$, as a function of time. The very first point has large errors in it because $\bar{r}_D$ is set equal to $\bar{r}$, i.e., there is no prediction. The curves are then fairly smooth until the staging region. Another discontinuity occurs at the 400 sec point where the intercept guidance is

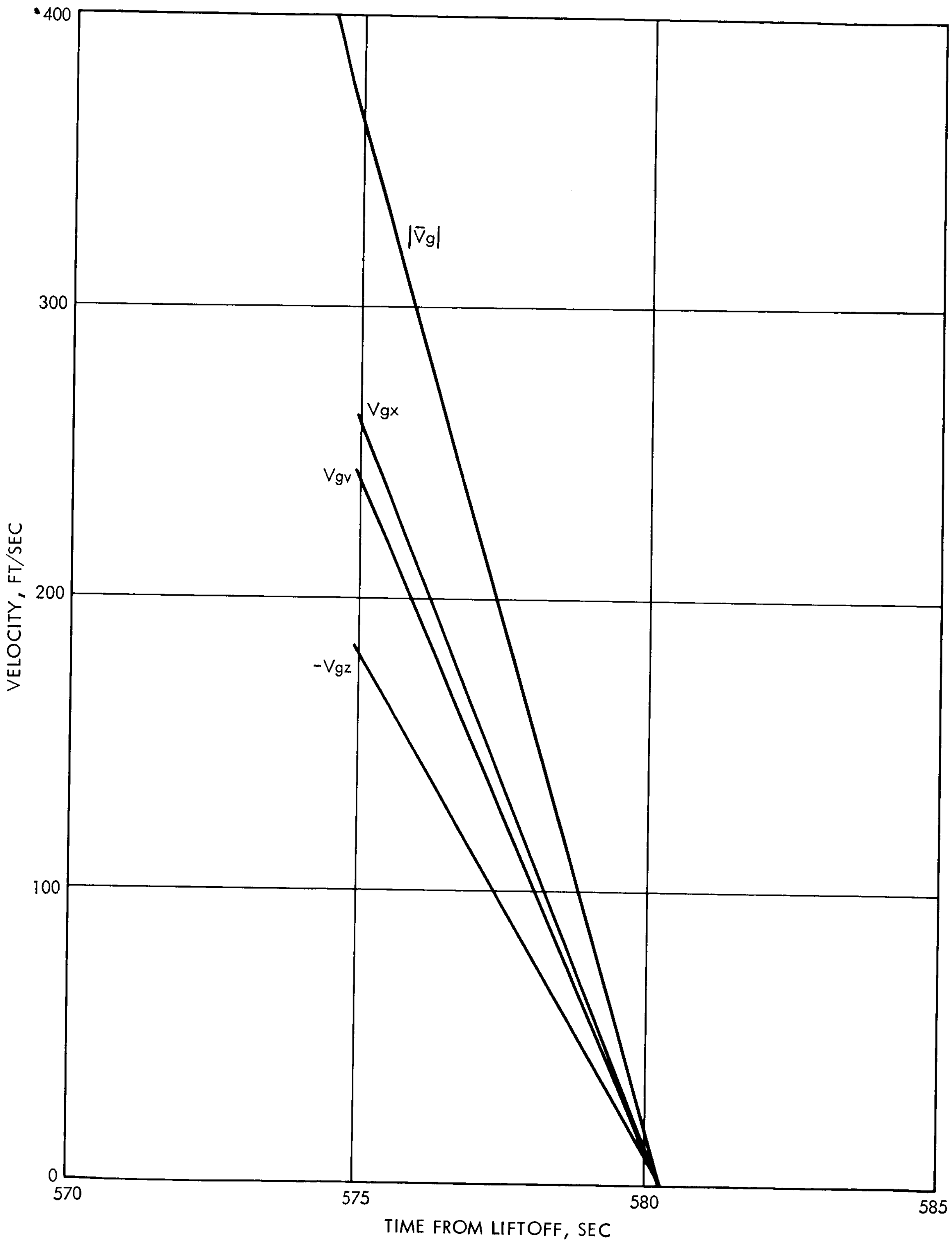

Figure 33. $\overline{V}_g$ Components Near Cutoff on the First Intercept Trajectory

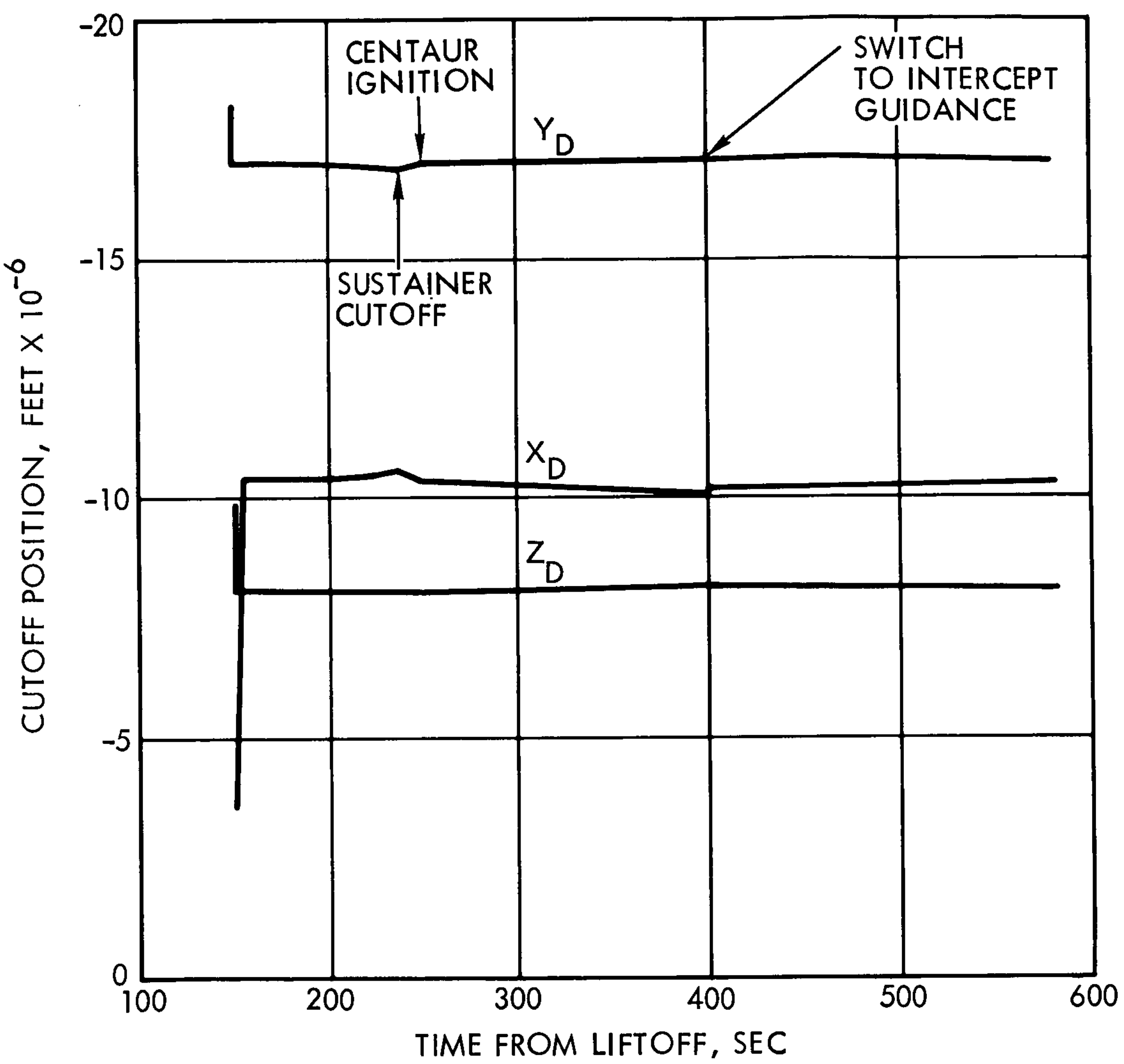

Figure 34. Predicted Cutoff Position on the First Intercept Trajectory

initiated. The curves are remarkably smooth, however, considering the fact that the vehicle is steering towards a parking orbit for the first 400 seconds.

Figure 35 shows the inertial components of desired velocity, $\bar{v}_d$, which is computed at the predicted cutoff position, $\bar{r}_D$. The initial values contain large errors because of the error in $\bar{r}_D$. The jumps at 400 seconds are due to the switch from circular orbit injection steering to intercept guidance. This change amounts to less than 1,000 ft sec^{-1}, however, which is relatively small. The small changes occurring past this time are due to errors in the prediction rountine, which cause $\bar{r}_D$ to change.

Figure 36 shows the time to go (T) as a function of time. Note the small jump in T at the 400 second point.

In summary, then it can be stated that the steering equations give satisfactory performance with respect to fuel consumption and accuracy when used in the intercept guidance mode.

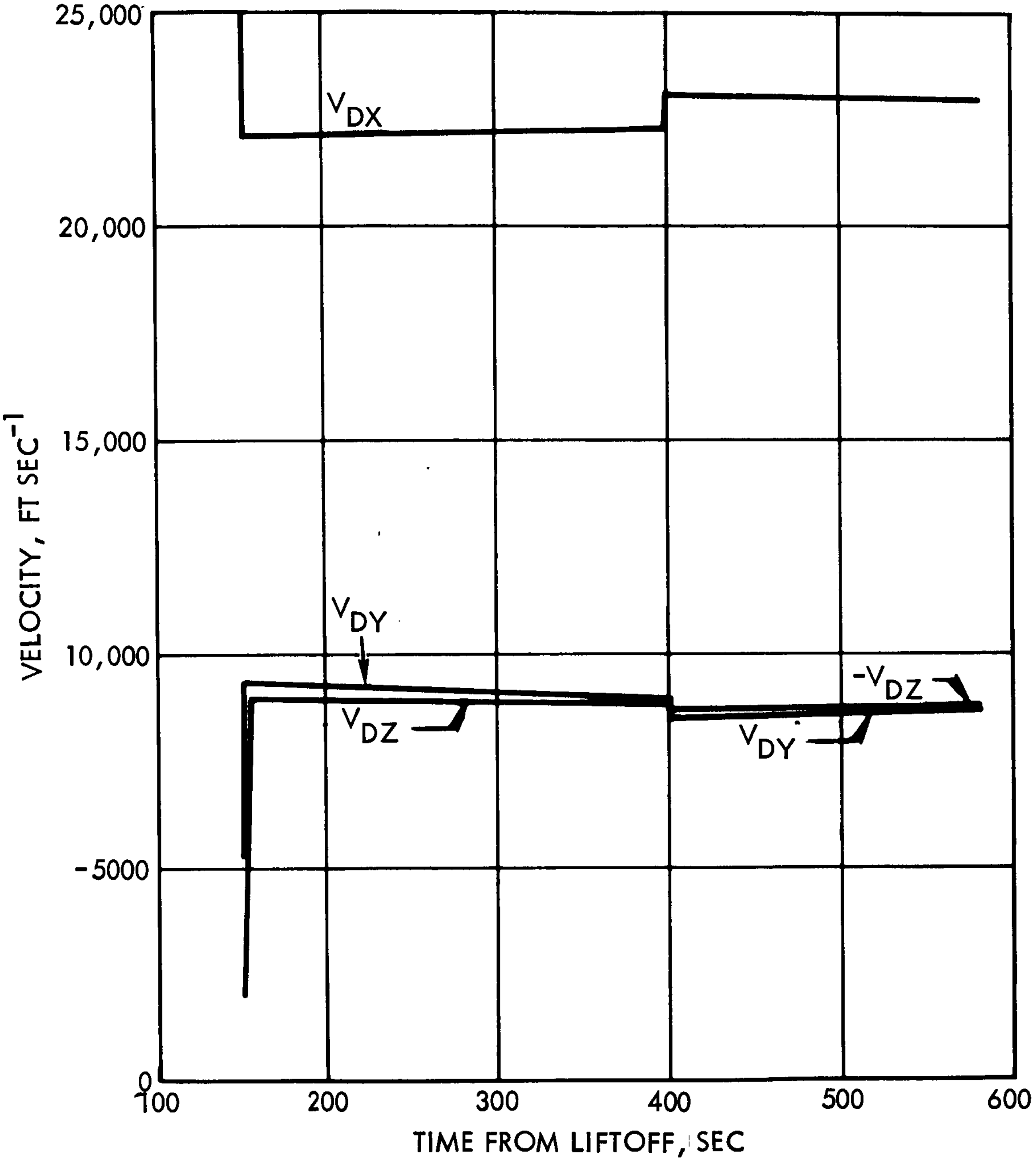

Figure 35. Desired Velocity Components on the First Intercept Trajectory

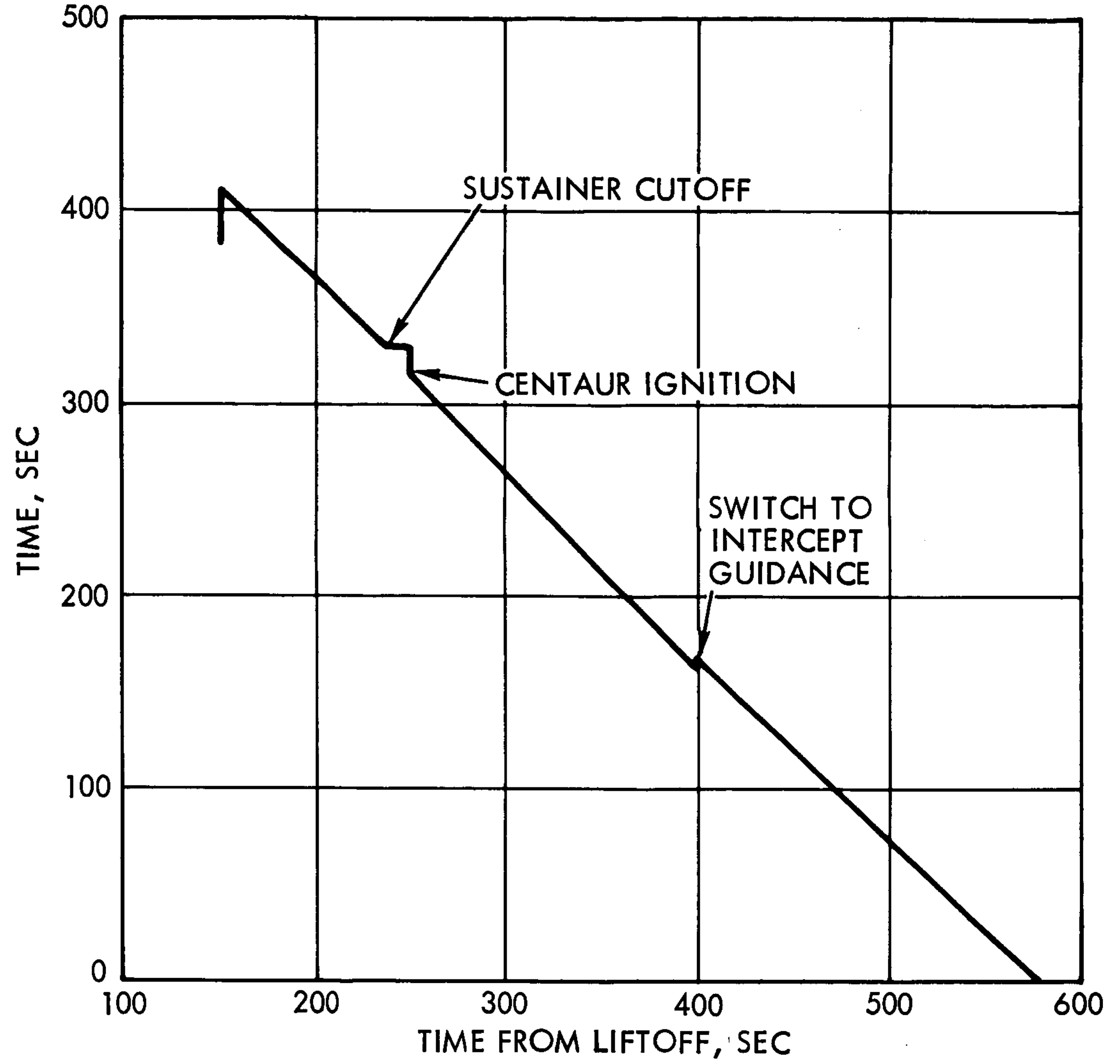

Figure 36. Time to go to Cutoff on the First Intercept Trajectory

7. PERFORMANCE OF INTERCEPT EQUATIONS

7.1 GENERAL

The intercept equations are used in any situation where it is desired to hit an earth satellite having a known ephemeris while using a minimum of fuel. These equations are used for intercept of artificial earth satellite, for lunar missions, and for Comsat missions. Comsat missions are handled by requiring intercept of a fictitious earth satellite in the desired Comsat orbit.

Whenever intercept is required, ν will be set to unity in the initialization equations of the flow charts, which calls into play the free-flight prediction equations, the p-iteration equations, and the search logic. The operation of this combination was described earlier in Section 5.3.1. The final output is the desired velocity, $\overline{v}_D$, needed at the predicted cutoff point to hit the target at an optimum rendezvous time, t_T. The purpose of this section is to give some performance data on each of these blocks of equations, and on the overall combination. The problem of introducing biases to account for earth's oblateness gravity effects and for lunar gravitational effects will also be discussed.

7.2 P-ITERATION EQUATIONS

In every case which was tested during the course of the study it was found that the p-iteration scheme converged to within sufficient accuracy after six iterations. Table 11 shows the results of each of these iterations in a typical case where the vehicle is near cutoff on a translunar injection. The actual difference between t_T and t_D was 226,163.71 sec., so the final value shown in Table 11 is in error by only 0.20 seconds. The corresponding error in the desired velocity, $\overline{v}_D$, was less than 0.03 ft. sec^{-1}, out of a total of about 36,000 ft. sec^{-1}.

In the case considered in Table 11 the initial value of h_D was far enough removed from the final value that five iterations were required for convergence. The scheme will generally converge even faster when used with the guidance equations because the initial value of h_D is taken to be the final value of h_D computed on the previous pass through the p-iteration

Table 11. Performance of the P-Iteration Equations

Iteration No.	τ_{12}	h_D
0	240,714.42 sec.	7.1900000×10^4 km^{2}sec^{-1}
1	238,806.13	7.1907189×10^4
2	226,854.83	7.1954822×10^4
3	226,198.80	7.1957576×10^4
4	226,163.91	7.1957722×10^4
5	226,163.91	7.1957722×10^4

equations. On the very first guidance cycle, however, it is always necessary to use an initial guess. This initial guess is denoted by K_3 in the flow charts. A fixed value of K_3 will generally serve quite well for a wide variety of conditions. For example, it was found that a fixed value of K_3 gave good results at a series of points taken across a lunar launch window on a direct ascent mission.

Even better accuracy on free fall time, τ_{12}, is obtained in other applications. For example, in the case of a low altitude satellite intercept run, the errors in τ_{12} were generally less than 0.001 seconds out of a total of about 3,000 seconds. All of these figures are, of course, independent of the errors arising from the use of two body equations to describe the motion of the vehicle, which neglects the gravity forces due to earth's oblateness and due to the mass of the moon.

The ratio of the initial value of Δh_D used in the iteration procedure, denoted by K_1 in the flow charts, to K_3 is quite mission dependent. For the low altitude satellite intercept it was found that $K_1 = 0.01\ K_3$ worked quite well, but such a value was too large on a translunar injection. In the latter application a value of $K_1 = 0.001\ K_3$ was found to work satisfactorily.

7.3 FREE-FLIGHT PREDICTION EQUATIONS

The rate of convergence of the iteration procedure used in solving Keplers equation was found to be highly dependent on the eccentricity of the orbit being predicted. Less than three iterations are required for low eccentricity orbits. However, highly eccentric orbits can require up to ten iterations for good results. Table 12 shows a typical iteration sequence for prediction of an orbit with an eccentricity of 0.985. The purpose of these iterations is to solve the transcendental equation

$$\Delta E = -S(1 - \cos\Delta E) + C \sin \Delta E + \Delta M$$

for ΔE. The actual mechanization is carried out by rewriting the above equation as $f(\Delta E) = 0$, and then iterating until a value of ΔE is found which will satisfy this equation.

Table 12 shows that in this case convergence is reached after the 8th iteration, even though a somewhat better solution was available on the 7th. The final solution for $f(\Delta E)$ is not actually zero because of round-off error in the digital computer. In this case it appears that after the 5th iteration the solution is essentially unchanged. However, in some other cases it was found that the use of seven iterations still led to some residual error, and that ten iterations were actually needed.

The final choice of the number of iterations to be used here will depend a great deal on the applications to be made of the free flight prediction equations. If they are only used in predicting the position of a target vehicle then a lower number of iterations might be acceptable, since most targets will have reasonably low eccentricities. However, there is the possibility that these equations might also be used as a

Table 12. Performance of the Free Flight Prediction Equations

Iteration No.	$f(\Delta E)$
0	-0.42208285
1	+4.68407780
2	-0.27248116
3	+0.15442495
4	+0.01146152
5	+0.00008622
6	-0.00000003
7	+0.00000000
8	-0.00000001
9	-0.00000001
10	-0.00000001

navigational aid, in which case they would be required to handle quite high eccentricities. For the present, it will be necessary to assume a worst case situation, i.e., that ten iterations are required.

Comparison of these solutions with those of numerical integration routines are somewhat useless, since they only show up the numerical integration errors.

7.4 BIAS EQUATIONS

The use of two body equations in free flight prediction and in computing $\overline{v}_D$ will, of course, lead to errors if nothing is done to account for the gravity forces due to the earth's oblateness and due to the mass of the moon. These effects can generally be ignored in the case of rendezvous with an artificial earth satellite, since they are small and can be detected via radar in the latter phases of the mission. The additional fuel needed to correct these errors is not a critical factor in such missions. However, in the lunar mission the effects of lunar gravity on the trajectory are relatively large, and the amount of fuel available for midcourse correction is quite limited. Hence, translunar injections require a rather accurate compensation of these effects. This section describes some of the work which was done to establish an effective method for making this compensation.

Figure 37 shows some of the variables involved in the biasing problem. The location of the center of the moon at the time of impact, t_T, is denoted by $\overline{R}_m$. The actual cutoff conditions needed to impact the desired point on the lunar surface, as determined by a complete numerical integration solution, are denoted as $\overline{r}_D$, $\overline{v}_D$, and t_D. If these conditions are used in the two body prediction routine then the resulting position at time t_T, denoted as $\overline{r}_T$, is displaced somewhat from the actual impact point. The difference, $\overline{r}_T - \overline{r}_M$, is the total bias vector, $\overline{b}$. The $\overline{b}$ vector gives the required compensation for the earth's oblateness gravity force, and also describes the target location on the lunar surface.

The guidance equations employ the free flight prediction routine to compute $\overline{r}_M$ for each value of t_T. The bias vector, $\overline{b}$, must then be added to $\overline{r}_M$ in order to obtain the aiming point, $\overline{r}_T$. If the prediction of $\overline{r}_M$ is correct, and if the proper $\overline{b}$ vector is added to $\overline{r}_M$, then the value of $\overline{v}_D$

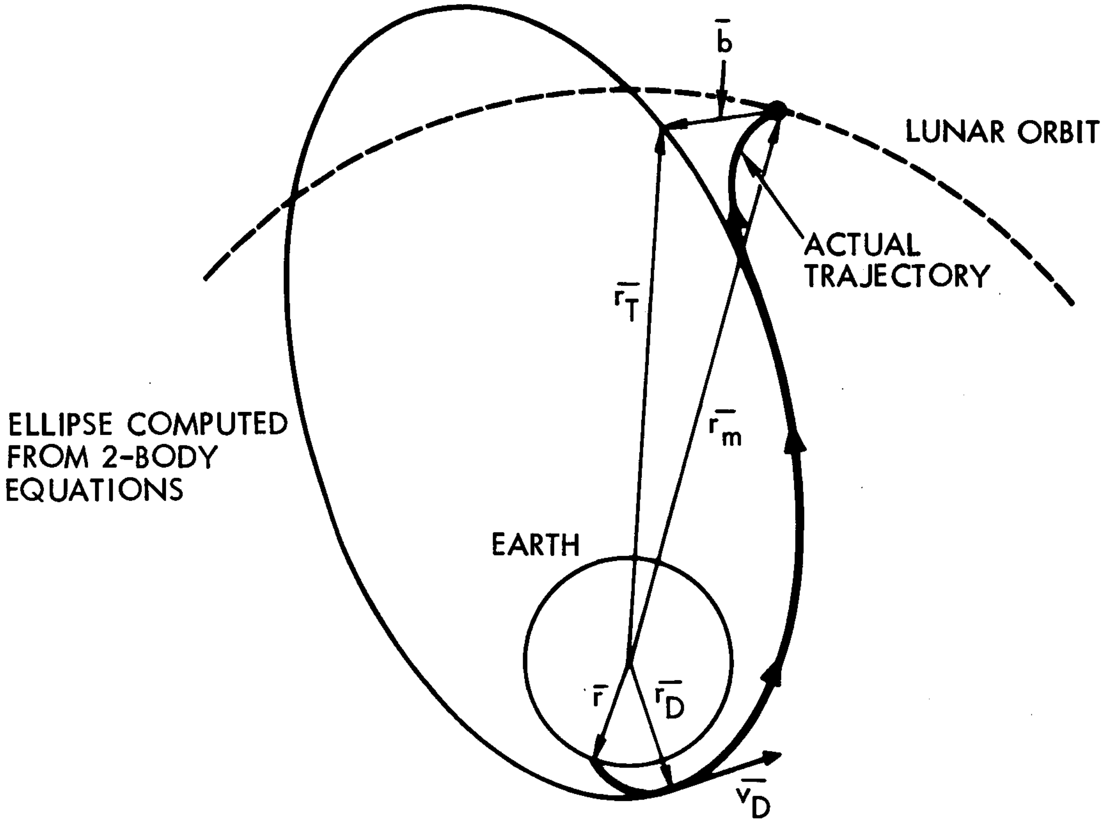
$\bar{b}$
LUNAR ORBIT
ACTUAL TRAJECTORY
$\bar{r}_T$
$\bar{r}_m$
ELLIPSE COMPUTED FROM 2-BODY EQUATIONS
EARTH
$\bar{r}$
$\bar{r}_D$
$\bar{v}_D$

Figure 37. Diagram of the Lunar Biasing Problem

computed by the p-iteration equations will, by necessity, be correct. The errors in predicting the moon's position and in computing the bias vector are then pertinent to the accuracy discussion.

The accuracy of predicting the moon's position was tested by comparing the results obtained from the free flight prediction routine with an actual ephemeris over the range of impact times encountered for a single launch window. The data which was used was that of the Centaur/Surveyor mission. The particular launch window was that of September 30, 1965. The free flight prediction routine was initialized by using the actual position and velocity of the moon at the impact time which was closest to the middle of the impact time range. Table 13 shows the resulting errors in inertial coordinate for six impact times which just about span the range of impact times for this launch window. The worst error is less than 0.5 km, which is quite satisfactory. The allowable uncorrected software miss at the surface of the moon is 2 deg for the present guidance system, which is equivalent to about 60 km. Judging from these results it might even be possible to initialize the free flight prediction equation only once during a launch opportunity of several days, rather than initializing at each launch window. Further work needs to be done to establish the time span over which this approach will work.

The $\overline{b}$ vector was also computed for several impact times during this same launch window to determine its behavior and to find the simplest way of representing it. Figure 38 shows the three coordinates of the $\overline{b}$ vector as a function of the impact time, t_T, as measured in inertial coordinates. Figure 39 shows a similar plot of $\overline{b}$ as measured in a

Table 13. Error in Predicting the Position of the Moon

Case	Impact Time	ΔX	ΔY	ΔZ
1	224,147.358 sec	-0.13 Km	-0.08 Km	-0.04 Km
2	224,597.884	-0.14	-0.08	-0.02
3	224,964.706	+0.26	-0.05	-0-
4	226,164.306	-0-	-0-	-0-
5	227,544.510	-0.45	-0.15	-0.03
6	229,709.744	-0.43	-0.38	-0.13

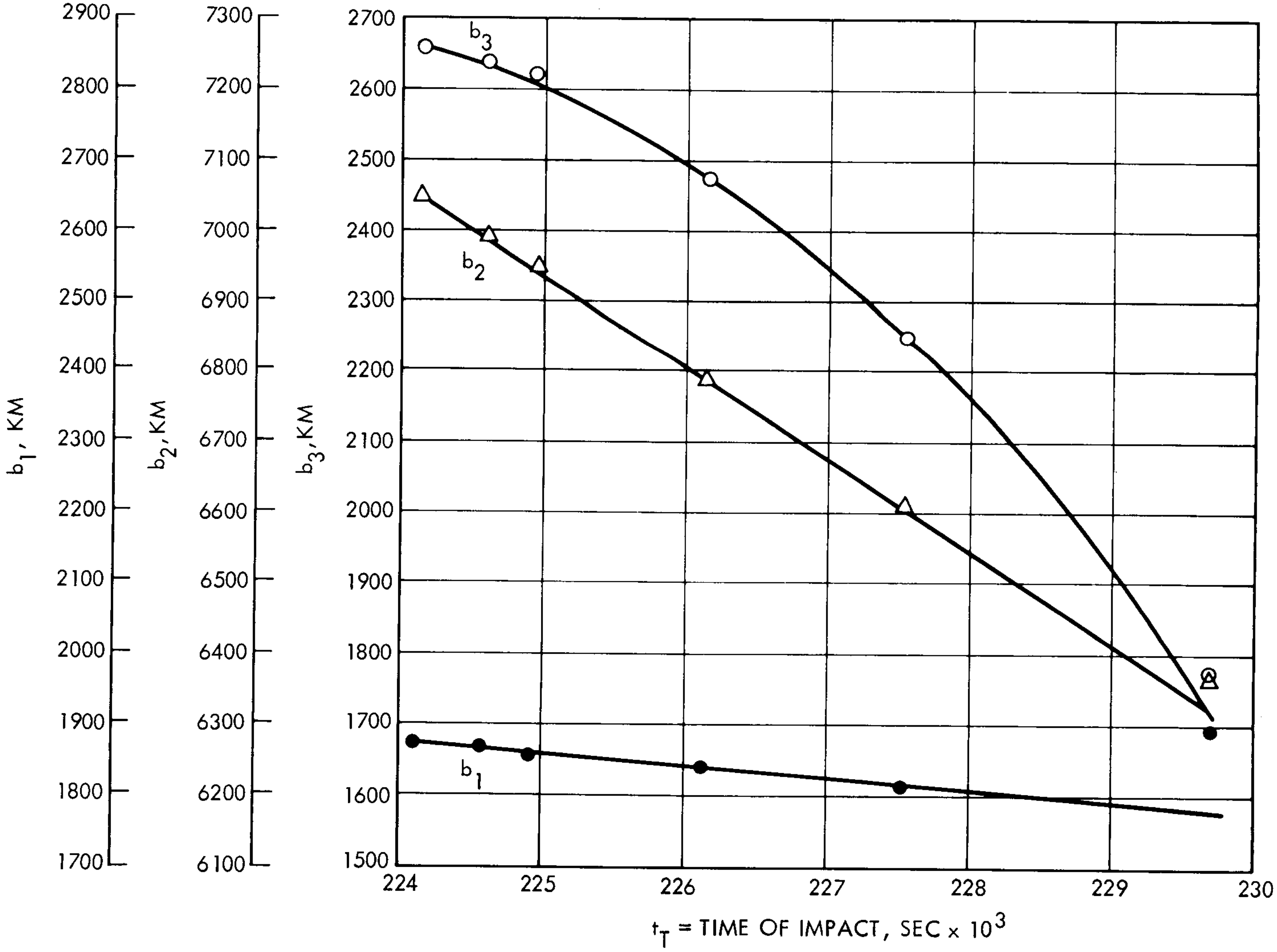

Figure 38. The b Vector in Inertial Coordinates vs. Time of Impact

cylindrical coordinate frame which rotates with the moon. There was some speculation that the $\overline{b}$ vector might be more nearly constant in the rotating coordinate frame than in the inertial frame. However, Figure 38 and 39 show that there is no advantage to using the rotating frame. The inertial representation is much easier to handle in the Airborne Digital Computer (ADC), and hence was chosen as the preferred mechanization.

The curves connecting the data points in Figure 38 were computed from the equations

$$b_1 = K_{61} + K_{62}(t_T - t_0)$$
$$b_2 = K_{63} + K_{64}(t_T - t_0)$$
$$b_3 = K_{65} + K_{66}(t_T - t_0) + K_{67}(t_T - t_0)^2$$

which will be used in the A.D.C. to compute the bias vector for a particular impact time. The coefficients in these equations will, of course, be dependent on the particular launch window in question and will have to be recomputed accordingly. The particular values used for Figure 38 were

$K_{61} = 1,843.11$ km
$K_{62} = -0.0166$ km sec^{-1}
$K_{63} = 6,788.0$ km
$K_{64} = -0.130$ km sec^{-1}
$K_{65} = 2477$ km
$K_{66} = -0.1342$ km sec^{-1}
$K_{67} = -0.222\text{x}10^{-4}$ km sec^{-2}

The quantity t_0 appearing in the bias equations was chosen to be the same as the time of initialization of the moon's position and velocity, which in this case was near the middle of the range of t_T values, i.e., at $t_T = 226,164.306$ seconds.

The nominal cutoff conditions employed in this study were obtained from closed loop runs using the existing Centaur guidance equations, which led to some impact error at the moon. The lunar latitudes and

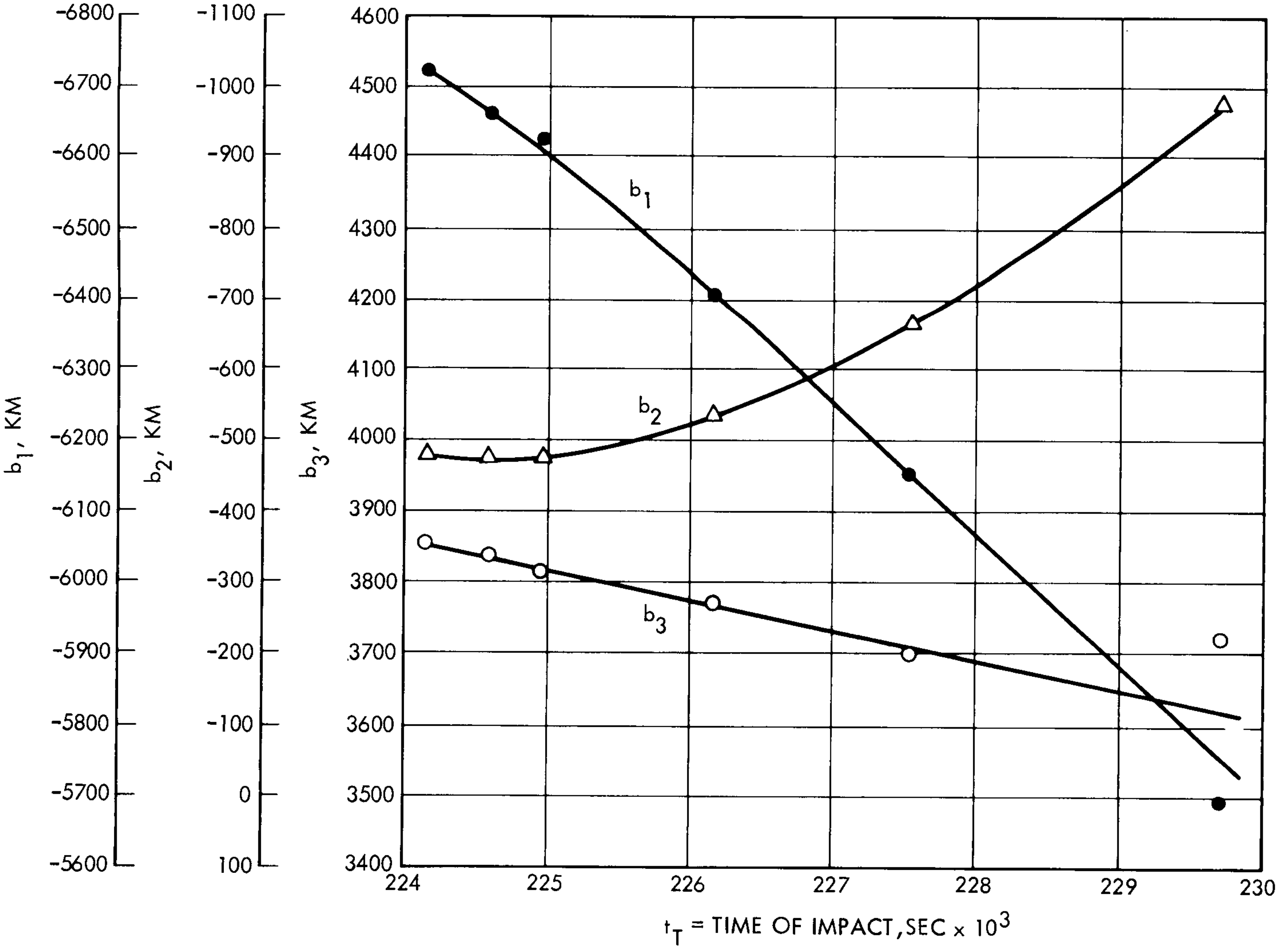

Figure 39. The b Vector in a Moon Oriented Rotating Coordinate Frame vs. Time of Impact

longitudes of the impact points obtained from these cutoff conditions are shown in Table 14. It can be seen from this table that there is a 3 deg variation in latitude between the six cases, and a 0.5 deg variation in longitude. If open loop nominals had been used, there would be a much smaller variation in impact position and less difficulty in defining the target location. As the situation stands, the target can be any point which has a 2 deg radius sphere about it that contains all the impact points. The target will thus be chosen to lie at 2.5 deg latitude and 154.5 deg longitude. These variations in the nominal impact points probably account for at least part of the error in fitting to the data of Figure 38.

The accuracy of the bias equations was proven by computing the desired velocity for the same six cases using the free flight prediction equations, the biasing equations, and the p-iteration equations. The exact impact time of the nominal trajectories were used for t_T values, so the search logic was not needed. It was assumed that the vehicle was at the nominal cutoff position and velocity when the computations were made. A complete numerical integration solution to the equations of motion was then used to predict the lunar impact point which would result from the use of this desired velocity. The resulting lunar latitude and longitude are given in Table 14.

The data in Table 15 follows that of Table 14 fairly closely over the first five data points. The worst deviation for this set of data is about 0.2 deg. The last point differs by about 2.0 deg in longitude. This deviation is undoubtedly correlated with the poor fit obtained on case 6 in

Table 14. Lunar Impact Points Obtained From The Nominal Cutoff Condition

Case	Latitude	Longitude
1	1.0813 deg	353.7157 deg
2	1.3284 deg	353.7455 deg
3	1.6235 deg	354.0027 deg
4	1.6253 deg	353.6730 deg
5	2.0838 deg	354.1659 deg
6	4.0950 deg	354.0064 deg

Table 15. Lunar Impact Points Obtained From The Computed Desired Velocities

Case	Latitude	Longitude
1	1.1163 $\widehat{\text{deg}}$	353.8444 $\widehat{\text{deg}}$
2	1.3211 $\widehat{\text{deg}}$	353.7784 $\widehat{\text{deg}}$
3	1.4144 $\widehat{\text{deg}}$	353.7228 $\widehat{\text{deg}}$
4	1.6528 $\widehat{\text{deg}}$	353.7046 $\widehat{\text{deg}}$
5	2.1145 $\widehat{\text{deg}}$	354.0339 $\widehat{\text{deg}}$
6	3.3870 $\widehat{\text{deg}}$	356.0063 $\widehat{\text{deg}}$

Figure 38. The fact remains, however, that all the impact points fall within 2.0 deg of the target, which is acceptable performance. The deviations from the original data are so small that it appears that if a consistent set of data had been used initially the final performance would have been quite good.

7.5 SEARCH LOGIC

The search logic essentially seeks out the t_T which minimizes the fuel consumption of the total rendezvous maneuver for any given set of initial conditions. The problem is constrained by requiring that the perigee altitude be kept above a certain minimum level.

In the original guidance equations of Reference 3 the search logic was initialized every guidance cycle and allowed to complete fifteen iterations. However, it was found that this number required too long a computing time, and did not give good convergence. The values of t_T were still changing enough near cutoff to cause changes in desired velocity, which led to some steering error. Hence, the logic was changed so that the equations were initialized only once during a given burn, and only three iterations were made per guidance cycle. This procedure reduced the computing time, and also caused the search logic to converge to its final answer well before cutoff occurred. In fact, in the intercept runs discussed earlier the search logic usually converged to its final answer within 10 seconds after the start of intercept guidance. The fuel consumption with this type of operation was no worse than with the original equations.

In order to determine whether the search logic could be used successfully on a translunar injection, a separate A-shot program was set up which contained only the free flight prediction equations, biasing equations, p-iteration equations and the search logic. No vehicle dynamics were included in this program, so it was necessary to enter position and velocity as additional inputs. The cutoff values of position and velocity at the same six points used in the lunar biasing study were employed here. The search logic was then used to find the optimum value of t_T and the corresponding desired velocity, $\overline{v}_D$. The program was allowed to go through 30 iterations. The object was to determine whether the program could find its own value of t_T for various launch times, and whether this value would be close to that of the nominal trajectory. It was also questionable whether the biasing equations would work properly for slightly non-nominal values of t_T. The coefficient values used in these runs are shown in Table 16.

The resulting values of t_T are shown in Table 17, along with the values from the nominal trajectories. It is clear from this table that the worst deviation in t_T is only 63.5 seconds, which is small compared to

Table 16. Coefficient Values for A-Shot Runs on Translunar Injection

$K_1 = 7.19 \text{ Km}^2 \text{ sec}^{-1}$
$K_2 = 5$
$K_3 = 71900 \text{ Km}^2 \text{ sec}^{-1}$
$K_4 = 3600 \text{ sec}$
$K_5 = 226,164.306 \text{ sec}$
$K_{10} = 500 \text{ sec}$
$K_{13} = 6475.6 \text{ Km}$
$K_{22} = 3600$
$K_{30} = 30.0$
$K_{31} = 0.050$
$\overline{r}_o = 108,723.76; -346,204.17; -174,909.96 \text{ Km}$
$\overline{v}_o = 0.93719289; 0.24830374; 0.03332489 \text{ Km sec}^{-1}$
$t_o = 226,164.306$
$\nu = 1$

Table 17. Values of t_T From Nominal Trajectories And From A-Shot Results

Case	Nominal t_T	A-Shot t_T
1	224.147.36 sec	224,147.12 sec
2	224.597.88 sec	224,590.09 sec
3	224,964.71 sec	224,901.22 sec
4	225,164.31 sec	226,166.85 sec
5	227,544.51 sec	227,536.18 sec
6	229,709.84 sec	229,729.93 sec

the total variation in t_T of over 5,500 seconds. This deviation does not represent a direct error either, because the position of the moon will still be computed properly for that time, and the p-iteration equations will give a proper value of $\overline{v}_D$ for the computed $\overline{t}_T$. This deviation may, however, cause some indirect error through the bias equations.

Table 18 shows a comparison between the nominal cutoff velocities and the $\overline{v}_D$ vector computed by the A-shot program. The worst deviation is 0.0014 km sec^{-1}, which is about 4.6 ft sec^{-1}. It must be remembered that this is not all error, since the routine chooses a slightly different impact time, which requires a different velocity.

The lunar impact points obtained from the A-shot $\overline{v}_D$ values are shown in Table 19. These points are very close to those of Table 13. Assuming again that the target lies at 2.5 deg latitude and 354.5 deg longitude, the impact points all fall within a 2 deg circle centered at the target. Therefore, the procedure meets the accuracy requirements imposed on the present software.

Figure 40 shows the iteration pattern obtained for case 4 when using the A-shot program. Only the first 15 of the 30 iterations are shown here, because the data density becomes too high after that. The minimum point on this curve is quite clearly defined, and it can be seen that the data points are rapidly approaching this minimum. The actual operation in the guidance computer would be somewhat different, however, because only 3 iterations would be made per guidance cycle. Also, the Δv curve would

Table 18. A Comparison Between the A-Shot $\overline{V}_d$ Vectors and the Nominal Cutoff Velocities

	NOMINAL CUTOFF VELOCITY			$\overline{V}_D$ from A-SHOT PROGRAM		
CASE	V_x (Km sec^{-1})	V_y (Km sec^{-1})	V_z (Km sec^{-1})	V_{Dx}	V_{Dy}	V_{Dz}
1	-9.9850547	-3.6534389	-2.7593531	-9.9850699	-3.6534453	-2.7592639
2	-9.9231285	-3.7788099	-2.8370595	-9.9231548	-3.7787866	-2.8370447
3	-9.8751798	-3.8644952	-2.9004344	-9.875269	-3.8644040	-2.9004231
4	-9.6553230	-4.1396023	-3.2472560	-9.6553163	-4.1396137	-3.2472454
5	-9.3698171	-4.2430575	-3.8474798	-0.3698241	-4.2432473	-3.8472686
6	-8.8141065	-3.8724886	-5.2157257	-8.8148783	-3.8710926	-5.2154675

Table 19. Lunar Impact Points Obtained from the $\bar{V}d$ Vectors Generated by the A-Shot Program

Case	Latitude	Longitude
1	1.1076 $\overset{\frown}{\text{deg}}$	353.8209 $\overset{\frown}{\text{deg}}$
2	1.2847 $\overset{\frown}{\text{deg}}$	353.7029 $\overset{\frown}{\text{deg}}$
3	1.4493 $\overset{\frown}{\text{deg}}$	353.8086 $\overset{\frown}{\text{deg}}$
4	1.6491 $\overset{\frown}{\text{deg}}$	353.7059 $\overset{\frown}{\text{deg}}$
5	2.1376 $\overset{\frown}{\text{deg}}$	354.0450 $\overset{\frown}{\text{deg}}$
6	3.2943 $\overset{\frown}{\text{deg}}$	355.9832 $\overset{\frown}{\text{deg}}$

be different on each guidance cycle because the required Δv is decreasing as the cutoff time is approached. The curve of Figure 40 is still rather helpful in visualizing the operation of the search logic.

It appears, then, that the search logic will give satisfactory performance on the translunar injection, as well as on the low altitude satellite intercept mission.

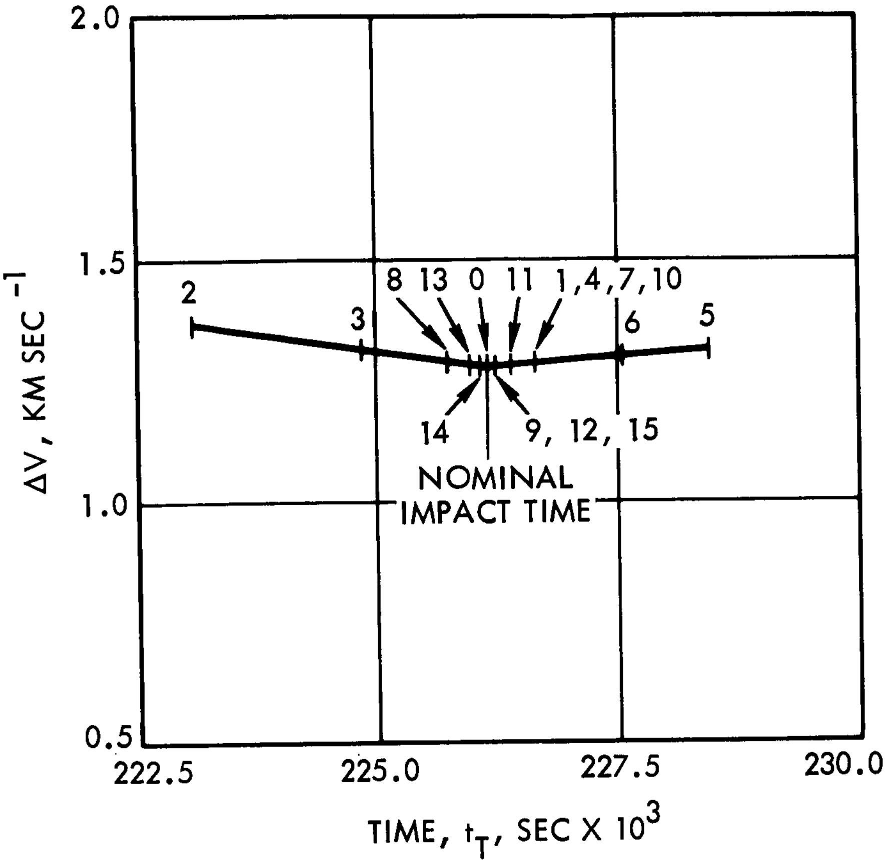

Figure 40. ΔV versus t_r, Lunar Injection, 30 September 1965, Case 4

8. STABILITY INTERFACE OF GENERALIZED EXPLICIT EQUATIONS WITH THE CURRENT ATLAS/CENTAUR CONTROL SYSTEM

A separate study was conducted at TRW Systems by J.P. Ivaska of the Performance Analysis Section of the Control Systems Department. The purpose of this study was to determine what, if any, interface problems existed when explicit guidance techniques were used with the current Centaur Control System. The report on this quite extensive study is included in this report as Appendix A. The plan of the study was to investigate the interface problem in two parts: The first, to determine whether explicit equations in the guidance loop fundamentally degrade the Centaur Control System performance seriously. The second to evaluate the effect of the explicit equations on the Centaur Control System with consideration given to the actual digital nature of the guidance loop.

In the first part the guidance equations used were a linearized version of those presented in this report, and the control system model was a linearized version of the Centaur Control System. The objectives of the first part of the study were pursued using a linearized analysis, with the conclusion that the incorporation of explicit guidance results in very little degradation of system stability prior to the approach of injection. However, as the time to injection becomes short the important stability margins are considerably reduced, though no instability results. The reason for this behavior can be appreciated by noting that the attitude commands as generated by guidance vary inversely with the time-to-go until engine cutoff. Thus attitude commands changes tend to be more extreme near cutoff than further away resulting in greater demands being put on the control system. In terms of the linearized analysis performed in Appendix A, the reduced values of time-to-go are shown to result in a higher gain constant in the linearized guidance loop, thus producing the degraded stability characteristics.

The second part of the study was performed by utilizing a sample data simulation. This simulation was capable of representing both the continuous nature of the control system dynamics as well as the digital nature of the guidance loop. The sampling periods were varied from 1 through 20 seconds for the case just prior to injection. The situation just prior to injection was chosen as a result of its relative criticality as indicated by the results of the first part of the study. The simulation showed that sampling times of up to 5 seconds were satisfactory but that instability occurred when longer sampling periods were used.

The results of this guidance-control interface study thus showed that the use of the type of explicit equations presented in this report does not cause serious problems of control as long as the guidance loop sampling periods are kept to about 5 seconds or less.

These timing limitations have the following implications:

1) An advanced flight computer (such as the LEM AGS) will have no speed problems performing the computations for the complete generalized equation package. Table 5 gives a maximum timing requirement of less than 0.1 second which is of course well below the 5 seconds required from the above stability analysis.

2) The current Centaur computer would take more than 13 seconds (See Table 5) to perform the powered flight computations for intercept problems which is well beyond the stability limit of 5 seconds. Thus the current Centaur computer could not accommodate the complete generalized equation package.

3) From Table 5, it can be seen that if intercept guidance is deleted from the equation package, the timing requirements using the current Centaur computer are 2.8 seconds which is within the 5 second limit. Thus if intercept guidance were not included in the overall capability of the equation set, the current Centaur computer would not be ruled out for reasons of insufficient speed.

9. CONCLUSIONS

The most important conclusions that can be drawn from this equation study and the related tasks performed within the Advanced Centaur Study are as follows:

1) The use of generalized equations to provide guidance for a multipurpose space system employing the Centaur vehicle together with the Atlas lower stages is feasible provided advanced computer hardware is supplied.

2) The use of explicit guidance techniques, as described and analysed in this report, provide high flexibility and long term economy with more than adequate performance accuracy for the generalized guidance purposes.

3) The current Centaur -3 Librascope computer might be able to handle a version of the generalized equations which did not include an intercept guidance capability. However, to do this the -3 would have to be modified to permit use of the entire memory during flight, and even then the squeeze would be tight.

10. FLOW CHARTS

The flow charts presented in this section are the mechanizations of the equations derived and discussed in the body of the report. The computer requirements estimates of Section 4.1 were made from these flow charts.

The flow chart number and title are listed below.

Flow Chart

1) Initial Guidance Loop Computations
2) Free Flight Prediction
3) P-Iteration
4) Search Logic
5) Cutoff Velocity Prediction
6) Exo-Atmospheric Steering
7) Error-Signal Equations
8) Cutoff Routine
9) Coast Trajectory Termination
10) Maneuver Sequencing
11) Atmosphere Steering
12) Navigation Equations
13) Atmospheric Navigation Parameters
14) Compensation Equations

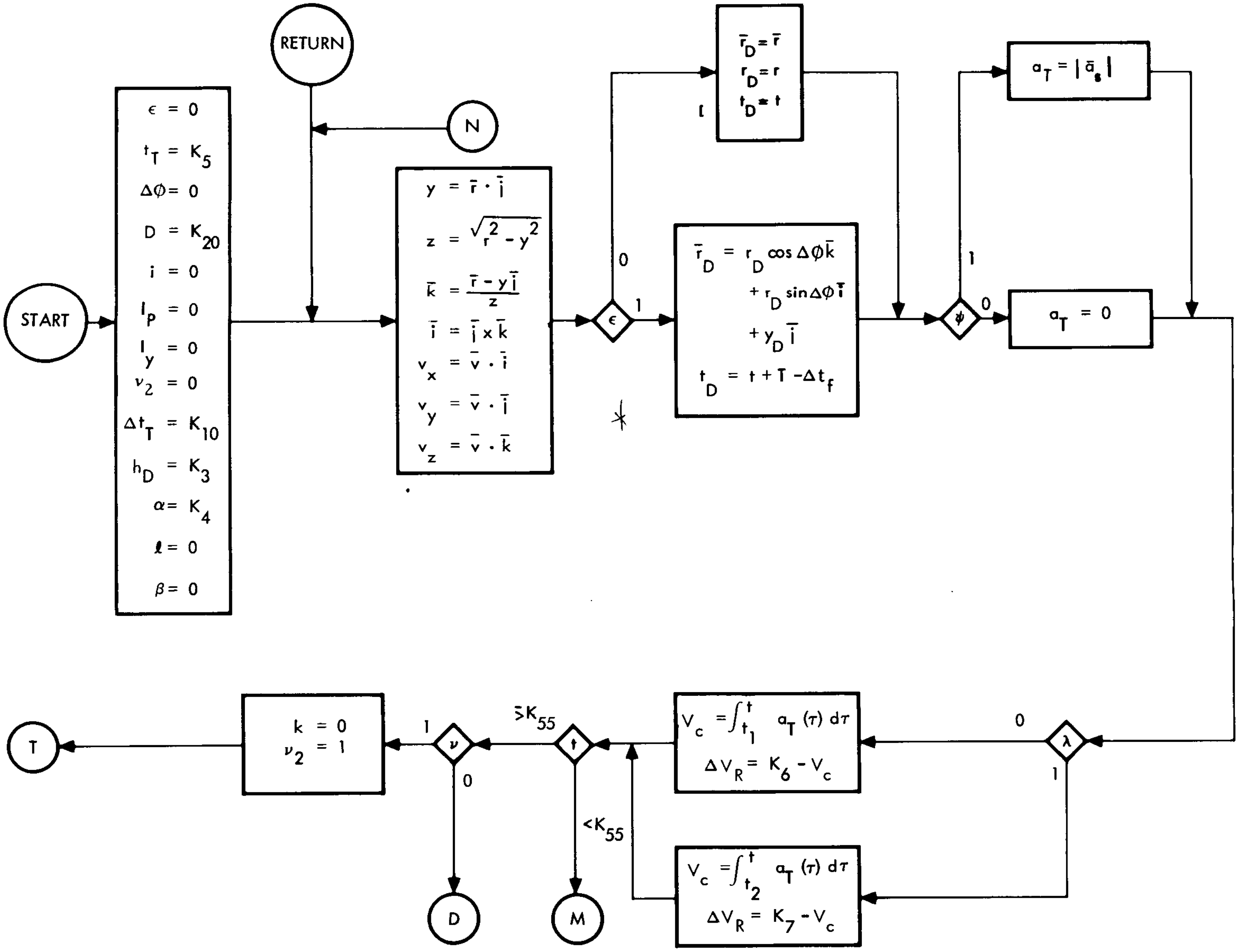
START
ϵ = 0
t_T = K_5
ΔΦ = 0
D = K_20
i = 0
I_P = 0
I_y = 0
ν_2 = 0
Δt_T = K_10
h_D = K_3
α = K_4
ℓ = 0
β = 0
RETURN
N
y = r̄ · j̄
z = √(r² - y²)
k̄ = (r̄ - yj̄)/z
ī = j̄ x k̄
v_x = v̄ · ī
v_y = v̄ · j̄
v_z = v̄ · k̄
ϵ
0
1
r̄_D = r̄
r_D = r
t_D = t
r̄_D = r_D cos ΔΦk̄ + r_D sinΔΦī + y_D j̄
t_D = t + T - Δt_f
ψ
1
0
a_T = |ā_s|
a_T = 0
λ
0
1
V_c = ∫_{t_1}^{t} a_T (τ) dτ
ΔV_R = K_6 - V_c
V_c = ∫_{t_2}^{t} a_T (τ) dτ
ΔV_R = K_7 - V_c
t
≥K_55
<K_55
M
ν
1
0
D
k = 0
ν_2 = 1
T

Flow Chart 1. Initial Guidance Loop Computations

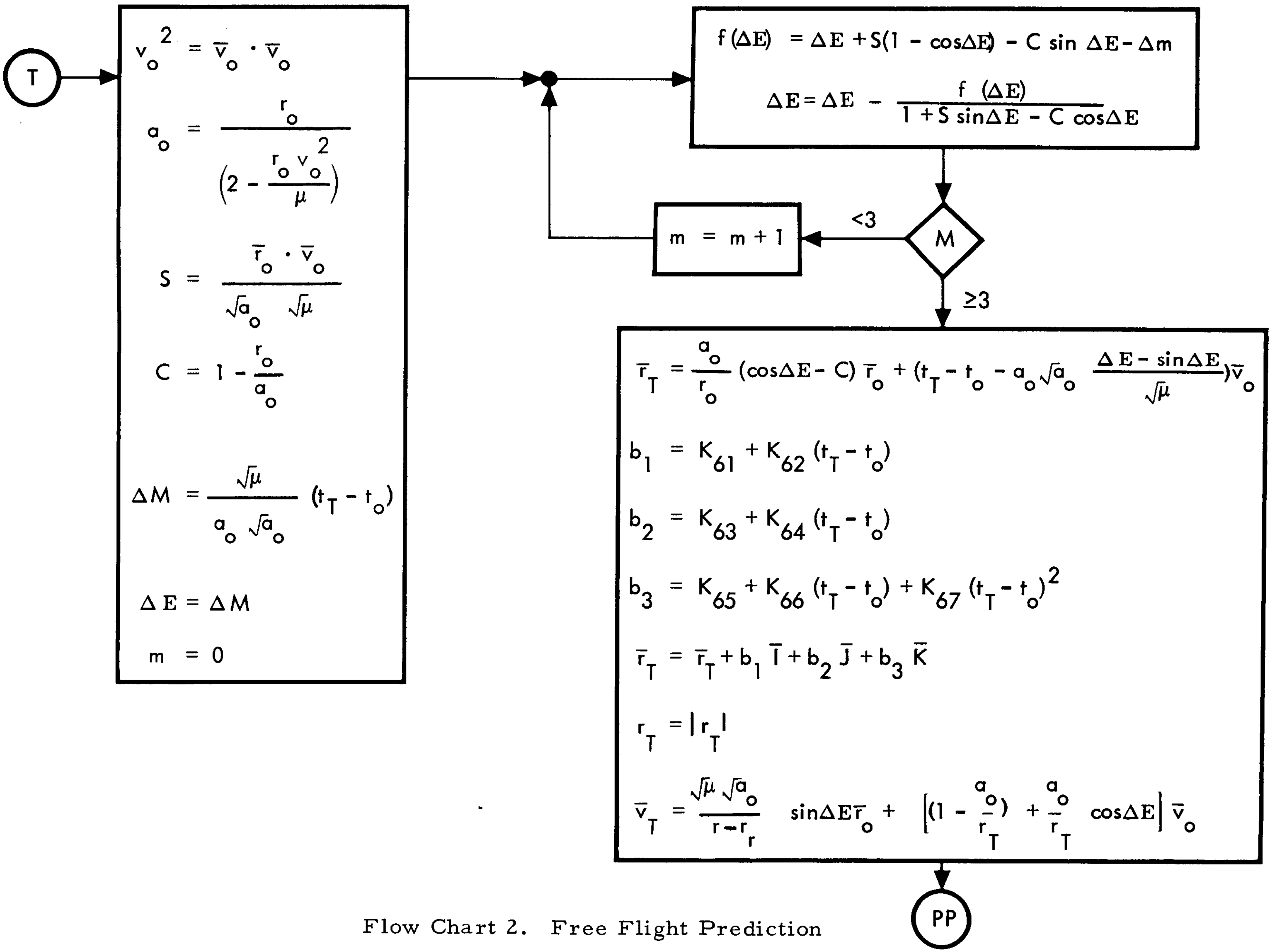

T
$v_o^2 = \bar{v}_o \cdot \bar{v}_o$
$a_o = \frac{r_o}{\left(2 - \frac{r_o v_o^2}{\mu}\right)}$
$S = \frac{\bar{r}_o \cdot \bar{v}_o}{\sqrt{a_o}\ \sqrt{\mu}}$
$C = 1 - \frac{r_o}{a_o}$
$\Delta M = \frac{\sqrt{\mu}}{a_o \sqrt{a_o}} (t_T - t_o)$
$\Delta E = \Delta M$
$m = 0$
$f(\Delta E) = \Delta E + S(1 - \cos\Delta E) - C \sin \Delta E - \Delta m$
$\Delta E = \Delta E - \frac{f(\Delta E)}{1 + S \sin\Delta E - C \cos\Delta E}$
M
<3
$m = m + 1$
≥ 3
$\bar{r}_T = \frac{a_o}{r_o} (\cos\Delta E - C)\, \bar{r}_o + (t_T - t_o - a_o\sqrt{a_o}\ \frac{\Delta E - \sin\Delta E}{\sqrt{\mu}})\bar{v}_o$
$b_1 = K_{61} + K_{62} (t_T - t_o)$
$b_2 = K_{63} + K_{64} (t_T - t_o)$
$b_3 = K_{65} + K_{66} (t_T - t_o) + K_{67} (t_T - t_o)^2$
$\bar{r}_T = \bar{r}_T + b_1 \bar{I} + b_2 \bar{J} + b_3 \bar{K}$
$r_T = |r_T|$
$\bar{v}_T = \frac{\sqrt{\mu}\sqrt{a_o}}{r - r_r}\ \sin\Delta E \bar{r}_o + \left[(1 - \frac{a_o}{r_T}) + \frac{a_o}{r_T}\ \cos\Delta E\right] \bar{v}_o$
PP

Flow Chart 2. Free Flight Prediction

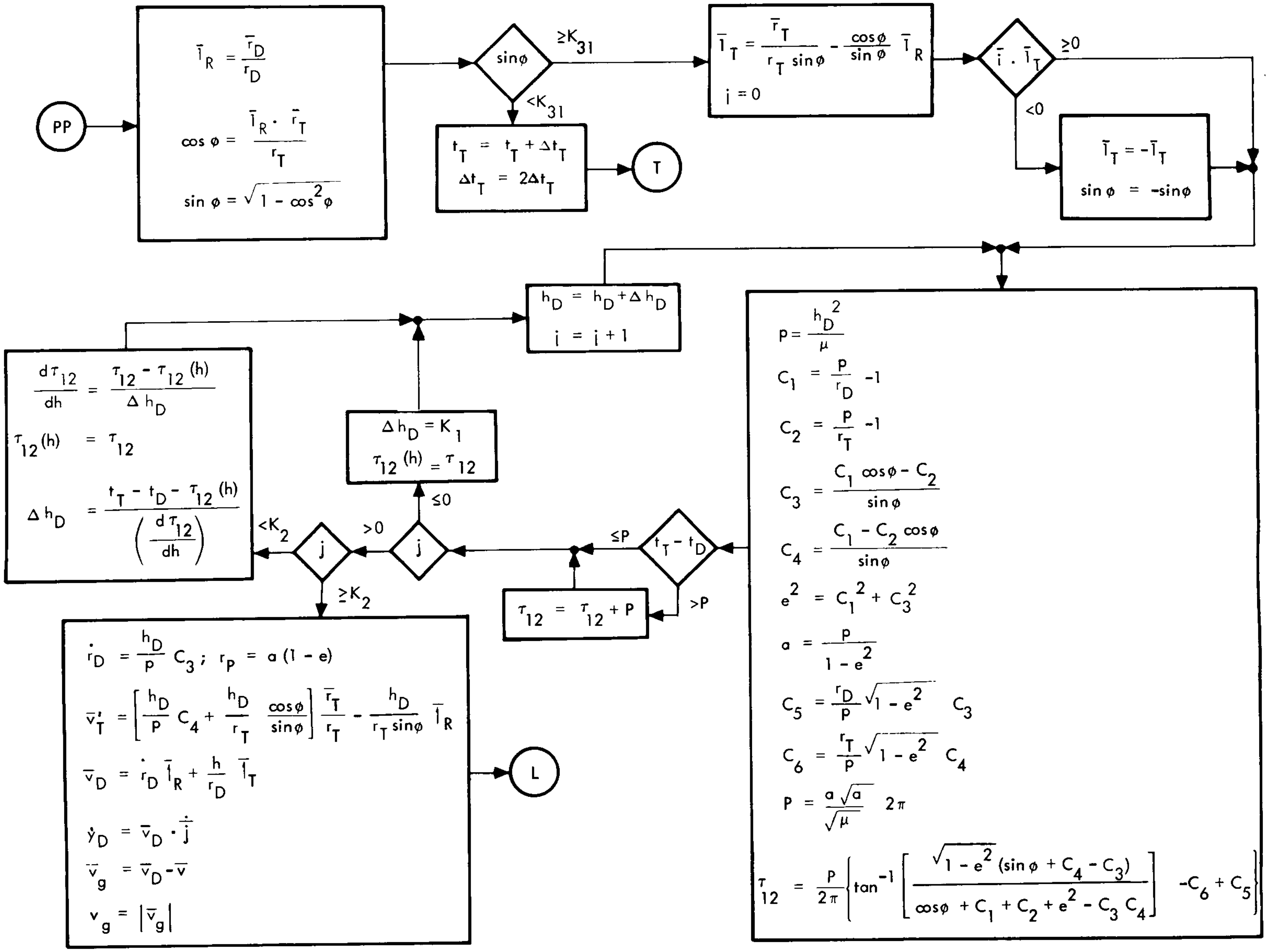
PP
$\bar{1}_R = \frac{\bar{r}_D}{r_D}$
$\cos\phi = \frac{\bar{1}_R \cdot \bar{r}_T}{r_T}$
$\sin\phi = \sqrt{1 - \cos^2\phi}$
$\sin\phi$
$\geq K_{31}$
$< K_{31}$
$t_T = t_T + \Delta t_T$
$\Delta t_T = 2\Delta t_T$
T
$\bar{1}_T = \frac{\bar{r}_T}{r_T \sin\phi} - \frac{\cos\phi}{\sin\phi}\,\bar{1}_R$
$i = 0$
$\bar{i} \cdot \bar{1}_T$
≥ 0
< 0
$\bar{1}_T = -\bar{1}_T$
$\sin\phi = -\sin\phi$
$h_D = h_D + \Delta h_D$
$i = i + 1$
$p = \frac{h_D^2}{\mu}$
$C_1 = \frac{p}{r_D} - 1$
$C_2 = \frac{p}{r_T} - 1$
$C_3 = \frac{C_1 \cos\phi - C_2}{\sin\phi}$
$C_4 = \frac{C_1 - C_2 \cos\phi}{\sin\phi}$
$e^2 = C_1^2 + C_3^2$
$a = \frac{p}{1 - e^2}$
$C_5 = \frac{r_D}{p}\sqrt{1 - e^2}\;C_3$
$C_6 = \frac{r_T}{p}\sqrt{1 - e^2}\;C_4$
$P = \frac{a\sqrt{a}}{\sqrt{\mu}}\;2\pi$
$\tau_{12} = \frac{P}{2\pi}\left\{\tan^{-1}\left[\frac{\sqrt{1 - e^2}\,(\sin\phi + C_4 - C_3)}{\cos\phi + C_1 + C_2 + e^2 - C_3 C_4}\right] - C_6 + C_5\right\}$
$t_T - t_D$
$\leq P$
$> P$
$\tau_{12} = \tau_{12} + P$
j
≤ 0
> 0
$\Delta h_D = K_1$
$\tau_{12}(h) = \tau_{12}$
j
$< K_2$
$\geq K_2$
$\frac{d\tau_{12}}{dh} = \frac{\tau_{12} - \tau_{12}(h)}{\Delta h_D}$
$\tau_{12}(h) = \tau_{12}$
$\Delta h_D = \frac{t_T - t_D - \tau_{12}(h)}{\left(\frac{d\tau_{12}}{dh}\right)}$
$\dot{r}_D = \frac{h_D}{p} C_3;\; r_p = a(1 - e)$
$\dot{\bar{v}}_T = \left[\frac{h_D}{p} C_4 + \frac{h_D}{r_T}\;\frac{\cos\phi}{\sin\phi}\right]\frac{\bar{r}_T}{r_T} - \frac{h_D}{r_T \sin\phi}\;\bar{1}_R$
$\bar{v}_D = \dot{r}_D\,\bar{1}_R + \frac{h}{r_D}\;\bar{1}_T$
$\dot{y}_D = \bar{v}_D \cdot \dot{\bar{j}}$
$\bar{v}_g = \bar{v}_D - \bar{v}$
$v_g = |\bar{v}_g|$
L

Flow Chart 3. P-Iteration

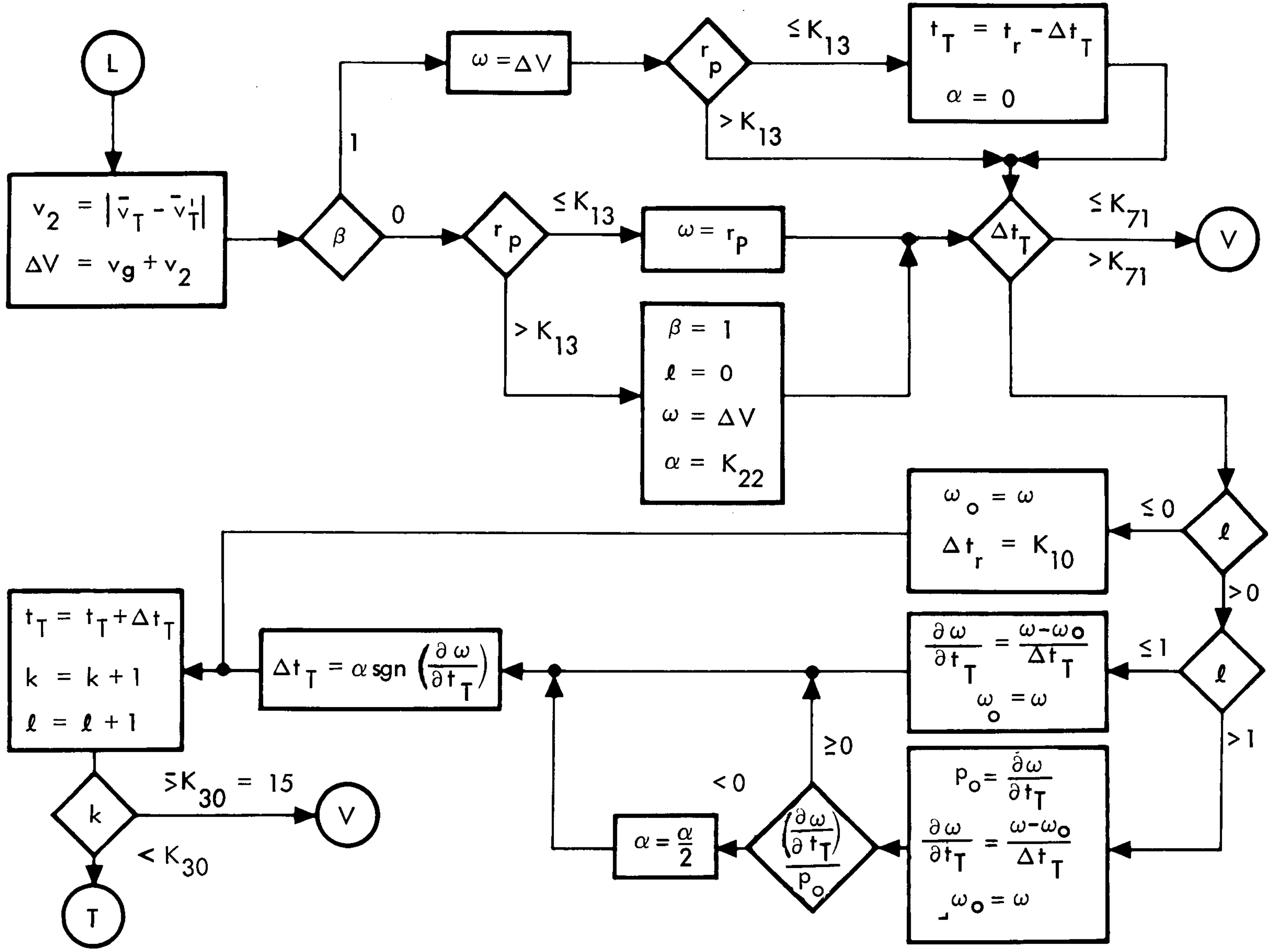
L
$v_2 = |\bar{v}_T - \bar{v}_T'|$
$\Delta V = v_g + v_2$
β
1
0
$\omega = \Delta V$
r_p
$\leq K_{13}$
$> K_{13}$
$t_T = t_r - \Delta t_T$
$\alpha = 0$
r_p
$\leq K_{13}$
$> K_{13}$
$\omega = r_p$
$\beta = 1$
$\ell = 0$
$\omega = \Delta V$
$\alpha = K_{22}$
Δt_T
$\leq K_{71}$
$> K_{71}$
V
ℓ
≤ 0
> 0
$\omega_o = \omega$
$\Delta t_r = K_{10}$
ℓ
≤ 1
> 1
$\frac{\partial \omega}{\partial t_T} = \frac{\omega - \omega_o}{\Delta t_T}$
$\omega_o = \omega$
$p_o = \frac{\partial \omega}{\partial t_T}$
$\frac{\partial \omega}{\partial t_T} = \frac{\omega - \omega_o}{\Delta t_T}$
$\omega_o = \omega$
$\frac{\left(\frac{\partial \omega}{\partial t_T}\right)}{p_o}$
≥ 0
< 0
$\alpha = \frac{\alpha}{2}$
$\Delta t_T = \alpha \operatorname{sgn} \left(\frac{\partial \omega}{\partial t_T}\right)$
$t_T = t_T + \Delta t_T$
$k = k + 1$
$\ell = \ell + 1$
k
$\geq K_{30} = 15$
$< K_{30}$
V
T

Flow Chart 4. Search Logic

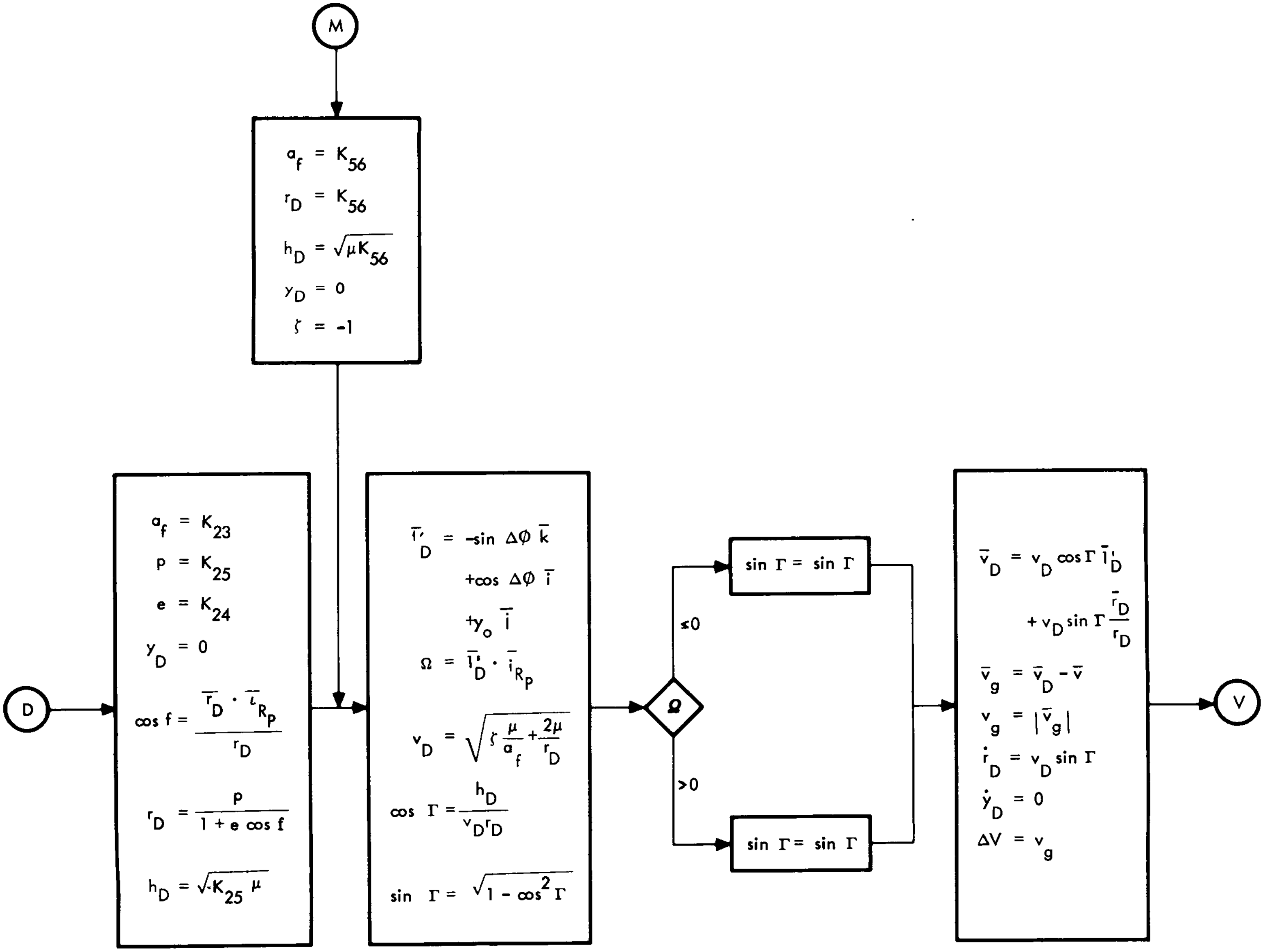

M
$a_f = K_{56}$
$r_D = K_{56}$
$h_D = \sqrt{\mu K_{56}}$
$y_D = 0$
$\zeta = -1$
D
$a_f = K_{23}$
$p = K_{25}$
$e = K_{24}$
$y_D = 0$
$\cos f = \frac{\bar{r}_D \cdot \bar{\iota}_{R_P}}{r_D}$
$r_D = \frac{p}{1 + e \cos f}$
$h_D = \sqrt{K_{25}\,\mu}$
$\bar{1}'_D = -\sin \Delta\phi \,\bar{k} + \cos \Delta\phi \,\bar{i} + y_o \,\bar{i}$
$\Omega = \bar{1}'_D \cdot \bar{i}_{R_P}$
$v_D = \sqrt{\zeta \frac{\mu}{a_f} + \frac{2\mu}{r_D}}$
$\cos \Gamma = \frac{h_D}{v_D r_D}$
$\sin \Gamma = \sqrt{1 - \cos^2 \Gamma}$
Ω
≤ 0
> 0
$\sin \Gamma = \sin \Gamma$
$\sin \Gamma = \sin \Gamma$
$\bar{v}_D = v_D \cos \Gamma \,\bar{1}'_D + v_D \sin \Gamma \frac{\bar{r}_D}{r_D}$
$\bar{v}_g = \bar{v}_D - \bar{v}$
$v_g = |\bar{v}_g|$
$\dot{r}_D = v_D \sin \Gamma$
$\dot{y}_D = 0$
$\Delta V = v_g$
V

Flow Chart 5. Cutoff Velocity Prediction

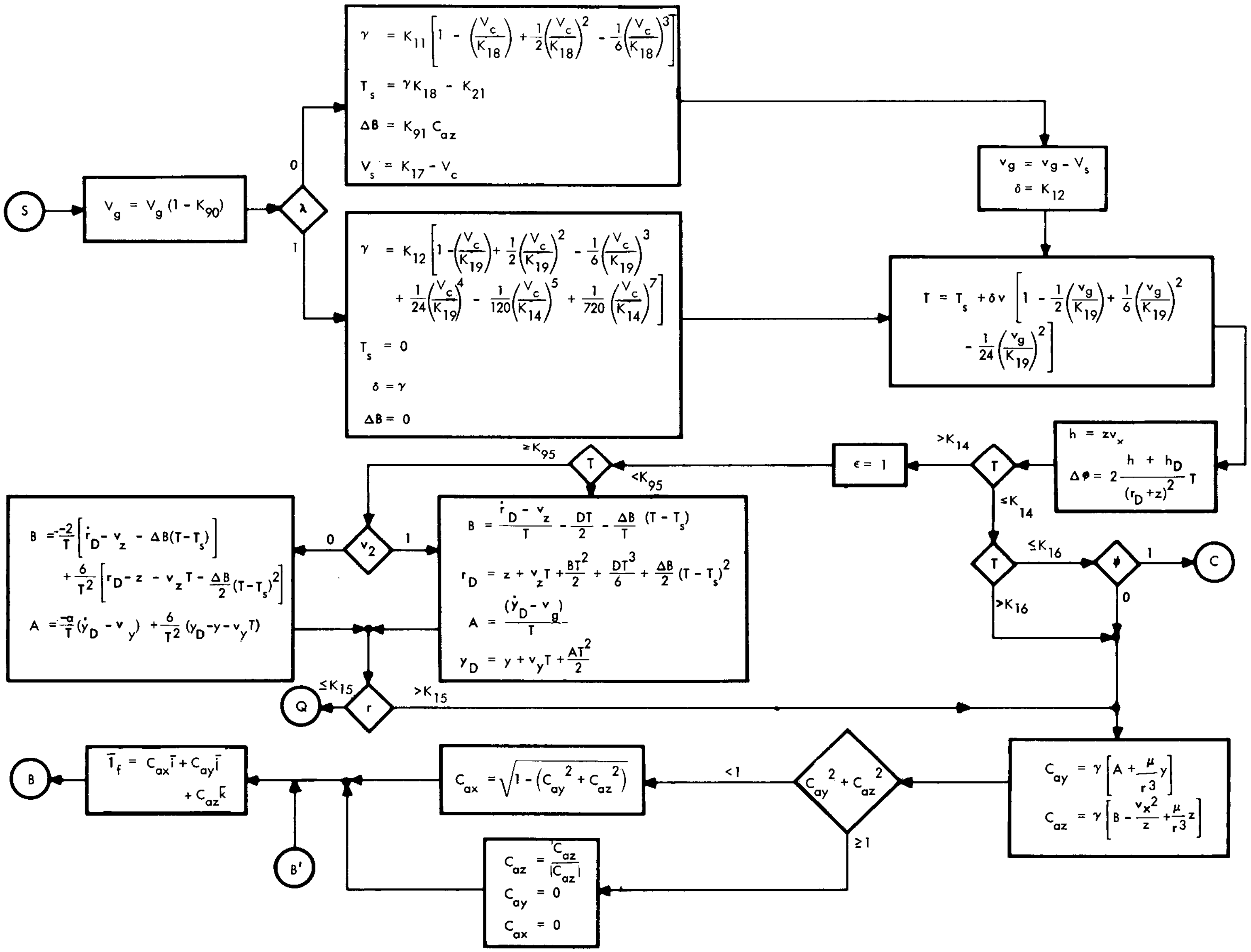

S
$V_g = V_g(1 - K_{90})$
λ
0
1
$\gamma = K_{11}\left[1 - \left(\frac{V_c}{K_{18}}\right) + \frac{1}{2}\left(\frac{V_c}{K_{18}}\right)^2 - \frac{1}{6}\left(\frac{V_c}{K_{18}}\right)^3\right]$
$T_s = \gamma K_{18} - K_{21}$
$\Delta B = K_{91} C_{az}$
$V_s = K_{17} - V_c$
$\gamma = K_{12}\left[1 - \left(\frac{V_c}{K_{19}}\right) + \frac{1}{2}\left(\frac{V_c}{K_{19}}\right)^2 - \frac{1}{6}\left(\frac{V_c}{K_{19}}\right)^3 + \frac{1}{24}\left(\frac{V_c}{K_{19}}\right)^4 - \frac{1}{120}\left(\frac{V_c}{K_{14}}\right)^5 + \frac{1}{720}\left(\frac{V_c}{K_{14}}\right)^7\right]$
$T_s = 0$
$\delta = \gamma$
$\Delta B = 0$
$v_g = v_g - V_s$
$\delta = K_{12}$
$T = T_s + \delta v\left[1 - \frac{1}{2}\left(\frac{v_g}{K_{19}}\right) + \frac{1}{6}\left(\frac{v_g}{K_{19}}\right)^2 - \frac{1}{24}\left(\frac{v_g}{K_{19}}\right)^2\right]$
$h = z v_x$
$\Delta\phi = 2\frac{h + h_D}{(r_D + z)^2} T$
T
$>K_{14}$
$\leq K_{14}$
$\epsilon = 1$
T
$\geq K_{95}$
$< K_{95}$
T
$\leq K_{16}$
$>K_{16}$
ϕ
1
0
C
v_2
0
1
$B = \frac{-2}{T}\left[\dot{r}_D - v_z - \Delta B(T - T_s)\right] + \frac{6}{T^2}\left[r_D - z - v_z T - \frac{\Delta B}{2}(T - T_s)^2\right]$
$A = \frac{-a}{T}(\dot{y}_D - v_y) + \frac{6}{T^2}(y_D - y - v_y T)$
$B = \frac{\dot{r}_D - v_z}{T} - \frac{DT}{2} - \frac{\Delta B}{T}(T - T_s)$
$r_D = z + v_z T + \frac{BT^2}{2} + \frac{DT^3}{6} + \frac{\Delta B}{2}(T - T_s)^2$
$A = \frac{(\dot{y}_D - v_g)}{T}$
$y_D = y + v_y T + \frac{AT^2}{2}$
r
$\leq K_{15}$
$>K_{15}$
Q
$C_{ay} = \gamma\left[A + \frac{\mu}{r^3} y\right]$
$C_{az} = \gamma\left[B - \frac{v_x^2}{z} + \frac{\mu}{r^3} z\right]$
$C_{ay}^2 + C_{az}^2$
<1
≥1
$C_{ax} = \sqrt{1 - (C_{ay}^2 + C_{az}^2)}$
$C_{az} = \frac{C_{az}}{|C_{az}|}$
$C_{ay} = 0$
$C_{ax} = 0$
B'
$\bar{I}_f = C_{ax}\bar{i} + C_{ay}\bar{j} + C_{az}\bar{k}$
B

Flow Chart 6. Exo-Atmospheric Steering

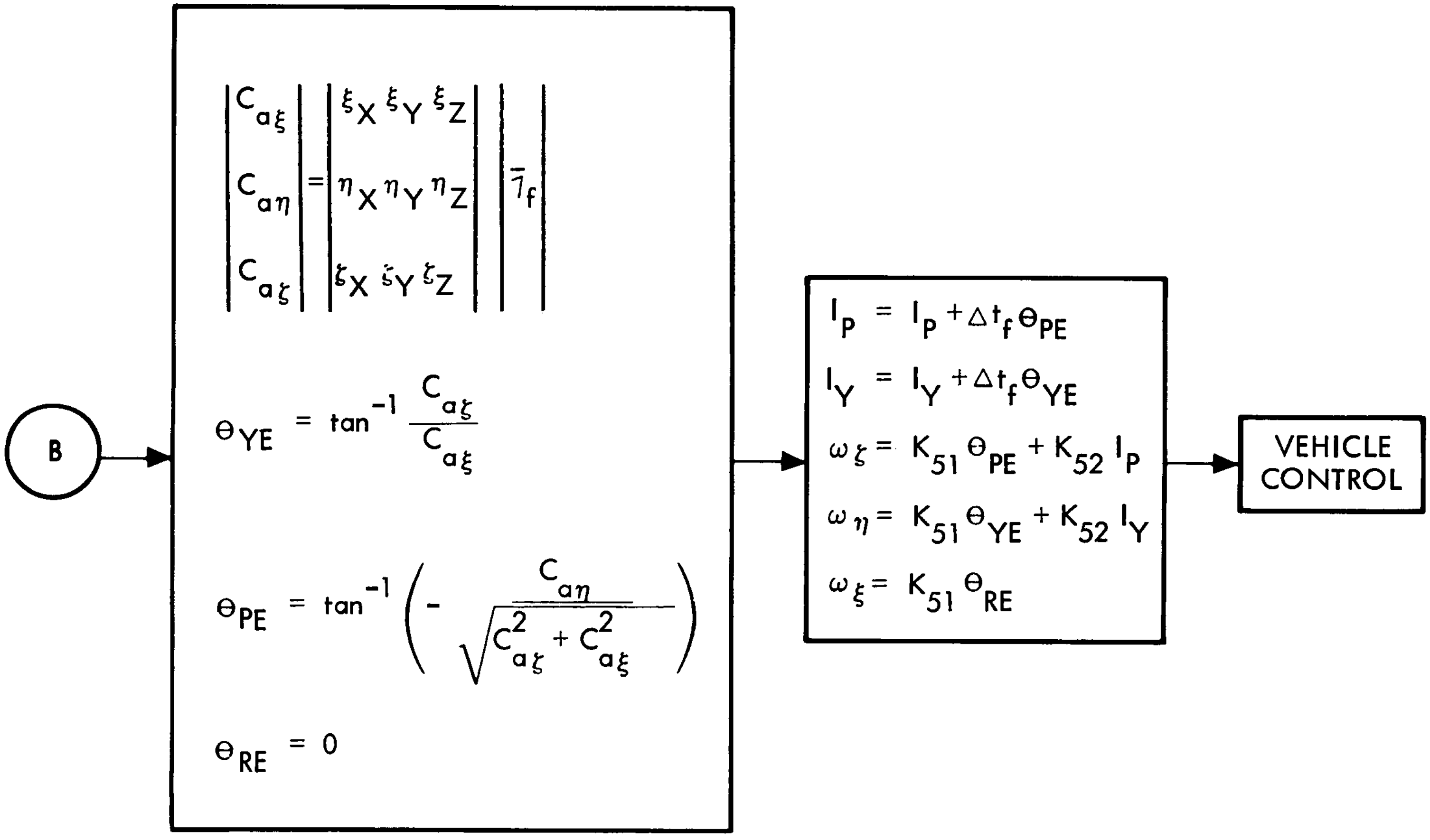
B
$\begin{vmatrix} C_{a\xi} \\ C_{a\eta} \\ C_{a\zeta} \end{vmatrix} = \begin{vmatrix} {}^{\xi}X & {}^{\xi}Y & {}^{\xi}Z \\ {}^{\eta}X & {}^{\eta}Y & {}^{\eta}Z \\ {}^{\zeta}X & {}^{\zeta}Y & {}^{\zeta}Z \end{vmatrix} \begin{vmatrix} \bar{\eta}_f \end{vmatrix}$
$\Theta_{YE} = \tan^{-1} \frac{C_{a\zeta}}{C_{a\xi}}$
$\Theta_{PE} = \tan^{-1} \left(- \frac{C_{a\eta}}{\sqrt{C_{a\zeta}^2 + C_{a\xi}^2}} \right)$
$\Theta_{RE} = 0$
$I_P = I_P + \Delta t_f \Theta_{PE}$
$I_Y = I_Y + \Delta t_f \Theta_{YE}$
$\omega_\zeta = K_{51} \Theta_{PE} + K_{52} I_P$
$\omega_\eta = K_{51} \Theta_{YE} + K_{52} I_Y$
$\omega_\xi = K_{51} \Theta_{RE}$
VEHICLE CONTROL

Flow Chart 7. Error Signal Equations

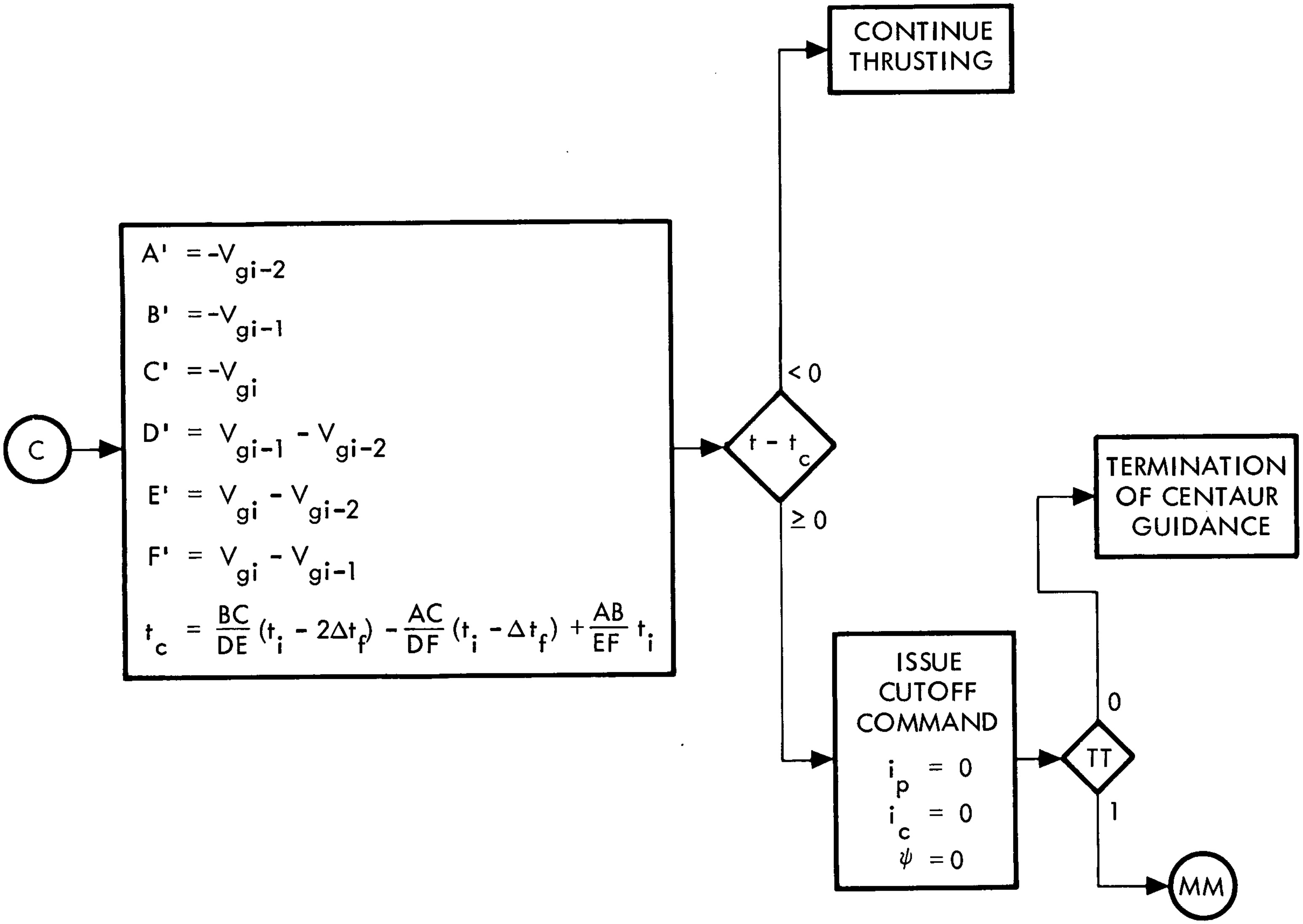

C
$A' = -V_{gi-2}$
$B' = -V_{gi-1}$
$C' = -V_{gi}$
$D' = V_{gi-1} - V_{gi-2}$
$E' = V_{gi} - V_{gi-2}$
$F' = V_{gi} - V_{gi-1}$
$t_c = \frac{BC}{DE}(t_i - 2\Delta t_f) - \frac{AC}{DF}(t_i - \Delta t_f) + \frac{AB}{EF} t_i$
$t - t_c$
< 0
≥ 0
CONTINUE THRUSTING
ISSUE CUTOFF COMMAND
$i_p = 0$
$i_c = 0$
$\psi = 0$
TT
0
1
TERMINATION OF CENTAUR GUIDANCE
MM

Flow Chart 8. Cutoff Routine

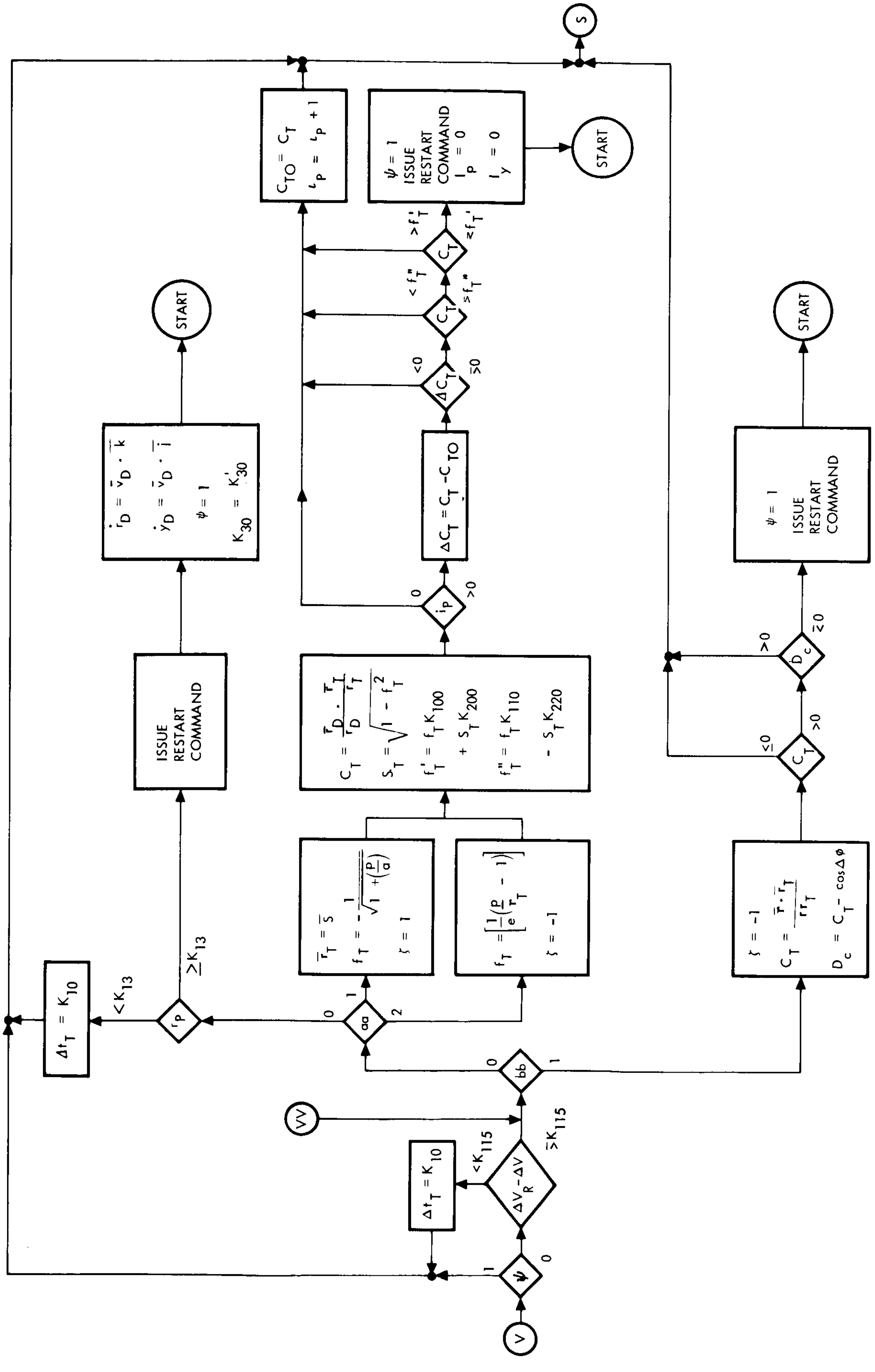
V
ψ
1
0
Δt_T = K_10
ΔV_R - ΔV
< K_115
≥ K_115
VV
bb
0
1
aa
0
1
2
r_P
< K_13
≥ K_13
Δt_T = K_10
ISSUE RESTART COMMAND
ṙ_D = v̄_D · k̄
ẏ_D = v̄_D · ī
ψ = 1
K_30 = K'_30
START
r̄_T = S̄
f_T = - 1 / √(1 + (p/a))
ζ = 1
f_T = [1/e (p/r_T - 1)]
ζ = -1
C_T = r̄_D · r̄_T / r_D r_T
S_T = √(1 - f_T²)
f'_T = f_T K_100 + S_T K_200
f"_T = f_T K_110 - S_T K_220
i_P
0
> 0
ΔC_T = C_T - C_TO
ΔC_T
< 0
≥ 0
C_T
< f"_T
≥ f"_T
C_T
> f'_T
≤ f'_T
C_TO = C_T
i_P = i_P + 1
ψ = 1
ISSUE RESTART COMMAND
I_P = 0
I_Y = 0
START
S
ζ = -1
C_T = r̄ · r̄_T / r r_T
D_c = C_T - cos Δφ
C_T
≤ 0
> 0
D_c
> 0
≤ 0
ψ = 1
ISSUE RESTART COMMAND
START

Flow Chart 9. Coast Trajectory Termination

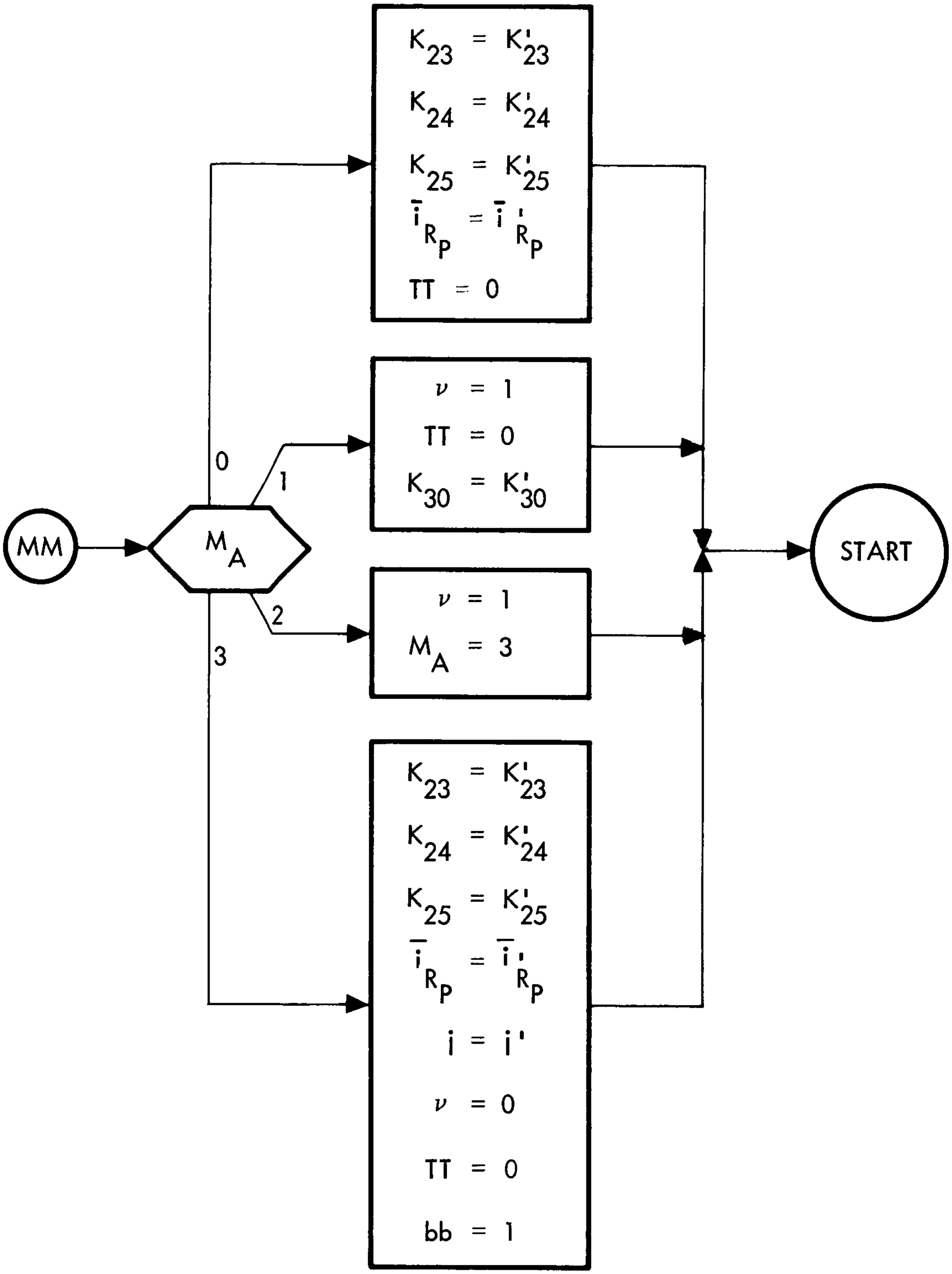

MM
M_A
0
1
2
3
$K_{23} = K'_{23}$
$K_{24} = K'_{24}$
$K_{25} = K'_{25}$
$\bar{i}_{R_P} = \bar{i}'_{R_P}$
TT = 0
$\nu = 1$
TT = 0
$K_{30} = K'_{30}$
$\nu = 1$
$M_A = 3$
$K_{23} = K'_{23}$
$K_{24} = K'_{24}$
$K_{25} = K'_{25}$
$\bar{i}_{R_P} = \bar{i}'_{R_P}$
i = i'
$\nu = 0$
TT = 0
bb = 1
START

Flow Chart 10. Maneuver Sequencing

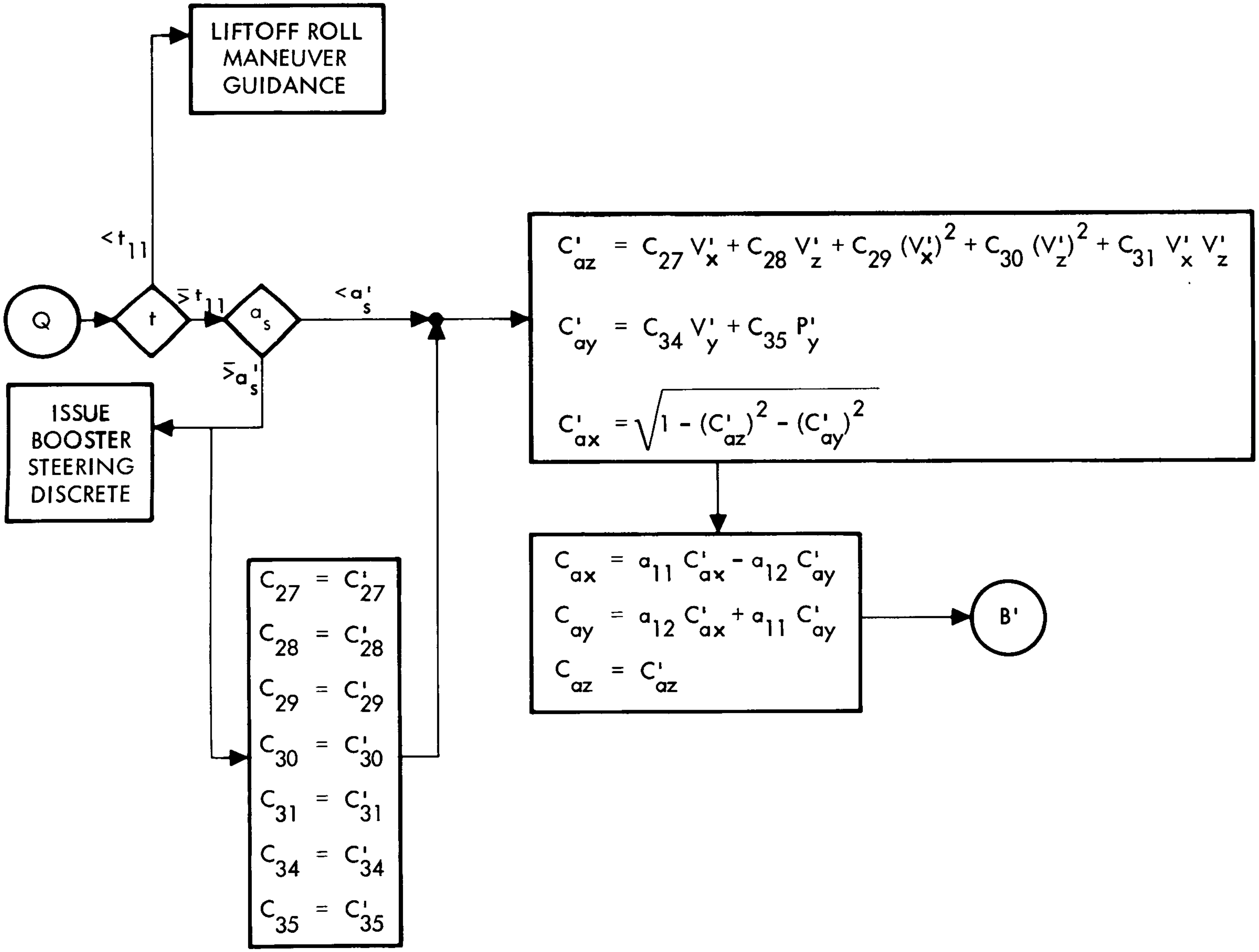
LIFTOFF ROLL MANEUVER GUIDANCE
Q
t
$<t_{11}$
$\geq t_{11}$
a_s
$<a'_s$
$\geq a'_s$
ISSUE BOOSTER STEERING DISCRETE
$C_{27} = C'_{27}$
$C_{28} = C'_{28}$
$C_{29} = C'_{29}$
$C_{30} = C'_{30}$
$C_{31} = C'_{31}$
$C_{34} = C'_{34}$
$C_{35} = C'_{35}$
$C'_{az} = C_{27} V'_x + C_{28} V'_z + C_{29} (V'_x)^2 + C_{30} (V'_z)^2 + C_{31} V'_x V'_z$
$C'_{ay} = C_{34} V'_y + C_{35} P'_y$
$C'_{ax} = \sqrt{1 - (C'_{az})^2 - (C'_{ay})^2}$
$C_{ax} = a_{11} C'_{ax} - a_{12} C'_{ay}$
$C_{ay} = a_{12} C'_{ax} + a_{11} C'_{ay}$
$C_{az} = C'_{az}$
B'

Flow Chart 11. Atmospheric Steering

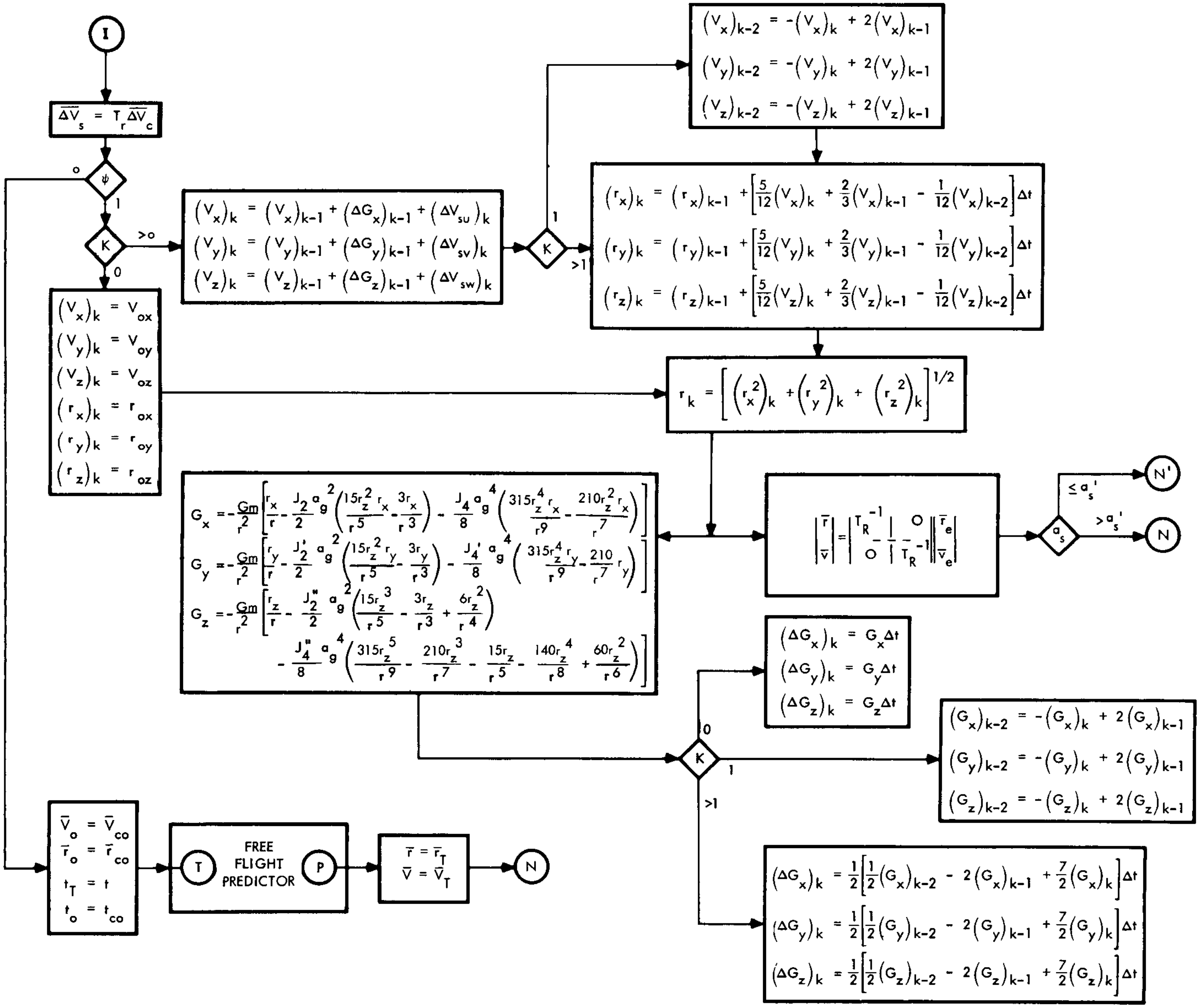
I
$\overline{\Delta V}_s = T_r \overline{\Delta V}_c$
ψ
0
1
K
>0
0
$(V_x)_k = V_{ox}$
$(V_y)_k = V_{oy}$
$(V_z)_k = V_{oz}$
$(r_x)_k = r_{ox}$
$(r_y)_k = r_{oy}$
$(r_z)_k = r_{oz}$
$(V_x)_k = (V_x)_{k-1} + (\Delta G_x)_{k-1} + (\Delta V_{su})_k$
$(V_y)_k = (V_y)_{k-1} + (\Delta G_y)_{k-1} + (\Delta V_{sv})_k$
$(V_z)_k = (V_z)_{k-1} + (\Delta G_z)_{k-1} + (\Delta V_{sw})_k$
K
1
>1
$(V_x)_{k-2} = -(V_x)_k + 2(V_x)_{k-1}$
$(V_y)_{k-2} = -(V_y)_k + 2(V_y)_{k-1}$
$(V_z)_{k-2} = -(V_z)_k + 2(V_z)_{k-1}$
$(r_x)_k = (r_x)_{k-1} + \left[\frac{5}{12}(V_x)_k + \frac{2}{3}(V_x)_{k-1} - \frac{1}{12}(V_x)_{k-2}\right]\Delta t$
$(r_y)_k = (r_y)_{k-1} + \left[\frac{5}{12}(V_y)_k + \frac{2}{3}(V_y)_{k-1} - \frac{1}{12}(V_y)_{k-2}\right]\Delta t$
$(r_z)_k = (r_z)_{k-1} + \left[\frac{5}{12}(V_z)_k + \frac{2}{3}(V_z)_{k-1} - \frac{1}{12}(V_z)_{k-2}\right]\Delta t$
$r_k = \left[\left(r_x^2\right)_k + \left(r_y^2\right)_k + \left(r_z^2\right)_k\right]^{1/2}$
$G_x = -\frac{Gm}{r^2}\left[\frac{r_x}{r} - \frac{J_2}{2}a_g^2\left(\frac{15r_z^2 r_x}{r^5} - \frac{3r_x}{r^3}\right) - \frac{J_4}{8}a_g^4\left(\frac{315r_z^4 r_x}{r^9} - \frac{210r_z^2 r_x}{r^7}\right)\right]$
$G_y = -\frac{Gm}{r^2}\left[\frac{r_y}{r} - \frac{J_2'}{2}a_g^2\left(\frac{15r_z^2 r_y}{r^5} - \frac{3r_y}{r^3}\right) - \frac{J_4'}{8}a_g^4\left(\frac{315r_z^4 r_y}{r^9} - \frac{210}{r^7}r_y\right)\right]$
$G_z = -\frac{Gm}{r^2}\left[\frac{r_z}{r} - \frac{J_2''}{2}a_g^2\left(\frac{15r_z^3}{r^5} - \frac{3r_z}{r^3} + \frac{6r_z^2}{r^4}\right) - \frac{J_4''}{8}a_g^4\left(\frac{315r_z^5}{r^9} - \frac{210r_z^3}{r^7} - \frac{15r_z}{r^5} - \frac{140r_z^4}{r^8} + \frac{60r_z^2}{r^6}\right)\right]$
$\begin{vmatrix}\bar{r}\\ \bar{v}\end{vmatrix} = \begin{vmatrix}T_R^{-1} & 0\\ 0 & T_R^{-1}\end{vmatrix}\begin{vmatrix}\bar{r}_e\\ \bar{v}_e\end{vmatrix}$
a_s
$\leq a_s'$
$> a_s'$
N'
N
K
0
1
>1
$(\Delta G_x)_k = G_x \Delta t$
$(\Delta G_y)_k = G_y \Delta t$
$(\Delta G_z)_k = G_z \Delta t$
$(G_x)_{k-2} = -(G_x)_k + 2(G_x)_{k-1}$
$(G_y)_{k-2} = -(G_y)_k + 2(G_y)_{k-1}$
$(G_z)_{k-2} = -(G_z)_k + 2(G_z)_{k-1}$
$(\Delta G_x)_k = \frac{1}{2}\left[\frac{1}{2}(G_x)_{k-2} - 2(G_x)_{k-1} + \frac{7}{2}(G_x)_k\right]\Delta t$
$(\Delta G_y)_k = \frac{1}{2}\left[\frac{1}{2}(G_y)_{k-2} - 2(G_y)_{k-1} + \frac{7}{2}(G_y)_k\right]\Delta t$
$(\Delta G_z)_k = \frac{1}{2}\left[\frac{1}{2}(G_z)_{k-2} - 2(G_z)_{k-1} + \frac{7}{2}(G_z)_k\right]\Delta t$
$\bar{V}_o = \bar{V}_{co}$
$\bar{r}_o = \bar{r}_{co}$
$t_T = t$
$t_o = t_{co}$
T
FREE FLIGHT PREDICTOR
P
$\bar{r} = \bar{r}_T$
$\bar{V} = \bar{V}_T$
N

Flow Chart 12. Navigation Equations

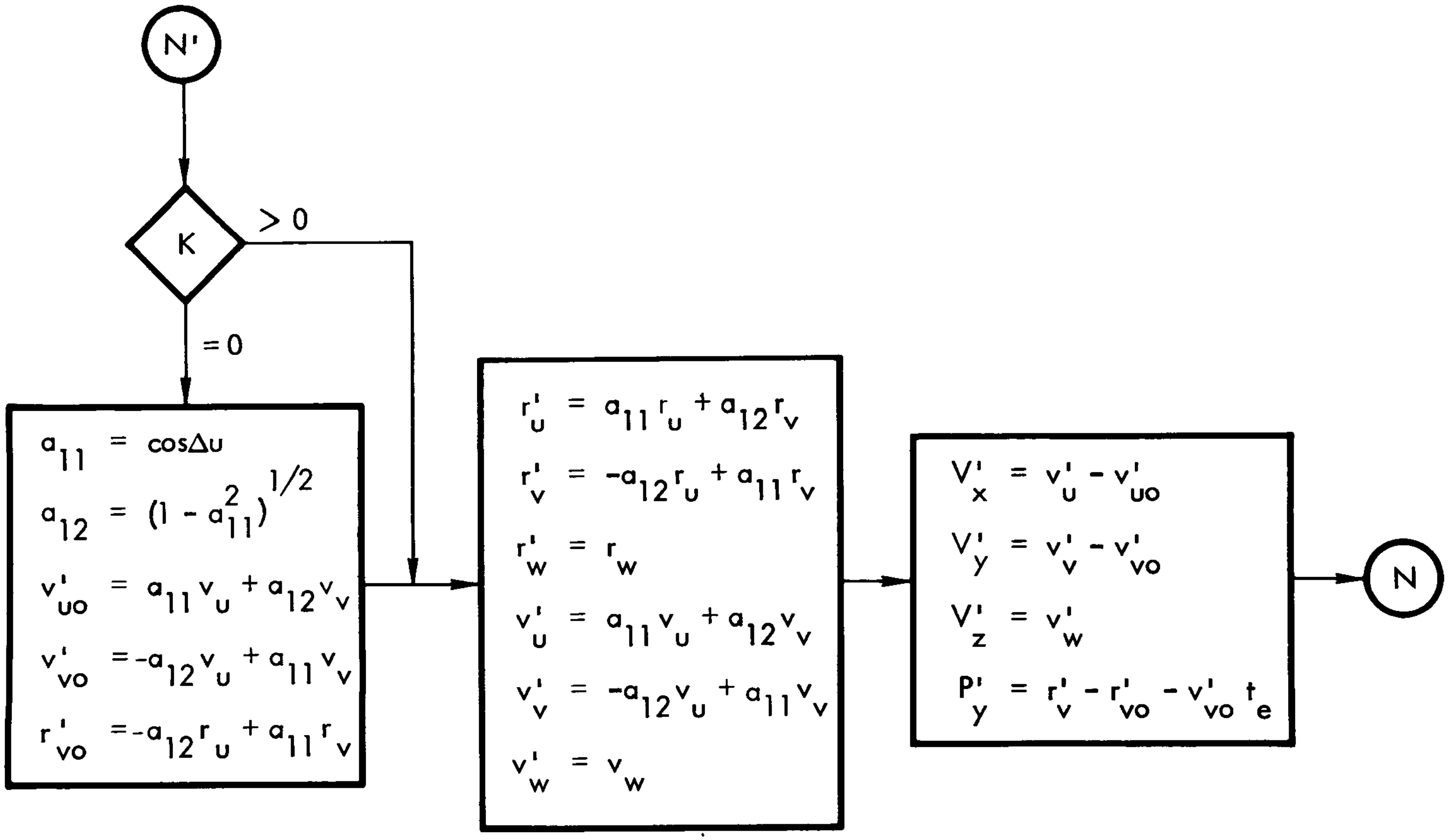
N'
K
> 0
= 0
$a_{11} = \cos\Delta u$
$a_{12} = (1 - a_{11}^2)^{1/2}$
$v'_{uo} = a_{11} v_u + a_{12} v_v$
$v'_{vo} = -a_{12} v_u + a_{11} v_v$
$r'_{vo} = -a_{12} r_u + a_{11} r_v$
$r'_u = a_{11} r_u + a_{12} r_v$
$r'_v = -a_{12} r_u + a_{11} r_v$
$r'_w = r_w$
$v'_u = a_{11} v_u + a_{12} v_v$
$v'_v = -a_{12} v_u + a_{11} v_v$
$v'_w = v_w$
$V'_x = v'_u - v'_{uo}$
$V'_y = v'_v - v'_{vo}$
$V'_z = v'_w$
$P'_y = r'_v - r'_{vo} - v'_{vo} t_e$
N

Flow Chart 13. Atmospheric Navigation Parameters

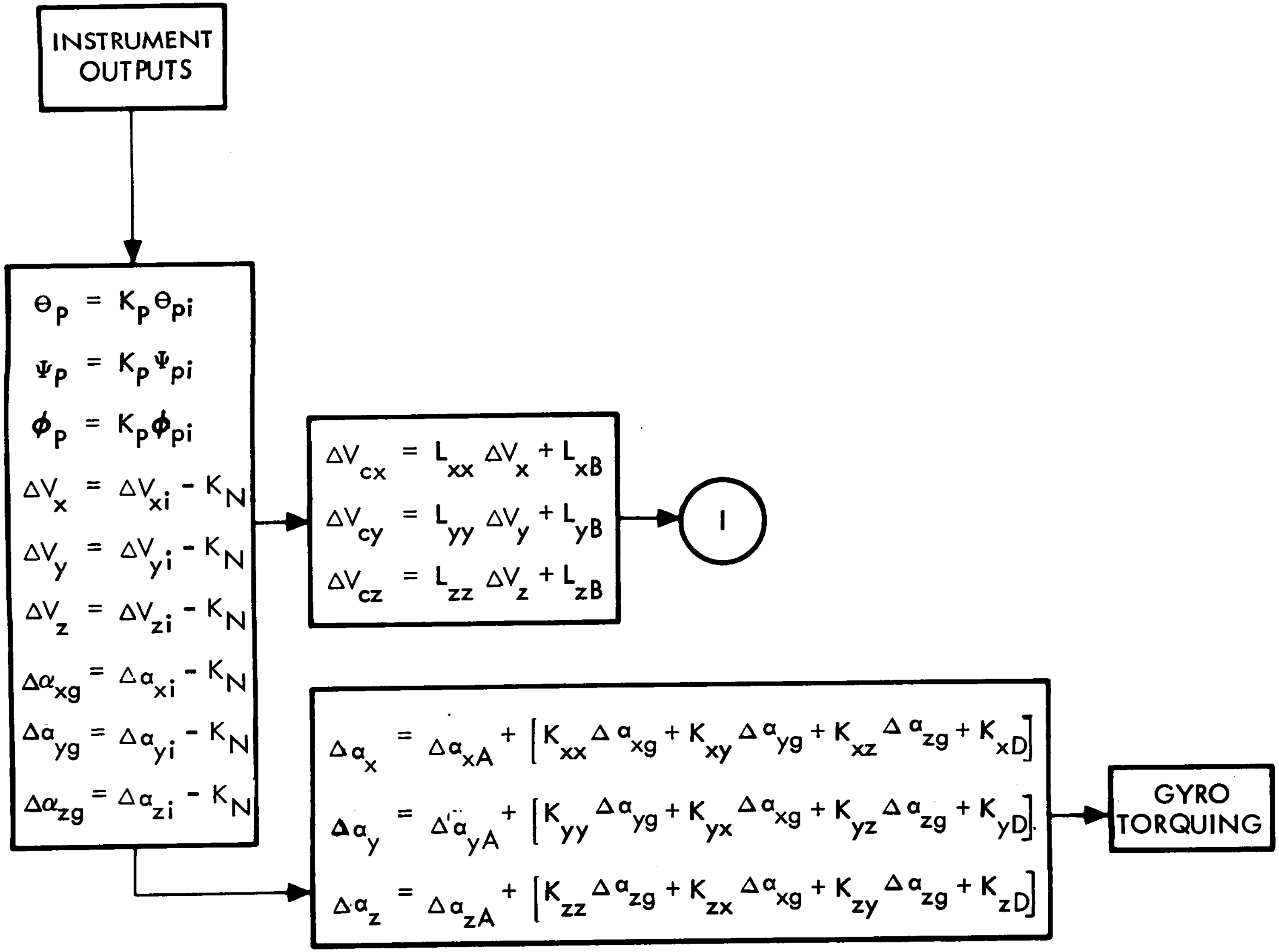
INSTRUMENT OUTPUTS
$\Theta_p = K_p \Theta_{pi}$
$\Psi_p = K_p \Psi_{pi}$
$\phi_p = K_p \phi_{pi}$
$\Delta V_x = \Delta V_{xi} - K_N$
$\Delta V_y = \Delta V_{yi} - K_N$
$\Delta V_z = \Delta V_{zi} - K_N$
$\Delta\alpha_{xg} = \Delta\alpha_{xi} - K_N$
$\Delta\alpha_{yg} = \Delta\alpha_{yi} - K_N$
$\Delta\alpha_{zg} = \Delta\alpha_{zi} - K_N$
$\Delta V_{cx} = L_{xx} \Delta V_x + L_{xB}$
$\Delta V_{cy} = L_{yy} \Delta V_y + L_{yB}$
$\Delta V_{cz} = L_{zz} \Delta V_z + L_{zB}$
1
$\Delta\alpha_x = \Delta\alpha_{xA} + \left[K_{xx} \Delta\alpha_{xg} + K_{xy} \Delta\alpha_{yg} + K_{xz} \Delta\alpha_{zg} + K_{xD}\right]$
$\Delta\alpha_y = \Delta\alpha_{yA} + \left[K_{yy} \Delta\alpha_{yg} + K_{yx} \Delta\alpha_{xg} + K_{yz} \Delta\alpha_{zg} + K_{yD}\right]$
$\Delta\alpha_z = \Delta\alpha_{zA} + \left[K_{zz} \Delta\alpha_{zg} + K_{zx} \Delta\alpha_{xg} + K_{zy} \Delta\alpha_{zg} + K_{zD}\right]$
GYRO TORQUING

Flow Chart 14. Compensation Equations

11. NOMENCLATURE

a = semi major axis of conic (p-iteration)

a_{11}, a_{12} = elements in transformation from platform to pitch plane oriented inertial system matrix

aa = $\begin{cases} 0 \text{ if coast trajectory is rendezvous or Com-Sat parking orbit} \\ 1 \text{ if coast trajectory is interplanetary parking orbit} \\ 2 \text{ if coast trajectory is translunar parking orbit} \end{cases}$

a_f = semi-major axis of conic (hyperbola or specified ellipse)

a_g = semi-major axis of earth's reference ellipsoidal

a_o = semi-major axis of target's orbit

a_T = magnitude of thrust acceleration

a'_s = acceleration level at which BECO occurs

$\bar{a}_s$ = sensed acceleration

A, B, B_1, D = steering coefficients

A', B', C', D', E', F' = Auxiliary variables in cutoff routine

A_x', A_y', A_z' = Components of acceleration in earth fixed system

$\bar{b}$ = lunar offset bias vector

b_1, b_2, b_3 = coefficients in biased lunar position vector determination

bb = $\begin{cases} 0 \text{ if coast trajectory is parking orbit} \\ 1 \text{ if coast trajectory is intercept orbit} \end{cases}$

c = coefficient used in free flight predictor

c_1-c_6 = variable used in p-iteration

C_{27}-C_{35} = Atmospheric steering coefficients

C_{ax}, C_{ay}, C_{az} = direction cosines of desired acceleration with respect to $\bar{i}\ \bar{j}\ \bar{k}$ frame

$C'_{ax}, C'_{ay}, C'_{az}$ = Direction cosines with respect to earth fixed system

$C_{a\xi}, C_{a\eta}, C_{a\zeta}$ = direction cosines of desired acceleration with respect to vehicle fixed axes (ξ, η, ζ)

e = eccentricity of conic

f = true anomaly

f_d = desired true anomaly

f_T = cosine of true anomaly of $\bar{r}_T$ or $\bar{s}$

f'_T = cosine of minimum angle between injection and target vector ($\bar{r}_T$ or $\bar{S}$)

f''_T = cosine of maximum angle between injection and target vector ($\bar{r}_T$ or $\bar{S}$)

G_x, G_y, G_z = Component of gravitational acceleration

h = angular momentum

h_d = desired angular momentum

i_p = counter in coast trajectory termination routine (monitor mode)

$\bar{i}, \bar{j}, \bar{k}$ = unit vectors along computational coordinate axes

$\bar{i}_{R_P}$ = unit vector in perigee direction of first specified conic

$\bar{i}'_{R_P}$ = unit vector in perigee direction of second specified conic

I_p, I_y = integral of θ_{PE} and θ_{YE} respectively

$\bar{j}$ = unit vector normal to desired orbit plane of first conic

$\bar{j}'$ = unit vector normal to desired orbit plane of second conic

J = variable used in p-iteration counter

J_2, J_4 ≡ Coefficients in spherical harmonic representation of earth's potential

k = variable used in search procedure counter

K = counter

K_1 = initial increment on h_D for p-iteration

K_2 = number of iterations to be used in p-iteration

K_3 = initial guess on h_D to be used in p-iteration

K_5 = initial value of t_T to be used in search logic

K_6 = velocity change capability of both stages

K_7 = velocity change capability of second stage

K_{10} = initial increment on t_T to be used in search procedure

K_{11} = reciprocal of initial sustainer acceleration

K_{12} = reciprocal of initial Centaur acceleration

K_{13} = limit on R_P to be used to switch from search on R_P to search on ΔV in search procedure

K_{14} = value of T for switching to constant coefficient steering

K_{15} = limit on r for atmospheric steering equations

K_{16} = limit on T for entering cutoff routine

K_{17} = velocity change capability of sustainer

K_{18} = exhaust velocity of sustainer

K_{19} = exhaust velocity of Centaur

K_{21} = ratio of mass to mass flow rate at sustainer fuel depletion

K_{23} = semi major axis of first specified conic

K'_{23} = semi major axis of second specified conic

K_{24} = eccentricity of first specified conic

K'_{24} = eccentricity of second specified conic

K_{25} = semi latus rectum of first specified conic

K'_{25} = semi latus rectum of second specified conic

K_{30} = number of iterations in search procedure

K_{27}-K_{33} = atmospheric steering constants

K_{34} = 180 degree test in p-iteration

K_{51} = rate command proportionality constant

K_{52} = gain for integral control loop

K_{55} = time at which steering to inject into desired orbit is initiated

K_{61}-K_{67} = lunar intercept offset constants

K_{71} = limit on Δt for entry to steering

K_{97} = maximum ratio of $\frac{V_c}{V_e}$

K_{100} = cosine of maximum allowable true anomaly at injection

K_{110} = cosine of minimum allowable true anomaly at injection

K_{115} = velocity capability pad

K_{200} = sine of maximum allowable true anomaly at injection

K_{210} = sine of minimum allowable true anomaly at injection

K_N = Null factor

K_P = Euler angle scale factor

K_{xD}, K_{yD}, K_{zD} = compensation constants for non-g sensitive gyro drift

$K_{xx}, K_{xy}, K_{xz}, K_{yx}, K_{yz}, K_{zz}, K_{zx}, K_{zy}$ = compensation constants for attitude rate scale factor errors

ℓ = variable used in search procedure counter

L_{xB}, L_{yB}, L_{zB} = compensation constants for accelerometer bias

L_{xx}, L_{yy}, L_{zz} = compensated scale factors for accelerometers

m = variable used in free flight predictor counter

$$M_A = \begin{cases} 0 & \text{for interplanetary mission (two burn) or} \\ & \text{pre-targeted lunar mission (two burn)} \\ 1 & \text{for rendezvous mission and in flight} \\ & \text{targeted lunar mission (two burn)} \\ 2 & \text{for com-sat mission (three burn)} \\ 3 & \text{for redefined internally in guidance program} \\ & \text{for three burn com-sat mission} \end{cases}$$

p = semi-latus rectum of conic

p_o = variable used in search logic

p'_y = component of position normal to pitch plane

P = period of transfer ellipse

r = $|\bar{r}|$

r_{ox}, r_{oy}, r_{oz} $\equiv$ Initial components of position in equatorial oriented inertial system

r_p = radius of perigee on transfer orbit

r_T = $|\bar{r}_T|$

r_u, r_v, r_w = components of r

r_{uo}, r_{vo}, r_{wo} = components of position at launch of launch site in platform coordinates

r'_u, r'_v, r'_w = components of $\bar{r}'$

$r'_{uo}, r'_{vo}, r'_{wo}$ = components of $\bar{r}'_o$

$\dot{r}_D$ = desired radial velocity at cutoff

$\bar{r}$ = present position vector in platform coordinates

$\bar{r}_e$ = position vector in equatorial oriented inertial coordinate system

r_o = $|\bar{r}_o|$

$\bar{r}_d$ = predicted cutoff position vector

$\bar{r}_o$ = position vector of target vehicle at t_o

$\bar{r}_{po}$ = position vector of launch site at "go inertial" in platform coordinates

$\bar{r}_T$ = position vector of target vehicle at t_T

$\bar{r}_t$ = target vector for pre-targeted translunar ellipse

$\bar{r}'$ = position vector in pitch plane oriented inertial coordinate system

$\bar{r}'_o$ = position vector of launch site at "go inertial" in pitch plane oriented inertial coordinate system

$(r_{po})_u, (r_{po})_v, (r_{po})_w$ = components of $\bar{r}_{po}$

$(r_x), (r_y), (r_z)$ ≡ components of position in equatorial oriented inertial system

S = constant used in free flight predictor

s_T = sine of true anomaly of $\bar{r}_T$ or $\bar{s}$

$\bar{s}$ = unit vector in direction of outward assymptote

t = present time

t_1 = time of ignition of sustainer

t_2 = time of first ignition of Centaur

t_{11} = time (from liftoff) at which liftoff roll maneuver ends

t_D = predicted time of cutoff

t_e = time since "go inertial"

t_ℓ = time of launch

t_o = time of last ephemeris of target vehicle

t_T = time of rendezvous with target

T = time to go until cutoff

τ = transformation from platform to pitch plane oriented inertial coordinate system

T_R = transformation from platform to equatorial oriented inertial coordinate system

T_s = time to go until sustainer burnout

$TT = \begin{cases} 0 & \text{if Centaur guidance is terminated} \\ 1 & \text{if Centaur engine will re-ignite} \end{cases}$

$v_2 = |\bar{v}_T - \bar{v}'_T|$

v_c = velocity consumed

$\bar{v}_D$ = desired velocity vector

$v_g = |\bar{v}_g|$

$v_o = |\bar{v}_o|$

v_{ox}, v_{oy}, v_{oz} ≡ Initial components of velocity in equatorial oriented system

$\bar{v}_T$ = velocity vector of target at t_T

v_u, v_v, v_w = components of $\bar{v}$

v_{uo}, v_{vo}, v_{wo} = components of velocity at launch of launch site in platform coordinates

v_x, v_y, v_z = components of $\bar{v}$ along $\bar{i}$ $\bar{j}$ $\bar{k}$ respectively

v'_u, v'_v, v'_w = components of $\bar{v}'$

$v'_{uo}, v'_{vo}, v'_{wo}$ $\equiv$ components of $\overline{v'_o}$

$\bar{v}$ = present velocity vector in platform coordinates

$\bar{v}_e$ = velocity vector in equatorial oriented inertial coordinate system

$\bar{v}_g$ = velocity to be gained vector

$\bar{v}_m$ = location of center of moon at impact

$\bar{v}_o$ = velocity vector of target at t_o

$\bar{v}_{po}$ = velocity vector of launch site at "go inertial" in platform coordinates

$\bar{v}'$ = velocity vector in pitch plane oriented inertial coordinate system

$\bar{v}'_o$ = velocity vector of launch site at "go inertial" in pitch plane oriented inertial coordinate system

$\bar{v}'_T$ = velocity vector of vehicle at t_T on transfer orbit

$(v_{po})_u, (v_{po})_v, (v_{po})_w$ $\equiv$ components of $\bar{v}_{po}$

V_s = velocity remaining in sustainer stage

V'_x, V'_y, V'_z = components of velocity earth fixed coordinate system

$(V_x), (V_y), (V_z)$ = components of velocity in equatorial oriented inertial system

W = dummy variable used in search logic

W_o = previous value of W

x, y, z = components of $\bar{r}$ along $\bar{i}\ \bar{j}\ \bar{k}$ respectively

y_D = desired velocity along $\bar{j}$ direction at cutoff

y_D, z_D = components of $\bar{r}_D$ along $\bar{j}$ and $\bar{k}$ axes respectively

$\bar{1}_f$ = unit vector along desired thrusting direction

$\bar{1}_D$ = unit vector normal to $\bar{r}_D$ and $\bar{j}$

$\bar{1}_R$ = unit vector in direction of $\bar{r}_o$

$\bar{1}_T$ = unit vector normal to $\bar{1}_R$ lying in plane of $\bar{r}_D$ and $\bar{r}_T$

$\bar{1}'_x, \bar{1}'_y, \bar{1}'_z$ ≡ unit vectors along x' y' z' axes respectively

α = magnitude of Δt_T in search procedure

β = $\begin{cases} 1 \text{ iterate on } \Delta V \text{ in search procedure} \\ 0 \text{ iterate on } r_p \text{ in search procedure} \end{cases}$

γ = reciprocal of thrust acceleration of sustainer

Γ = flight path angle

δ = reciprocal of thrust acceleration of Centaur

$\theta_{pi}, \psi_{pi}, \phi_{pi}$ = Euler angle outputs

θ_p, ψ_p, ϕ_p = scaled Euler angle outputs

ΔB = steering constant

ΔE = change in eccentric anomaly

Δh_D = change in h_D

ΔM = change in mean anomaly

Δt = guidance computation cycle time

Δt_c = guidance cycle time

Δt_f = time increment used in cutoff routine

Δt_T = change in t_T

Δv_R = velocity remaining in both stages

ΔV = total velocity change needed to complete Centaur mission from present state

ΔV_R = velocity capability remaining in Centaur

$\Delta V_x, \Delta V_y, \Delta V_z$ = uncompensated incremental velocity components in platform coordinates

$\Delta V_x, \Delta V_y, \Delta V_z$ = referenced accelerometer output in platform coordinates

$\Delta v_{xi}, \Delta v_{yi}, \Delta v_{zi}$ = accumulated raw accelerometer output in platform coordinates

$\Delta \overline{V}_c$ ≡ velocity increment in platform coordinates

$\Delta \overline{V}_s$ ≡ velocity increment in computational coordinates

$(\Delta G_x), (\Delta G_y), (\Delta G_z)$ ≡ components of integrated gravity increments

$(\Delta V_{su}), (\Delta V_{sv}), (\Delta V_{sw})$ = components of sensed velocity in platform coordination

$\Delta \alpha_x, \Delta \alpha_y, \Delta \alpha_z$ = compensated commanded incremental rotational components

$\Delta \alpha_{xA}, \Delta \alpha_{yA}, \Delta \alpha_{zA}$ = commanded rotational increments

$\Delta \alpha_{xg}, \Delta \alpha_{yg}, \Delta \alpha_{zg}$ = gyro referenced output

$\Delta \alpha_{xi}, \Delta \alpha_{yi}, \Delta \alpha_{zi}$ = raw gyro output

Δu = angle between alignment azimuth and launch azimuth at "go inertial"

$\Delta \theta$ = predicted change in central angle during powered flight

$$\epsilon = \begin{cases} 1 \text{ if } T > K_{14} \\ 0 \text{ if } T \leq K_{14} \text{ and on initial guidance computation} \end{cases}$$

$$\epsilon = \begin{cases} 1 \text{ if prediction of burnout position is desired} \\ 0 \text{ if prediction of burnout position is not desired} \end{cases}$$

$\theta_{YE}, \theta_{PE}, \theta_{RE}$ = yaw, pitch, roll angle errors

$$\zeta = \begin{cases} 1 \text{ hyperbola} \\ -1 \text{ ellipse} \end{cases}$$

Υ_{12} = predicted time of free flight

$$\lambda = \begin{cases} 0 \text{ sustainer engine} \\ 1 \text{ Centaur engine} \end{cases}$$

μ = universal gravitation constant times mass of earth

$$\nu = \begin{cases} 1 \text{ if intercept guidance is desired} \\ 0 \text{ if hyperbolic or specified ellipse guidance is desired} \end{cases}$$

$$\nu_2 = \begin{cases} 1 \text{ if steering is to null velocity errors only} \\ 0 \text{ if sterring is to null both position and velocity errors} \end{cases}$$

$\bar{\xi}, \bar{\eta}, \bar{\zeta}$ = unit vectors along vehicle roll, yaw, pitch, axes respectively

$\xi_x, \xi_y, \xi_x, \eta_x, \eta_y, \eta_z, \zeta_x, \zeta_y, \zeta_z$ = elements of guidance to vehicle coordinate transformation matrix

$$\psi = \begin{cases} 1 \text{ engine on} \\ 0 \text{ engine off} \end{cases}$$

ϕ = central angle between $\bar{r}_D$ and $\bar{r}_T$

$\omega_\xi, \omega_\eta, \omega_\zeta$ = roll, yaw, pitch rate commands

$$\Omega = \begin{cases} \leq 0 & 0 \leq f < \pi \\ > 0 & \pi \leq f < 2\pi \end{cases}$$

12. REFERENCES

1. TRW Systems document 4222-6036-RU000 titled A Feasibility Study of Incorporating Closed - Loop Steering Into the Advanced Atlas/Centaur Vehicle, dated 24 June 1965.

2. R. H. Battin, Astronautical Guidance, McGraw-Hill Inc., 1964.

3. TRW Systems document 4222-6034-K0000 titled, Guidance Equations for Advanced Centaur Guidance System Study, dated 7 June 1965.

4. TRW Systems document 4222-6031-RU-000 titled Advanced Centaur Computer Requirements, dated 21 May 1965.

5. Standardized Space Guidance System (SSGS), SSGS Guidance Equation Studies (U), SECRET, TRW Systems Report 5154-6042-RZ000.

APPENDIX A

TRW SYSTEMS INTEROFFICE CORRESPONDENCE 65.9352.8-104

PRELIMINARY STUDY OF EXPLICIT GUIDANCE - CONTROL SYSTEM INTERFACE FOR ATLAS/CENTAUR

DATED 20 AUGUST, 1965 BY J.P. IVASKA, JR.

TRW SPACE TECHNOLOGY LABORATORIES
THOMPSON RAMO WOOLDRIDGE INC.
INTEROFFICE CORRESPONDENCE

65.9352.8-104
Page 1

TO: File
CC: See Distribution
DATE: 20 August 1965

SUBJECT: Preliminary Study of Explicit Guidance-Control System Interface for Atlas/Centaur

FROM: J. P. Ivaska, Jr.
BLDG. R2
ROOM 1170
EXT. 22407

REFERENCES:

1. 4222-6034-K0000, "Guidance Equations for Advanced Centaur Guidance System Study," R. P. Davis and C. M. Staley, 7 June 1965
2. GD/A-DDE65-004 (General Dynamics/Astronautics document), "Flight Dynamics and Control Analysis of the Centaur Vehicle (Atlas/Centaur AC-5)," K. C. Bonine, January 1965

I. SUMMARY

This investigation analyzed the Atlas/Centaur guidance-control interface problems associated with the incorporation of the explicit guidance scheme developed in Reference 1. This preliminary study was divided into two distinct sections.

The first was conducted under the assumption that the guidance commands are updated continuously; it showed that explicit guidance loop would not degrade system stability excessively. The second section evaluated the effects of the digital nature of the guidance loop; it determined that the stability degradation remains tolerable with this more realistic representation of the guidance loop. This analysis also showed that the range of guidance loop sampling periods which yield acceptable system stability characteristics is between zero and five seconds.

The conclusions of this preliminary study are: (1) from a control system viewpoint, the explicit guidance scheme can be incorporated into the Atlas/Centaur vehicle; and (2) the guidance commands should be updated at least once every five seconds.

II. INTRODUCTION

A. General

TRW Systems Group is conducting a study program in support of Atlas/Centaur for the National Aeronautics and Space Administration, Lewis Research Center, under Contract Number NAS 3-3231. The program consists of six major tasks, most of which are concerned with guidance of Atlas sustainer or Centaur stages. This report contains analysis supporting Task VI, one objective of which is the development of a set of explicit guidance equations for use during exoatmospheric flight. The analysis is devoted to an investigation of the guidance-control interface problems caused by the incorporation of this explicit guidance scheme into the Atlas/Centaur vehicle.

B. Background

For the purposes of stability analysis, guidance equations may be classified into two very general divisions. One class consists of open-loop guidance schemes; the commands generated are functions only of time, not of any quantity describing vehicle state.

A second class consists of closed-loop guidance schemes; the commands are functions of vehicle state, though they may also depend on time. Within this class are two further classifications. One is delta guidance equations; the commands are functions of the differences between certain vehicle state variables and the corresponding desired end conditions. The key equation of such a scheme is usually a truncated power series. The second classification is comprised of explicit guidance methods, which are dependent on present vehicle state and which use equations in closed form.

The two basic classes, open- and closed-loop guidance schemes, differ markedly in their impact on system stability characteristics. Because a closed-loop guidance approach is dependent on certain vehicle state variables, some of which may be measured and used by the control system, its incorporation may alter vehicle stability characteristics. Experience has shown that system stability is generally degraded by inclusion of closed-loop guidance. However, an open-loop guidance scheme, which utilizes no vehicle state information, does not change vehicle stability characteristics.

For the same reason, the two classes also differ strikingly in their capability in handling non-nominal situations. Open-loop guidance does not sense off-nominal conditions and cannot correct for them. Closed-loop guidance is sensitive to variations from nominal and, therefore, includes possibilities of compensating for them.

Whenever a new closed-loop guidance approach is proposed, it must be evaluated with respect to several considerations. It should possess certain capabilities which can be assessed without regard to guidance-control interface problems. Among these is the capability to minimize off-nominal errors. However, it is equally important that its effects on system stability characteristics be tolerable.

The present Atlas/Centaur uses closed-loop delta guidance equations. However, a set of closed-loop explicit guidance equations has been developed under Task VI for use on later Atlas/Centaur vehicles; the derivation is presented in Reference 1. Its various attributes are presently being investigated, and important among these is the impact of its incorporation on system stability characteristics.

C. Objectives of Study

The basic objective of this study is to evaluate interface problems between the explicit guidance scheme of Reference 1 and the vehicle control system. The incorporation of this guidance method must not result in excessive degradation of vehicle stability.

There is an additional aspect to the problem. The guidance equations are to be implemented digitally; this raises the question of how often the guidance commands should be updated. Generally, the more frequently the updating is performed, the less stability characteristics are degraded. This implies that there exists a minimum allowable sampling frequency which can be formulated just on the basis of vehicle stability considerations. An evaluation of the interface between guidance and control must include the development of such a requirement.

III. GENERAL APPROACH

This section presents the approach used to evaluate the guidance-control interface problems resulting from incorporation of explicit guidance into Atlas/Centaur. Details of the actual analysis are deferred until later sections. Through the procedure outlined below, it was possible to determine whether the explicit guidance scheme can be used in Atlas/Centaur without intolerable alterations in vehicle stability.

A. Choice of Trajectory

The Atlas/Centaur explicit guidance scheme is designed to accommodate a wide class of possible trajectories. However, to make the problem tractable, a typical trajectory had to be selected. This is not a serious limitation on the value of the analysis since the guidance-control interface problems were not expected to be greatly trajectory dependent. The trajectory chosen for this study should not be extreme and should be typical of missions projected for future Atlas/Centaur missions.

B. Stability Analysis for Vehicle Without Closed-Loop Guidance

After the trajectory selection, the next step was to evaluate vehicle stability characteristics in the absence of open-loop guidance. This provided a basis for comparison through which subsequent results were evaluated. First, it had to be decided whether the analysis was to be conducted in the pitch plane or in the yaw plane or whether studies for both planes were necessary. After this decision, the following tasks were performed.

1. Linearization of System Equations

In launch vehicle or missile design, stability investigations are generally started by linearizing the vehicle total equations. The resulting set of linear differential equations characterize system behavior in the small. Coefficients of the equations are fixed at values corresponding to critical flight times, and conventional linear control system techniques are employed to derive vehicle stability portraits. The basic assumption is that the rate of change of the coefficients of the equations is low compared to the frequencies of interest, usually an easily justifiable assumption.

Since the primary purpose of this analysis was to examine the guidance-control interface, related topics such as slosh limit cycle and actuator nonlinearities which may affect the basic system characteristics were ignored. These effects should be examined later in more detailed studies.

2. Choice of Flight Times

In launch vehicle and missile control system design, particularly for atmospheric flight, the choice of flight times for which to evaluate system stability is comparatively straightforward. Those generally selected are Liftoff, Max-Q (the time of flight at which aerodynamic pressure is maximum), Burnout, and flight times when gain changes occur.

For this problem, the choice of flight times is not as clear, for two reasons. First, the explicit guidance scheme is not used until the exoatmospheric phase of flight, which eliminates several of the above possibilities. Second, the times selected should be those when the guidance scheme-control system interface problems are comparatively severe, which is difficult to estimate a priori.

A reasonable solution is to spread all but one of the selected times of flight fairly evenly throughout the period of use of the explicit guidance scheme and choose the remaining flight time near the end of that period. Experience has shown that incorporation of a closed-loop guidance scheme generally results in greatest degradation of vehicle stability characteristics near the end of its employment, when the matching of boundary conditions is completed.

3. Linear Analysis

After linearization of system equations and choice of flight times, conventional control system techniques were used to obtain the appropriate stability portraits. Gain-phase plots were used, and values of critical stability margins were read from these. The details of the use of the gain-phase plot and the significance of various stability margins are explained in Section 5.2.

C. Stability Analysis for Vehicle Incorporating Explicit Guidance

Tasks similar to those described above were also completed for a vehicle including explicit guidance, so that the severity of guidance-control interface problems could be assessed.

1. Linearization of Guidance Equations

The linearization of system equations for a vehicle without closed-loop guidance is comparatively straightforward, because the dynamic and control system equations for different launch vehicles are similar in form. However, different guidance schemes generally use far different sets of total equations, and the linearization of sets of guidance equations must be done individually.

After completion of guidance equation linearization, a complete set of small-angle equations was available for a vehicle including explicit guidance. Stability portraits were then obtained for such a vehicle for the flight conditions previously selected.

2. Comparison of Results

Comparisons of corresponding stability portraits determined the severity of the guidance-control interface problems. The results can dictate whether the explicit guidance approach can be incorporated into the Atlas/Centaur without intolerable degradation of vehicle stability.

The representation of the guidance loop in these foregoing analyses was continuous. In actual fact, the guidance commands are computed digitally; this means aggravation of any interface problems. The above comparison simply determines whether the explicit guidance can be included in the somewhat idealized case for which the guidance commands are updated continuously.

3. Determination of Minimum Allowable Sampling Frequency

To complete the examination of guidance-control interface problems, a minimum allowable frequency for updating the guidance commands must be established. There exists no standardized procedure for this task, but it should begin with an examination of the previous results.

For the flight times for which the introduction of continuously updated explicit guidance caused little degradation of stability characteristics, significant alteration because of sampling effects in the guidance loop is very unlikely. However, for each flight time for which there is considerable degradation for a continuous representation of the guidance loop, a further analysis should be conducted to determine the lowest sampling frequency which results in adequate system stability. If there is more than one such flight time, the highest such sampling frequency must be used so that satisfactory stability characteristics exist for all flight times.

IV. ANALYSIS

This section provides the details of the analysis, the structure of which is outlined in the preceding section.

A. Selection of Trajectory

The trajectory selected for this study places the payload in a 580-nautical mile circular orbit. The flight is divided into three distinct segments. The first is Atlas booster flight, which extends from Liftoff to Booster Engine Cutoff (BECO), at 140.09 seconds after Liftoff. Atlas sustainer flight is the second phase; it extends from BECO until Sustainer Engine Cutoff (SECO), which occurs at 238.07 seconds after Liftoff. The third phase is Centaur flight, lasting from SECO until Main Engine Cutoff (MECO), nominally at 566.25 seconds after Liftoff.

The explicit guidance scheme is designed for operation during portions of the flight when aerodynamic forces are no longer significant. It is initiated when the vehicle achieves a certain prespecified altitude. This occurs during sustainer flight, the exact flight time being dependent on the altitude selected. Consequently, this explicit guidance scheme is used from some point in the sustainer phase until MECO. The period of time between Liftoff and MECO listed above is nominal; for particular flights, non-nominal conditions can cause a change in that time in accordance with the action of the explicit guidance methods.

B. Stability Analysis for Vehicle Without Explicit Guidance

The following discussion presents the stability characteristics for an Atlas/Centaur launch vehicle which does not include any form of closed-loop guidance. It provides a basis for comparison by which the effects of explicit guidance on vehicle stability can be evaluated.

All analyses were conducted in the pitch plane, as it was judged that the guidance-control interface problems are more severe there than in the yaw plane. For the latter plane, the purpose of the guidance loop is simply to maintain the vehicle within the desired flight plane; no trajectory shaping is needed. However, in the pitch plane, trajectory shaping is required, because the vehicle must be placed in a prespecified orbit.

1. System Descriptions

First, the system representations used for analysis of Atlas sustainer and Centaur phases should be presented. The vehicle dynamic equations are very similar to many sets previously used in launch vehicle and missile design but are considerably simplified by the fact that aerodynamic forces are insignificant. The set summarized in Section 5.1 is applicable to both sustainer and Centaur phases. The control systems used for the two phases differ considerably and are responsible for the fundamental differences in system descriptions.

a. System Description for Sustainer Phase

Figure 1 is a conventional block diagram applicable to sustainer phase without closed-loop guidance. The control system gains differ from those used for Centaur flight, but there are only two essential differences between that diagram and the corresponding one for Centaur phase. The first is the inclusion of the 25-radian-per-second simple lag filter for sustainer phase; no filtering is used during Centaur flight. The second is that the effects of gyro dynamics may be neglected for sustainer phase.

For both phases, the engine actuator hydraulics were simulated by a simple lag; the time constants for the two segments of the trajectory differ slightly.

b. System Description for Centaur Phase

Figure 2 is the system block diagram for Centaur stage without closed-loop guidance. Gyro dynamics must be included for this phase, because the gyros in the two control systems differ considerably. The dynamics of the Centaur gyro, an overdamped type, become significant at a frequency much lower than the corresponding frequency for the Atlas gyro; experience has shown that the degradation of vehicle stability due to incorporation of closed-loop guidance is generally concentrated at low frequencies. Because the Centaur gyro is an overdamped type, its dynamics may be simulated by a simple lag. The time constant, as given by Reference 2, is 0.03 seconds.

2. Flight Times Selected

Before the system stability portraits can be obtained, the flight times must be chosen for which to conduct the linear analyses. In accordance with the philosophy explained in the previous section, the following four times of flight were selected: (1) 200 seconds after Liftoff, approximately at the midpoint of the sustainer phase; (2) 360 seconds after Liftoff, approximately at the midpoint of the period of use of the explicit guidance scheme; (3) 520 seconds after Liftoff, during the latter portion of that period; and (4) 560 seconds after Liftoff, nominally just 6.25 seconds before MECO. Table 1 gives the vehicle dynamic parameters for these times of flight.

3. Stability Portraits

Figures 3 through 6 show the system stability portraits for a vehicle without closed-loop guidance for the above four times of flight. The graphs are gain-phase plots of the frequency responses of the transfer functions from commanded engine actuator angle to control system output. System stability margins may be read from these graphs and are listed in Table 2. (Section 5.2 discusses the use of such gain-phase plots for analysis of exoatmospheric flight of launch vehicles or missiles; it also presents desirable values for the various stability margins.)

A comparison of the gain-phase plots for the latter three times of flight shows that the shapes of the three graphs are identical and that the only differences are in the location of the zero-decibel line. This reflects the fact that the only differences in the three systems of equations are in the value of the control coefficient (μ_c), to which the loop feedforward gain is linearly related. The control coefficient increases with time during Centaur flight, because the engine thrust remains constant and vehicle moment of inertia decreases; the result is that both low-frequency gain margin and rigid body phase margin increase with time from their relatively low values for 360 seconds after Liftoff. High-frequency rigid body gain margin decreases with time but is always more than adequate throughout exoatmospheric flight.

C. Stability Analysis for Vehicle Incorporating Explicit Guidance

This portion contains the stability analysis conducted for an A/C vehicle using explicit guidance. A procedure was followed that is very similar to that used for an Atlas/Centaur without closed-loop guidance.

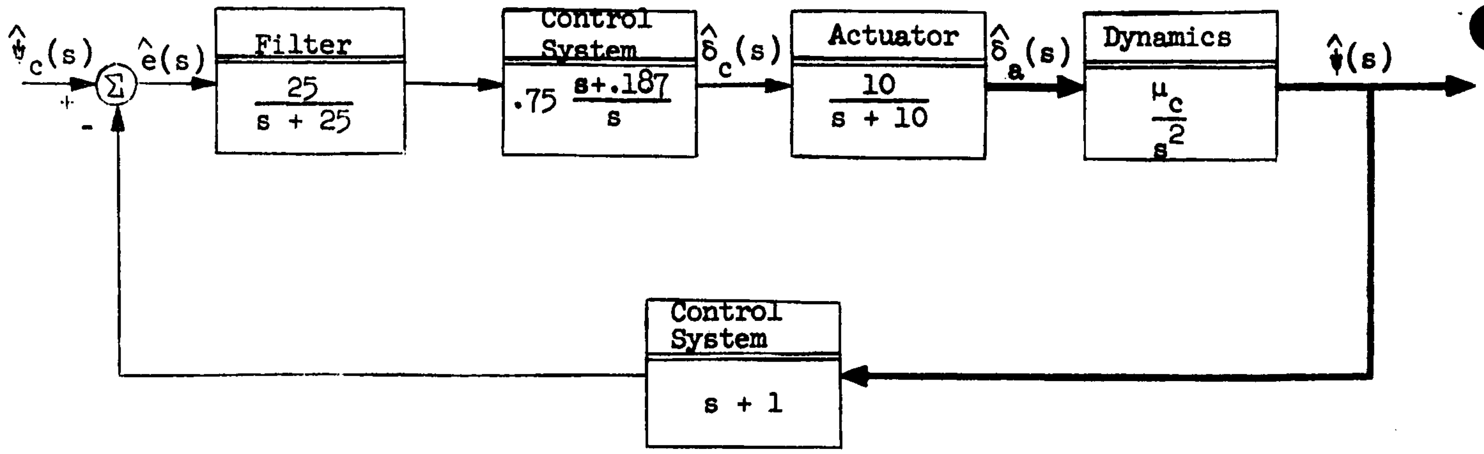
$\hat{\psi}_c(s)$
+
-
Σ
$\hat{e}(s)$
Filter
$\frac{25}{s+25}$
Control System
$.75\,\frac{s+.187}{s}$
$\hat{\delta}_c(s)$
Actuator
$\frac{10}{s+10}$
$\hat{\delta}_a(s)$
Dynamics
$\frac{\mu_c}{s^2}$
$\hat{\psi}(s)$
Control System
$s+1$
Legend
Electrical Signal
Dynamic Quantity

Figure 1. System Block Diagram (Sustainer Phase) for Vehicle Without Closed-Loop Guidance

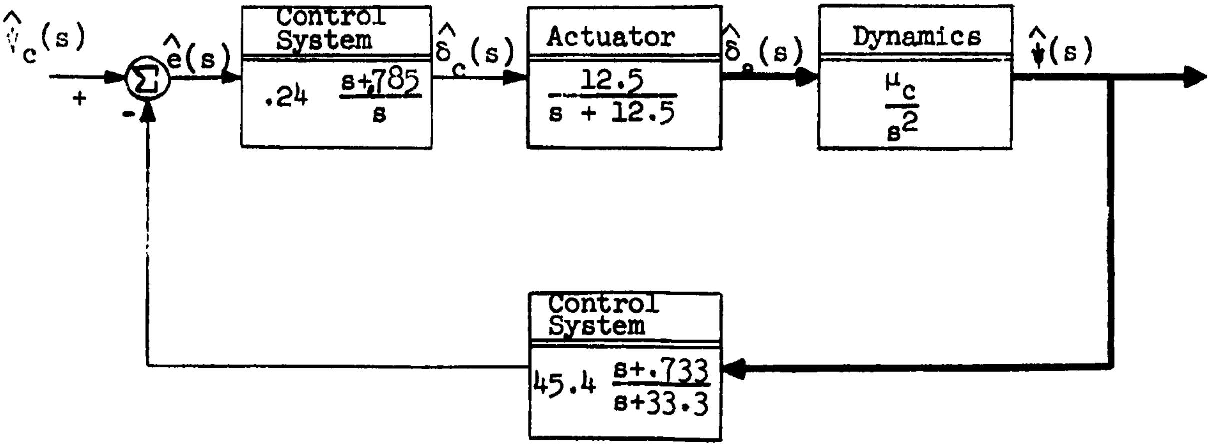
$\hat{\psi}_c(s)$
+
-
Σ
$\hat{e}(s)$
Control System
$.24\,\frac{s+.785}{s}$
$\hat{\delta}_c(s)$
Actuator
$\frac{12.5}{s+12.5}$
$\hat{\delta}_a(s)$
Dynamics
$\frac{\mu_c}{s^2}$
$\hat{\psi}(s)$
Control System
$45.4\,\frac{s+.733}{s+33.3}$
Legend
Electrical Signal
Dynamic Quantity

Figure 2. System Block Diagram (Centaur Phase) for Vehicle Without Closed-Loop Guidance

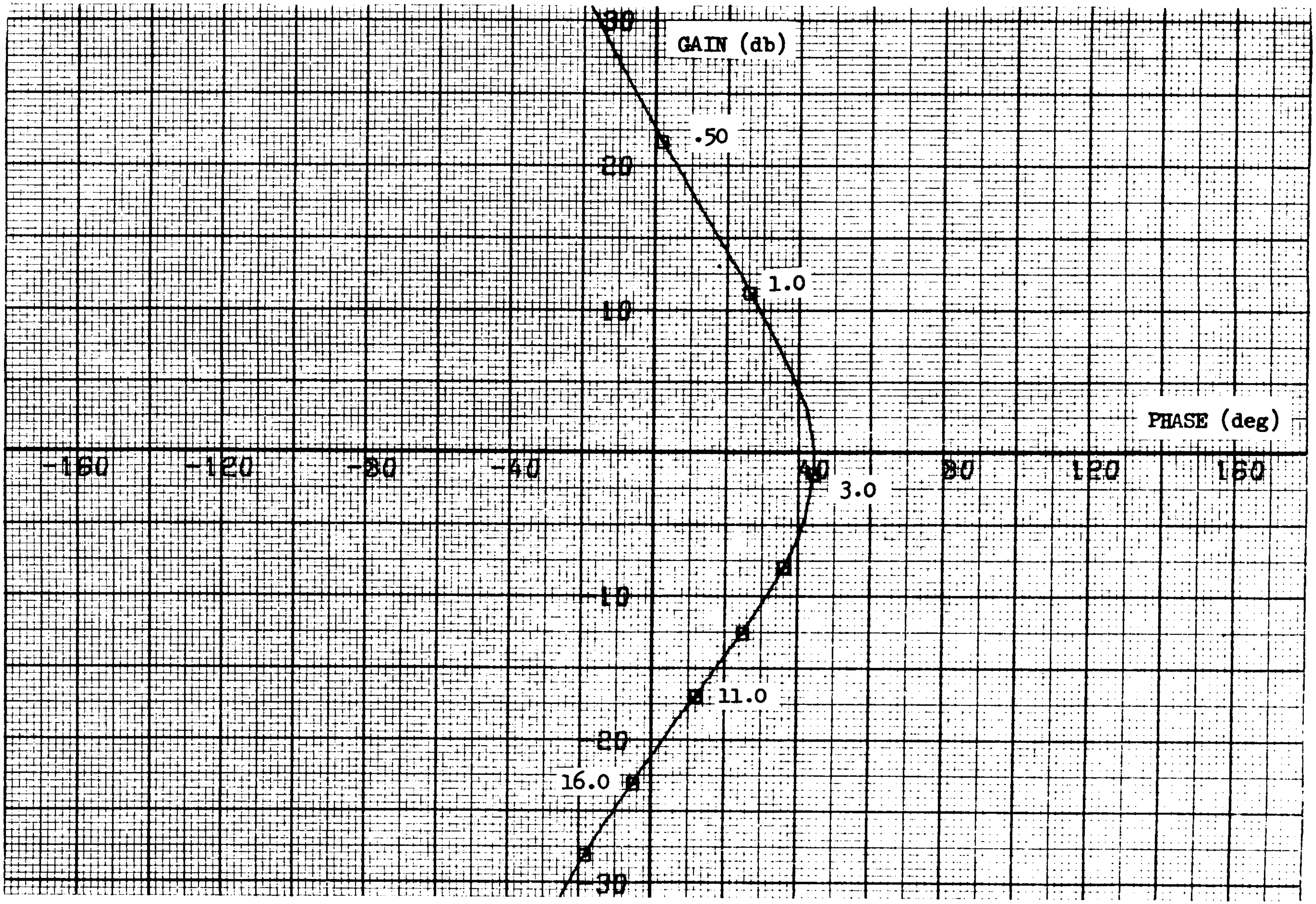

Figure 3. Gain-Phase Plot for 200 Seconds After Liftoff for Vehicle Without Closed-Loop Guidance

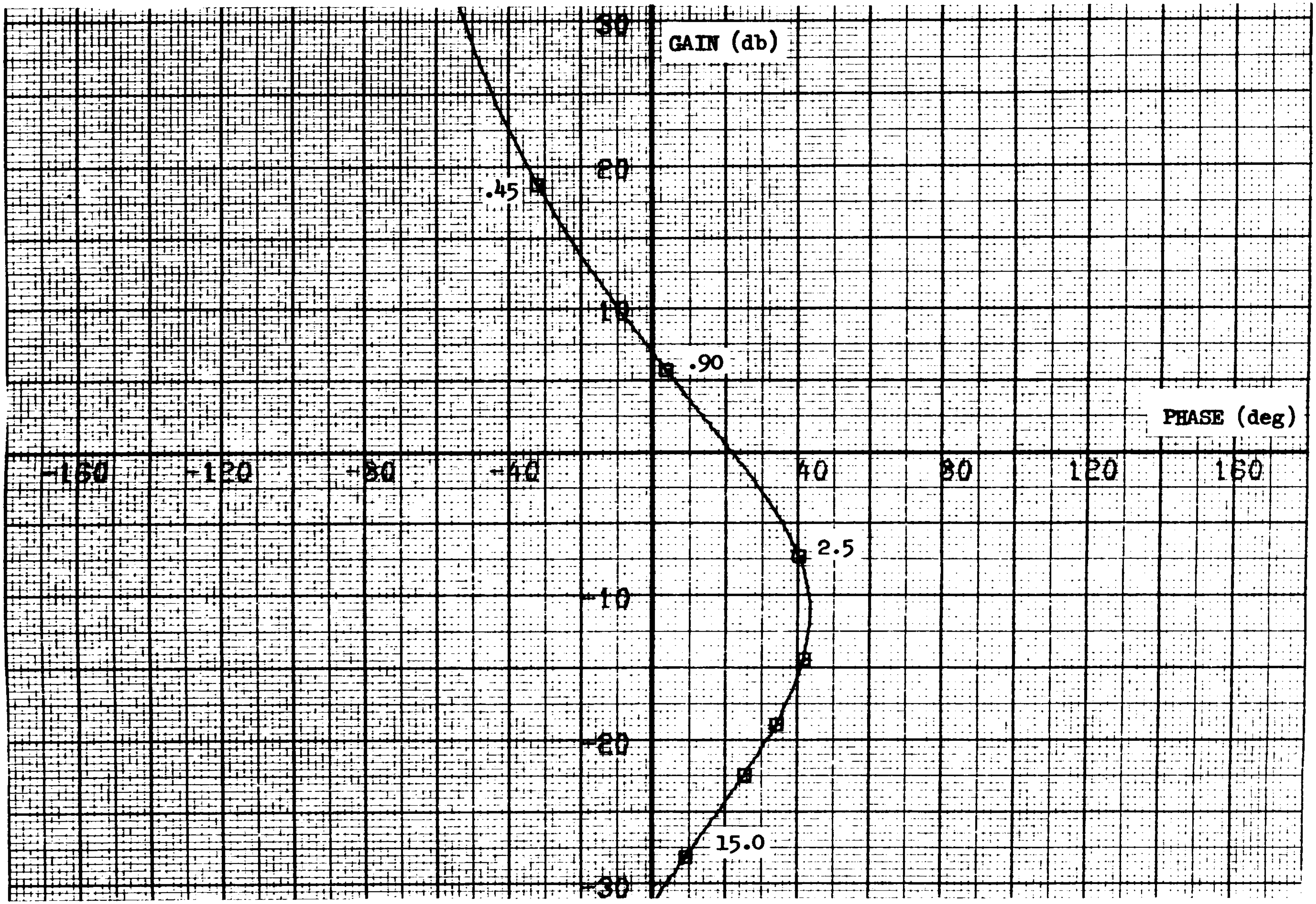

Figure 4. Gain-Phase Plot for 360 Seconds After Liftoff for Vehicle Without Closed-Loop Guidance

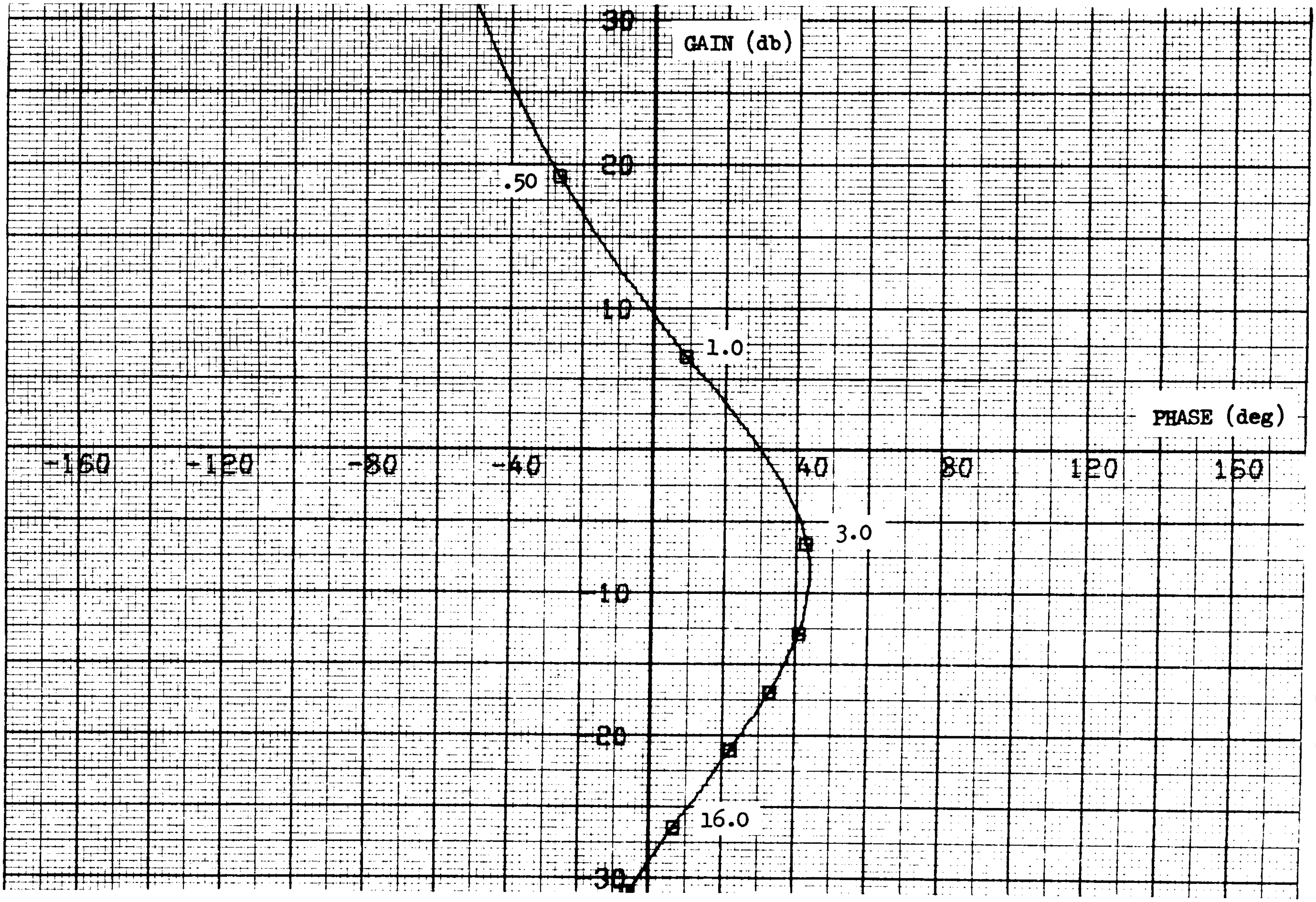

Figure 5. Gain-Phase Plot for 520 Seconds After Liftoff for Vehicle Without Closed-Loop Guidance

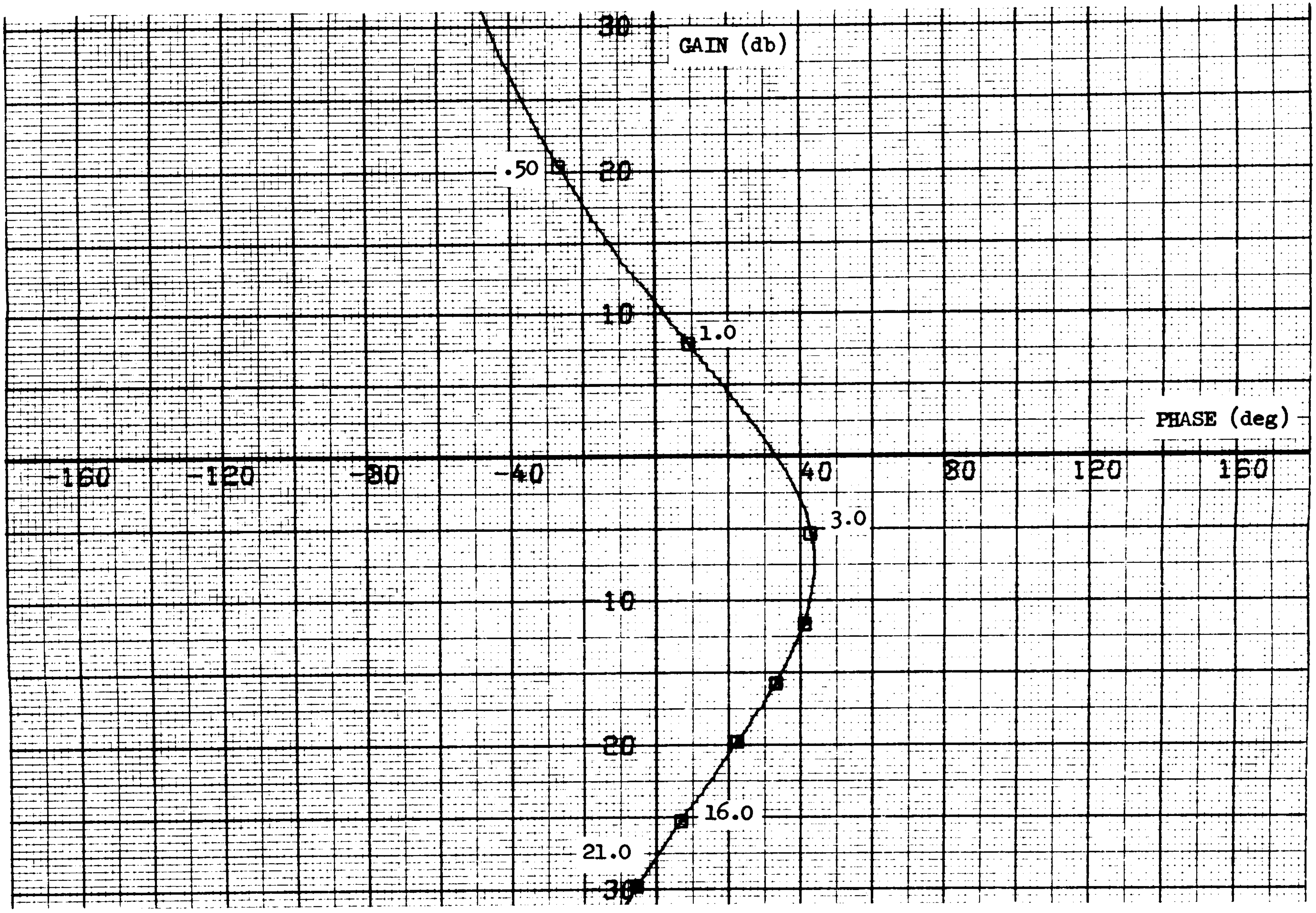

Figure 6. Gain-Phase Plot for 60 Seconds After Liftoff for Vehicle Without Closed-Loop Guidance

Table 1. Vehicle Dynamic Parameters

T(time after Liftoff-sec)	a_c(ft/sec^2)	μ_c(sec^{-2})	ℓ_p(ft)
200	46.5	3.35	32.0
360	33.8	3.13	16.4
520	55.2	4.16	15.3
560	65.9	4.73	14.6

Table 2. System Stability Margins for a Vehicle Without Closed-loop Guidance

T(time after Liftoff-sec)	Low-frequency Gain Margin (db)	Rigid Body Phase Margin (deg)	High-frequency Rigid Body Gain Margin (db)
200	22.5	44.0	21.3
360	7.1	22.5	31.6
520	9.6	29.5	29.0
560	10.8	32.5	27.9

1. System Descriptions

The first task was linearization of the guidance equations so that an entire set of perturbed equations was available for a vehicle with explicit guidance. The details of the derivation are presented in Section 5.3, but the results are summarized in Figure 7. The natures of the linearized models of the guidance loop for sustainer and Centaur phases are identical, and the values of the linearized coefficients are given in Table 3.

2. Stability Portraits

Figures 8 through 11 are the stability portraits for a vehicle with explicit guidance for the four flight times. Each is a gain-phase plot of the frequency response of the transfer function from commanded engine actuator angle to control system output. The stability margins are listed in Table 4 and can be compared with the corresponding figures for an Atlas/Centaur without explicit guidance.

3. Comparison of Results

The corresponding stability margins were compared for two purposes; the most important was to determine whether explicit guidance can be integrated into Atlas/Centaur under the idealized condition of continuous updating of guidance commands. The second purpose was to determine which times of flight should be subjected to further analysis for derivation of minimum allowable sampling frequency.

The changes in stability margins are tabulated in Table 5. For 200, 360 and 520 seconds after Liftoff, the introduction of explicit guidance causes no significant reduction in stability margins. For the second of these flight times, the rigid body phase margin is lower than desirable both with and without explicit guidance, but this fact is traceable to the control system design, not any characteristic of the guidance scheme.

For 560 seconds after Liftoff, there is considerable degradation of vehicle stability characteristics. Though the high-frequency rigid body gain margin is not significantly altered, both the low-frequency gain margin and the rigid body phase margin are reduced to very low levels.

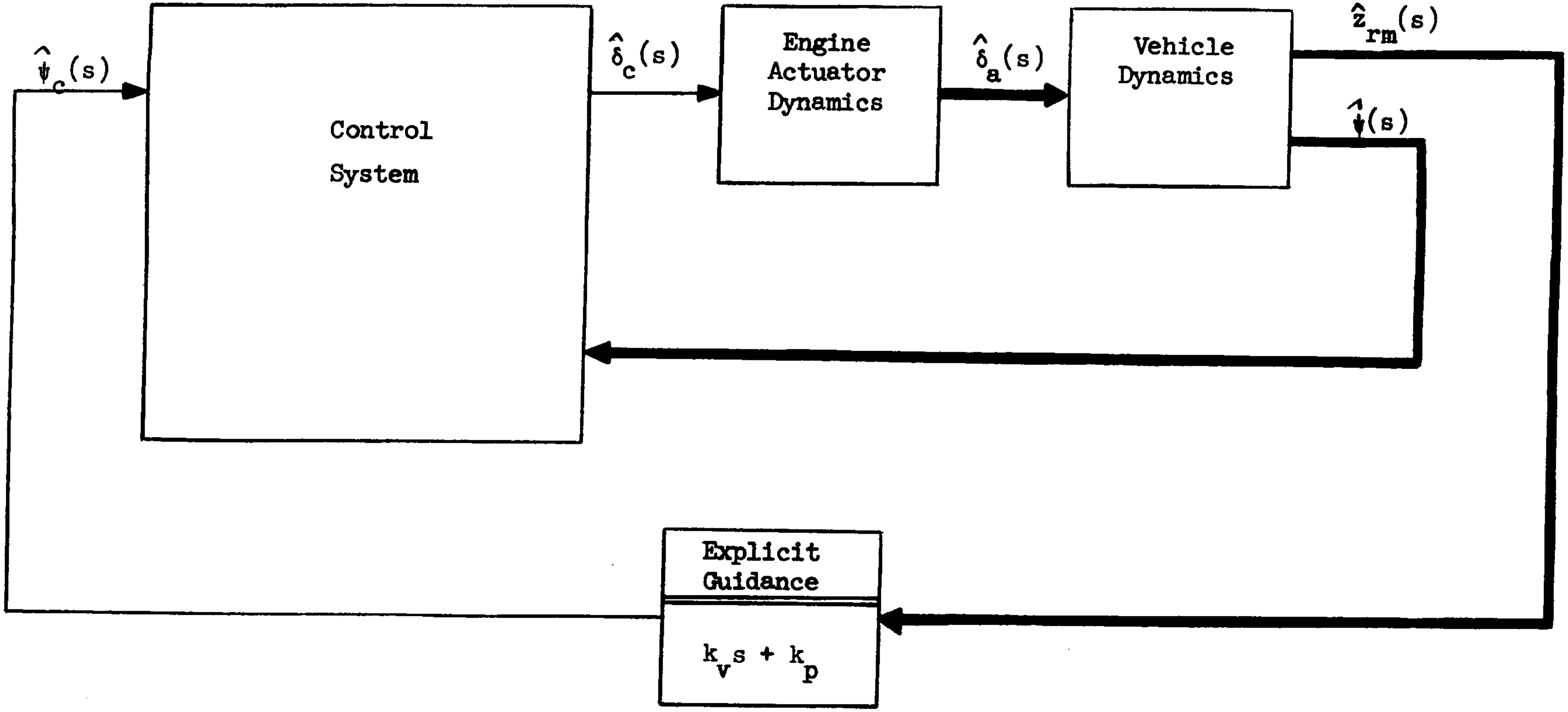
$\hat{\psi}_c(s)$
Control System
$\hat{\delta}_c(s)$
Engine Actuator Dynamics
$\hat{\delta}_a(s)$
Vehicle Dynamics
$\hat{z}_{rm}(s)$
$\hat{\psi}(s)$
Explicit Guidance
$k_v s + k_p$

Legend
Electrical Signal
Dynamic Quantity

Figure 7. General System Block Diagram Representation for Vehicle Incorporating Explicit Guidance

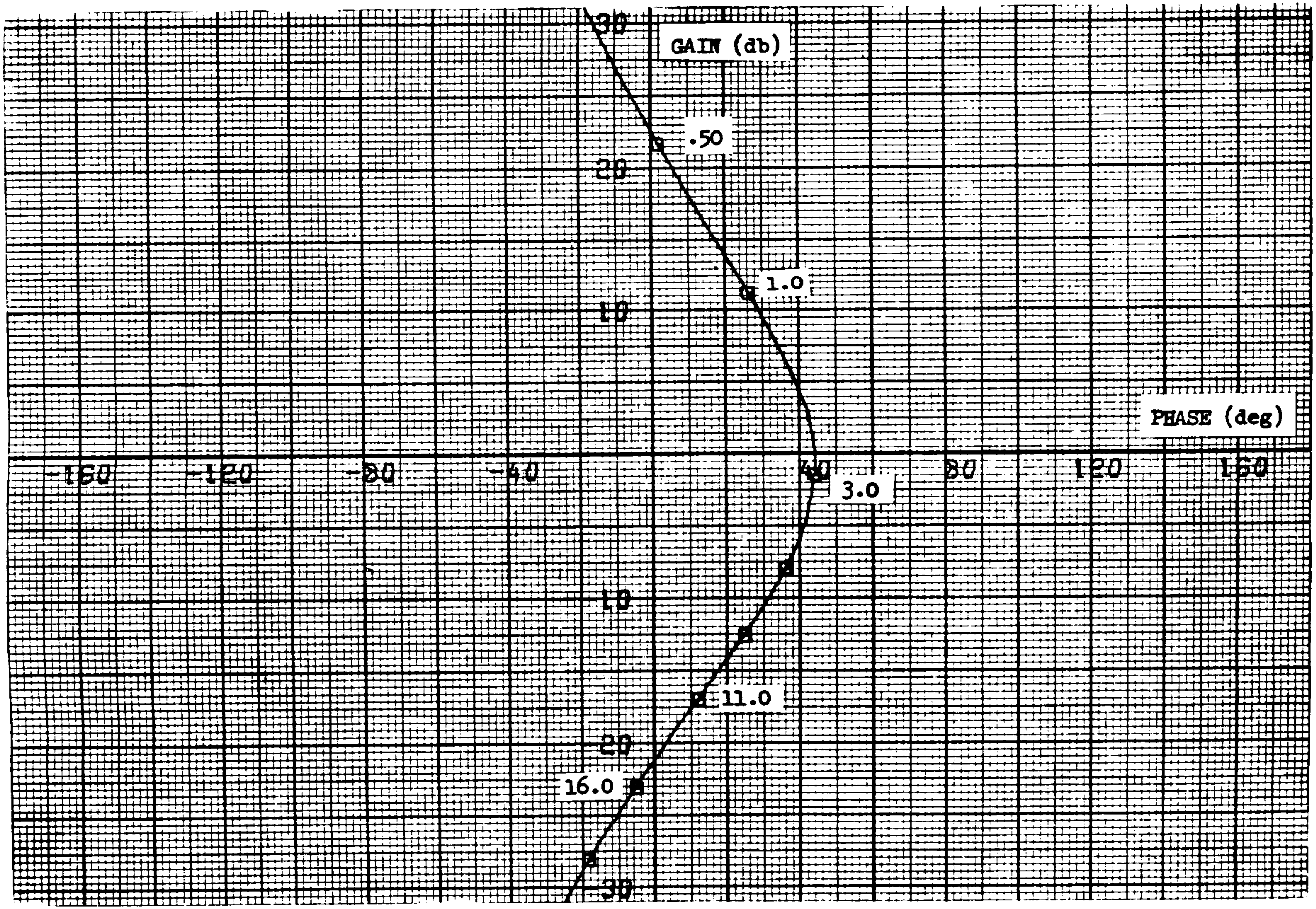

Figure 8. Gain-Phase Plot for 200 Seconds After Liftoff for Vehicle Incorporating Explicit Guidance

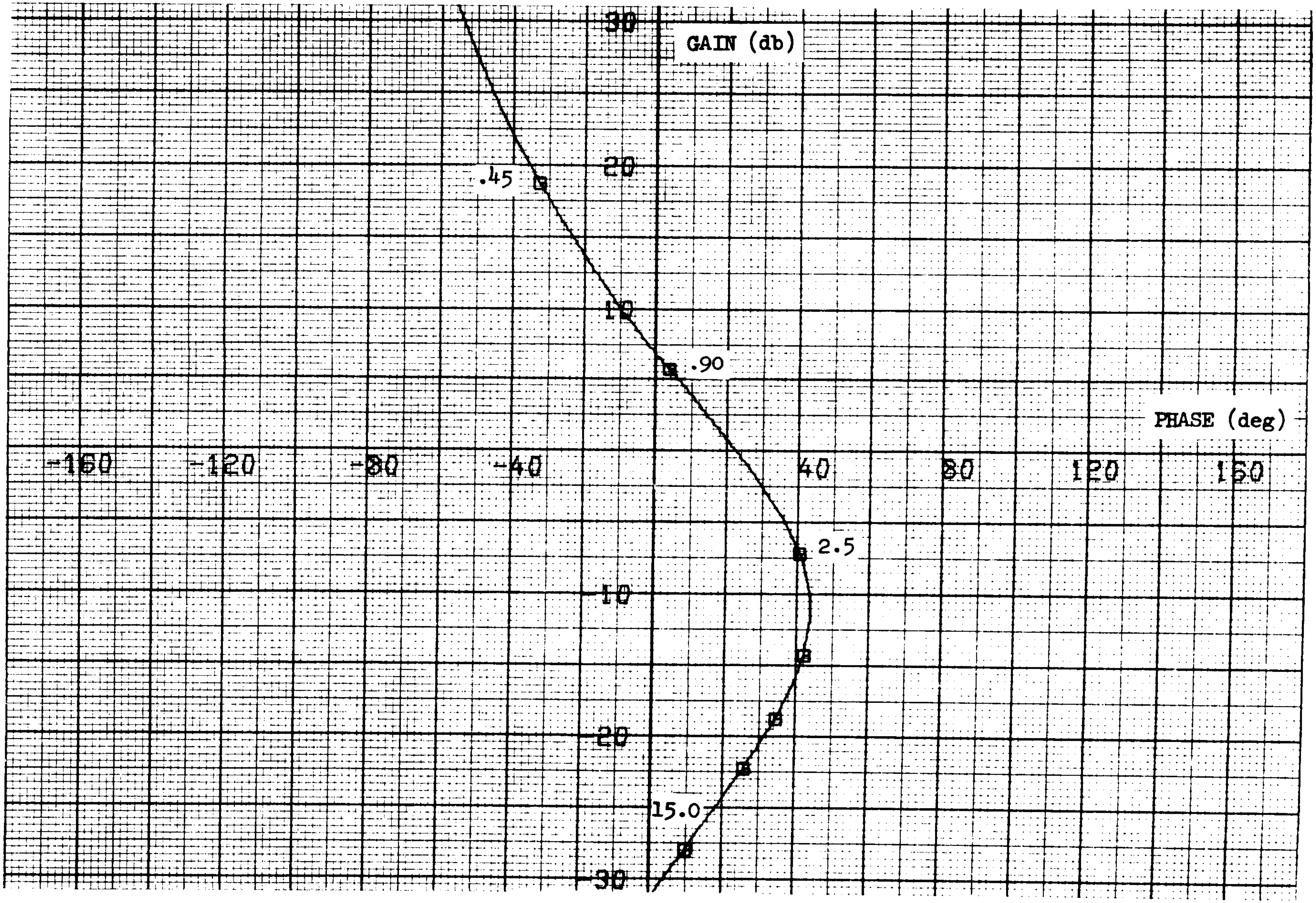

Figure 9. Gain-Phase Plot for 360 Seconds After Liftoff for Vehicle Incorporating Explicit Guidance

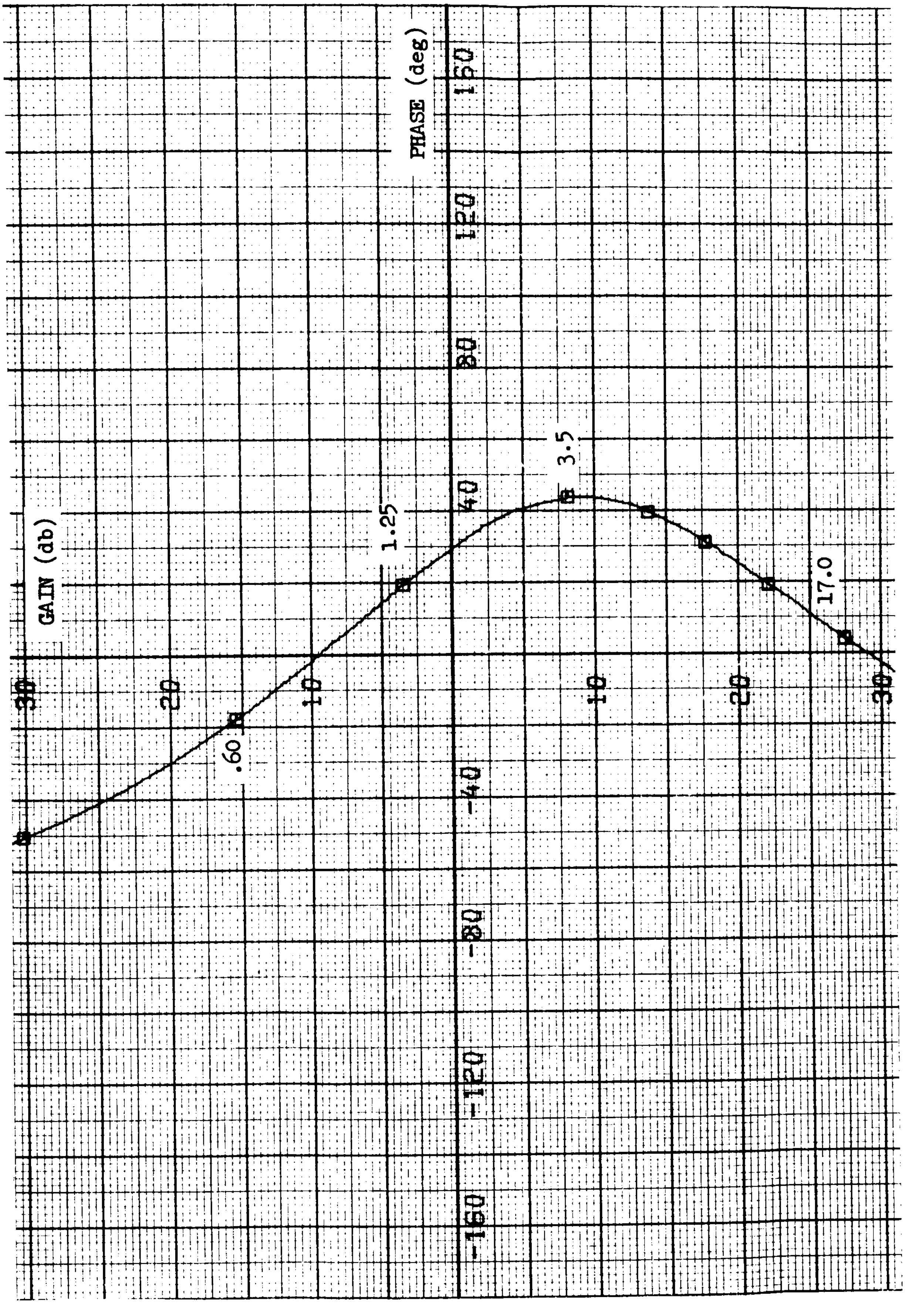

Figure 10. Gain-Phase Plot for 520 Seconds After Liftoff for Vehicle Incorporating Explicit Guidance

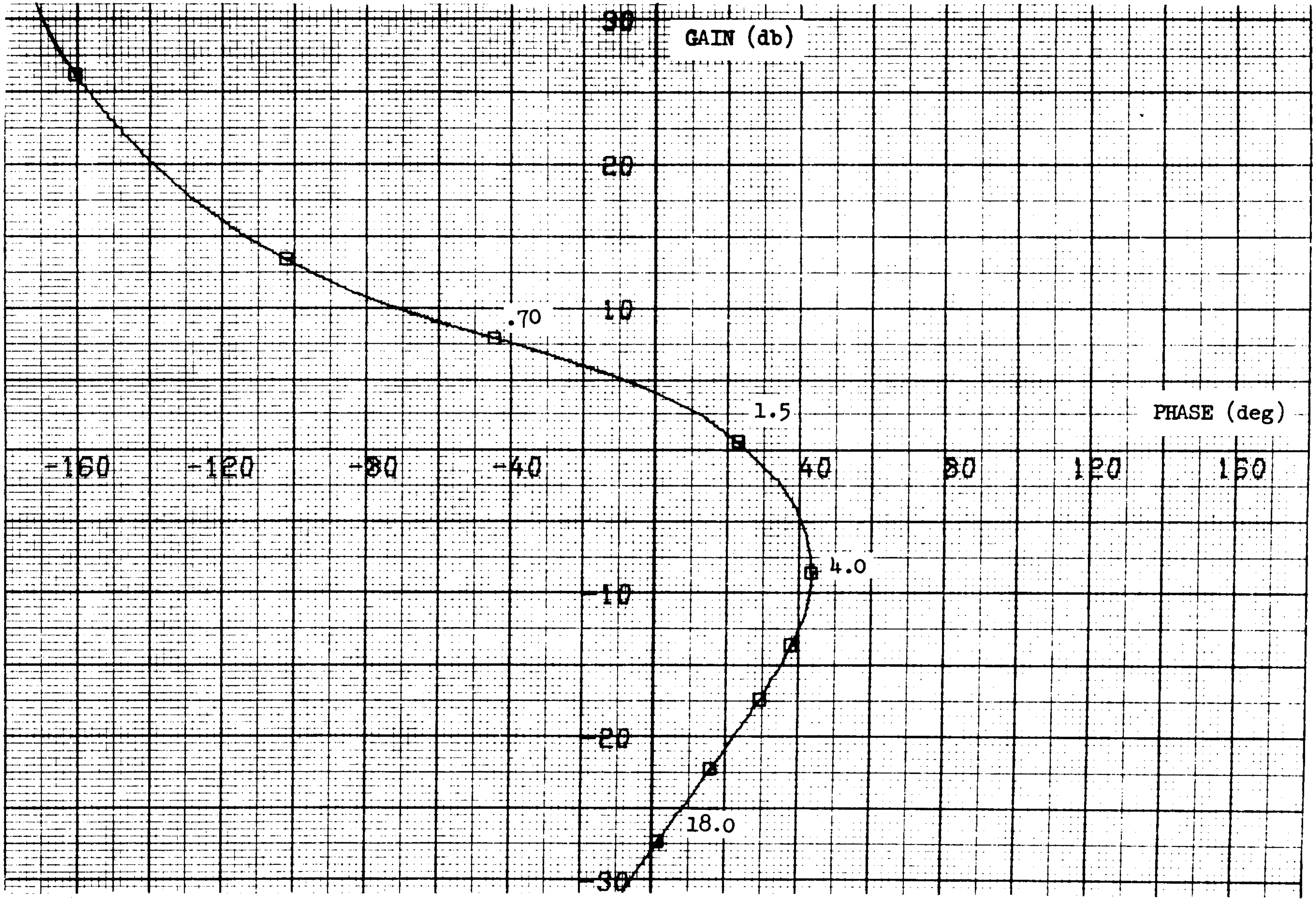

Figure 11. Gain-Phase Plot for 560 Seconds After Liftoff for Vehicle Incorporating Explicit Guidance

Table 3. Values of Linearized Guidance Loop Coefficients

T (time after Liftoff-sec)	K_v(sec/ft)	K_p(ft^{-1})
200	$-.198(10^{-3})$	$-.958(10^{-6})$
360	$-.381(10^{-3})$	$-.463(10^{-5})$
520	$-.240(10^{-3})$	$-.507(10^{-4})$
560	$-.903(10^{-2})$	$-.233(10^{-2})$

Table 4. System Stability Margins for a Vehicle Incorporating Explicit Guidance

T(time after Liftoff-sec)	Low-frequency Gain Margin (db)	Rigid Body Phase Margin (deg)	High-frequency Rigid Body Gain Margin (db)
200	22.5	44.0	21.3
360	7.0	22.2	31.5
520	9.5	28.8	29.0
560	4.0	24.8	27.9

Table 5. Changes in System Stability Margins Caused by Incorporation of Explicit Guidance

T(time after Liftoff-sec)	Change in Low-frequency Gain Margin (db)	Change in Rigid Body Phase Margin (deg)	Change in High-frequency Rigid Body Gain Margin (db)
200	0.0	0.0	0.0
360	-0.1	-0.3	-0.1
520	-0.1	-0.7	0.0
560	-6.8	-7.7	0.1

However, several special considerations must be recognized in a discussion of results for a flight time so late in the mission. The first is that MECO nominally occurs just 6.25 seconds later. Also, the explicit guidance scheme discontinues updating of commands five seconds before MECO, or only 1.25 seconds after the flight time under consideration. When the guidance commands are no longer updated, the stability characteristics revert to those for a vehicle without closed loop guidance. For 560 seconds after Liftoff, the latter margins are satisfactory.

Consequently, although the stability characteristics for a vehicle with explicit guidance are poor at 560 seconds after Liftoff, they are applicable only for a very short period of time. This is significantly different from the more usual situation in which stability characteristics change only very slowly with flight time and poor stability margins are likely to have more serious consequences.

Furthermore, the primary assumption upon which these linear analyses were based is considerably less justifiable for an Atlas/Centaur with explicit guidance near MECO than for the other situations treated. It was always assumed that the linearized coefficients change at frequencies much lower than the frequencies of interest. However, as can be seen from Table 3, the coefficients of the guidance loop change comparatively rapidly late in flight (for reasons discussed in Appendix C in connection with the derivation of the literal expressions for the coefficients), and the assumption of quasi-constant linearized coefficients was more dubious than usual. The significance of stability margins was therefore reduced.

Because of these considerations, the effects of the incorporation of explicit guidance were judged tolerable for 560 seconds after Liftoff, because the analysis showed that instability does not result. For the other flight times, the effects were found acceptable because the stability characteristics were altered very little by the inclusion of explicit guidance.

4. Determination of the Minimum Allowable Sampling Frequency

In the analyses explained above, the representation of the guidance loop was continuous; the guidance commands were assumed to be updated instantaneously. In fact, the commands are computed digitally and are updated only at intervals.

Also, the computer requires a finite time to process information to generate updated commands. Both effects cause degradation of system stability characteristics.

Incorporation of explicit guidance causes very little change in vehicle stability for 200, 360 and 520 seconds after Liftoff, and the addition of the above two effects to the system models was expected to cause very little more for realistic values of sampling frequency and computation time. Consequently, the flight time nearest MECO was investigated further for determination of the minimum allowable sampling frequency.

A sampled-data simulation was used for this purpose. It is capable of representing both the continuous nature of the vehicle control system and dynamics and the digital nature of the guidance loop. The computational delay was estimated at 0.5 seconds and used throughout. Five sampling periods (lengths of intervals between guidance command updatings) were selected for study and were intended to cover the range of reasonable possibilities. They were 1, 2, 5, 10 and 20 seconds.

Any sampling period was considered acceptable which did not result in instability for 560 seconds after Liftoff, in accordance with the reasons which lead to the earlier conclusion that the effects of explicit guidance are tolerable for that flight time. Figures 12 through 16 are vehicle stability portraits for the five sampling periods tested. They show that the system is stable for periods of 1, 2 and 5 seconds, but unstable for values of 10 and 20 seconds.

Figures 12 through 16 are gain-phase plots of the frequency responses of the transfer functions from commanded vehicle body angle to output of the guidance loop. This is a different transfer function from the one used to draw the gain-phase plots discussed previously. Consequently, the general shapes of the curves for the two sets of gain-phase plots differ markedly, and the stability margins have different meanings. However, this is not important, because all that was wanted from the second set was an indication of whether the systems including explicit guidance and sampling effects are stable.

A comparison of the five plots shows that the maximum allowable sampling period is between 5 and 10 seconds, very likely only slightly greater than the former value. Five seconds may be taken as the maximum allowable period.

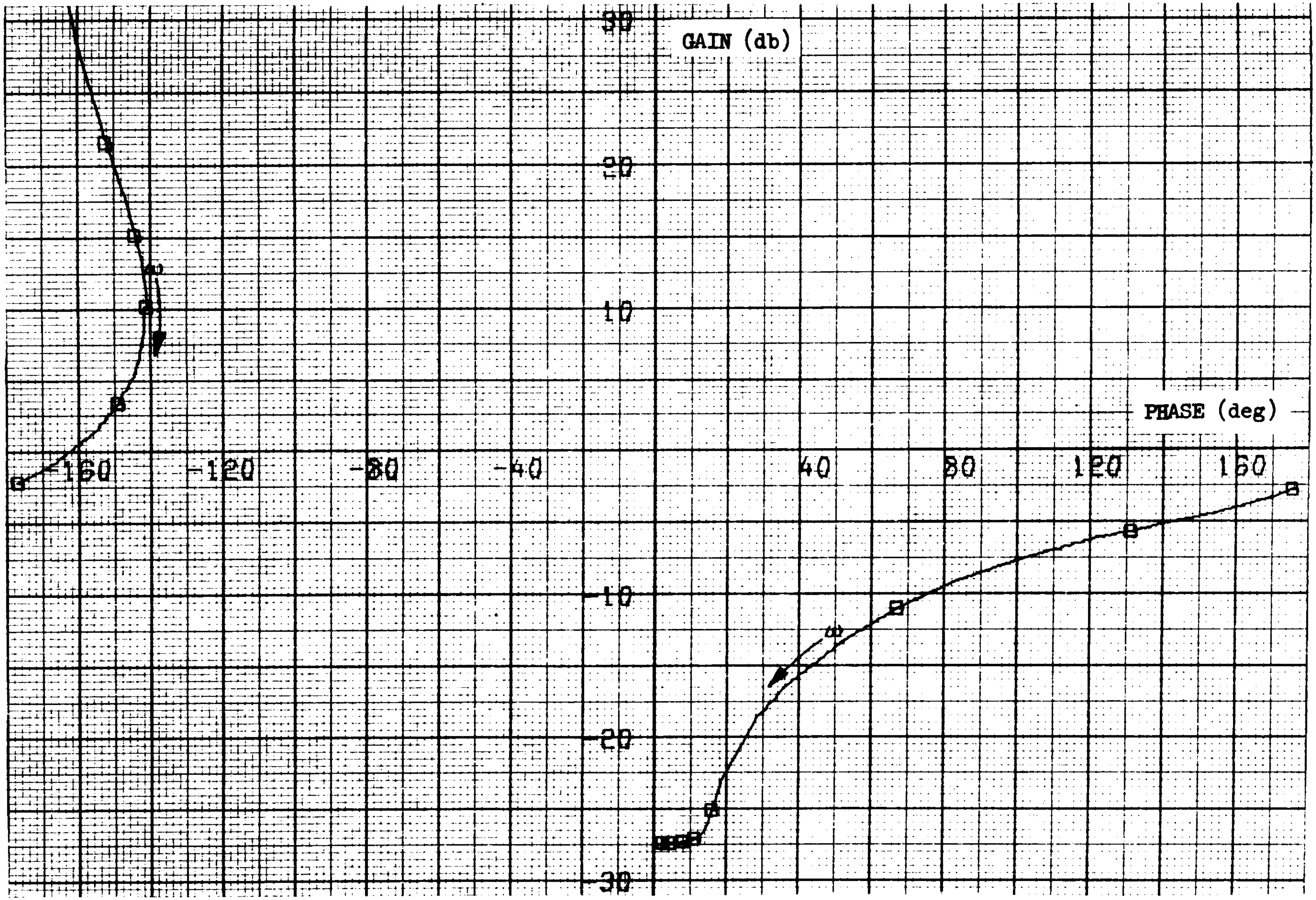

Figure 12. Gain-Phase Plot for 560 Seconds After Liftoff for Vehicle Incorporating Explicit Guidance (1-Second Sampling Period)

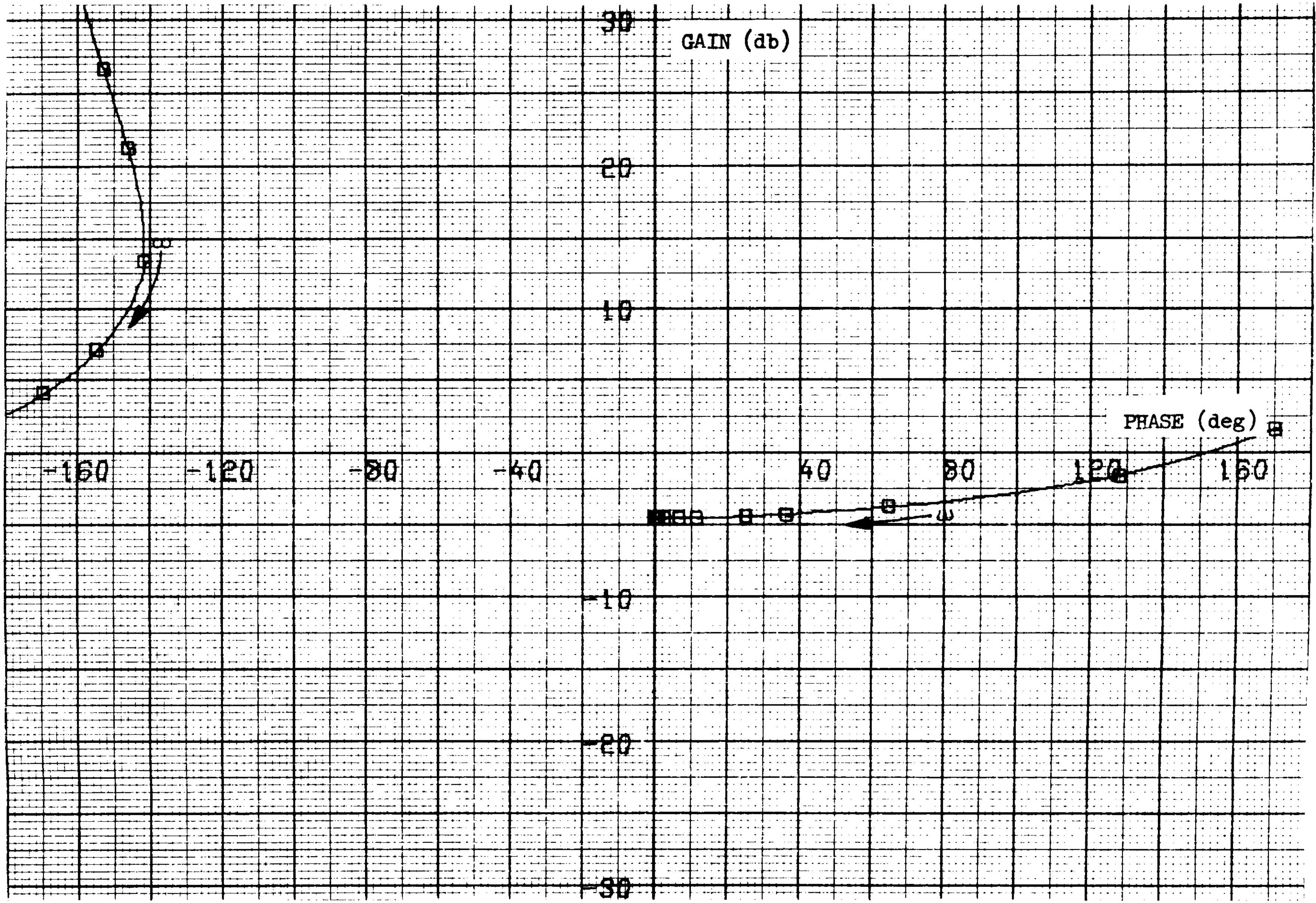

Figure 13. Gain-Phase Plot for 560 Seconds After Liftoff for Vehicle Incorporating Explicit Guidance (2-Second Sampling Period)

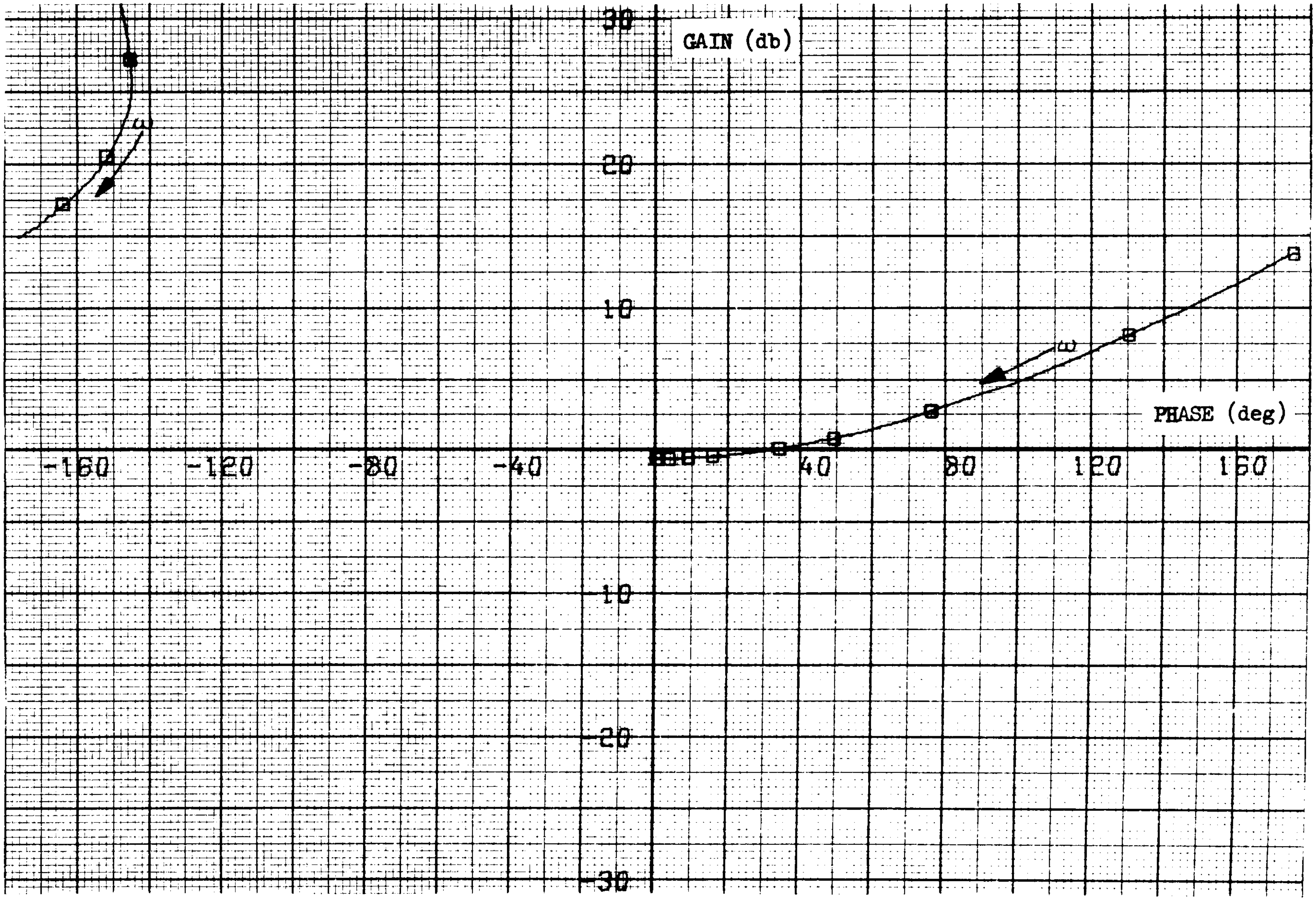

Figure 14. Gain-Phase Plot for 560 Seconds After Liftoff for Vehicle Incorporating Explicit Guidance (5-Second Sampling Period)

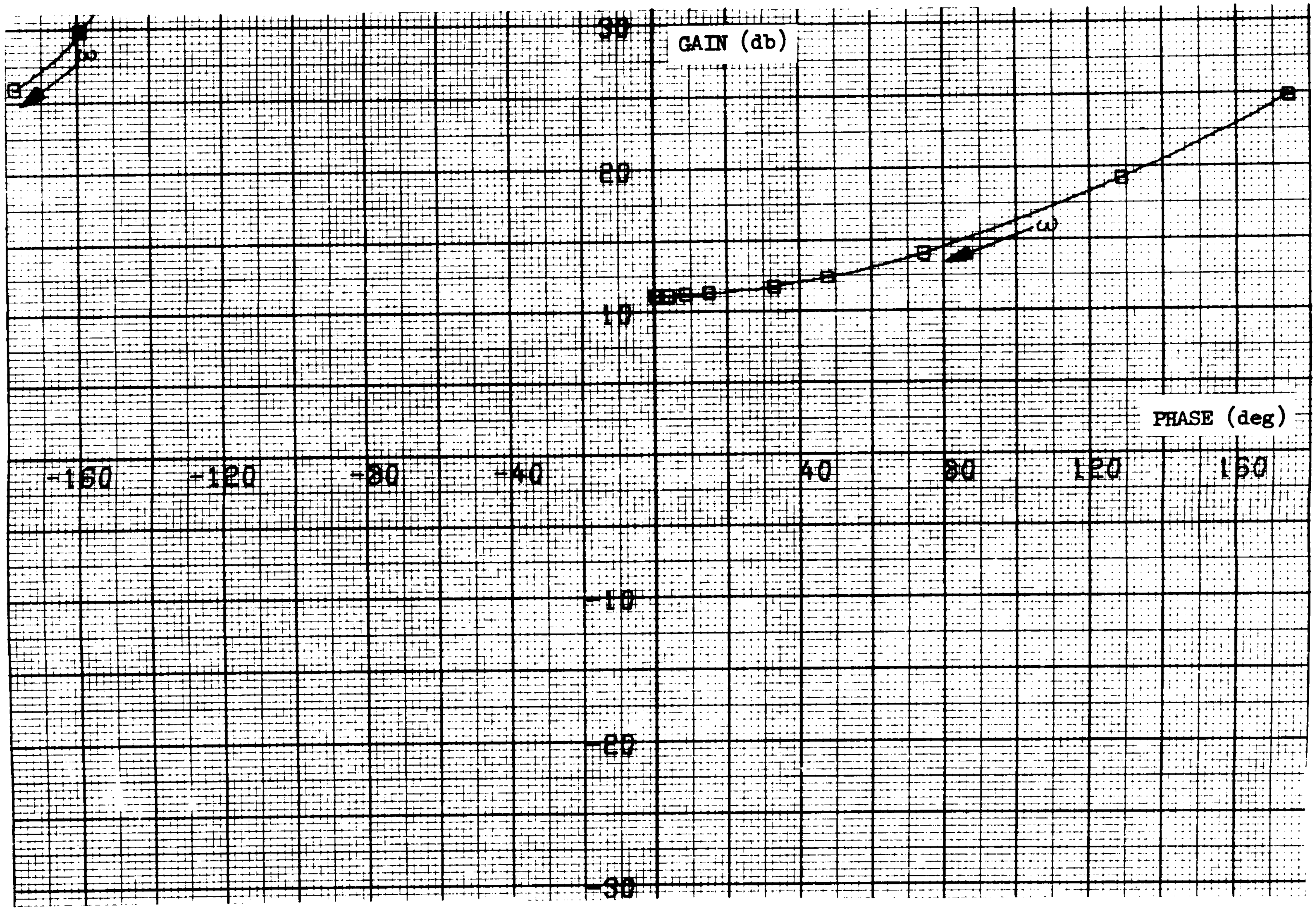

Figure 15. Gain-Phase Plot for 560 Seconds After Liftoff for Vehicle Incorporating Explicit Guidance (10-Second Sampling Period)

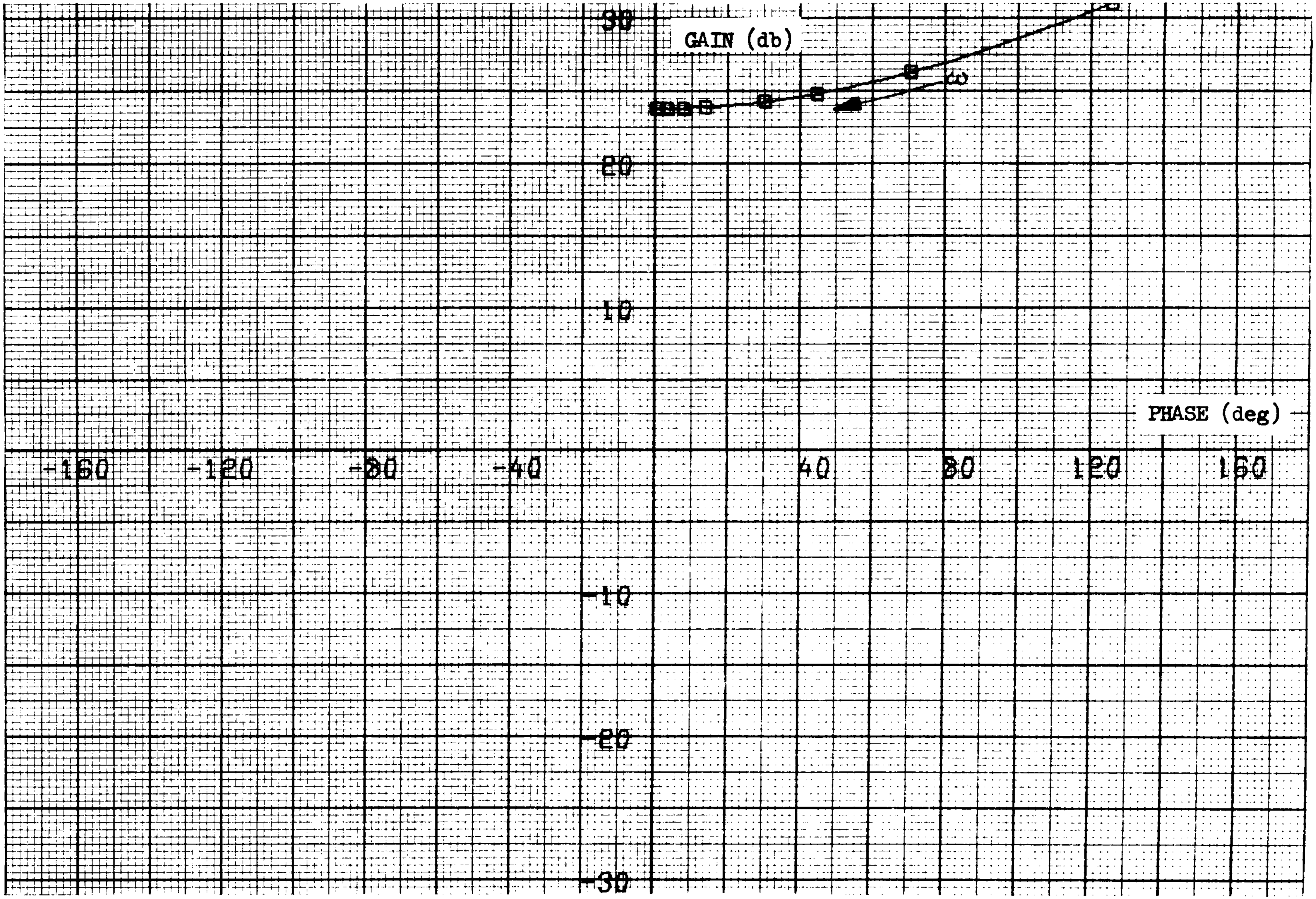

Figure 16. Gain-Phase Plot for 560 Seconds After Liftoff for Vehicle Incorporating Explicit Guidance (20-Second Sampling Period)

G. Summary

The first portion of the analysis was devoted to study of the guidance-control interface problems under the assumption of continuous updating of guidance commands. It was found that incorporation of explicit guidance results in very little degradation of system stability for all flight times but those close to MECO. Near MECO, there is considerable reduction of important stability margins, but the vehicle remains stable even for those times of flight.

The second portion was an investigation of the effects on system stability of the digital nature of the guidance computations. These effects are important only for flight times near MECO; for 560 seconds after Liftoff, the vehicle is stable for sampling periods of 5 seconds or shorter, but unstable for periods longer than 5 seconds.

V. ANALYSIS METHODS

A. Linearized Vehicle Dynamics Equations

In this appendix the dynamics equations used in support of the stability analyses described in Sections III and IV are presented. Although the total dynamics equations are nonlinear with time-varying coefficients, they were linearized for control systems analyses, and the system was studied for fixed times of flight. Two sets of linearized launch vehicle dynamics equations are included below. The first is for the more general situation for which areodynamic forces are significant. The second set can be obtained directly from the first; it applies only to the exoatmospheric case which includes all of the Atlas sustainer and Centaur phases.

- General Case

The equations listed below describe the perturbed vehicle pitch plane rigid body dynamics for the general case in which aerodynamics are significant. The important variables are illustrated in Figure A-1. The fifth equation in the list accounts for the fact that the inertial platform is displaced from the vehicle center of gravity. This set of vehicle dynamics equations is typical of those used in linear analyses:

$$\ddot{\psi} = \mu_c \delta + \mu_a \alpha_T \text{ (moment equation)}$$

$$\ddot{z}_r = a_c \delta - a_\alpha \alpha_T - a_\psi \psi \text{ (translational equation)}$$

$$\dot{\alpha}_V = \dot{\psi} + \frac{a_c}{V} \delta - \frac{1}{V} (a_\psi - g \cos\beta) \alpha_V - \frac{a_\alpha}{V} \alpha_T - \frac{C \cos\beta}{V} \psi \text{ (normal force equation)}$$

$$\alpha_T = \alpha_V + \alpha_W$$

$$z_{rm} = z_r \ell_p \psi$$

where the variables are defined as follows:

ψ = vehicle body angle (rad)

δ = actual engine angle (rad)

α_T = total effective angle of attack (rad)

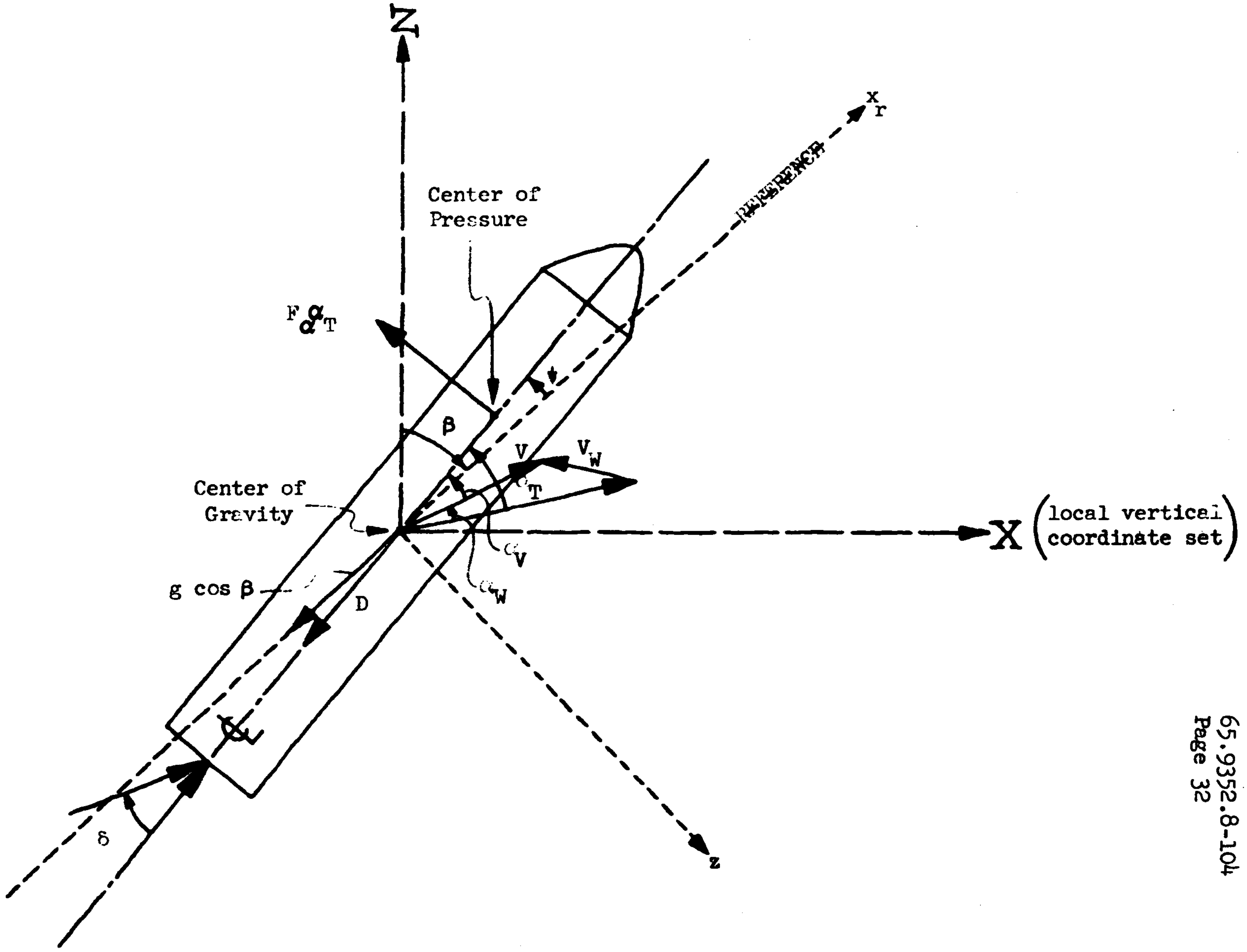
Z
x_r
REFERENCE
Center of Pressure
$F_{\alpha}\alpha_T$
β
V
V_W
α_T
Center of Gravity
X (local vertical coordinate set)
α_V
α_W
g cos β
D
℄
δ
z

Figure A-1.
Definition of Variables in Linearized Dynamics Equations

α_V = actual vehicle angle of attack (rad)

α_W = equivalent wind angle of attack (rad)

z_r = distance of vehicle center of gravity normal to reference axis from nominal point in the pitch plane (ft)

z_{rm} = distance (as measured in vehicle guidance loop) of vehicle center of gravity normal to reference axis from nominal point in the pitch plane (ft)

The parameters involved in the above four equations are defined by these relations:

$\mu_c = T_c \ell_c / I$

$\mu_\alpha = F_\alpha \ell_\alpha / I$

$a_c = T_c / M$

$a_\alpha = F\ell_\alpha / M$

$a_{\downarrow} = (T-D)/M$

where:

M = vehicle mass (slugs)
I = vehicle inertia about pitch axis (slug-ft^2)
T = total thrust (lb)
T_c = control thrust (lb)
F_α = aerodynamic force per unit total angle of attack (lb/rad)
D = vehicle drag force (lb)
V = vehicle velocity (ft/sec)
g = acceleration of gravity (ft/sec^2)

ℓ_c = distance parallel to roll axis between vehicle center of gravity and engine gimbal point (ft)

ℓ_α = distance parallel to roll axis between vehicle center of gravity and vehicle center of pressure (ft)

ℓ_p = distance parallel to roll axis between vehicle center of gravity and vehicle inertial platform (ft)

β = nominal vehicle flight path angle (rad)

o Exoatmospheric Case

The second set of linearized launch vehicle dynamics equations applies only to the exoatmospheric case. This set is a simplified version of the first list. The aerodynamic parameters, a_α and μ_α, become zero, which eliminates the need for computing angle of attack. Also, the parameters a_c and a_ψ become identical, because the drag force goes to zero and the control thrust equals the total vehicle thrust. The result is a group of only three equations, as compared with the five previously required:

$$\ddot{\psi} = \mu_c \delta$$

$$\ddot{z}_r = a_c \delta - a_c \psi$$

$$z_{rm} = z_r - \ell_p \psi$$

where both the variables and parameters are defined as above. Figure A-2 is a block diagram representation of these relations expressed in Laplace Transform notation.

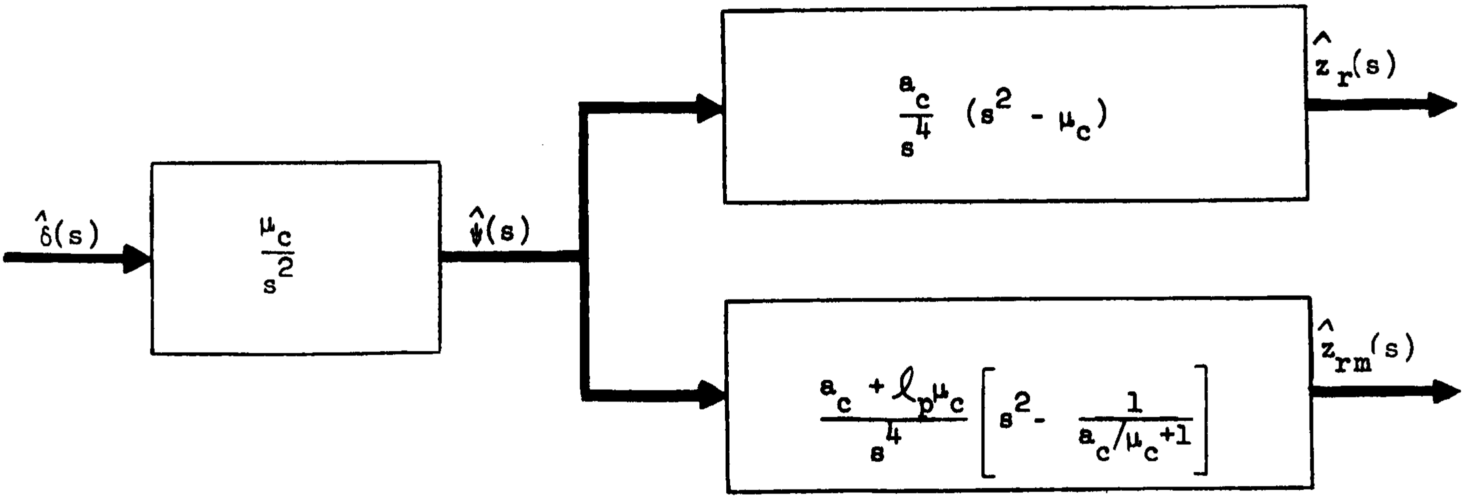
$\hat{\delta}(s)$
$\frac{\mu_c}{s^2}$
$\hat{\psi}(s)$
$\frac{a_c}{s^4}(s^2 - \mu_c)$
$\hat{z}_r(s)$
$\frac{a_c + \ell_p \mu_c}{s^4}\left[s^2 - \frac{1}{a_c/\mu_c + 1}\right]$
$\hat{z}_{rm}(s)$

Figure A-2. Block Diagram Representation of Exoatmospheric Vehicle Dynamics

B. Gain-Phase Plots For Launch Vehicles During Exoatmospheric Flight

This appendix presents a brief discussion of the use of gain-phase plots for launch vehicle stability analyses. It concentrates particularly on their utility for treatment of flight times during exoatmospheric phases.

The gain-phase plot is a graph of the frequency response of a system open-loop feedforward transfer function. The coordinates are the gain and phase of the frequency response, with input frequency as a parameter. Though the plot is drawn for an open-loop transfer function, its features have significance in terms of system closed-loop stability, just as do the features of the Bode plot. In fact, a gain-phase plot is actually a Bode plot expressed in terms of two orthogonal coordinates.

The transfer function generally used in control system analysis and synthesis is from commanded engine actuator angle to control system output. Figure B-1 shows schematically the relationship of these two variables and the relative positions of all components of the system in the feedforward loop. Figure B-2 is a typical gain-phase plot for this transfer function for a launch vehicle or missile operating above the atmosphere.

If the system is to be stable when operating in the closed-loop mode, the origin must always be on the right of the trace as it is traversed from low to high input frequencies. Moreover, it is not enough that the system be stable; to insure adequate vehicle response characteristics, certain minimum levels should be maintained for the various stability margins.

Generally, there are no more than three important stability margins for flight outside the atmosphere. They are low-frequency gain margin, rigid body phase margin, and high-frequency rigid body gain margin, all of which are defined in Figure B-2. For each time of flight treated, each gain margin should be 6 decibels or greater, and the rigid body phase margin should be at least 30 degrees. For vehicles which do not include integrators in their control systems for exoatmospheric flight, there exists no low-frequency gain margin.

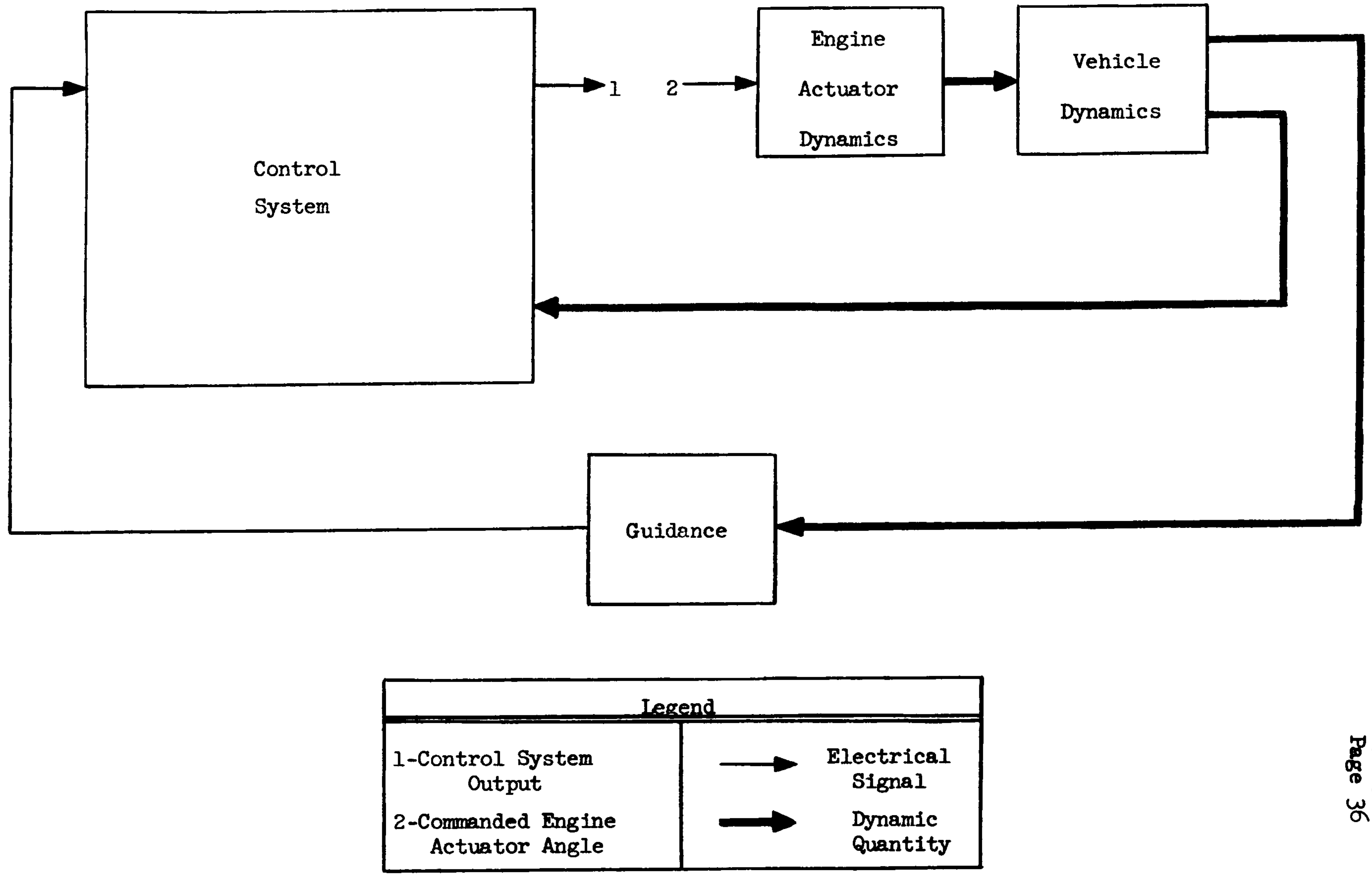
Control
System
1
2
Engine
Actuator
Dynamics
Vehicle
Dynamics
Guidance
Legend
1-Control System Output
2-Commanded Engine Actuator Angle
Electrical Signal
Dynamic Quantity

Figure B-1. Relationship of Variables of Transfer Function Generally Used for Gain-Phase Plots

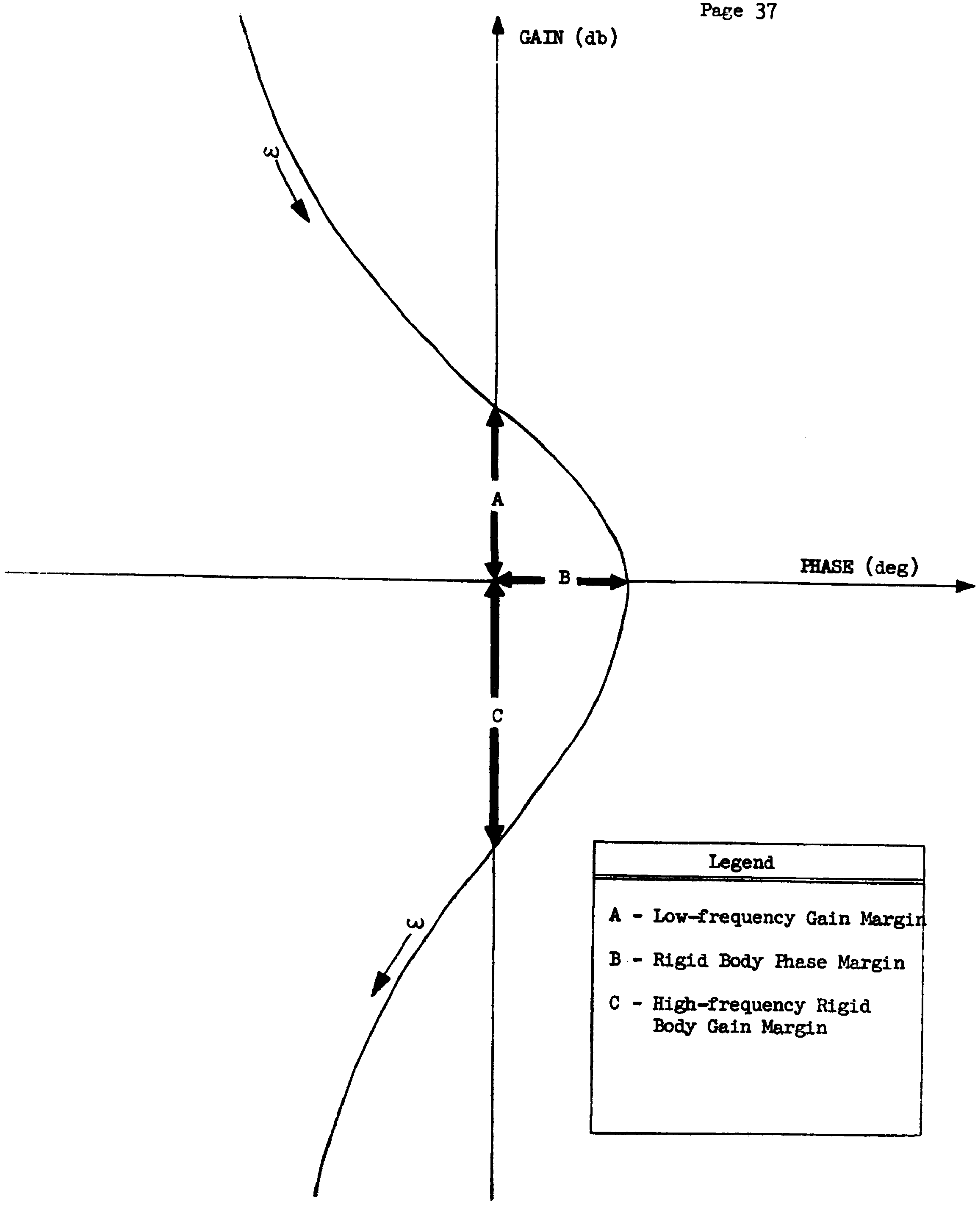
GAIN (db)
ω
A
B
PHASE (deg)
C
ω
Legend
A - Low-frequency Gain Margin
B - Rigid Body Phase Margin
C - High-frequency Rigid Body Gain Margin

Figure B-2. Typical Gain-phase Plot for Launch Vehicle During Exoatmospheric Flight

The exoatmospheric case is considerably simpler than the atmospheric situation, for which there is a greater number of significant stability margins. In the latter case, bending, engine actuator nonlinearities, and slosh are important and must be included in the analysis. In the former case, such modes can usually be neglected, as they generally cause only very minor modifications in vehicle stability portraits.

C. Linearization of Explicit Guidance Equations

This appendix presents the linearization of the explicit guidance equations. The result is a linear, constant coefficient differential equation which describes the small-angle behavior of the guidance scheme. With the perturbed equations for the vehicle dynamics and control system, it was used in conjunction with conventional linear analysis techniques to obtain system stability portraits for an Atlas/Centaur vehicle incorporating explicit guidance.

o Assumptions

Several simplifying assumptions were used during the linearization. Their utility can be understood through a brief discussion of the essentials of the guidance scheme.

At the end of each guidance cycle, the explicit guidance equations produce a commanded orientation expressed in an inertial coordinate frame. The Centaur resolver chain translates this and the actual vehicle orientation into error signals in body axes. The equations also yield an estimate of the remaining burn arc required for injection into the prespecified orbit; the estimate is expressed as the difference in true anomaly between the present vehicle position and the predicted vehicle position at MECO. The vehicle anomaly at MECO is not fixed as this set of guidance equations is intended to place the payload in a prespecified orbit, but not at any prespecified point or time. This burn arc estimate is used as the starting point for the computations of the next guidance cycle.

For the purposes of analysis, however, it was assumed that the true anomaly at injection is constant. Any change in the burn arc remaining is attributed to change in vehicle position. While this is not strictly true, the frequencies at which the commanded injection conditions change are expected to be low, considerably lower than the system frequencies of interest.

Another important assumption is that the Centaur acceleration also changes very slowly. In the explicit guidance equations, that quantity is not measured; it is computed as a function of the velocity consumed. However, in the linearized analyses, it was treated as a constant.

- Linearization

Figure 8 of Reference 1 includes most of the equations involved in the guidance-control interface as limited by the above assumptions. This diagram is complicated by the fact that it is very general and includes some equations not applicable to the Atlas/Centaur problem. It also includes equations which, after linearization, affect only the yaw plane. Figure C-1 includes only the equations necessary for the Atlas/Centaur pitch-plane analysis, though they are not in perturbed form.

The independent variables in Figure C-1, those which are independent whereever they appear in the diagram, are v_g, v_x, v_z and z. They are defined as follows:

v_g = velocity-to-go during remainder of Centaur flight
v_x = horizontal component of vehicle in-plane velocity
v_z = vertical component of vehicle in-plane velocity
z = vehicle distance from center of earth

This reflects the fact that the explicit guidance scheme is conceptually based on a local vertical coordinate frame, illustrated in Figure C-2. The commanded vehicle orientation in the pitch plane is given by the direction cosine c_{az}:

c_{az} = direction cosine of the angle between the local vertical and the commanded vehicle roll axis.

The above variable is the lone completely independent quantity in the diagram and is directly related only to: (1) distance from the center of the earth; (2) the horizontal component of the vehicle in-plane velocity; and (3) the

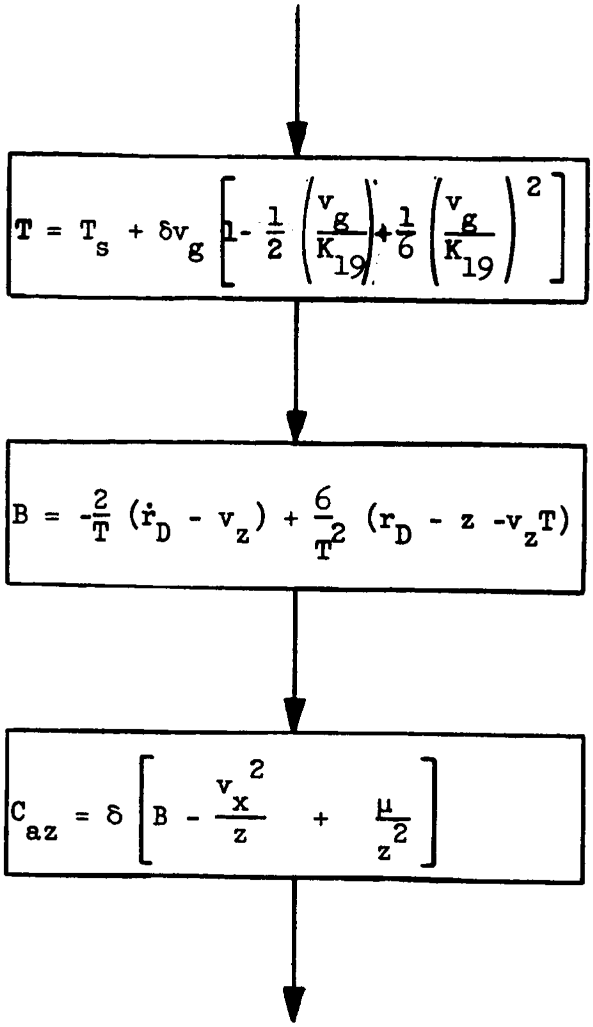

$$T = T_s + \delta v_g \left[1 - \frac{1}{2} \left(\frac{v_g}{K_{19}} \right) + \frac{1}{6} \left(\frac{v_g}{K_{19}} \right)^2 \right]$$

$$B = -\frac{2}{T} (\dot{r}_D - v_z) + \frac{6}{T^2} (r_D - z - v_z T)$$

$$C_{az} = \delta \left[B - \frac{v_x^2}{z} + \frac{\mu}{z^2} \right]$$

Definitions

B = steering coefficient

K_{19} = exhaust velocity of Centaur

r_D = desired radius at injection

$\dot{r}_D$ = desired radial velocity at injection

T_s = time-to-go until sustainer burnout

δ = reciprocal of thrust acceleration

μ = universal gravitational constant times mass of earth

Figure C-1. Computational Flow Diagram for the Pitch Plane Case

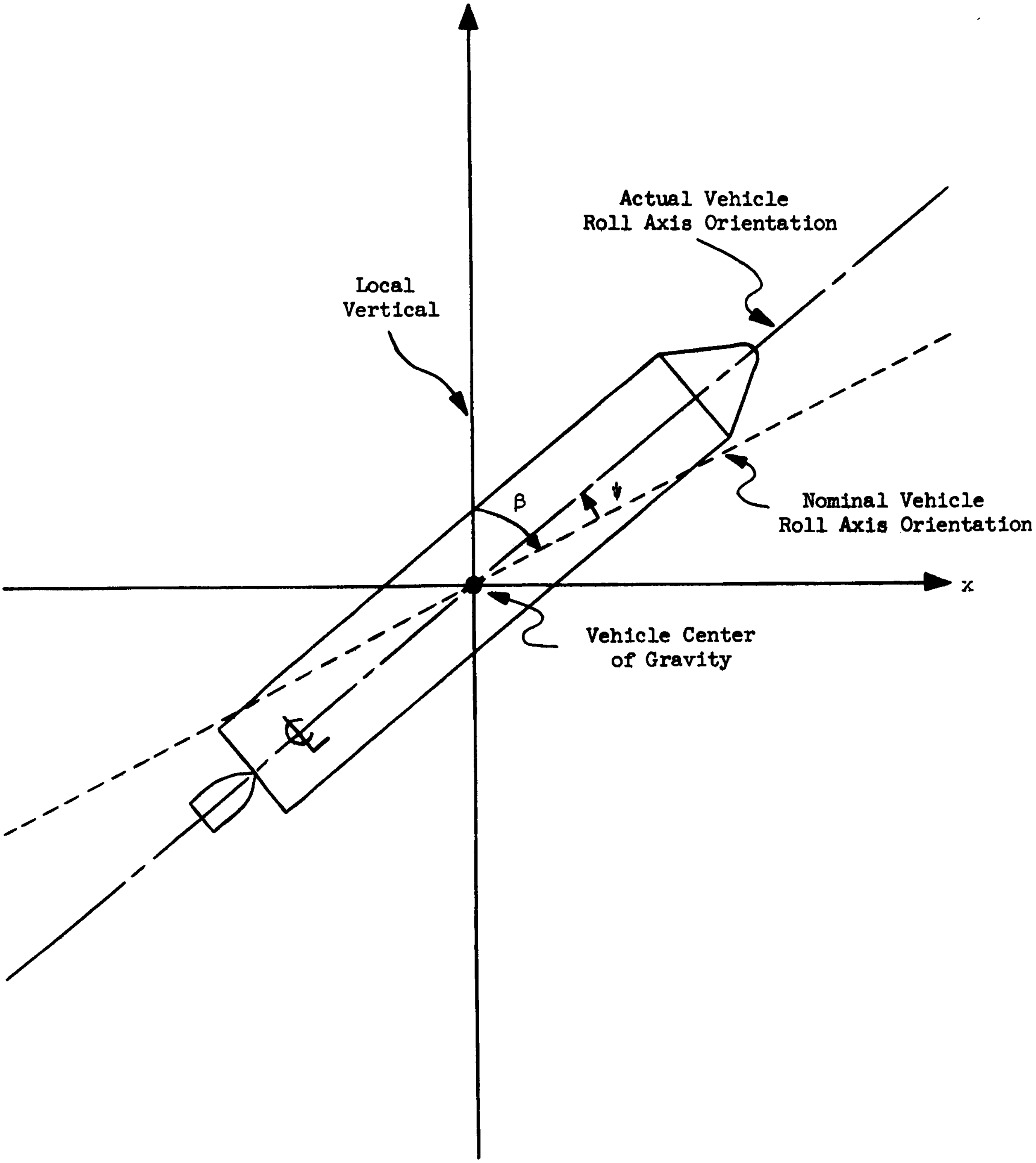
z
Actual Vehicle
Roll Axis Orientation
Local
Vertical
β
ψ
Nominal Vehicle
Roll Axis Orientation
x
Vehicle Center
of Gravity
℄

Figure C-2. Local Vertical Coordinate System
Used in Explicit Guidance Equations

steering coefficient B. The total differential for the direction cosine is given by:

$$dc_{az} = \frac{\partial c_{az}}{\partial v_x} dv_x + \frac{\partial c_{az}}{\partial z} dz + \frac{\partial c_{az}}{\partial B} dB$$

The steering coefficient B is itself directly dependent on three quantities, two of which are independent variables in the diagram of Figure C-1. They are: (1) the vertical component of vehicle in-plane velocity; and (2) vehicle distance from the center of the earth. The third quantity is defined as follows:

T = time-to-go until MECO

The total differential for the steering coefficient B is:

$$dB = \frac{\partial B}{\partial v_z} dv_z + \frac{\partial B}{\partial z} dz + \frac{\partial B}{\partial T} dT$$

Substitution yields:

$$dc_{az} = \frac{\partial c_{az}}{\partial v_x} dv_x + \frac{\partial c_{az}}{\partial B} \frac{\partial B}{\partial v_z} dv_z + \left[\frac{\partial c_{az}}{\partial z} + \frac{\partial c_{az}}{\partial B} \frac{\partial B}{\partial z} \right] dz + \frac{\partial c_{az}}{\partial B} \frac{\partial B}{\partial T} dT$$

The time-to-go until MECO is directly dependent just on velocity-to-go during present phase of flight, and the total differentials for these two variables are related by:

$$dT = \frac{\partial T}{\partial v_g} dv_g$$

Consequently, the total differential of the direction cosine can be expressed as:

$$dc_{az} = \frac{\partial c_{az}}{\partial v_x} dv_x + \frac{\partial c_{az}}{\partial B} \frac{\partial B}{\partial v_z} dv_z + \left[\frac{\partial c_{az}}{\partial z} + \frac{\partial c_{az}}{\partial B} \frac{\partial B}{\partial z} \right] dz + \frac{\partial c_{az}}{\partial B} \frac{\partial B}{\partial T} \frac{\partial T}{\partial v_g} dv_g$$

However, the velocity-to-go during the Centaur phase of flight is a function only of the horizontal and vertical components of vehicle in-plane velocity. For Centaur phase, the equation is:

$$v_g = \sqrt{(v_x - v_{xf})^2 + (v_z - v_{zf})^2}$$

where v_{xf} and v_{zf} express the desired vehicle velocity at MECO in the local vertical coordinate frame for the present time of flight. For sustainer flight, the equation is identical except that the nominal vehicle velocity at SECO is subtracted from the right-hand side. The total differential of velocity-to-go is:

$$dv_g = \frac{\partial v_g}{\partial v_x} dv_x + \frac{\partial v_g}{\partial v_z} dv_z$$

In the linearized equations describing the vehicle control system, commanded vehicle attitude is stated in terms of an angle:

ψ_c = commanded vehicle body angle (rad)

Its zero point corresponds to the nominal vehicle attitude, and it depends only on the direction cosine c_{az}:

$$d\psi_c = \frac{\partial \psi_c}{\partial c_{az}} dc_{az}$$

When several of the above relations are appropriately combined, the total differential of the linearized flight path angle can be expressed in the following general terms:

$$d\psi_c = \frac{\partial\psi_c}{\partial\alpha_{az}}\left[\left(\frac{\partial\alpha_{az}}{\partial v_x} + \frac{\partial\alpha_{az}}{\partial\beta}\ \frac{\partial\beta}{\partial\Gamma}\ \frac{\partial\Gamma}{\partial v_g}\ \frac{\partial v_g}{\partial v_x}\right) dv_x + \left(\frac{\partial\alpha_{az}}{\partial\beta}\ \frac{\partial\beta}{\partial v_z}\right.\right.$$

$$\left.\left. + \frac{\partial\alpha_{az}}{\partial\beta}\ \frac{\partial\beta}{\partial\Gamma}\ \frac{\partial\Gamma}{\partial v_g}\ \frac{\partial v_g}{\partial v_z}\right) dv_z + \left(\frac{\partial\alpha_{az}}{\partial z} + \frac{\partial\alpha_{az}}{\partial\beta}\ \frac{\partial\beta}{\partial z}\right)dz\right]$$

This expression is a function of differentials of quantities expressed in the local vertical coordinate frame. For a representation of the entire guidance loop, it must be a function of differentials of quantities defined in body coordinates. The transformation in the pitch plane from body axis to a local vertican set can be written very generally as:

$$[T] = \begin{bmatrix} T_{11} & T_{12} \\ T_{21} & T_{22} \end{bmatrix}$$

With the inclusion of the above transformation, the equation describing the guidance loop assumes the following form when written in Laplace Transform notation:

$$\hat{\psi}_c(s) = (k_v s + k_p)\ \hat{z}_{rm}(s)$$

where the variable on the right-hand side is as defined in Appendix A and the linearized guidance loop coefficients, k_p and k_v, are given by:

$$k_v = \frac{\partial\psi_c}{\partial\alpha_{az}}\left[T_{12}\left(\frac{\partial\alpha_{az}}{\partial v_x} + \frac{\partial\alpha_{az}}{\partial\beta}\ \frac{\partial\beta}{\partial\Gamma}\ \frac{\partial\Gamma}{\partial v_g}\ \frac{\partial v_g}{\partial v_x}\right) + T_{22}\left(\frac{\partial\alpha_{az}}{\partial\beta}\ \frac{\partial\beta}{\partial v_z} + \frac{\partial\alpha_{az}}{\partial\beta}\ \frac{\partial\beta}{\partial\Gamma}\ \frac{\partial\Gamma}{\partial v_g}\ \frac{\partial v_g}{\partial v_z}\right)\right]$$

$$k_p = T_{22} \frac{\partial \psi_c}{\partial \alpha_{az}} \left[\frac{\partial \alpha_{az}}{\partial z} + \frac{\partial \alpha_{az}}{\partial B} \frac{\partial B}{\partial z} \right]$$

These coefficients must now be written in more specific terms. The following expressions are easily derived from equations presented earlier or contained in Figure C-1:

$$\frac{\partial \alpha_{az}}{\partial v_x} = -\frac{2\delta v_x}{z}$$

$$\frac{\partial \alpha_{az}}{\partial z} = \frac{\delta}{z^2} \left(v_x{}^2 - \frac{2\mu}{z} \right)$$

$$\frac{\partial \alpha_{az}}{\partial B} = \delta$$

$$\frac{\partial B}{\partial v_z} = -\frac{4}{T}$$

$$\frac{\partial B}{\partial z} = -\frac{6}{T^2}$$

$$\frac{\partial B}{\partial T} = \frac{2}{T^2} \left(\dot{r}_D + 2 v_z - 6 \frac{r_D - 2}{T} \right)$$

$$\frac{\partial T}{\partial v_g} = \delta \left[1 - \frac{v_g}{K_{19}} + \frac{1}{2} \left(\frac{v_g}{K_{19}} \right)^2 \right]$$

$$\frac{\partial v_g}{\partial v_x} = \frac{v_x - v_{xf}}{v_g}$$

$$\frac{\partial v_g}{\partial v_z} = \frac{v_z - v_{zf}}{v_g}$$

The remaining partial derivative and the elements of the transformation are expanded as follows in accordance with the definitions of polarity included in Figure C-2:

$$\frac{\partial \psi_c}{\partial c_{az}} = \csc \beta$$

$$T_{12} = \cos \beta$$

$$T_{22} = -\sin \beta$$

The linearized guidance loop coefficients can now be written in terms of vehicle state variables:

$$k_v = 2\delta \left\{ \frac{2}{T} - \frac{v_x}{z} \cot \beta + \frac{\delta}{T v_g^{\,2}} \left[\dot{r}_D + 2\, v_z - 6\, \frac{r_D - z}{T} \right] \left[1 - \frac{v_g}{K_{19}} \right. \right.$$

$$\left. \left. + \frac{1}{2} \left(\frac{v_g}{K_{19}} \right)^2 \right] \left[(v_x - v_{xf}) \cot \beta - (v_z - v_{zf}) \right] \right\}$$

$$k_p = \delta \left[\frac{6}{T^2} - \frac{1}{z} \left(v_x - \frac{2\mu}{z} \right) \right]$$

This completes the linearization of the explicit guidance equations for the pitch plane case.

In Table 3 of Section IV, it is seen that, when the above expressions are evaluated for particular flight times, the resulting linearized coefficient values become relatively very large for flight times near MECO. The reason for this is contained in the above equations. As the vehicle nears MECO, the terms which involve inverse powers of time-to-go until MECO tend toward infinity. So do the values of the linearized guidance loop coefficients, since both the above expressions contain at least one such term.

VI. CONCLUSIONS AND RECOMMENDATIONS

On the basis of the results of this preliminary study, it is concluded that the effects on vehicle stability of incorporation of the explicit guidance scheme are acceptable if the guidance commands are updated every 5 seconds or more frequently.

Further studies should be more detailed in several aspects:

(1) when the classes of trajectories have been delineated more specifically, several representative missions should be selected and similar analyses performed to corroborate the assumption that the results are not trajectory dependent;

(2) the vehicle dynamics equations should be modified to include bending and sloshing to verify the assumption that there exists little interaction between the guidance loop and these modes;

(3) a time-varying simulation should be conducted and the resulting time responses examined to determine the consequences of possible low stability margins for flight times very close to MECO.

APPENDIX B

DERIVATION OF ORBIT PARAMETERS, FROM THE MISSION CONSTRAINTS C_3, R_p, $\bar{s}$ FOR ESCAPE HYPERBOLA

A. CONIC PARAMETERS (a, e, p)

For a hyperbola the following two relations are well known,

$$p = a\left(e^2 - 1\right) \qquad \text{(1A)}$$

$$R_p = a\,(e - 1) \qquad \text{(2A)}$$

from which

$$a = \frac{R_p}{e - 1} \qquad \text{(3A}$$

Combining (1A), (2A), and (3A) and noting that for a conic

$$h^2 = \mu p \qquad \text{(4A)}$$

we get

$$e = \frac{h^2}{\mu R_p} - 1 \qquad \text{(5A)}$$

Now, at perigee

$$h^2 = R_p{}^2 \; V_p{}^2 \qquad \text{(6A)}$$

where from vis-viva

$$V_p{}^2 = \mu\left(\frac{2}{R_p} + \frac{1}{a}\right) \qquad \text{(7A)}$$

and at infinity

$$V\infty = \mu\left(\frac{1}{\infty} + \frac{1}{a}\right) = \frac{\mu}{a} = C_3 \qquad \text{(8A)}$$

Combining (6A), (7A), and (8A)

$$h^2 = 2R_p\mu + R_p{}^2\, C_3 \qquad \text{(9A)}$$

and substituting this into (5A)

$$e = 1 + \frac{R_p C_3}{\mu} \tag{10A}$$

Also substituting (8A) into (1A) we get

$$p = \frac{\mu (e_2 - 1)}{C_3} \tag{11A}$$

Thus (8A), (10A), (11A) provide a, e, and p from R_p and C_3

B. DIRECTION OF PERIGEE ($\bar{i}_{R_p}$)

Let θ be the acute angle between $\bar{i}_{R_p}$ and $\bar{s}$. Then

$$\bar{i}_{R_p} \times \bar{s} = \bar{j} \sin \theta \tag{12A}$$

If both sides of (12A) are crossed with $\bar{s}$

$$\bar{s} \times (\bar{i}_{R_p} \times \bar{s}) = \bar{s} \times \bar{j} \sin \theta \tag{13A}$$

or employing the familiar vector identity for triple cross products, (13A) becomes

$$\bar{i}_{R_p} - \bar{s} (\bar{s} \cdot \bar{i}_{R_p}) = \bar{s} \times \bar{j} \cos \theta \tag{14A}$$

But

$$\bar{s} \cdot \bar{i}_{R_p} = - \cos \theta \tag{15A}$$

Thus

$$\bar{i}_{R_p} = \bar{s} \times \bar{j} \sin \theta - \bar{s} \cos \theta \tag{16A}$$

where, for a hyperbola

$$\theta = \tan^{-1} \left[\sqrt{e^2 - 1} \right] \tag{17A}$$

APPENDIX C

DERIVATION OR ORBIT PARAMETERS FROM THE MISSION CONSTRAINTS R_T, V_T AND R_p FOR TRANSLUNAR ELLIPTIC TRAJECTORIES

A. CONIC PARAMETER (a, e, p)

Repeating steps similar to (1A) through (5A) in Appendix A it can readily be shown for an ellipse.

$$e = \frac{h^2}{\mu R_p} - 1 \tag{1B}$$

Noting again that

$$h^2 = R_p^2 V_p^2 \tag{6A}$$

we get

$$e = \frac{R_p V_p^2}{\mu} - 1 \tag{2B}$$

From the vis-viva law,

$$V_p^2 = \frac{2\mu}{R_p} - \frac{\mu}{a} \tag{3B}$$

and

$$V_T^2 = \frac{2\mu}{R_T} - \frac{\mu}{a} \tag{4B}$$

When (2B), (3B) and (4B) are combined the expression for e is

$$e = 1 - R_p \left[\frac{2}{R_T} - \frac{V_T^2}{\mu} \right] \tag{5B}$$

Now from (4B) 'a' can be obtained and then 'p' can be computed from

$$p = a(1 - e^2) \tag{6B}$$

B. DIRECTION OF PERIGEE, (L_{R_p})

Referring to Figure 1B, and the more generalized vector diagram (2B) we can express $\bar{R}_p$ in terms of $\bar{R}_T$ and $\bar{V}_T$ as

$$\bar{R}_p = a\frac{\bar{R}_T}{R_T} - b\frac{\bar{V}_T}{V_T} \tag{7B}$$

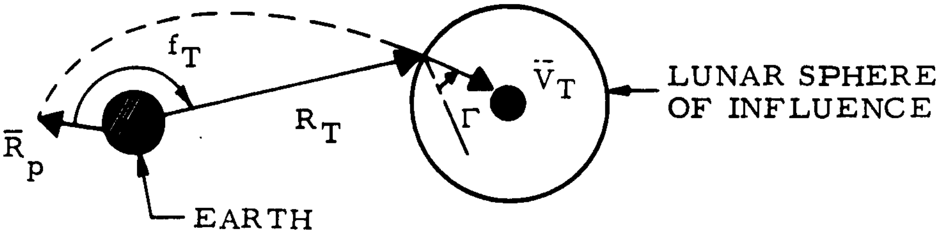
f_T
$\bar{R}_p$
R_T
$\bar{V}_T$
Γ
LUNAR SPHERE OF INFLUENCE
EARTH

Figure 1B

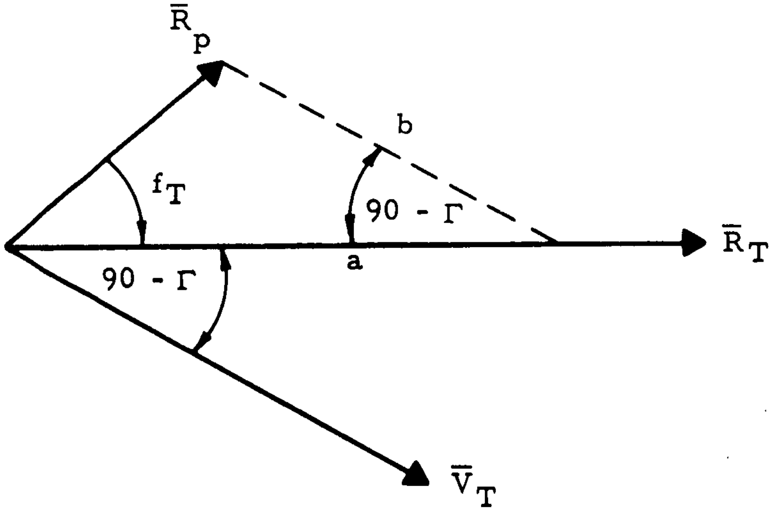
$\bar{R}_p$
b
f_T
90 - Γ
$\bar{R}_T$
a
90 - Γ
$\bar{V}_T$

Figure 2B

From the law of sines

$$\frac{b}{\sin f_T} = \frac{R_p}{\sin (90 - \Gamma)} \qquad (8B)$$

or

$$b = \frac{R_p \sin f_T}{\cos \Gamma} \qquad (9B)$$

Also we have from Figure 2B

$$a = R_p \cos f + b \sin \Gamma \qquad (10B)$$

Thus, putting (9B) and (10B) into (7B) yields

$$\bar{R}_p = R_p \left| \cos f_T + \sin f_T \frac{\sin \Gamma}{\cos \Gamma} \right| \frac{\bar{R}_T}{R_T} - \left[R_p \frac{\sin f_T}{\cos \Gamma} \frac{\bar{V}_T}{V_T} \right] \qquad (11B)$$

or

$$\bar{i}_{R_p} = \frac{1}{\cos} \left[\cos (f_T - \Gamma) \frac{\bar{R}_T}{R_T} - \sin f \frac{\bar{V}_T}{V_T} \right] \qquad (12B)$$

Now, from Figure 1B)

$$= \sin^{-1} \left[\frac{\bar{R}_T \cdot \bar{V}_T}{R_T \, V_T} \right] \qquad (13B)$$

and from the polar equation of the ellipse

$$f_T = \cos^{-1} \left\{ \frac{1}{e} \left[\frac{p}{R_T} - 1 \right] \right\} \qquad (114B)$$

Thus with (13B) and (14B), $\bar{i}_{R_p}$ is defined.

APPENDIX D

ANGLE BETWEEN PERIGEE AND OUTWARD ASSYMPTOTE OF ESCAPE HYPERBOLA

If 'a' is one half the transverse axis and 'b' is one half the conjugate axis the angle f_t, between the transverse axis and an assymptote is given by

$$f_T = \tan \frac{b}{a} \qquad (1A)$$

Now, for a hyperbola the, eccentricity, e, is

$$e = \frac{\sqrt{a^2 + b^2}}{a} = \sqrt{1 + \frac{b^2}{a^2}} \qquad (2a)$$

or

$$e^2 - 1 = \frac{b^2}{a^2} = \tan^2 f_T \qquad (3a)$$

If 'p' is the semi-latus rectum, then it can be shown that

$$\frac{p}{e} = e^2 - 1 \qquad (4a)$$

Substituting 4a into 3a we have

$$f_t = \tan^{-1} \sqrt{\frac{p}{a}} \qquad (5a)$$

Since we are interested in the angle between the perigee vector and the outward assymptote, the angle, f_T, is given by

$$f_T = 180 - \tan^{-1} \sqrt{\frac{p}{a}}$$

APPENDIX E

TABULATION OF INPUTS FOR EACH MISSION

Below are tabulated the inputs associated with these guidance equations, for each mission. With these inputs the maneuver proceeds automatically to completion of the Centaur Guidance role.

A. INPUTS COMMON TO ALL PROPOSED MANEUVERS

K_6
K_7
K_{11}
K_{12}
K_{14}
K_{15}

K_{16}
K_{17}
K_{18}
K_{19}
K_{20}
K_{21}

K_{27} - K_{48}
K_{51}
a_s
Δt_f
t_{11}
ω
$\psi = 1$
$\lambda = 0$

B. INPUTS FOR SPECIFIED EARTH ORBIT IN ADDITION TO A

K_{23}
K_{24}
K_{25}

$\bar{i}_{R_p} = 0$ circular orbit
$\neq 0$ elliptic orbit
$\bar{j}$

$\zeta = -1$
$\nu = 0$
$TT = 0$

C. INPUTS FOR INTERPLANETARY MISSION IN ADDITION TO A (1 BURN)

K_{23}
K_{24}
K_{25}

$\bar{i}_{R_p}$
$\bar{s}$
$\bar{j}$

$\zeta = 1$
$\nu = 0$
$TT = 0$

D. INPUTS FOR PRE-TARGETED LUNAR MISSION IN ADDITION TO A (1 BURN)

K_{23}
K_{24}
K_{25}

$\bar{i}_{R_p}$
$\bar{r}_T$
$\bar{j}$

$\nu = 0$
$TT = 0$

E. INPUTS FOR INTERPLANETARY MISSION IN ADDITION TO A (2 BURN)

K_{23}, K_{23}'

K_{24}, K_{24}'

K_{25}, K_{25}'

$\bar{i}R_p, \bar{i}R_p'$

$\bar{j}$

$\bar{s}$

f_T

S_T

K_{100}

K_{200}

K_{110}

K_{210}

K_{115}

$t_T = 1$

$bb = 0$

$aa = 1$

$\zeta = -1$

$\nu = 0$

F. INPUTS FOR PRE-TARGETED LUNAR MISSION IN ADDITION TO A (2 BURN)

K_{23}, K_{23}'

K_{24}, K_{24}'

K_{25}, K_{25}'

$\bar{i}R_p, \bar{i}R_p'$

$\bar{j}$

$\bar{r}_T$

f_T

s_T

K_{100}

K_{200}

K_{110}

K_{210}

K_{115}

$\zeta = -1$

$\nu = 0$

$TT = 1$

$M_A = 0$

$bb = 0$

$aa = 2$

G. INPUTS FOR RENDEZVOUS MISSIONS AND IN-FLIGHT TARGETED LUNAR MISSIONS IN ADDITION TO A (1 BURN)

K_1

K_2

K_3

K_5

K_{10}

K_{13}

K_{30}

$\nu = 1$

$TT = 0$

H. INPUTS FOR RENDEZVOUS MISSIONS AND IN-FLIGHT TARGETED LUNAR MISSIONS IN ADDITION TO A (2 BURN)

K_1

K_2

K_3

K_5

K_{10}

K_{13}

K_{23}

K_{24}

K_{25}

K_{30}

K_{115}

$\bar{i}_{R_p}$

$\bar{j}$

$\zeta = -1$

$\nu = 0$

$TT = 1$

$M_A = 1$

$bb = 0$

$aa = 0$

J. INPUTS FOR COM-SAT MISSION IN ADDITION TO A (3 BURN)

K_1

K_2

K_3

K_5

K_{10}

K_{13}

K_{23}, K_{23}'

K_{24}, K_{24}'

K_{25}, K_{25}'

K_{30}

K_{115}

$\bar{i}_{R_p}, \bar{i}_{R_p}'$

$\bar{j}, \bar{j}'$

$\zeta = -1$

$\nu = 0$

$TT = 1$

$M_A = 3$

$bb = 0$

$aa = 0$